

MICRO-STRUCTURAL CHARACTERISATION OF NON- EASEL PAINTED ARTWORKS

By

Lynn Chua

A thesis submitted for the
Degree of Master of Science (Research)

University of Technology, Sydney

August 2016

CERTIFICATE OF AUTHORSHIP AND ORIGINALITY

I certify that the work in this thesis has not previously been submitted for a degree nor has it been submitted as part of the requirements for a degree except as fully acknowledged within the text.

I also certify that the thesis has been written by me. Any help that I have received in my research work and the preparation of the thesis itself has been acknowledged. In addition, I certify that all the information sources and literature used are indicated in the thesis.

Lynn Chua

22 Aug 2016

ACKNOWLEDGEMENT

I like to personally thank my academic supervisor, Associate Professor Barbara Stuart and co-supervisor, Dr. Paul Thomas, for their continuous encouragement and feedback throughout my research. Special thanks to Dr. Brian Reedy, Dr. Katie McBean, Dr. Linda Xiao and Dr. Verena Taudte for the instrumentation training and assistance in my technical questions at UTS. I also wish to express my gratitude to Mr. Jean-Pierre Guerbois (UTS) for his assistance in HF analysis, Dr. Elizabeth Carter (USyd) for her assistance in vivianite analysis and Dr. Ilaria Bonaduce (UniPisa) for assistance in my questions on the GC/MS analytical protocol for binder characterisation. In addition, Dr. Nick Proschogo (USyd) and Dr. Russel Pickford (BMSF, UNSW)'s provision of MS data processing softwares are much appreciated.

I wish to express my deepest gratitude to my internship supervisor, Dr. Gregory Dale Smith, senior conservation scientist at the IMA. The extensive learning experiences acquired at the IMA would not be possible without Greg's passionate and unequivocal guidance in conservation science research. Greg also contributed his feedback on the writing of the thesis. Special thanks to Dr. Victor Chen, dye analyst and full-time volunteer at the IMA (retiree chemist from Eli Lilly and Company). Victor taught me the spirit of perseverance in science and to think in the chemistry way, even if it is 'art' we are talking about. I also wish to thank John Goodpaster, IMA visiting professor from IUPUI, who guided me with practical experience through several days of GC-MS troubleshooting.

Lastly it was an enjoyable experience working with the conservators through various projects. I like to thank Kerry Head (Objects Conservator at the AGNSW) and Natalie Wilson (Curator of Australian art at the AGNSW) for organising the sampling rounds and their enthusiasm in discussion of PNG highlands paint materials. I am also inspired and thankful to Claire Hoevel (Paper Conservator at the IMA), for her dedication and inquisitive mind in the conservation of artworks, which have kick-started most of the projects undertaken. I also like to acknowledge the contributions in data collection by Dr. Jay A. Siegel (IMA visiting professor from IUPUI) and conservation documentation by Richard McCoy (Conservator of objects and variable art) for the "*Numbers 0-9*" project.

PUBLICATIONS AND CONFERENCE PRESENTATIONS

Accepted

Chua, L., Head, K., Thomas, P. & Stuart, B. 2016, 'Micro-characterisation of the colour palette of ceremonial objects from the Papua New Guinea Highlands: Transition from natural to synthetic pigments', *Microchemical Journal*, vol. 124, pp. 547-58.

Chua, L., Maynard-Casely, H.E., Thomas, P.S., Head, K. & Stuart, B.H. 2016, 'Characterisation of blue pigments from ceremonial objects of the Southern Highlands in Papua New Guinea using vibrational spectroscopy and X-ray diffraction', *Vibrational Spectroscopy*, vol. 85, pp. 43-7.

Chua, L. Hoeval, C., Smith, G.D. 2016, 'Characterization of Haku Maki Prints from the "Poem" Series using Light-Based Techniques', *Heritage Science*, vol. 4, no. 1.

Pending

Chua, L. Head, K. Thomas, P. & Stuart, B., 'Raman and FTIR Microscopy of organic binders and extraneous organic materials on painted ceremonial objects from the Highlands of Papua New Guinea', *Microchemical Journal*

Chua, L., McCoy R., Siegel, J., Smith, G.D. 'Polyurethane enamel paint characterization in Robert Indiana "Numbers 0-9" outdoor sculpture: Comparison of Paint failure before and after Conservation', *Studies in Conservation*

Conference Presentations

Chua, L., Head, K., Thomas, P. & Stuart, B. (2015, April). *Investigation of paints on ceremonial objects from the Highlands of Papua New Guinea*. Paper presented at the TECHNART Conference, Catania, Italy

TABLE OF CONTENTS

CERTIFICATE OF AUTHORSHIP AND ORIGINALITY	II
ACKNOWLEDGEMENTS	III
PUBLICATIONS AND CONFERENCE PRESENTATIONS	IV
TABLE OF CONTENTS	V
LIST OF TABLES	IX
LIST OF FIGURES	X
ABSTRACT	XVII
CHAPTER 1:INTRODUCTION.....	1
1.1 BACKGROUND	2
1.2 THESIS AIM	3
1.3 REFERENCES	5
CHAPTER 2:LITERATURE REVIEW.....	7
2.1 PAINT COMPOSITION.....	8
2.2 SAMPLING CONSIDERATIONS	9
2.3 INSTRUMENTAL TECHNIQUES	10
2.3.1 Vibrational Spectroscopy	11
2.3.1.1 FTIR spectroscopy.....	11
2.3.1.2 Raman Spectroscopy	13
2.3.1.3 Mapping/ Imaging	16
2.3.1.4 Data processing	16
2.3.2 Elemental Analysis	17
2.3.2.1 ed-XRF	17
2.3.2.2 SEM-EDS	18
2.3.3 GC/MS and Py-GC/MS	18
2.3.3.1 Sample Preparation Methods.....	19
2.3.3.2 Data Interpretation	21
2.4 CONCLUSIONS	24
2.5 REFERENCES.....	25
CHAPTER 3:CHARACTERISATION OF PAINT MATERIALS ON CEREMONIAL OBJECTS FROM THE HIGHLANDS OF PAPUA NEW GUINEA.....	47
3.1 BACKGROUND.....	48

3.2	MATERIALS AND METHODS	50
3.2.1	Techniques that eliminate interference for binder identification	50
3.2.1.1	Solvent extraction	51
3.2.1.2	HF pretreatment	52
3.2.2	FTIR microscopy	52
3.2.3	Raman microscopy	52
3.2.4	SEM-EDS	53
3.2.5	XRD	53
3.2.6	GC/MS	53
3.3	RESULTS AND DISCUSSION	54
3.3.1	White Clays	60
3.3.2	Black charred wood	62
3.3.3	Coloured pigments	64
3.3.3.1	Blue vivianite	65
3.3.3.2	Red and yellow ochres	70
3.3.3.3	Synthetic pigments	71
3.3.4	Binders	73
3.3.4.1	Plant-based organic matter	73
3.3.4.2	Lipid	77
3.3.4.3	Wax and wax ester	83
3.3.4.4	Natural resin	85
3.3.4.5	Synthetic resin	87
3.3.5	Metal Soaps	89
3.3.6	Extraneous organic materials	91
3.4	CONCLUSIONS	95
3.5	REFERENCES	97
CHAPTER 4:NON-INVASIVE ANALYSIS OF PIGMENTS AND LIGHTFASTNESS OF “POEM” SERIES PRINTS BY JAPANESE ARTIST HAKU MAKI		104
4.1	BACKGROUND	105
4.2	MATERIALS AND METHODS	106
4.2.1	Reference samples	106
4.2.2	Optical Microscopy	107
4.2.3	FTIR Microspectroscopy	107
4.2.4	Raman Microspectroscopy	107
4.2.5	Microfocus X-ray Spectroscopy (XRF)	107
4.2.6	Microfade Testing (MFT)	108

4.3	RESULTS AND DISCUSSION	108
4.3.1	White Haze.....	108
4.3.2	Pigments Identification	110
4.3.3	Microfade testing	118
4.4	CONCLUSIONS	122
4.5	REFERENCES.....	123
CHAPTER 5: INVESTIGATING CAUSES FOR POLYURETHANE PAINT FAILURE ON MODERN OUTDOOR SCULPTURES “NUMBERS 0-9” BY ARTIST ROBERT INDIANA		
126		
5.1	BACKGROUND.....	127
5.2	MATERIALS AND METHODS.....	131
5.2.1	Paint samples	131
5.2.2	UV-Vis microscopy and stereo-microscopy	132
5.2.3	SEM-EDS	132
5.2.4	Raman microscopy.....	133
5.2.5	FTIR microscopy	133
5.2.6	Py-GC/MS	134
5.2.7	Colorimetric measurements	134
5.3	RESULTS AND DISCUSSION	134
5.3.1	Layer stratigraphy	134
5.3.2	Foundation layers.....	139
5.3.2.1	Inorganic Extenders.....	140
5.3.2.2	Binder	141
5.3.3	Topcoat Binder.....	143
5.3.4	Topcoat Pigments.....	146
5.3.4.1	Characterisation of lead chromate family pigments in magenta, red, orange and yellow topcoats	146
5.3.5	Colour Measurements	150
5.4	CONCLUSIONS	152
5.5	SUPPLEMENTARY DATA	153
5.6	REFERENCES.....	154
CHAPTER 6: ANALYSIS OF “ESTES PARK, COLORADO” PREPARATORY SKETCH BY ARTIST GUSTAVE BAUMANN		
157		
6.1	INTRODUCTION.....	158
6.2	MATERIALS AND METHODS.....	159
6.2.1	FTIR Micro-spectroscopy	159

6.2.2	GC/MS	159
6.3	RESULTS AND DISCUSSION	160
6.3.1	FTIR micro-spectroscopy results	160
6.3.2	GC/MS results.....	162
6.3.3.1	Fatty acid fraction	162
6.3.3.2	Amino acid fraction	163
6.3.3.3	Monosaccharide fraction	164
6.4	CONCLUSIONS	165
6.5	REFERENCES.....	166
CHAPTER 7: CONCLUSIONS		169
7.1	CHOICE OF INSTRUMENTAL TECHNIQUES	171
7.2	DATA INTERPRETATION	172
7.3	OUTCOMES	173
7.4	FUTURE STUDIES.....	174
APPENDIX: VALIDATION OF ANALYTICAL PROCEDURE FOR MULTI-CLASS BINDER CHARACTERISATION IN THE SAME PAINT SAMPLE WITH GC/MS ..		176
A.1	INTRODUCTION.....	176
A.2	MATERIALS AND METHODS	179
A.2.1	Reagents	180
A.2.2	Method	180
A.2.3	Sample.....	181
A.3	RESULTS: METHOD VALIDATION	182
A.3.1	Phase 1- Validation with pure standards and raw materials.....	182
A.3.1.1	Monosaccharide fraction	183
A.3.1.2	Amino acid fraction	188
A.3.1.3	Fatty acid/ Terpenoid fraction	194
A.3.2	Phase 2- Validation with mock-up pigment/binder mixtures.....	196
A.3.2.1	Egg yolk.....	196
A.3.2.2	Egg yolk: Linseed oil (3p: 1p).....	198
A.3.2.3	Gum arabic: egg yolk (2p:1p).....	199
A.3.2.4	Gum arabic: gum tragacanth (1p:1p), zinc white, basium sulphate	200
A.3.2.5	Kaolin: mars yellow (1p:1p), deionised water	201
A.3.3	Phase 3- Validation with Baumann studio materials, comparing against Py-GC/MS and FTIR results.....	202
A.4	CONCLUSIONS	204
A.5	REFERENCES.....	205

LIST OF TABLES

Table 3-1: Photos of sampled areas of painted ceremonial objects collected from PNG Highlands	54
Table 3-2: Coloured pigments identified in the artefacts collected from the PNG Highlands	64
Table 3-3: List of natural vivianite sources in PNG Highlands	67
Table 4-1: Summary of the results from Raman and XRF analyses of pigments on selected Haku Maki prints from the “Poem” series	114
Table 5-1: Summary of pigment results identified in original and restoration paints	147
Table 7-1: Summary of case-study results	170
Table A-1: Binder class in raw materials	183
Table A-2: Percentage (%) monosaccharides composition in gum references	187
Table A-3: Percentage (%) amino acid composition of protein references.....	193
Table A-4: Percentage (%) aldose and uronic acid composition for single binders: gum arabic references and gum tragacanth reference, in comparison with mixed binders: gum arabic/ gum tragacanth and gum arabic/ egg yolk. Values in bold distinguishes a mixed binder from a single binder	201
Table A-5: Results of powder and varnish samples obtained from Baumann’s painting studio	203

LIST OF FIGURES

- Figure 3-1: Materials identified in PNG Highlands ceremonial objects 54
- Figure 3-2: FTIR spectra of white clay samples from (a) #258.1978 shield, (b) #245.1977 ceremonial hat, (c) #290.1979 tree fern head, where K = kaolinite, O = organic matter, Q = quartz, M = montmorillonite..... 61
- Figure 3-3: FTIR spectra of (a) fibre obtained from plant substrate on *Shield* (#490.1979) (b) black undercoat obtained from *Shield* (#265.1977), (c) black particles that filled the woven plant fibre on left arm of *Yupini* (#283.1978), (d) black particle obtained from grey paint on *Shield* (#260.1978) and (e) black particles from the black areas of *Sacred Stone* (#272.1978); L= lignin, C= cellulose, T= tannin, HT= hydrolysable tannin, CT= condensed tannin 63
- Figure 3-4: Raman spectra of blue vivianite sample taken from Timbuwara (#580.1979), (a) 785 nm, low power, no color change, (b) 785 nm, higher power, discoloration to yellow 66
- Figure 3-5: Raman spectra of blue vivianites at 514 nm in the spectral region 2700-3800 cm^{-1} (a) blue vivianite from Timbu wara (#18.2005) (b) blue vivianite from Mortar (#279.1977), the band at 3485 cm^{-1} suggests partial oxidation of Fe^{2+} to Fe^{3+} 67
- Figure 3-6: Distribution of blue pigments detected in the ceremonial objects, collected by Moriarty from various regions of the PNG Highlands between 1961 and 1972. Red dotted circle highlights the isolated occurrence of ceremonial objects containing vivianite..... 69
- Figure 3-7: Optical microscopic image of vivianite sample dispersed in glycerine at 200X magnification, collected from *Timbu wara* (#580.1979). Top left photo courtesy of AGNSW. 70
- Figure 3-8: (a) Distribution map of headquarters, sub-district posts and patrol posts recorded in PNG Highlands in 1966 (b) Distribution of red pigments identified on ceremonial objects obtained from different Highlands localities by Moriarty between 1961 and 1972..... 74

- Figure 3-9: Exemplar FTIR spectra of red ochres containing (a) substantial organic matter (shield #302.1978) and (b) little organic matter (apron adorer #294.1977) 75
- Figure 3-10: FTIR spectra of various colored samples of residue (a) after water extraction and (b) after 10% HF pretreatment, S= plant sap or SOM. 77
- Figure 3-11: Generic illustration of various binder classes of lipid, wax and wax esters containing long chain alkanes, esters and other functional groups. 78
- Figure 3-12: FTIR spectra of (a)(i) unaged pork lard reference (ii) red ochre paint on *Sacred Stone* (#272.1978), (iii) black particles from scrotum of *Yupini* (#283.1978), (iv) red SOP paint on *Judge's Wig* (#553.1979) and (v) Microcrystalline wax reference b) corresponding Raman spectrum of the samples in (a) collected at 785 nm 82
- Figure 3-13: a) FTIR spectrum and b) Raman spectrum collected at 785 nm, of samples containing wax or wax esters..... 84
- Figure 3-14: FTIR spectra of various resins identified 86
- Figure 3-15: Total ion chromatogram of (a) #239.1977 varnish and (b) Tigaso oil reference..... 87
- Figure 3-16: FTIR spectra of black particles obtained from black undercoat of *Shield* (#265.1977) (a) orange residue from CHCl₃/MeOH (2:1 v/v) extract (b) raw black particles, without solvent extraction, A = acrylate, T = tannin 89
- Figure 3-17: EDS mapping of red synthetic paint containing zinc carboxylate soap from *Effigy* (#818.1979) 90
- Figure 3-18: FTIR spectra of a) #533.1979 bark belt- white sample at the periphery of the red synthetic paint shows an abundance of zinc oleate (ZO) and zinc palmitate or zinc stearate (ZP/ ZS) b) #666.1979 mortar-grey sample shows an abundance of calcium palmitate (CP) and potassium stearate (PS)..... 91

- Figure 3-19: SEM image at around 2000 X magnification c) FTIR spectrum and d) Raman spectrum collected at 785 nm, of the “white paint” on *shield* (#302.1978) in comparison with a bird excrement reference 92
- Figure 3-20: Photo of white efflorescence (indicated by black arrows) on *Shield* (#490.1979). FTIR spectrum of multiple spots on the white efflorescence sample shows a) C-chalk, b) possible gum-like binder or unresolved features of fungi, c) fungi features; d) SEM image of white efflorescence details fungal morphology residing at the surface of a substrate 94
- Figure 4-1: Prints by Haku Maki. (a) *Poem 71-29*, 1970, IMA#2013.419, 10.5”x7.25”, (b) *Poem 70-90*, 1970 IMA#2013.418, 6.5”x4.75”, (c) *Poem 70-70*, 1970, IMA#2013.417, 6.5”x4.5”, and (d) *Poem 71-61*, 1971, IMA#2013.420, 17.24”x10.5”. Gifts of Donald A. and Loryne M. Coffin. White efflorescence is visible in the black fields of (a). Photos courtesy of IMA..... 105
- Figure 4-2: Photomicrographs of the white efflorescence on *Poem 71-29*: (a) thin and soft web-like layer, (b) thicker clump of white filaments, and (c) transmission optical image of the fungal hyphae 109
- Figure 4-3: FTIR spectrum of (a) the white filaments shown in Fig. 4.2b and (b) a paper fiber taken from the print *Poem71-29*..... 110
- Figure 4-4: FTIR spectral comparison of (a) the black paint in *Poem 71-29* and (b) an aniline black reference pigment whose structure is shown in the inset ($n \approx 3$, $X^- = \text{HCrO}_4^-$, Cl^-) 111
- Figure 4-5: Raman spectrum collected at 532 nm, of the black background in (a) *Poem 70-70* compared to (b) a reference sample of aniline black watercolour. A similar match is obtained when (c) aniline black is diluted in a 4:1 ratio with lamp black in watercolour medium 113
- Figure 4-6: Raman spectra of (a) the orange paint in *Poem 71-29* at 785 nm, (b) chrome yellow (PY34) at 633 nm, (c) chrome orange (PO21) at 633 nm, (d) the red artist’s seal in *Poem 70-90* at 633 nm and (e) molybdate orange (PR104) at 633 nm..... 116

- Figure 4-7: Detail of the XRF elemental spectra of *Poem 71-29* (a) orange paint, (b) black paint, and (c) yellow paint.....118
- Figure 4-8: ΔE fading curves for the coloured areas of *Poem 71-29*. The colours being analysed are as indicated in the data traces, and the blue lines indicate average fading (with error bars) for the triplicate analyses of BWS 2 (upper) and BWS 3 (lower).....119
- Figure 4-9: ΔE fading curves for pure BASF aniline black (black squares) and in equal admixture with carbon black (black triangles) prepared as watercolour paints. These curves are compared to BWS 2 and 3120
- Figure 5-1: Image of “*Numbers 0-9*”, Robert Indiana, 1988.241-250, automotive paint on aluminum, Top: Before restoration in 2011, first displayed at IMA in 1992; Bottom: 4 years after restoration in 2011. Photos Courtesy of IMA.....127
- Figure 5-2: Close-up photos of some damages seen in “*Numbers 0-9*”, Robert Indiana, 1988.241-250, taken 4 years after restoration (a) paint delamination over a significant area revealing the aluminum surface in *Number 8* (b) paint delamination in *Number 2* reveals original paint that has not been properly removed. (c) paint loss along edge in *Number 7* reveals primer layer and signs of repainting.....130
- Figure 5-3: Example of the original paint system fabricated by Lippincott from *Number 2*. using terms based on original equipment manufacture (OEM).....136
- Figure 5-4: Front/back facings and side colours of *Number 7* original vs *Number 2* restored.....137
- Figure 5-5: Some examples of restored paint cross-sections demonstrating inconsistency in layer stratigraphy138
- Figure 5-6: Left: Front/ back paint cross-section of original *Number 5* with vis-microscopy. Right: SEM image shows that the first blue layer was formed by two coats, as seen by a distinct line in the middle139

- Figure 5-7: SEM image of *Number 0* paint cross-section taken from front/ back area, where aluminum (Al) and oxygen (O) represents aluminum oxides below the faring layer139
- Figure 5-8: White surfacer (layer 2) in cross-section of *Number 3* fluoresces yellow and is analogous to the distribution of Zn (zinc) in the EDS Hypermap image. Similar distribution of Zn is observed in white primer/surfacers in original *Numbers 0, 3, 4, 6, 7, 8 and 9* and Restored *Numbers 3, 5, 8 and 9*140
- Figure 5-9: Column 1- FTIR spectra of primer/surfacers in original (a-c) and restored (d-g) paints, where T - talc, K - kaolinite, M -magnesite, A - acrylate, NC - nitrocellulose, E -epoxy, U - urethane; Column 2- corresponding Py-GC/MS pyrolyzates; Column 3- the Numbers that contain the exemplar primer/surfacers142
- Figure 5-10: Images of cross-section in Original *Number 0* Grey reveal paint failure. Left: Optical microscopic image; Right: SEM image.....143
- Figure 5-11: Pyrogram of restored paint (*Number 6* red) vs original paint (*Number 2* green)144
- Figure 5-12: FTIR spectrum (a) at surface of topcoat original paint and (b) deeper within the topcoat original paint (c) restored paint after 3 years curing145
- Figure 5-13: Raman spectra (collected at 785 nm) and FTIR spectra of magenta, red, orange and yellow original topcoats. Selective spectral regions enable discrimination of molybdate orange (PR104) and chrome yellow (PY34), and allow relative pigment proportions in the paint mixture to be determined. 825, 340, 358 cm^{-1} are characteristic peaks for PR104, whereas 838 cm^{-1} and a fountain series of peaks centering at 340 cm^{-1} are characteristic of PY34.....151
- Figure 5-14: FTIR spectra of (a) Pigment reference PR122; (b) #48 red paint from uncured tin for *Number 6*, after extraction of binder with acetone; (c) the same paint as (b) without acetone extraction, where A : acrylate152

Figure 6-1:	Coloured pigments and varnishes in Baumann's studio.....	158
Figure 6-2:	Left: <i>Estes Park, Colorado</i> , 1926, Gustav Baumann, IMA# 2008.54, tempera over graphite on brown paper. Loose paint flakes available for analysis were purple, beige and white (Original location of paint is unknown). Purple sample: Sky area, Beige sample: Cloud area, White sample: White margin that borders the painting. Gift of Ann Baumann. Photo Courtesy of IMA. Right: A photomicrograph showing severe delamination of the paint.....	159
Figure 6-3:	FTIR spectrum of purple, beige and white samples indicate the presence of metal carboxylates.....	161
Figure 6-4:	Fatty acid profile of Blank (top) and Beige sample (Bottom), phthalic acid is attributed to contamination from vial cap	163
Figure 6-5:	Amino acid profile of blank (top), beige sample (middle) and egg yolk reference (bottom).....	164
Figure 6-6:	Monosaccharide profile of beige sample (top) and blank (bottom). Ions are extracted at $m/z = 249, 319, 408$	165
Figure A-1:	Summary of GC/MS combined analytical procedure	179
Figure A-2:	Schematic pathway of mercaptalation and derivatisation of carbohydrates.....	184
Figure A-3:	TIC of IS (mannitol), aldoses and uronic acids in a monosaccharide standard solution, whereby one peak represents one monosaccharide. Peak at $R_t = 27.85$ min also occurs in blanks.....	186
Figure A-4:	TIC of gum arabic (top), gum tragacanth (middle) and cherry gum (bottom).....	186
Figure A-5:	TIC of gum arabic (top trace) compared to the same sample with an extracted ion profile at 248, 304, 319 and 407 (bottom trace)	187
Figure A-6:	TIC of blank (top) and amino acid pure standard (bottom). Chemical structures of marker compounds indicate the extent of derivatisation	190

Figure A-7: Comparison of amino acid fractions: TIC of bone glue, hide glue and casein.....	192
Figure A-8: (a) TIC of HCl, (b) TIC of bone glue with conventional heating in 6M pure HCl, (c) TIC of an aliquot of the same bone glue hydrolysate in (b) after 5 cycles of rinsing with deionised water, EtOH and evaporation dry with N ₂ stream.....	194
Figure A-9: Fatty acid profile of pure standard	195
Figure A-10: TIC of linseed oil/ manila copal fatty acid/terpenoid fraction.....	196
Figure A-11: TIC of amino acid fractions from an unpigmented, unaged, dried egg yolk sample (top) 500 µg and (bottom) 460 µg, subjected to the same analytical procedure	198
Figure A-12: Fatty acid profile of (a) egg yolk:linseed oil (3p:1p), (b) egg yolk only and (c) linseed oil only. Samples are unpigmented and unaged. Retention times vary due to concentration difference	199
Figure A-13: Extracted ion profile (m/z= 249, 305, 319, 408) of gum fraction in gum arabic/egg yolk mix (top) and egg yolk reference (bottom).....	200
Figure A-14: Fatty acid profile of Baumann studio “printing varnishes”: A-S2-33 (top), D-S3-18 (middle) and H-S3-13 (bottom)	204

Abstract

Artist paint is one of the most heterogeneous materials encountered in museum conservation. While many scientific studies have been carried out on European easel paintings, less work has focused on other painted artworks, as well as works from other geographic regions. This thesis compiles results from four technical analysis projects on different types of non-easel painted artworks at the Indianapolis Museum of Art (IMA) and the Art Gallery of New South Wales (AGNSW), applying micro-analytical techniques, including FTIR microscopy, Raman microscopy, SEM-EDS, micro-XRF, XRD, Py-GC/MS, GC/MS and MFT. The painted artworks include 20th century ethnographic collections from the Highlands of Papua New Guinea, inked prints from the “Poem series” by Japanese artist Haku Maki, Robert Indiana’s painted aluminum outdoor sculptures, and Gustave Baumann’s home-made paint on paper. These works have not been previously investigated scientifically, and each presents specific museum curatorial and conservation concerns such as technical art history, lightfastness, paint degradation and treatment considerations. A range of natural and synthetic pigments, paint binders and deterioration products were characterized, contributing to the technical art history and understanding of paint degradation that informs conservation practices.

Chapter 1

Introduction

1.1 Background

In the process of documenting and conserving artworks, museum professionals such as conservators, collection managers and curators may have a number of questions about the artwork, which materially stems from an unknown question: “What did the artist use at that time?” This question is often presented to the 20th century conservator and conservation scientist, who then employs different techniques coupled with knowledge of art materials to investigate the issue. Through a scientific inquiry process, material-related questions can be addressed with more certainty and results can be beneficial for interventive and preventive aspects of paintings conservation, technical art history and issues surrounding authenticity (P.N.A Sciences 2005).

The beginnings of scientific studies on artwork began around the late 18th century, but it was not until the 20th century when results begun to meet the standard of reliability (Townsend & Boon 2012). Presently in the 21st century, instrumental techniques have evolved into a wide range that suit the challenges of characterising painted artworks. Broadly categorised into handheld or portable, mid-range bench-top instruments and high end instruments, the mid-range forms the mainstay techniques that are most widely practised in paint characterisation. To present, mid-range techniques capable of micro-structural characterisation, namely microscopy, spectroscopy and gas chromatography-mass spectrometry with pyrolyser, have been frequently applied. As a result, a non-exhaustive list of databases, flowcharts and spectral signatures relating these techniques to known artist paint materials have developed (Burgio & Clark 2001; Derrick, Stulik & Landry 1999; Scherrer et al. 2009).

Regarding materials encountered in the museum, paint itself is a heterogeneous substrate that makes it one of the more complex materials to analyse. Depending on the ingredients present in the paint, how the paint is applied and the environment that the paint is exposed to, many chemical reactions can happen at a micro-level that explains for its appearance and associated degradation. With respect to the museum field, paint characterisation by the afore-mentioned mainstay instrumentation techniques have been well studied on easel paintings, especially oil paintings originating from Western Europe.

Characterisation studies have accumulated numerous pigment, binder and varnish data constituting artists' oil painting recipes from different genres and Western art periods (Mayer 1950; Wallert, Hermens & Peek 1995). Reference paint mock-ups have been prepared via natural or artificial ageing, in either pure or mixed ingredients, to investigate the deteriorating mechanisms. However, studies relating to paintings from other geographical regions are less common. Paints that do not come from artist's tubes, such as printing inks and industrial paints, are potentially found on artworks, yet these had not been commonly analysed. Paints prepared by home-made recipes, either sourced from the natural environment or commercial sources, are un-conventional and may contain materials previously unknown to the conservation field.

1.2 Thesis Aim

This thesis examines how instrumentation techniques can be applied to the scientific study of painted artworks in museum context. To get a brief understanding of past research carried out in this area, [Chapter 2](#) provides a literature review of micro-characterisation instrumentation techniques applied to paint materials in the museum conservation field, highlighting the type of paint constituents found on artworks, issues encountered in instrumental techniques and ways to overcome these difficulties.

The thesis then reports primary data obtained from case-study projects ([Chapters 3-6](#)) formulated in collaboration with the Indianapolis Museum of Art (IMA) and the Art Gallery of New South Wales (AGNSW). Each case-study aims to address specific conservation and curatorial questions or problems associated with unknown painted materials on non-easel painted artworks (ethnographical paints, printing inks, industrial paint and home-made recipes).

Firstly, [Chapter 3](#) features a scientific investigation of pigments and binders in painted ceremonial objects collected from the Highlands of Papua New Guinea in the 1960s, an area of research that has not been previously explored. Colours symbolise different important meanings to the Highlanders and by identifying the pigments used for each colour, it can contribute to the knowledge gap in technical art history. The possible presence of natural vivianite, a rare blue pigment, seen in several objects first drew

interest to its scientific analysis. In addition, a number of bright colours indicative of modern pigments were also seen on the objects, generating an interest in tracing the source of pigment in the Highlands. Highlanders favour paints with a high pigment to binder ratio for better opacity, which makes it even more difficult to detect the organic binder analytically. As such, sample or technique modifications were applied, revealing a wide range of organic materials used.

Turning from investigating hand-made paints to ready-made paints, Chapter 4 describes the characterisation of pigments used in printing inks, found on the 'Poem series' prints, created in the 1970s by Haku Maki, a Japanese printmaker well-known for his unusual style of embossed printmaking technique that appears to pop out with an illusion 3-D effect. One of the paintings received particular attention because of an unknown white efflorescence enveloping thinly on the black background. The conservator was also concerned with lightfastness issues, as the pigments appeared too bright for a printing ink and was deemed unusual for a print. Taking a micro-sample in this case is not preferred, particularly because the fine print is in good condition and the paint layer is thin. Hence, methods applied onto these prints are mainly non-invasive (i.e. Raman and XRF spectroscopy). The results aim to characterise the white efflorescence that is aesthetically disturbing, the pigment composition forming Maki's palette and the lightfastness of the colours.

While indoor paints have been commonly analysed in museum artworks, outdoor painted sculptures receive less attention. Chapter 5 presents the scientific investigation of material composition in "Numbers 0-9", the first set of sculptures by Robert Indiana. Originally fabricated in the 1980s, the sculptures comprise of industrial polyurethane paint on welded aluminium. Signs of recurring paint failure in spite of conservation attempts motivated for an in-depth scientific study. Scientific characterisation of the paint layer stratigraphy serves to uncover the inherent causes for loss of gloss and paint adhesion.

Chapter 6 studies the home-made recipe of one of Gustave Baumann's preparatory sketches. Baumann is known to make his own paints, yet the ingredients in his studio lack evidences of a binder, hence there has been an ongoing interest to determine the binder

he used. The preparatory sketch of painted paper in this study shows one of the worst damages amongst Baumann's collections, and it has been a conservation interest to determine the causes for the extensive paint delamination. In this case study, the determination of organic binder by spectroscopy means was found to be insufficient and another technique was sought to complement the data interpretation. The technique developed by the research group in University of Pisa, is able to simultaneously identify more than one binder class in the same paint micro-sample using GC/MS (Lluveras et al. 2010), making it a promising technique for this application. This technique was validated in [Appendix A](#) and applied to the analysis of the organic binder in Baumann's paint sample.

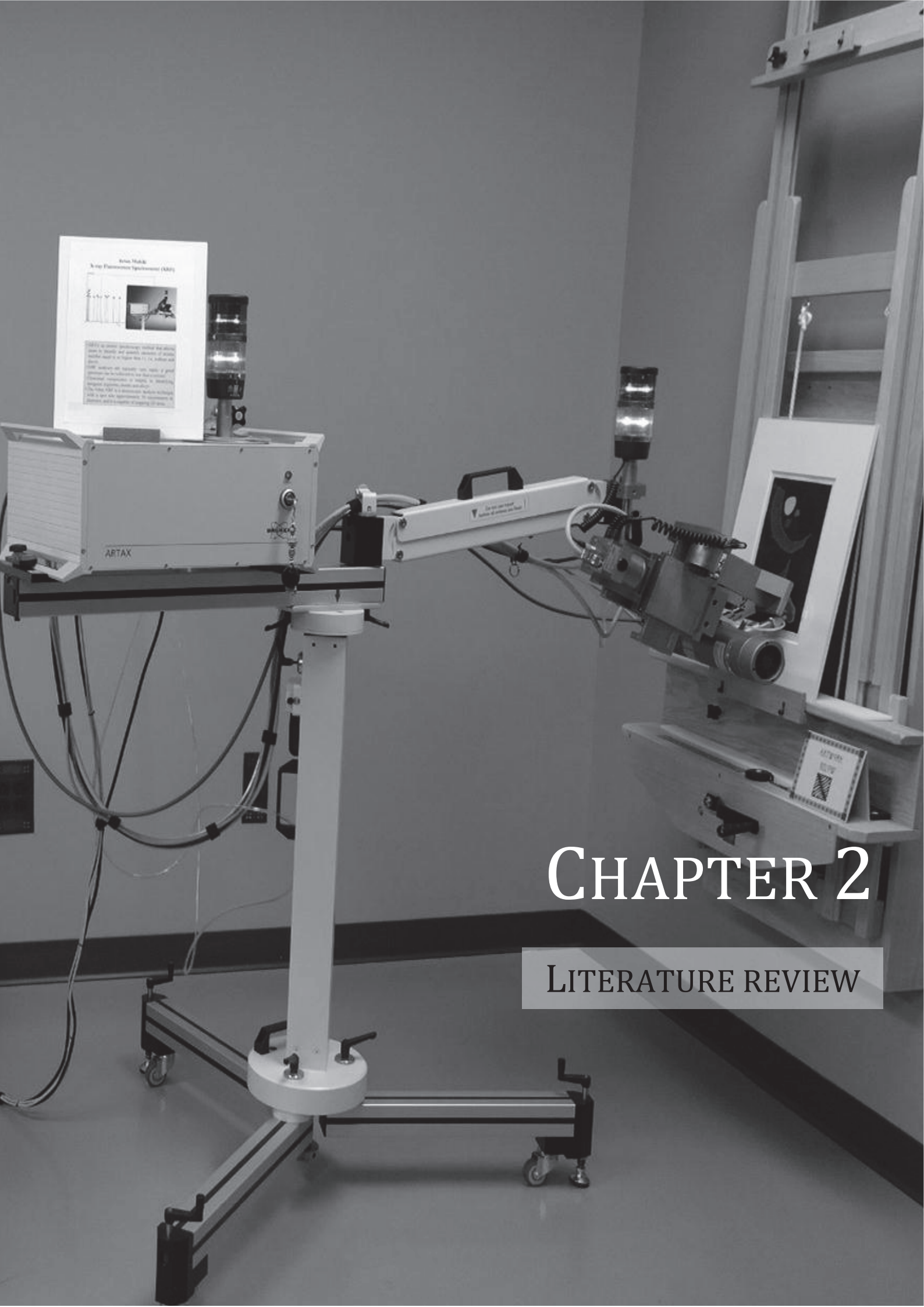
Lastly, [Chapter 7](#) concludes the results of the case-studies, focusing on the selection of instrumental methods and data interpretation. The results and discussion also generates potential topics for future research.

1.3 References

- Burgio, L. & Clark, R.J.H. 2001, 'Library of FT-Raman spectra of pigments, minerals, pigment media and varnishes, and supplement to existing library of Raman spectra of pigments with visible excitation', *Spectrochimica Acta Part A: Molecular and Biomolecular Spectroscopy*, vol. 57, no. 7, pp. 1491-521.
- Derrick, M.R., Stulik, D. & Landry, J.M. 1999, *Infrared Spectroscopy in Conservation Science*, The Getty Conservation Institute, USA.
- Lluveras, A., Bonaduce, I., Andreotti, A. & Colombini, M.P. 2010, 'GC/MS Analytical Procedure for the Characterization of Glycerolipids, Natural Waxes, Terpenoid Resins, Proteinaceous and Polysaccharide Materials in the Same Paint Microsample Avoiding Interferences from Inorganic Media', *Analytical Chemistry*, vol. 82, no. 1, pp. 376-86.
- Mayer, R. 1950, *The artist's handbook of materials and techniques*, The Viking Press, New York.
- P.N.A Sciences 2005, (*Sackler NAS Colloquium*) *Scientific Examination of Art: Modern Techniques in Conservation and Analysis*, National Academies Press.
- Scherrer, N.C., Stefan, Z., Françoise, D., Annette, F. & Renate, K. 2009, 'Synthetic organic pigments of the 20th and 21st century relevant to artist's paints: Raman spectra reference collection', *Spectrochimica Acta Part A: Molecular and Biomolecular Spectroscopy*, vol. 73, no. 3, pp. 505-24.

Townsend, J. & Boon, J. 2012, 'Research and Instrumental Analysis in the Materials of Easel Paintings', in R. Rushfield & J.H. Stoner (eds), *The Conservation of Easel Paintings*, Routledge: London and New York, pp. 341-65.

Wallert, A., Hermens, E. & Peek, M. 1995, 'Historical painting techniques, materials, and studio practice : preprints of a symposium', Getty Conservation Institute, University of Leiden, the Netherlands.



Series Mobile
X-ray Fluoroscopic System (XRF)

ARTAX is a mobile fluoroscopic system that allows you to perform and observe procedures of patients under mobile X-ray (C-arm, mobile and fixed).

ARTAX features the highest quality, mobile of good performance for fluoroscopy for diagnostic, interventional, orthopedic, urology, or dentistry. The mobile ARTAX is a portable mobile system which is used for emergency, the maintenance of equipment, and the location of imaging of the site.

ARTAX

CHAPTER 2

LITERATURE REVIEW

2.1 PAINT COMPOSITION

Paint consists of finely divided pigment particles evenly dispersed in a liquid medium or vehicle; it has the property of drying to form a continuous, adherent film when applied to a surface for decorative or protective purpose (Mayer & Sheehan 1991; Steele, Stern & Stott 2010). In the context of ancient art and archaeology, paint has been encountered from the earliest beginnings on wall paintings in caves, shelters and rock surfaces. Pigments and associated inorganic salts such as carbon black, red and yellow ochres, brown plattnerite, white whewellite, weddellite and chalk were reported (Edwards & Chalmers 2005). The binding media used varies and arises from the natural environment, including beeswax (Gomes et al. 2013), egg, blood, fat, saliva (Prinsloo et al. 2013), plant saps and animal glue (Scott et al. 2009; Wong & Agnew 2013). The different techniques of applying paint have evolved a variety of paintings spanning across time periods, cultures and continents. Paintings range from Eastern scrolls (pigments, water-soluble gum or proteinaceous binder), Western murals and easels (pigments, oils, wax) to other forms of painted art, such as woodblock prints (inks containing linseed oil, natural resin or driers applied with pressure onto a paper) and contemporary sculptures (mostly synthetic resins and pigments). Comprehensive works outlining the historical paint materials and recipes are best described by Rutherford and Stout (Rutherford & Stout 1966) and Mayer and Sheehan (Mayer & Sheehan 1991). The chemistry of organic binders (Mills & White 1994), historical pigments (Eastaugh 2013) and modern pigments (Buxbaum & Pfaff 2005; Herbst & Hunger 2002) were also well studied.

Traditionally, pigments were made by careful selection of minerals, followed by sieving and grinding into fine powder, which was later dispersed in different binding media by hand-grinding to form paint of a desired consistency. The traditional recipe frequently employs linseed oil, poppy oil, walnut oil, gum arabic, casein, egg, natural terpenoid resins (dammar, copal, mastic etc.) and various inorganic pigments and fillers (e.g. chalk, gypsum). The combinations of different pigments, binders and substrate can alter the properties of paint, such as accelerated drying of oil paints containing Pb, Mn and Cu pigments (Tumosa & Mecklenburg 2005), pigment discoloration (Daniels, Stacey & Middleton 2004; Goltz et al. 2003; White 2007) and formation of metal lead soaps (Cotte et al. 2006; Plater et al. 2003; Robinet &

Corbeil 2003). These also change with respect to relative humidity, temperature and light (Bayne & Butler 2013; Gervais et al. 2013; Saunders & Kirby 2004; Tan et al. 2013).

Since the first paint tube was invented in 1841, the production of ready-mix paints increased with popular demand. From 1965 onwards, numerous companies were marketing them under different brand names (Learner 2000). This trend is parallel to the discovery of synthetic polymers and resins in the early 20th century. The modern day recipe contains a wider variety in paint composition, of which synthetic organic pigments, additives, driers, drying oils, non-drying oils, and synthetic resin were often encountered (Learner 2004). In modern oil paints, non-drying oil is added to drying oils to impart slower drying and reduce cost (Izzo 2010). Synthetic binders such as polyvinylacetate (PVA) (resin: 1914, emulsion: 1940s), nitrocellulose (mid-1920s), phenol-formaldehyde (late 1920s), alkyds (late 1930s), polyurethane (ca. 1937), acrylic solutions (late 1940s), acrylic emulsion (late 1950s) and water mixable oils (1990s) have been introduced and employed on artworks (Learner 2000; Standeven 2011). New lines of pigments, namely synthetic organic pigments with high tinting strength and lightfastness (Lomax & Learner 2006) and DayGlo pigments (fluorescent dyes and polymeric materials that emits intense light even in daylight) were increasingly found in modern day paints and inks (Fremout & Saverwyns 2014). Characterisation of modern paints reveals new conservation problems such as plasticiser migration, dirt pickup, water sensitivity, soap formation, lightfastness of synthetic organic pigments (Burnstock & van den Berg 2014; Ghelardi, Degano, Colombini, Mazurek, Schilling, Khanjian, et al. 2015; Learner 2007; Ormsby & Learner 2009) or to some effect, an improper choice of primer (Llamas & Talamantes 2014; Maor & Murray 2007).

2.2 SAMPLING CONSIDERATIONS

Sampling is considered destructive to the artwork and should be avoided where possible. Nevertheless, micro-sampling of artworks is still frequently practised as the pros of sampling in giving a more detailed and confident material information outweigh its cons, especially when the paint matrix is heterogeneous and multilayered. In certain museum institutions, permission should be sought to justify the purpose of sampling an artwork. As a general guide, the amount sampled and method of sampling depends on the choice of instrumentation technique. Sample

amounts required for spectroscopy are usually much lower than chromatography. It is generally considered acceptable as long as the physical damage is not visible to the unaided eye, which also depends on other factors such as the type of artwork, surface topography, colour, position of sampling etc.

2.3 INSTRUMENTAL TECHNIQUES

The technical analysis of artefacts often employs non-invasive or micro-destructive techniques. Non-invasive techniques are considerably beneficial when extracting a micro-sample from an artwork is neither permitted nor feasible. In particular, non-invasive imaging techniques have been developed to analyse artworks. From early use of X-ray, UV and infrared, imaging of artwork has expanded to use of NIR confocal laser scanning microscopy (Daffara, Fontana & Pezzati 2009) and optical coherence topography (Targowski & Iwanicka 2012) that offers optical sectioning of painted layers, reflectance transformation imaging that reveals surface texture (Tamayo, Andres & Pons 2013), high resolution digital microscopy that produces focused images of greater depth of field and 3D profile of the paint surfaces (Boon 2014). Aside from imaging, characterisation using portable handheld XRF is by far the most popular of such non-invasive techniques (Shugar & Mass 2012). Portable XRF coupled with XRD was used to obtain simultaneous elemental and phase information from paintings (Eveno, Moignard & Castaing 2011). Fibre optics reflectance spectroscopy has been used to distinguish pigments based on the spectral distribution (Cheilakou, Troullinos & Kouï 2014; Poldi & Caglio 2013).

Performances of portable and handheld instruments have not superseded the quality of data (signal to noise ratio (SNR) and spectral resolution) achievable with benchtop instrumentation, due to miniaturisation of optical and electronic components and instrumental constraints to variation (Vandenabeele et al. 2007). Benchtop instrumentation have been modified to suit non-invasive analysis; a Raman benchtop instrumentation can be fitted on a moveable gantry to analyse moderately sized works in-situ (e.g. manuscripts, books and paper-based work) (Ernst 2010). A combination of micro-Raman and micro-XRF spectroscopy with sample spot size collimated to microns ($< 100 \mu\text{m}$) have been shown to produce reliable results in a number of pigment characterisation studies (Aibéo et al. 2008; Castro et al. 2008; Fremout et al. 2006). Over the past decade, portable and handheld instruments with imaging and characterising

capabilities have shown improved performances, narrowing their gap with benchtop instrumentation (Brunetti et al. 2016). However, it should be highlighted that non-invasive techniques are still more suited to routine-based analysis of homogeneous samples, whereas detailed chemical information of unknown heterogeneous or layered paint samples still requires micro-sampling and complementary benchtop micro-analysis (Aceto et al. 2012; Mazzeo, Roda & Prati 2011).

To present, a number of analytical techniques have been maturely developed in conservation science labs and affiliated research institutions (Madariaga 2015; Stuart 2007; Townsend & Boon 2012). These mainstay techniques include microscopy, vibrational, X-ray spectroscopy and chromatographic analysis with mass spectrometry, which shall be further elaborated in the following sections.

2.3.1 VIBRATIONAL SPECTROSCOPY

2.3.1.1 FTIR SPECTROSCOPY

With Fourier transform Infrared (FTIR) spectroscopy, the class of compounds such as inorganic/organic pigments, dyes, inorganic salts, substrates, and binders may be determined (Derrick, Stulik & Landry 1999) and the study of paint ageing and changes of chemical composition are also possible (Duce et al. 2014). One of the most comprehensive review focuses the widespread applications of FTIR spectroscopy to various polychrome works of art (Casadio & Toniolo 2001), due in part to the ease of performing a direct measurement and in part to the versatility of different analyses modes. The interpretation of spectral data is highly dependable on an in-house database or referencing literature and online databases, complemented with functional group analysis. IRUG (Infrared and Raman Users Group) forms the most common platform for shared database on art materials (Price & Pretzel 2007).

Amongst all modes of analyses, transmission mode has shown the most success with paint and associated art materials and the quality of the spectra allows the development of reference libraries. Solid powders compressed between diamond cells form a suitably thin layer for transmission FTIR microscopy. Due to the diffraction limit at 20 μm , the sample size required needs only be about 50-100 μm to achieve a reasonable SNR and account for sample loss. The second most frequently used mode of analysis with regards to paint samples is attenuated total

reflectance (ATR), where sufficient contact of the ATR tip with sample is necessary. ATR-FTIR spectra provides information about surfaces, as the IR radiation penetrated only the upper few microns of the paint, facilitating surface deterioration studies. ATR produces a spectrum resembling transmission spectra, hence is suited for comparison to most existing reference libraries. However, it should be noted that ATR spectra may show slight peak shifts to lower wavenumbers and higher relative intensities at lower wavenumbers when compared to transmission spectra libraries (Smith 2011). If a micro Ge-ATR is used, the effective spatial resolution is reduced from 20 μm (diffraction limit) further to 5 μm , suitable for analysis of thin paint cross-sections (Joseph et al. 2010; Kaszowska et al. 2013; Rizzo 2008). Another mode of analysis that is less frequently mentioned is the use of IR photoacoustic spectroscopy (PAS). PAS-FTIR spectroscopy has been applied to inorganic pigments analysis (Von Aderkas et al. 2010), and has been shown to prevail over transmission FTIR when analyzing fungal growth on alkyd paints (Cappitelli et al. 2005). While reflection (specular or diffuse) is ideal in preserving the paint sample integrity, it is not often the choice of analysis due to its tendency to spectrum distortion, poor SNR, the requirement for polished or flat surfaces and incompatibility with existing IR databases (Sessa, Bagán & García 2013; Vetter & Schreiner 2011). Although specular reflection has been applied successfully to the characterisation of historical paint cross-sections employing mathematical Kramers-Kronig transformation (Van der Weerd et al. 2002), the same research group reported in a subsequent study that the overall spectral quality from specular reflectance was poor (Van der Weerd, Heeren & Boon 2004). Fixing a long optical fibre probe from the benchtop FTIR spectrometer further decreases the sensitivity. As such, its use is not favourable with irregular painted surfaces encountered in most art samples. Additionally, 'transflection' or 'absorption/reflection' mode can be employed, which is a reflection mode that requires a thin sample placed on an infrared reflective glass slide. This technique is more commonly used for liquid paint smears and has been used to identify the surfactant in water extracts of aged acrylic dispersion gel media (Learner 2007). The double transmission in a 'tranflection' mode allows higher signal to be obtained from a thin sample, however, spectra obtained via this mode can possibly undergo spectral distortions (Bassan et al. 2009).

As paint layers contain a multitude of organic and inorganic materials, nearly the whole IR spectrum can be exploited. Mid-IR is most frequently used to provide information on the binder, synthetic organic pigments and extenders or fillers. While the far IR ($600\text{-}50\text{ cm}^{-1}$) has been

employed in differentiating inorganic pigments and ochres (Kendix et al. 2009; Vahur, Ulla & Leito 2009), it is not available with a FTIR microscope, which implies the need for relatively larger sample amount (in the order of milligrams) for analysis in a spectrometer equipped with far IR detector. Near-IR microscopy (NIR) is comparatively underutilised in cultural heritage investigations, but a few studies have shown that the combination and overtone bands in NIR complement mid-IR, allowing binders of similar compositions to be interpreted (Sciutto et al. 2014; Tommaso et al. 2012).

The main problem of FTIR spectroscopy lies in the overlapping IR bands contributed by a mixture of compounds. Secondly, FTIR spectroscopy detects the bulk of the material, which means trace or minor components may not be identifiable in a mixed matrix. The spectrum is usually sensitive to inorganic materials (i.e. clay, fillers, salts), which give distinct strong bands that obscure other bands due to binder or pigments. Some ways to minimise or eliminate interfering IR bands include solvent extractions (Doménech-Carbó et al. 2001; Sarmiento et al. 2011) and treatment of sample with HF (Smith, Newton & Altherr 2015). Deconvolution of spectra helps to an extent in defining peak maxima of shoulders or broad bands, in which case was shown to be able to identify < 1 % of resin in mixed furniture finishes (Derrick 1989).

2.3.1.2 RAMAN SPECTROSCOPY

Raman spectroscopy, when coupled to a microscope, only requires a sample size of less than a micron, allowing Raman signals to be obtained from tiny particles and layers in paint cross-sections. The application of Raman spectroscopy to heritage materials and artworks had been extensively reviewed (Bersani & Lottici 2016; Centeno 2015; Edwards & Chalmers 2005; Smith & Clark 2004; Vandenabeele, Edwards & Moens 2007; Yu & Butler 2015). A number of studies have generated databases for the interpretation of artist pigments and minerals (Bell, Clark & Gibbs 1997; Burgio & Clark 2001; Burrafato et al. 2004; Castro et al. 2005), synthetic organic pigments (Colombini & Kaifas 2010; Fremout & Saverwyns 2012; Scherrer et al. 2009; Vandenabeele, Moens, et al. 2000), natural binders (Daher et al. 2010; Vandenabeele, Wehling, et al. 2000) and synthetic binders (Anghelone, Jembrih-Simbürger & Schreiner 2014).

The ease of degradation of pigments under laser illumination, especially those that are darkly colored, means that pigments require an initial low power (< 1 mW) for a Raman experiment. Pigments respond differently to different lasers and the general rule is to use a laser close to

the color of the pigment (Analytical Methods Committee 2015). This rule may not apply when pigments are mixed with other substances, and the sensitivity of the pigment of interest may prove better at other wavelengths. Furthermore, the rule does not take into account of resonance raman, a phenomenon whereby the excitation wavelength coincides with the electronic transition of the molecule, enhances the Raman scattering intensities and leads to selective enhancement of certain vibrational modes. At different laser wavelengths of excitation, some pigments such as PG7 (phthalocyanine green) can generate a different fingerprint spectrum, possibly due to resonance raman in effect. Resonance Raman has been used to enhance the scattering intensities in the study of synthetic ultramarine (Clark, Dines & Kurmoo 1983). Heterogeneity in the sample matrix can also present difficulty in data acquisition. For example, the Raman spectrum can be obtained successfully when analysed on raw pigments, but when mixed with other pigments or fillers (e.g. clay), some spectral bands are suppressed, while others are enhanced. This is because the relationship of pigment proportion and scattering intensity is non-linear (Breitman, Ruiz-Moreno & Gil 2007). Raman signals can be entirely swamped by fluorescence, the most common limitation faced in Raman spectroscopy. Pigments with poor Raman scattering property mixed with oil binding media suffered from fluorescence effects even after long acquisition scans (Burrafato et al. 2004). While solvents may separate unpolymerised binders from a pigment, separating different pigments or polymerised binder by solvent solubility is not feasible.

A number of ways have been proposed for reducing problems with fluorescence in Raman spectroscopy. The use of lasers at longer wavelengths (i.e. 785 nm or FT-Raman (1064 nm)) generates less or no photoluminescence and have been well-applied to a range of pigments and binders (Burgio & Clark 2001; Ellis, Claybourn & Richards 1990). Pulse UV irradiation (non-thermal photoablation) (López-Gil, Ruiz-Moreno & Miralles 2006) and photobleaching of samples may also be able to reduce the photoluminescent background. Mathematical processing techniques such as shift excitation Raman difference spectroscopy (SERDS), which involves the use of two closely spaced excitation wavelengths (tunable laser), and shift subtracted Raman spectroscopy (SSRS), which consists of taking the difference between two closely spaced spectral shifts (different grating positions), have been reported as ways to remove fluorescence background and enhance the SNR of the peaks (Bell, Bourguignon & Dennis 1998; Osticioli, Zoppi & Castellucci 2006; Rosi et al. 2010). The success of such spectral

processing methods, however, is limited to improving SNR of weak Raman signals above a photoluminescent background and is not effective where the background photoluminescence occurs in orders greater than the Raman signals (Tuschel 2016).

More notably, the surface-enhanced Raman spectroscopy (SERS) technique has shown much success for its potential to enhance quantum yield, permitting analysis of highly fluorescent dyes and lakes at low concentrations not otherwise feasible with conventional Raman direct analysis. The most recent review of SERS applied to characterising organic colourants in artworks provided a comprehensive overview of current analytical procedures and recent innovations (Pozzi & Leona 2016). Most commonly, silver nanoparticles are prepared following the protocol by Lee and Meiser (Lee & Meiser 1982). A small drop of silver nanoparticles adjacent to the paint specimen, coupled with aggregating agents (e.g. NaClO_4 , KNO_3), can multiply the amplitude of the Raman signals from the dye to orders ranging to 10^{10} or greater above the photoluminescent background (Shadi et al. 2004). The reason for such enhancement is unclear, but has been proposed as due to chemical means (polarity enhancement leads to charge transfer between metal and molecule) or electromagnetic means (plasmon resonance occurs in the field of metal) (Wustholz et al. 2009). Several studies have shown the applicability of SERS to identify the dyes from sample amounts of a few tens of micron-sized dyed fibre (Bruni, Guglielmi & Pozzi 2010; Bruni et al. 2011; Chen et al. 2006). The SERS method for detection of colourants on fibres has evolved from classical extraction of dye, to in-situ 'on-the-sample' non-extraction hydrolysis (Leona & Lombardi 2007; Leona, Stenger & Ferloni 2006), to direct 'on-the-fibre' analysis without need for pre-treatment (Casadio et al. 2010; Jurasekova et al. 2008). The range of dyes analysed by SERS also expanded to other sample forms, including micro-sized grains of oil paint samples (Oakley et al. 2011), pigment grains from a watercolor painting (Brosseau, Casadio & Van Duyne 2011) and direct SERS analysis on paint cross-sections (Frano et al. 2014). Other than dye molecules, SERS has also found application to natural and synthetic organic pigments on pastel artworks (Brosseau, Rayner, et al. 2009), quinacridone synthetic organic pigments (Del Puerto et al. 2011), PB15 pigments in house paints (Harroun et al. 2011) and natural resins (Lau, Livett & Prawer 2008). Recently, Leona et al. innovated a non-invasive SERS technique without a mechanical removal of sample from an artwork. The method used a hydrogel to transfer the dye or ink from paper, followed by SERS analysis on the hydrogel and no observable change is seen on the paper (Leona et al. 2011). Despite the extent

of applied literature, the application of the technique SERS is still at an initial stage. SERS spectra are different from those obtained with dispersive spectroscopy and SERS databases are limited to natural and synthetic dyestuffs (Bruni, Guglielmi & Pozzi 2011; Casanova-González et al. 2012; Pozzi, Porcinai, et al. 2013). Mixtures of dyes present difficulty in interpretation and studies combining TLC with SERS appears promising (Brosseau, Gambardella, et al. 2009; Cañamares et al. 2014; Geiman, Leona & Lombardi 2009; Pozzi, Shibayama, et al. 2013).

2.3.1.3 MAPPING/IMAGING

A paint chip's complex stratigraphy containing multiple material layers (i.e. cracks, localized dirt, pigments, fillers) or heterogeneous ingredients, can capitalize on the benefits of mapping or imaging (Boon, Ferreira & Keune 2005; Joseph et al. 2010; Kaszowska et al. 2013; Spring et al. 2008). With mapping or imaging capability, the spectral information is distributed over a larger area. It requires the preparation of a paint cross-section with a flat, polished surface that is free from resin contamination, especially of concern regarding FTIR mapping/ imaging. The classical method of preparing a paint cross-section often encounters two problems: (1) resin smearing over the paint cross-section and (2) resin infiltrating the spaces of a porous paint, coating the pigment particles (Derrick et al. 1994). To overcome these problems, methods of preparing cross-sections were introduced, which include compression between two diamond cells (Van der Weerd, Heeren & Boon 2004), microtoming with polycarbonate foil (Pouyet et al. 2014), replacement of resin with AgCl (Pouyet et al. 2014), KBr (Kopecká & Svobodová 2014) or NaCl (Prati et al. 2013), encapsulation of the sample utilising cyclododecane (CCD or C₁₂H₂₄) as barrier to resin (Kopecká & Svobodová 2014; Martin de Fonjaudran et al. 2008; Prati et al. 2010), polishing devices (Loon 2008; Mazzeo et al. 2007) and ion milling system (Boon & Asahina 2006).

2.3.1.4 DATA PROCESSING

When comparing fingerprint regions of multiple samples, the subtle differences may not be cogent enough for analysis. With chemometric processing methods such as Principal component analysis (PCA), a type of Eigenvector analysis, the variances of a large set of data can be reduced to principal components, enabling similar samples to be distinguished by geographical location, age, or original source. PCA combined with spectroscopy data is a powerful tool applied to the heritage field. It has been used to discriminate common binding

media in artworks (Sarmiento et al. 2011), separate natural and synthetic indigo (Vandenabeele & Moens 2003), discriminate fresh and naturally aged lipidic binders (Manzano et al. 2012), differentiate of artificially and naturally aged protein-based binding media (Nevin et al. 2008), semi-quantify pigment/binder ratio in lead-based paints (Pallipurath et al. 2014) and improve the drawbacks of FORS data arising from irregularities on an artwork surface (Sessa, Bagán & García 2014).

2.3.2 ELEMENTAL ANALYSIS

2.3.2.1 ENERGY DISPERSIVE X-RAY FLUORESCENCE (EDXRF) SPECTROSCOPY

A few excellent resources of portable/ handheld XRF applied to the field of archaeology and heritage have been published, including segments pertaining to paints (Potts & West 2008; Shackley 2010; Shugar & Mass 2012). Although portable/ handheld XRF has been advocated as a non-invasive technique, it should be noted that high energy X-rays penetrating into the artwork material do cause permanent modification at the atomic level. However, these effects are minor and not of major concern. The most visible damages observed were reported as darkening of polished copper, transparent glass and yellowing of white fabrics (Mantler & Schreiner 2000).

Problems with overlapping peaks, artifact peaks, inter-elemental absorption effects, layering/shielding effects, detection of low-Z pigments, and modern pigments are commonly encountered with XRF applied to painted artworks. Round-robin tests using XRF on the same paint model samples highlighted the difficulty in differentiating Cd in modern pigment from Pb sum peak and detection of low Z blue pigments in the presence of Cu based blue, and the detection of unusual elements (e.g. Hafnium) in modern pigments (Namowicz, Trentelman & McGlinchey 2009). The limitation of XRF in detecting light elements constituting dyes, lakes and ultramarine (or lapis lazuli) has been highlighted (Bonizzoni et al. 2007). The identification of mixtures containing barium with titanium, or lead white, vermilion with orpiment is challenging due to closely spaced characteristic x-rays, while small amounts such as cobalt blue were difficult to detect in earth pigments (McGlinchey 2012).

While XRF has commonly been used in qualitative analysis, quantitation is not considered appropriate in artists' paints, considering that the composition of each paint layer, the degree

of homogeneity and variable thickness in each paint layer are usually unknown. Interpretation of layered paint surfaces remains uncertain with solely in situ-XRF and almost always requires destructive sampling of paint cross-sections. However, where the paint recipe is known, XRF quantitation studies on paintings can be potentially useful for revealing the technique. By inserting XRF datasets into an algorithmic software for multilayer analysis (Solé et al. 2007), the non-destructive ability to approximate thicknesses of varnishes and glazes (De Viguerie, Sole & Walter 2009) and paint composition in multilayer paintings (De Viguerie et al. 2010) have been reported. XRF mapping/ imaging coupled with synchrotron source that are performed over painted surfaces, offers a high resolution visual distribution of the elemental composition hidden in paintings (Anitha et al. 2011; Dik et al. 2008; Howard et al. 2012).

2.3.2.2 SCANNING-ELECTRON MICROSCOPY (SEM)-ENERGY DISPERSIVE SPECTROSCOPY (EDS)

Similarly to XRF, quantitation using EDS for unknown heterogeneous paint samples is unreliable. With the advent of partial vacuum or environmental SEM, the need to carbon coat non-conductive paint cross-sections surfaces is avoided. Mapping functions also allow the detailed elemental composition to be determined across the layers.

With regards to elemental database, a comprehensive book reporting on the EDS spectra of over 60 minerals present in sedimentary rocks is a good reference resource (Severin 2004). As elemental interpretation is usually restricted to qualitative analysis, the lack of database as compared to spectroscopy is not surprising. However, a database of elemental intensity ratios in mixtures of artist pigments and standard paint formulations may be potentially useful for interpreting modern paint mixtures.

2.3.3 GAS-CHROMATOGRAPHY (GC)/ MASS SPECTROMETRY (MS) AND PYROLYSIS (PY)-GC/MS

Binders found on painted artworks can simultaneously contain one or more of the following chemical classes: carbohydrates, proteins, glycerolipids, wax esters, wax, natural and synthetic resins. Although FTIR spectroscopy and Secondary Ion Mass Spectrometry (SIMS) have been applied to binder analysis, the identification has been limited to the binder class (Edwards & Vandenabeele 2012). Since early studies of binder characterisation, GC/MS has been most

widely employed, and the applicability was extended with the addition of a pyrolyser. Several reviews including GC/MS applied to paint binders, along with exemplary case-studies, serve as excellent resources (Colombini & Modugno 2009; Doménech-Carbó 2008; Edwards & Vandenabeele 2012; Hutanu, Woods & Darie 2013), with the most recent updating on the latest progresses of analytical methods including the degradation of organic materials in artworks (Bonaduce et al. 2016). In general, the paint sample size required for Py-GC/MS can be as low as about 10 µg while for GC/MS, about 0.2-0.5 mg is needed, which is more than that required by spectroscopy and is often considered a macro analysis. Nevertheless, the detail of information obtained from separating the chemical components provides more information beyond the chemical class.

2.3.3.1 SAMPLE PREPARATION METHODS

2.3.3.1.1 GC/MS

Since art paint samples are mostly solid particles that are not sufficiently volatile, a sample pre-treatment by wet chemistry processes is of fundamental importance. This usually involves time-consuming solvent extraction, hydrolysis, clean-up and derivatisation (Edwards & Vandenabeele 2012). The choice of method depends on the chemical class of compounds suspected in the sample. Numerous methods targeting the analysis of a single chemical class have been developed and tested on common art binding media (Colombini et al. 2000; Gimeno-Adelantado et al. 2002; Marinach, Papillon & Pepe 2004; Mateo-Castro et al. 2001; Schilling 2005). Common cations (i.e. Ca^{2+} , Fe^{2+} , Cu^{2+}) in pigments can interfere with protein and lipid analysis (Gimeno-Adelantado et al. 2001). To overcome such pigment-binder interferences, insoluble salts have been removed via ammonia extraction of proteins into aqueous solution, whereas soluble cations such as Cu^{2+} were removed by passing the amino acid hydrolysate through cation exchange resins and eluting with ammonia (Colombini, Modugno & Giacomelli 1999). Similarly for carbohydrates, a double exchange resin for removal of soluble salts was found necessary (Andreotti et al. 2006). Sugars that undergo methanolysis and silylation with HMDS (hexamethyldisilazane) (Marinach, Papillon & Pepe 2004) or hydrolysis with TFA followed by silylation with HMDS (Vallance et al. 1998) produces highly complex chromatograms, where 1 to 5 peaks can appear for each monosaccharide. To avoid the formation of multiple peaks, sugars are converted to acyclic methoximes, followed by acetylation and this procedure generates two peaks per monosaccharide (Lliveras-Tenorio et al. 2012a; Pitthard et al. 2006).

However it does not detect uronic acids. On the other hand, by mercaptalating the anomeric carbon with EtSH:TFA (2:1) and silylating with HMDS or BSTFA (N,O-Bis (trimethylsilyl) trifluoroacetamide), a simple chromatogram with only one peak for each analyte is produced, in which both aldoses and uronic acids can be detected (Bonaduce et al. 2007; Dhakal & Armitage 2013; Pitthard & Finch 2001). Softer resins such as sandarac, certain copal and elemis can be simply extracted with solvent prior to derivatisation, without the need for hydrolysis (Marinach, Papillon & Pepe 2004). Where resins are hard or have extensively esterified (e.g. shellac), hydrolysis is required (Derry 2012; Pitthard et al. 2006; Sutherland 2010). Pure wax such as paraffin wax does not need sample pretreatment as the aliphatic alkanes are volatile enough to be separated by GC. To extract the wax into liquid phase, non-polar solvent cyclohexane has been used (Marinach, Papillon & Pepe 2004). Wax esters (e.g. beeswax and canauba wax) and non-drying oils may or may not require hydrolysis, depending on the unsaturation content and extent of C=C oxidation or hydrolysis (Bonaduce & Colombini 2004; Kimpe, Jacobs & Waelkens 2002; Mottram et al. 1999; Regert, Langlois & Colinart 2005; Steele, Stern & Stott 2010). In contrast, drying oils found on aged artworks have largely polymerised and usually undergoes alkaline hydrolysis, acidification, fatty acid extraction and derivation (Andreotti et al. 2006; Colombini et al. 2002).

Most sample pretreatment methods have been devoted to identifying a single class of compound. Only a few works have been able to identify more than one class of compounds in the same paint micro-sample (Castro et al. 1997; Singer & McGuigan 2007), and even fewer have employed microwave hydrolysis, which is advantageous in certain ways (Colombini et al. 1999; Rampazzi et al. 2002). The study by Lluveras et al. (Lluveras et al. 2010) contains the most updated protocol built up from previous literature and allows the identification of glycerolipids, proteins, carbohydrates, wax and terpenoids in the same microsample (Andreotti et al. 2006; Bonaduce, Cito & Colombini 2009). By using ammonia extraction in the first step, proteins, gums and organic acids are separated from wax, unsaponified resins and unhydrolysed triglycerides. An ether extraction of organic acids in combination with the residue from the first step constitutes the neutral lipid-resin-wax fraction. The aqueous gum/protein solution was acidified and C4 OMIX tips (sorbents with high binding capacity for polypeptides) were used to extract the polypeptides to form the protein fraction. The remaining solution then constitutes

the gum fraction. Each of these fractions were then hydrolyzed, cleaned-up and derivatised before analysis by GC/MS.

2.3.3.1.2 PY-GC/MS

With Py-GC/MS, the solid sample can be directly pyrolyzed or treated with TMAH in MeOH prior to pyrolysis. However, use of TMAH has its limitations, including decarboxylation reactions of carboxylic acids (loss of a CO₂), isomerisation of polyunsaturated fatty acids (shift in C=C position), formation of dehydration products (loss of H₂O). Therefore, other derivatising agents such as HMDS, Methprep II (a methanolic solution of m-trifluoromethylphenyl trimethylammonium hydroxide) are used as well (Colombini & Modugno 2009).

2.3.3.2 DATA INTERPRETATION

2.3.3.2.1 TRADITIONAL BINDERS BY GC/MS

Interpretation of GC/MS data often rely on markers and intensity ratios, which has been most commonly employed in the identification of fatty acids. As palmitic and stearic acids are stable with age, the P/S (palmitic/ stearic) ratio is most often used to differentiate these drying oils. P/S = 1-2 is linseed oil, P/S = 2-3 is walnut oil and P/S = 3-8 is poppyseed oil, P/S = 2.5-3.5 is egg (Colombini & Modugno 2009; Edwards & Vandenabeele 2012). Care should be taken in assessing P/S ratios, as it is found to be unreliable when more than one binder exists (such as egg and wax), or when other microorganisms contribute and alter the level of fatty acids (Colombini & Modugno 2009). Similarly, the presence of pigments and age of paint also changes the P/S ratios (Bonaduce et al. 2012). Other useful markers include O/S (oleic/ stearic) ratio (for differentiating young and aged oil paints), A/P (azelaic/ palmitic) ratios (for differentiating drying oil and egg tempera) (Colombini & Modugno 2009), D/G ratio (where D represents the sum of dicarboxylic acid and G= glycerol, indicate photo-oxidative reactions) and P/G ratio (migration of fatty acids) (Schilling 2005). However, modern oil paints composing varied amounts of drying and non-drying oil, with possible inclusion of stearate or other additives, require a different set of ratios (A/P, D/P, A/Sub (suberic), O/S, P/G, A/G, P/S, S/G, A/S, D/S) for composition analysis (Izzo 2010).

The GC/MS characterisation of various terpenoid resins relevant to paintings have been studied in detail, both aged and unaged (Cartoni et al. 2004; Dietemann et al. 2009; Doelen 1999; Osete-Cortina et al. 2004). The complications arise from the complex composition of different

compounds in the resin, from harvest to photo-oxidation with light and applied as a varnish (Dietemann 2003; Doelen 1999). In addition, the interpretation can be complicated by different age, grade and geographical origin of the resin. An overview of the analytical steps for sample treatment and the data evaluation specific to protein binders has been reviewed (Colombini & Modugno 2004). To classify the protein binders (collagen, milk protein, egg yolk, egg glair), amino acid ratios such as gly/glu, gly/asp, pro/asp, glu/pro, glu/asp, glu/ala, ala/pro, ala/gly ratios are often used (where gly: glycine; glu: glutamic acid; asp: aspartic acid; pro: proline; ala: alanine) (Castro et al. 1997; Colombini et al. 1999; Keck & Peters 1969). However, these data may not be applicable for intra- and inter-laboratory comparisons, as responses of amino acid change with the analytical procedure (Colombini & Modugno 2004). One of the main difficulties encountered in protein characterisation is the low yield of amino acids in the chromatogram. Cations, especially lead, copper, calcium, iron and manganese, often found in pigments, have a high tendency to form complexes with amino acids, lowering the yield (Colombini, Modugno & Giacomelli 1999; De la Cruz-Cañizares et al. 2004). Monosaccharides from the substrate and gum binder can also condense with amino acids, leading to a lower yield. In general, the initial proportion of proteins in the paint sample, the tendency of protein loss with increasing transfer steps, the experimental conditions taken in protein hydrolysis and the amount of proteins extracted into the sample aliquot, all have a potential to affect the final yield of the amino acids (Colombini & Modugno 2004; Colombini & Modugno 2009; Edwards & Vandenabeele 2012). To characterise the type of gum, the relative amounts of monosaccharides in unknown paint samples were compared to that of reference gum samples (Bonaduce et al. 2007). However, the data evaluation may be complicated by different issues, such as the potential contamination of substrate sugars, protein-sugar reaction, pigment-sugar interaction, differences in monosaccharide recovery, ageing effects and other causes due to sample (season, maturity, part of plant) (Lliveras-Tenorio et al. 2012a, 2012b).

2.3.3.2.2 SYNTHETIC BINDERS BY PY-GC/MS AND GC/MS

The use of Py-GC/MS has been largely applied to the characterisation of synthetic polymers such as acrylics, alkyds, PVA emulsions, nitrocellulose and polyurethanes (Hiltz 2015; Osete-Cortina & Doménech-Carbó 2006; Ploeger, Scalarone & Chiantore 2008; Wei, Pintus & Schreiner 2012, 2013). Marker compounds for characterising synthetic binders are clearly highlighted and often serves as a good starting reference (Learner 2004). The issue becomes

complicated when more than one type of binder exist in the paint chip, complicating the data evaluation. In such cases, Schilling et al. used an atypical analytical treatment method with GC/MS, enabling the characterization of artist's oil colours mixed with alkyd house paints in Jackson Pollock's drip paintings (Learner 2007). Additives that are commonly found in modern paints are usually difficult to detect analytically due to their low concentration, large molar mass and vast number of commercially available products. A few papers have demonstrated the Py-GC/MS characterisation of additives, such as plasticisers in poly vinyl acetate (PVAc) paint (Silva et al. 2009), polyethylene glycol (PEG) surfactants in acrylic emulsion paints (Scalarone & Chiantore 2004), wetting agents, defoamers, metal soap and stabiliser in commercial oil, acrylic and emulsion paints (Izzo et al. 2014). The characterisation of polyoxyethylene (POE) additives in water-mixable oils (WMO) paints using the analytical procedure (n-butylamine, BSTFA and HMDS) with GC/MS was also demonstrated (Learner 2007). Synthetic organic pigments can also appear in the pyrogram, which may or may not interfere with the binder identification. A number of studies provided markers for characterising common synthetic organic pigments in paints using Py-GC/MS (Germinario, van der Werf & Sabbatini 2015; Ghelardi, Degano, Colombini, Mazurek, Schilling & Learner 2015; Learner 2004; Russell et al. 2011; Sonoda 1999).

The application of Py-GC/MS to traditional binders of oils, proteins, carbohydrates, resins and waxes seems promising in some studies (Chiantore, Riedo & Scalarone 2009; Colombini & Modugno 2009; Fabbri & Chiavari 2001; Ling et al. 2007; Stevanato et al. 1997). However, it should be highlighted that the specimens tested in these studies were either unpigmented reference samples or commercial paints with single binder classes and it has been reported that Py-GC/MS is not reliable when applied to many traditional binders (Cappitelli 2004; Learner 1996). In the case of proteins, identification can be complicated by rearrangement reactions and the low recovery of amino acids (Edwards & Vandenabeele 2012). Markers for proteins appear differently even when the same derivatising agent is used, making it difficult to compare data across literature (Colombini & Modugno 2009). In the case of gums, the technique may result in incomplete derivatisation and yield, hence it is not useful to quantify or detect minor components, which are important in attributing to the type of gum (Colombini & Modugno 2009; Tommaso et al. 2012). Even different portions taken from the same gum sample for analysis can correlate poorly to each other (Shedrinsky et al. 1989). When using Py-GC/MS to

characterise resins, oils and waxes in aged and heterogeneous samples, results seem more promising, as demonstrated in the study of violin varnishes (Chiavari, Montalbani & Otero 2008) and animal fats mixed with oil-based paints in Picasso paintings (Cappitelli & Koussiaki 2006). However, a study comparing Py-GC/MS and GC/MS shows that for the same sample, weaker resinous peaks are obtained in Py-GC/MS (De la Cruz-Cañizares et al. 2005).

2.4 CONCLUSIONS

Paint is a heterogeneous mix of varying proportions of pigments (inorganic pigments, organic dye/lakes, synthetic organic pigment) and binding media (protein, carbohydrate, lipid, resin, wax, wax esters). Fillers (or extenders) and additives may be added in paints. The composition varies depending on the source (e.g. artist's prepared recipe vs a ready-made paint), the period (e.g. traditional oil paint vs modern oil paint) and the technique (e.g. style of application). Pigment characterisation can be further complicated by its origin (natural or synthetic).

Although various techniques have been frequently applied to paint materials, the acquisition of good quality data and data interpretation on painted artworks can be challenging, considering that the paint sample is usually heterogeneous, multi-layered, of an unknown composition, aged or degraded and that only micro-amounts are available or sometimes not permitted for sampling. The success of a confident characterisation is highly dependable on the availability of relevant references, sample type, sample quantity and technique development. Vibrational spectroscopy may be easy to operate due to a simplified design, but the interpretation is often hampered by a lack of database or mixture of compounds. In Raman spectroscopy, fluorescence is often the main obstacle. Fortunately, different techniques have been proposed for overcoming fluorescence, of which SERS has received most attention due to its notable capability of Raman scattering enhancement. To complement the characterisation of pigment/filler, elemental information can be obtained using XRF and SEM-EDS. While elemental analysis is usually straightforward, the interpretation of data has to consider different instrumental limits, source contamination and sample matrix. As artist's techniques of application and paint recipes differs, preparation of universal standards qualified for quantitative analysis is not feasible and elemental analysis has been carried out qualitatively with semi-quantification.

In the case of GC/MS applications, the sample preparation procedures and data interpretation is more time-consuming and tedious compared to spectroscopy techniques. It demands an understanding of organic chemistry pertaining to the paint constituents, which determines the type of sample treatment, derivatisation and instrumentation parameters. Where this information is unknown, spectroscopic techniques can be used as a first analysis prior to deciding the sample preparation method. While Py-GC/MS requires less sample amount and involves a simpler sample preparation procedure than GC/MS, piecing the fragments to the original structure may not always be achievable. The production of secondary fragments overlaps with parent peaks or creates additional peaks that complicate interpretation. Comparison of chromatographic results cannot solely rely on published data due to variances in instrumentation design, method and sample methodology and largely depends on a well-established in-house database. Despite these drawbacks, chromatographic mass spectrometry is still an invaluable technique to organic analysis of paint materials.

2.5 References

- Aceto, M., Agostino, A., Fenoglio, G., Gulmini, M., Bianco, V. & Pellizzi, E. 2012, 'Non invasive analysis of miniature paintings: Proposal for an analytical protocol', *Spectrochimica Acta Part A: Molecular and Biomolecular Spectroscopy*, vol. 91, pp. 352-9.
- Aibéo, C.L., Goffin, S., Schalm, O., van der Snickt, G., Laquiere, N., Eyskens, P. & Janssens, K. 2008, 'Micro-Raman analysis for the identification of pigments from 19th and 20th century paintings', *Journal of Raman Spectroscopy*, vol. 39, no. 8, pp. 1091-8.
- Analytical Methods Committee 2015, 'Raman spectroscopy in cultural heritage: Background paper', *Analytical Methods*, vol. 7, no. 12, pp. 4844-7.
- Andreotti, A., Bonaduce, I., Colombini, M.P., Gautier, G., Modugno, F. & Ribechini, E. 2006, 'Combined GC/MS Analytical Procedure for the Characterization of Glycerolipid, Waxy, Resinous, and Proteinaceous Materials in a Unique Paint Microsample', *Analytical Chemistry*, vol. 78, no. 13, pp. 4490-500.
- Anghelone, M., Jembrih-Simbürger, D. & Schreiner, M. 2014, 'Micro-Raman and ATR-FTIR for the study of modern paints containing synthetic organic pigments (SOPs): characterization of the photodegradation processes', *11th Infrared and Raman Users Group Conference 5-7 November 2014 Museum of Fine Arts, Boston*, pp. 1-6.

- Anitha, A., Brasoveanu, A., Duarte, M.F., Hughes, S.M., Daubechies, I., Dik, J., Janssens, K. & Alfeld, M. 2011, 'Virtual underpainting reconstruction from X-ray fluorescence imaging data', *Signal Processing Conference, 2011 19th European*, Barcelona, pp. 1239-43.
- Bassan, P., Byrne, H.J., Lee, J., Bonnier, F., Clarke, C., Dumas, P., Gazi, E., Brown, M.D., Clarke, N.W. & Gardner, P. 2009, 'Reflection contributions to the dispersion artefact in FTIR spectra of single biological cells', *Analyst*, vol. 134, no. 6, pp. 1171-5.
- Bayne, J.M. & Butler, I.S. 2013, 'Effect of temperature and pressure on selected artists' pigments', *New Journal of Chemistry*, vol. 37, no. 12, pp. 3833-9.
- Bell, I.M., Clark, R.J.H. & Gibbs, P.J. 1997, 'Raman spectroscopic library of natural and synthetic pigments (pre- ≈ 1850 AD)', *Spectrochimica Acta Part A: Molecular and Biomolecular Spectroscopy*, vol. 53, no. 12, pp. 2159-79.
- Bell, S.E.J., Bourguignon, E.S.O. & Dennis, A. 1998, 'Analysis of luminescent samples using subtracted shifted Raman spectroscopy', *Analyst*, vol. 123, no. 8, pp. 1729-34.
- Bersani, D. & Lottici, P. 2016, 'Raman spectroscopy of minerals and mineral pigments in archaeometry', *Journal of Raman Spectroscopy*, vol. 47, no. 5, pp. 499-530.
- Bonaduce, I., Brecolaki, H., Colombini, M.P., Lluveras, A., Restivo, V. & Ribechini, E. 2007, 'Gas chromatographic–mass spectrometric characterisation of plant gums in samples from painted works of art', *Journal of Chromatography A*, vol. 1175, no. 2, pp. 275-82.
- Bonaduce, I., Carlyle, L., Colombini, M.P., Duce, C., Ferrari, C., Ribechini, E., Selleri, P. & Tine, M.R. 2012, 'New insights into the ageing of linseed oil paint binder: a qualitative and quantitative analytical study', *PLoS ONE*, vol. 7, no. 11, p. e49333.
- Bonaduce, I., Cito, M. & Colombini, M.P. 2009, 'The development of a gas chromatographic–mass spectrometric analytical procedure for the determination of lipids, proteins and resins in the same paint micro-sample avoiding interferences from inorganic media', *Journal of Chromatography A*, vol. 1216, no. 32, pp. 5931-9.
- Bonaduce, I. & Colombini, M.P. 2004, 'Characterisation of beeswax in works of art by gas chromatography–mass spectrometry and pyrolysis–gas chromatography–mass spectrometry procedures', *Journal of Chromatography A*, vol. 1028, no. 2, pp. 297-306.
- Bonaduce, I., Ribechini, E., Modugno, F. & Colombini, M.P. 2016, 'Analytical Approaches Based on Gas Chromatography Mass Spectrometry (GC/MS) to Study Organic Materials in Artworks and Archaeological Objects', *Topics in Current Chemistry*, vol. 374, no. 1, pp. 1-37.

- Bonizzoni, L., Galli, A., Poldi, G. & Milazzo, M. 2007, 'In situ non-invasive EDXRF analysis to reconstruct stratigraphy and thickness of Renaissance pictorial multilayers', *X-Ray Spectrometry*, vol. 36, no. 2, pp. 55-61.
- Boon, J.J. 2014, 'New Light on the Surface of Art Objects in the Conservation Studio with a 3D Digital Hirox Microscope Mounted on an XYZ Stand', *ICOM-CC 17th Triennial Conference*, Melbourne.
- Boon, J.J. & Asahina, S. 2006, 'Surface preparation of cross sections of traditional and modern paint using the Argon ion milling polishing CP system', *Microscopy and Microanalysis*, vol. 12, no. S02, pp. 1322-3.
- Boon, J.J., Ferreira, E.S.B. & Keune, K. 2005, 'Imaging Analytical Studies of Old Master Paints Using FTIR, SIMS and SEMEDX of Embedded Paint Cross Sections', *Microscopy and Microanalysis*, vol. 11, pp. 1370-1.
- Breitman, M., Ruiz-Moreno, S. & Gil, A.L. 2007, 'Experimental problems in Raman spectroscopy applied to pigment identification in mixtures', *Spectrochimica Acta Part A: Molecular and Biomolecular Spectroscopy*, vol. 68, no. 4, pp. 1114-9.
- Brosseau, C.L., Casadio, F. & Van Duyne, R.P. 2011, 'Revealing the invisible: using surface-enhanced Raman spectroscopy to identify minute remnants of color in Winslow Homer's colorless skies', *Journal of Raman Spectroscopy*, vol. 42, no. 6, pp. 1305-10.
- Brosseau, C.L., Gambardella, A., Casadio, F., Grzywacz, C.M., Wouters, J. & Van Duyne, R.P. 2009, 'Ad-hoc surface-enhanced Raman spectroscopy methodologies for the detection of artist dyestuffs: thin layer chromatography-surface enhanced Raman spectroscopy and in situ on the fiber analysis', *Analytical Chemistry*, vol. 81, no. 8, pp. 3056-62.
- Brosseau, C.L., Rayner, K.S., Casadio, F., Grzywacz, C.M. & Van Duyne, R.P. 2009, 'Surface-enhanced Raman spectroscopy: a direct method to identify colorants in various artist media', *Analytical chemistry*, vol. 81, no. 17, pp. 7443-7.
- Brunetti, B., Miliani, C., Rosi, F., Doherty, B., Monico, L., Romani, A. & Sgamellotti, A. 2016, 'Non-invasive Investigations of Paintings by Portable Instrumentation: The MOLAB Experience', *Topics in Current Chemistry*, vol. 374, no. 1, pp. 1-35.
- Bruni, S., Guglielmi, V. & Pozzi, F. 2010, 'Surface-enhanced Raman spectroscopy (SERS) on silver colloids for the identification of ancient textile dyes: Tyrian purple and madder', *Journal of Raman Spectroscopy*, vol. 41, no. 2, pp. 175-80.

- Bruni, S., Guglielmi, V. & Pozzi, F. 2011, 'Historical organic dyes: a surface-enhanced Raman scattering (SERS) spectral database on Ag Lee–Meisel colloids aggregated by NaClO₄', *Journal of Raman Spectroscopy*, vol. 42, no. 6, pp. 1267-81.
- Bruni, S., Guglielmi, V., Pozzi, F. & Mercuri, A.M. 2011, 'Surface-enhanced Raman spectroscopy (SERS) on silver colloids for the identification of ancient textile dyes. Part II: pomegranate and sumac', *Journal of Raman Spectroscopy*, vol. 42, no. 3, pp. 465-73.
- Burgio, L. & Clark, R.J.H. 2001, 'Library of FT-Raman spectra of pigments, minerals, pigment media and varnishes, and supplement to existing library of Raman spectra of pigments with visible excitation', *Spectrochimica Acta Part A: Molecular and Biomolecular Spectroscopy*, vol. 57, no. 7, pp. 1491-521.
- Burnstock, A. & van den Berg, K.J. 2014, 'Twentieth Century Oil Paint. The Interface Between Science and Conservation and the Challenges for Modern Oil Paint Research', in K.J.v.d. Berg, A. Burnstock, M.d. Keijzer, J. Krueger, T. Learner, A. de Tagle & G. Heydenreich (eds), *Issues in Contemporary Oil Paint*, Springer International Publishing, Cham, Switzerland, pp. 1-19.
- Burrafato, G., Calabrese, M., Cosentino, A., Gueli, A.M., Troja, S.O. & Zuccarello, A. 2004, 'ColoRaman project: Raman and fluorescence spectroscopy of oil, tempera and fresco paint pigments', *Journal of Raman Spectroscopy*, vol. 35, no. 10, pp. 879-86.
- Buxbaum, G. & Pfaff, G. 2005, *Industrial Inorganic Pigments*, 3 edn, Wiley-VCH, Germany.
- Cañamares, M.V., Reagan, D., Lombardi, J. & Leona, M. 2014, 'TLC-SERS of mauve, the first synthetic dye', *Journal of Raman Spectroscopy*, vol. 45, no. 11-12, pp. 1147-52.
- Cappitelli, F. 2004, 'THM-GCMS and FTIR for the study of binding media in Yellow Islands by Jackson Pollock and Break Point by Fiona Banner', *Journal of Analytical and Applied pyrolysis*, vol. 71, no. 1, pp. 405-15.
- Cappitelli, F. & Koussiaki, F. 2006, 'THM-GCMS and FTIR for the investigation of paints in Picasso's Still Life, Weeping Woman and Nude Woman in a Red Armchair from the Tate Collection, London', *Journal of analytical and applied pyrolysis*, vol. 75, no. 2, pp. 200-4.
- Cappitelli, F., Vicini, S., Piaggio, P., Abbruscato, P., Princi, E., Casadevall, A., Nosanchuk, J.D. & Zanardini, E. 2005, 'Investigation of fungal deterioration of synthetic paint binders using vibrational spectroscopic techniques', *Macromolecular bioscience*, vol. 5, no. 1, pp. 49-57.

- Cartoni, G., Russo, M.V., Spinelli, F. & Talarico, F. 2004, 'GC-MS Characterisation and Identification of Natural Terpenic Resins Employed in Works of Art', *Annali di chimica*, vol. 94, no. 11, pp. 767-82.
- Casadio, F., Leona, M., Lombardi, J.R. & Van Duyne, R. 2010, 'Identification of Organic Colorants in Fibers, Paints, and Glazes by Surface Enhanced Raman Spectroscopy', *Accounts of Chemical Research*, vol. 43, no. 6, pp. 782-91.
- Casadio, F. & Toniolo, L. 2001, 'The analysis of polychrome works of art: 40 years of infrared spectroscopic investigations', *Journal of Cultural Heritage*, vol. 2, no. 1, pp. 71-8.
- Casanova-González, E., García-Bucio, A., Ruvalcaba-Sil, J.L., Santos-Vasquez, V., Esquivel, B., Falcón, T., Arroyo, E., Zetina, S., Roldán, M.L. & Domingo, C. 2012, 'Surface-enhanced Raman spectroscopy spectra of Mexican dyestuffs', *Journal of Raman Spectroscopy*, vol. 43, no. 11, pp. 1551-9.
- Castro, K., Abalos, B., Martínez-Arkarazo, I., Etxebarria, N. & Madariaga, J.M. 2008, 'Scientific examination of classic Spanish stamps with colour error, a non-invasive micro-Raman and micro-XRF approach: The King Alfonso XIII (1889–1901 “Pelón”) 15 cents definitive issue', *Journal of Cultural Heritage*, vol. 9, no. 2, pp. 189-95.
- Castro, K., Pérez-Alonso, M., Rodríguez-Laso, M.D., Fernández, L.A. & Madariaga, J.M. 2005, 'On-line FT-Raman and dispersive Raman spectra database of artists' materials (e-VISART database)', *Analytical and Bioanalytical Chemistry*, vol. 382, no. 2, pp. 248-58.
- Castro, R.M., Dome, M., Marti, V.P., Adelantado, J.G. & Reig, F.B. 1997, 'Study of binding media in works of art by gas chromatographic analysis of amino acids and fatty acids derivatized with ethyl chloroformate', *Journal of Chromatography A*, vol. 778, no. 1, pp. 373-81.
- Centeno, S.A. 2015, 'Identification of artistic materials in paintings and drawings by Raman spectroscopy: some challenges and future outlook', *Journal of Raman Spectroscopy*, vol. 47, no. 1, pp. 9-15.
- Cheilakou, E., Troullinos, M. & Kouli, M. 2014, 'Identification of pigments on Byzantine wall paintings from Crete (14th century AD) using non-invasive Fiber Optics Diffuse Reflectance Spectroscopy (FORS)', *Journal of Archaeological Science*, vol. 41, pp. 541-55.
- Chen, K., Leona, M., Vo-Dinh, K.-C., Yan, F., Wabuyele, M.B. & Vo-Dinh, T. 2006, 'Application of surface-enhanced Raman scattering (SERS) for the identification of anthraquinone dyes used in works of art', *Journal of Raman Spectroscopy*, vol. 37, no. 4, pp. 520-7.

- Chiantore, O., Riedo, C. & Scaralone, D. 2009, 'Gas chromatography–mass spectrometric analysis of products from on-line pyrolysis/silylation of plant gums used as binding media', *International Journal of Mass Spectrometry*, vol. 284, no. 1–3, pp. 35-41.
- Chiavari, G., Montalbani, S. & Otero, V. 2008, 'Characterisation of varnishes used in violins by pyrolysis-gas chromatography/mass spectrometry', *Rapid Communications in Mass Spectrometry*, vol. 22, no. 23, pp. 3711-8.
- Clark, R.J.H., Dines, T.J. & Kurmoo, M. 1983, 'On the nature of the sulfur chromophores in ultramarine blue, green, violet, and pink and of the selenium chromophore in ultramarine selenium: characterization of radical anions by electronic and resonance Raman spectroscopy and the determination of their excited-state geometries', *Inorganic Chemistry*, vol. 22, no. 19, pp. 2766-72.
- Colombini, A. & Kaifas, D. 2010, 'Characterization of some orange and yellow organic and fluorescent pigments by Raman spectroscopy', *Preservation Science*, vol. 7, pp. 14-21.
- Colombini, M., Modugno, F., Giannarelli, S., Fuoco, R. & Matteini, M. 2000, 'GC-MS characterization of paint varnishes', *Microchemical Journal*, vol. 67, no. 1, pp. 385-96.
- Colombini, M.P. & Modugno, F. 2004, 'Characterisation of proteinaceous binders in artistic paintings by chromatographic techniques', *Journal of Separation Science*, vol. 27, no. 3, pp. 147-60.
- Colombini, M.P. & Modugno, F. 2009, *Organic Mass Spectrometry in Art and Archaeology*, Wiley, Chichester.
- Colombini, M.P., Modugno, F., Fuoco, R. & Tognazzi, A. 2002, 'A GC-MS study on the deterioration of lipidic paint binders', *Microchemical Journal*, vol. 73, no. 1–2, pp. 175-85.
- Colombini, M.P., Modugno, F. & Giacomelli, A. 1999, 'Two procedures for suppressing interference from inorganic pigments in the analysis by gas chromatography–mass spectrometry of proteinaceous binders in paintings', *Journal of chromatography A*, vol. 846, no. 1, pp. 101-11.
- Colombini, M.P., Modugno, F., Giacomelli, M. & Francesconi, S. 1999, 'Characterisation of proteinaceous binders and drying oils in wall painting samples by gas chromatography–mass spectrometry', *Journal of Chromatography A*, vol. 846, no. 1–2, pp. 113-24.

- Cotte, M., Checroun, E., Susini, J., Dumas, P., Tchoreloff, P., Besnard, M. & Walter, P. 2006, 'Kinetics of oil saponification by lead salts in ancient preparations of pharmaceutical lead plasters and painting lead mediums', *Talanta*, vol. 70, no. 5, pp. 1136-42.
- Daffara, C., Fontana, R. & Pezzati, L. 2009, 'NIR confocal microscopy for painting diagnostics', vol. 7391, pp. 73910M-M-8.
- Daher, C., Paris, C., Le Hô, A.S., Bellot-Gurlet, L. & Échard, J.P. 2010, 'A joint use of Raman and infrared spectroscopies for the identification of natural organic media used in ancient varnishes', *Journal of Raman Spectroscopy*, vol. 41, no. 11, pp. 1494-9.
- Daniels, V., Stacey, R. & Middleton, A. 2004, 'The Blackening of Paint Containing Egyptian Blue', *Studies in Conservation*, vol. 49, no. 4, pp. 217-30.
- De la Cruz-Cañizares, J., Doménech-Carbó, M.-T., Gimeno-Adelantado, J.-V., Mateo-Castro, R. & Bosch-Reig, F. 2005, 'Study of Burseraceae resins used in binding media and varnishes from artworks by gas chromatography–mass spectrometry and pyrolysis-gas chromatography–mass spectrometry', *Journal of Chromatography A*, vol. 1093, no. 1–2, pp. 177-94.
- De la Cruz-Cañizares, J., Doménech-Carbó, M.T., Gimeno-Adelantado, J.V., Mateo-Castro, R. & Bosch-Reig, F. 2004, 'Suppression of pigment interference in the gas chromatographic analysis of proteinaceous binding media in paintings with EDTA', *Journal of Chromatography A*, vol. 1025, no. 2, pp. 277-85.
- De Viguerie, L., Sole, V.A. & Walter, P. 2009, 'Multilayers quantitative X-ray fluorescence analysis applied to easel paintings', *Analytical and bioanalytical chemistry*, vol. 395, no. 7, pp. 2015-20.
- De Viguerie, L., Walter, P., Laval, E., Mottin, B. & Solé, V.A. 2010, 'Revealing the sfumato Technique of Leonardo da Vinci by X-Ray Fluorescence Spectroscopy', *Angewandte Chemie International Edition*, vol. 49, no. 35, pp. 6125-8.
- Del Puerto, E., Sánchez-Cortés, S., García-Ramos, J.V. & Domingo, C. 2011, 'Solution SERS of an insoluble synthetic organic pigment-quinacridone quinone-employing calixarenes as dispersive cavitands', *Chemical Communications*, vol. 47, no. 6, pp. 1854-6.
- Derrick, M. 1989, 'Fourier Transform Infrared Spectral Analysis of Natural Resins Used in Furniture Finishes', *Journal of the American Institute for Conservation*, vol. 28, no. 1, pp. 43-56.

- Derrick, M., Luiz, S., Tanya, K., Henry, F. & Dusan, S. 1994, 'Embedding Paint Cross-Section Samples in Polyester Resins: Problems and Solutions', *Journal of the American Institute for Conservation*, vol. 33, no. 3, pp. 227-45.
- Derrick, M.R., Stulik, D. & Landry, J.M. 1999, *Infrared Spectroscopy in Conservation Science*, The Getty Conservation Institute, USA.
- Derry, J. 2012, 'Investigating Shellac: Documenting the Process, Defining the Product.', University of Oslo, Norway.
- Dhakal, B. & Armitage, R.A. 2013, 'GC-MS Characterization of Carbohydrates in an Archaeological Use Residue: A Case Study from the Coahuila Desert', *Archaeological Chemistry VIII*, vol. 1147, American Chemical Society, pp. 157-70.
- Dietemann, P. 2003, 'Towards More Stable Natural Resin Varnishes for Paintings', PhD thesis, Swiss Federal Institute of Technology (ETH), Zurich.
- Dietemann, P., Higgitt, C., Kälin, M., Edelmann, M.J., Knochenmuss, R. & Zenobi, R. 2009, 'Aging and yellowing of triterpenoid resin varnishes—Influence of aging conditions and resin composition', *Journal of Cultural Heritage*, vol. 10, no. 1, pp. 30-40.
- Dik, J., Janssens, K., Van Der Snickt, G., van der Loeff, L., Rickers, K. & Cotte, M. 2008, 'Visualization of a lost painting by Vincent van Gogh using synchrotron radiation based X-ray fluorescence elemental mapping', *Analytical chemistry*, vol. 80, no. 16, pp. 6436-42.
- Doelen, G. 1999, 'Molecular studies of fresh and aged triterpenoid varnishes'.
- Doménech-Carbó, M.T. 2008, 'Novel analytical methods for characterising binding media and protective coatings in artworks', *Analytica Chimica Acta*, vol. 621, no. 2, pp. 109-39.
- Doménech-Carbó, M.T., Doménech-Carbó, A., Gimeno-Adelantado, J.V. & Bosch-Reig, F. 2001, 'Identification of Synthetic Resins Used in Works of Art by Fourier Transform Infrared Spectroscopy', *Applied Spectroscopy*, vol. 55, no. 12, pp. 1590-602.
- Duce, C., Della Porta, V., Tiné, M.R., Spepi, A., Ghezzi, L., Colombini, M.P. & Bramanti, E. 2014, 'FTIR study of ageing of fast drying oil colour (FDOC) alkyd paint replicas', *Spectrochimica Acta Part A: Molecular and Biomolecular Spectroscopy*, vol. 130, pp. 214-21.
- Eastaugh, N. 2013, *The pigment compendium : a dictionary and optical microscopy of historical pigments*, Routledge, New York.
- Edwards, H.G.M. & Chalmers, J.M. 2005, *Raman Spectroscopy in Archaeology and Art History*, Royal Society of Chemistry, Great Britain.

- Edwards, H.G.M. & Vandenabeele, P. 2012, *Analytical Archaeometry: Selected Topics*, Royal Society of Chemistry, Cambridge, United Kingdom.
- Ellis, G., Claybourn, M. & Richards, S.E. 1990, 'Applications of Fourier Transform Raman Spectroscopy The application of fourier transform raman spectroscopy to the study of paint systems', *Spectrochimica Acta Part A: Molecular Spectroscopy*, vol. 46, no. 2, pp. 227-41.
- Ernst, R.R. 2010, 'In situ Raman microscopy applied to large Central Asian paintings', *Journal of Raman Spectroscopy*, vol. 41, no. 3, pp. 275-84.
- Eveno, M., Moignard, B. & Castaing, J. 2011, 'Portable apparatus for in situ X-ray diffraction and fluorescence analyses of artworks', *Microscopy and Microanalysis*, vol. 17, no. 05, pp. 667-73.
- Fabbri, D. & Chiavari, G. 2001, 'Analytical pyrolysis of carbohydrates in the presence of hexamethyldisilazane', *Analytica Chimica Acta*, vol. 449, no. 1–2, pp. 271-80.
- Franco, K.A., Mayhew, H.E., Svoboda, S.A. & Wustholz, K.L. 2014, 'Combined SERS and Raman analysis for the identification of red pigments in cross-sections from historic oil paintings', *Analyst*, vol. 139, no. 24, pp. 6450-5.
- Fremout, W. & Saverwyns, S. 2012, 'Identification of synthetic organic pigments: the role of a comprehensive digital Raman spectral library', *Journal of Raman Spectroscopy*, vol. 43, no. 11, pp. 1536-44.
- Fremout, W. & Saverwyns, S. 2014, 'Characterization of daylight fluorescent pigments in contemporary artists' paints by Raman spectroscopy', *11th Infrared and Raman Users Group Conference 5-7 November 2014 Museum of Fine Arts, Boston*, p. 39.
- Fremout, W., Saverwyns, S., Peters, F. & Deneffe, D. 2006, 'Non-destructive micro-Raman and X-ray fluorescence spectroscopy on pre-Eyckian works of art—verification with the results obtained by destructive methods', *Journal of Raman Spectroscopy*, vol. 37, no. 10, pp. 1035-45.
- Geiman, I., Leona, M. & Lombardi, J.R. 2009, 'Application of Raman Spectroscopy and Surface-Enhanced Raman Scattering to the Analysis of Synthetic Dyes Found in Ballpoint Pen Inks', *Journal of Forensic Sciences*, vol. 54, no. 4, pp. 947-52.
- Germinario, G., van der Werf, I.D. & Sabbatini, L. 2015, 'Pyrolysis gas chromatography mass spectrometry of two green phthalocyanine pigments and their identification in paint systems', *Journal of Analytical and Applied Pyrolysis*, vol. 115, pp. 175-83.

- Gervais, C., Languille, M.-A., Reguer, S., Gillet, M., Pelletier, S., Garnier, C., Vicenzi, E.P. & Bertrand, L. 2013, 'Why does Prussian blue fade? Understanding the role(s) of the substrate', *Journal of Analytical Atomic Spectrometry*, vol. 28, no. 10, pp. 1600-9.
- Ghelardi, E., Degano, I., Colombini, M.P., Mazurek, J., Schilling, M., Khanjian, H. & Learner, T. 2015, 'A multi-analytical study on the photochemical degradation of synthetic organic pigments', *Dyes and Pigments*, vol. 123, pp. 396-403.
- Ghelardi, E., Degano, I., Colombini, M.P., Mazurek, J., Schilling, M. & Learner, T. 2015, 'Py-GC/MS applied to the analysis of synthetic organic pigments: characterization and identification in paint samples', *Analytical and bioanalytical chemistry*, vol. 407, no. 5, pp. 1415-31.
- Gimeno-Adelantado, J., Mateo-Castro, R., Doménech-Carbó, M., Bosch-Reig, F., Doménech-Carbó, A., Casas-Catalán, M. & Osete-Cortina, L. 2001, 'Identification of lipid binders in paintings by gas chromatography: Influence of the pigments', *Journal of Chromatography A*, vol. 922, no. 1, pp. 385-90.
- Gimeno-Adelantado, J., Mateo-Castro, R., Doménech-Carbó, M., Bosch-Reig, F., Doménech-Carbo, A., De la Cruz-Canizares, J. & Casas-Catalan, M. 2002, 'Analytical study of proteinaceous binding media in works of art by gas chromatography using alkyl chloroformates as derivatising agents', *Talanta*, vol. 56, no. 1, pp. 71-7.
- Goltz, D., McClelland, J., Schellenberg, A., Attas, M., Cloutis, E. & Collins, C. 2003, 'Spectroscopic studies on the darkening of lead white', *Applied spectroscopy*, vol. 57, no. 11, pp. 1393-8.
- Gomes, H., Rosina, P., Holakooei, P., Solomon, T. & Vaccaro, C. 2013, 'Identification of pigments used in rock art paintings in Gode Roriso-Ethiopia using Micro-Raman spectroscopy', *Journal of Archaeological Science*, vol. 40, no. 11, pp. 4073-82.
- Harroun, S., Bergman, J., Jablonski, E. & Brosseau, C. 2011, 'Surface-enhanced Raman spectroscopy analysis of house paint and wallpaper samples from an 18th century historic property', *Analyst*, vol. 136, no. 17, pp. 3453-60.
- Herbst, W. & Hunger, K. 2002, *Industrial Organic Pigments: Production, Properties, Applications*, Wiley-VCH, Germany.
- Hiltz, J.A. 2015, 'Analytical pyrolysis gas chromatography/mass spectrometry (Py-GC/MS) of poly(ether urethane)s, poly(ether urea)s and poly(ether urethane-urea)s', *Journal of Analytical and Applied Pyrolysis*, vol. 113, pp. 248-58.

- Howard, D.L., de Jonge, M.D., Lau, D., Hay, D., Varcoe-Cocks, M., Ryan, C.G., Kirkham, R., Moorhead, G., Paterson, D. & Thurrowgood, D. 2012, 'High-definition X-ray fluorescence elemental mapping of paintings', *Analytical chemistry*, vol. 84, no. 7, pp. 3278-86.
- Hutanu, D., Woods, A.G. & Darie, C.C. 2013, 'Recent Applications of Mass Spectrometry in Paint Analysis', *Modern Chemistry & Applications*, vol. 1, no. 3, pp. 1-3.
- Izzo, F.C. 2010, '20th century artists' oil paints: A chemical-physical survey', PhD thesis, University Ca Foscari, Venice.
- Izzo, F.C., Balliana, E., Pinton, F. & Zendri, E. 2014, 'A preliminary study of the composition of commercial oil, acrylic and vinyl paints and their behaviour after accelerated ageing conditions', *Conservation Science in Cultural Heritage*, vol. 14, no. 1, pp. 353-69.
- Joseph, E., Prati, S., Sciutto, G., Ioele, M., Santopadre, P. & Mazzeo, R. 2010, 'Performance evaluation of mapping and linear imaging FTIR microspectroscopy for the characterisation of paint cross sections', *Analytical and Bioanalytical Chemistry*, vol. 396, no. 2, pp. 899-910.
- Jurasekova, Z., Domingo, C., Garcia-Ramos, J.V. & Sanchez-Cortes, S. 2008, 'In situ detection of flavonoids in weld-dyed wool and silk textiles by surface-enhanced Raman scattering', *Journal of Raman Spectroscopy*, vol. 39, no. 10, pp. 1309-12.
- Kaszowska, Z., Malek, K., Pańczyk, M. & Mikołajska, A. 2013, 'A joint application of ATR-FTIR and SEM imaging with high spatial resolution: Identification and distribution of painting materials and their degradation products in paint cross sections', *Vibrational Spectroscopy*, vol. 65, pp. 1-11.
- Keck, S. & Peters, T. 1969, 'Identification of protein-containing paint media by quantitative amino acid analysis', *Studies in Conservation*, vol. 14, no. 2, pp. 75-82.
- Kendix, E., Prati, S., Joseph, E., Sciutto, G. & Mazzeo, R. 2009, 'ATR and transmission analysis of pigments by means of far infrared spectroscopy', *Analytical and Bioanalytical Chemistry*, vol. 394, no. 4, pp. 1023-32.
- Kimpe, K., Jacobs, P. & Waelkens, M. 2002, 'Mass spectrometric methods prove the use of beeswax and ruminant fat in late Roman cooking pots', *Journal of chromatography A*, vol. 968, no. 1, pp. 151-60.
- Kopecká, I. & Svobodová, E. 2014, 'Methodology for infrared spectroscopy analysis of sandwich multilayer samples of historical materials', *Heritage Science*, vol. 2, no. 1, pp. 1-8.

- Lau, D., Livett, M. & Prawer, S. 2008, 'Application of surface-enhanced Raman spectroscopy (SERS) to the analysis of natural resins in artworks', *Journal of Raman Spectroscopy*, vol. 39, no. 4, pp. 545-52.
- Learner, T. 1996, 'The characterisation of acrylic painting materials and implications for their use, conservation and stability', PhD thesis, Birkbeck (University of London).
- Learner, T. 2000, 'A review of synthetic binding media in twentieth-century paints', *The Conservator*, vol. 24, no. 1, pp. 96-103.
- Learner, T. 2004, *Analysis of modern paints*, Getty Conservation Institute, Los Angeles.
- Learner, T. 2007, *Modern Paints Uncovered: Proceedings from the Modern Paints Uncovered Symposium*, Getty Conservation Institute, Los Angeles.
- Lee, P.C. & Meisel, D. 1982, 'Adsorption and surface-enhanced Raman of dyes on silver and gold sols', *The Journal of Physical Chemistry*, vol. 86, no. 17, pp. 3391-5.
- Leona, M., Decuzzi, P., Kubic, T.A., Gates, G. & Lombardi, J.R. 2011, 'Nondestructive identification of natural and synthetic organic colorants in works of art by surface enhanced Raman scattering', *Analytical chemistry*, vol. 83, no. 11, pp. 3990-3.
- Leona, M. & Lombardi, J.R. 2007, 'Identification of berberine in ancient and historical textiles by surface-enhanced Raman scattering', *Journal of Raman Spectroscopy*, vol. 38, no. 7, pp. 853-8.
- Leona, M., Stenger, J. & Ferloni, E. 2006, 'Application of surface-enhanced Raman scattering techniques to the ultrasensitive identification of natural dyes in works of art', *Journal of Raman Spectroscopy*, vol. 37, no. 10, pp. 981-92.
- Ling, H., Maiqian, N., Chiavari, G. & Mazzeo, R. 2007, 'Analytical characterization of binding medium used in ancient Chinese artworks by pyrolysis–gas chromatography/mass spectrometry', *Microchemical Journal*, vol. 85, no. 2, pp. 347-53.
- Llamas, R. & Talamantes, M.C. 2014, 'An analytical study of polypropylene as a support for paint layers. From concept to material in contemporary art', *Journal of Cultural Heritage*, vol. 15, no. 2, pp. 136-43.
- Lliveras-Tenorio, A., Mazurek, J., Restivo, A., Colombini, M.P. & Bonaduce, I. 2012a, 'Analysis of plant gums and saccharide materials in paint samples: comparison of GC-MS analytical procedures and databases', *Chemistry Central Journal*, vol. 6, no. 1, pp. 115-30.

- Lliveras-Tenorio, A., Mazurek, J., Restivo, A., Colombini, M.P. & Bonaduce, I. 2012b, 'The Development of a New Analytical Model for the Identification of Saccharide Binders in Paint Samples', *PLoS ONE*, vol. 7, no. 11, p. e49383.
- Lliveras, A., Bonaduce, I., Andreotti, A. & Colombini, M.P. 2010, 'GC/MS Analytical Procedure for the Characterization of Glycerolipids, Natural Waxes, Terpenoid Resins, Proteinaceous and Polysaccharide Materials in the Same Paint Microsample Avoiding Interferences from Inorganic Media', *Analytical Chemistry*, vol. 82, no. 1, pp. 376-86.
- Lomax, S.Q. & Learner, T. 2006, 'A Review of the Classes, Structures, and Methods of Analysis of Synthetic Organic Pigments', *Journal of the American Institute for Conservation*, vol. 45, no. 2, pp. 107-25.
- Loon, A.V. 2008, 'Color changes and chemical reactivity in seventeenth-century oil paintings', PhD thesis, University of Amsterdam.
- López-Gil, A., Ruiz-Moreno, S. & Miralles, J. 2006, 'Optimum acquisition of Raman spectra in pigment analysis with IR laser diode and pulsed UV irradiation', *Journal of Raman Spectroscopy*, vol. 37, no. 10, pp. 966-73.
- Madariaga, J.M. 2015, 'Analytical chemistry in the field of cultural heritage', *Analytical Methods*, vol. 7, no. 12, pp. 4848-76.
- Mantler, M. & Schreiner, M. 2000, 'X-ray fluorescence spectrometry in art and archaeology', *X-Ray Spectrometry*, vol. 29, no. 1, pp. 3-17.
- Manzano, E., García-Atero, J., Dominguez-Vidal, A., Ayora-Cañada, M.J., Capitán-Vallvey, L.F. & Navas, N. 2012, 'Discrimination of aged mixtures of lipidic paint binders by Raman spectroscopy and chemometrics', *Journal of Raman Spectroscopy*, vol. 43, no. 6, pp. 781-6.
- Maor, Y. & Murray, A. 2007, 'Delamination of Oil Paints on Acrylic Grounds', *MRS Proceedings*, vol. 1047, pp. 1047-Y04-01.
- Marinach, C., Papillon, M.-C. & Pepe, C. 2004, 'Identification of binding media in works of art by gas chromatography–mass spectrometry', *Journal of Cultural Heritage*, vol. 5, no. 2, pp. 231-40.
- Martin de Fonjaudran, C., Nevin, A., Piqué, F. & Cather, S. 2008, 'Stratigraphic analysis of organic materials in wall painting samples using micro-FTIR attenuated total reflectance and a novel sample preparation technique', *Analytical and Bioanalytical Chemistry*, vol. 392, no. 1-2, pp. 77-86.

- Mateo-Castro, R., Gimeno-Adelantado, J., Bosch-Reig, F., Domenech-Carbo, A., Casas-Catalan, M., Osete-Cortina, L., De la Cruz-Canizares, J. & Domenech-Carbo, M. 2001, 'Identification by GC-FID and GC-MS of amino acids, fatty and bile acids in binding media used in works of art', *Fresenius Journal of Analytical Chemistry*, vol. 369, no. 7-8, pp. 642-6.
- Mayer, R. & Sheehan, S. 1991, *The artist's handbook of materials and techniques*, Faber & Faber, London, United Kingdom.
- Mazzeo, R., Joseph, E., Prati, S. & Millemaggi, A. 2007, 'Attenuated Total Reflection–Fourier transform infrared microspectroscopic mapping for the characterisation of paint cross-sections', *Analytica Chimica Acta*, vol. 599, no. 1, pp. 107-17.
- Mazzeo, R., Roda, A. & Prati, S. 2011, 'Analytical chemistry for cultural heritage: a key discipline in conservation research', *Analytical and Bioanalytical Chemistry*, vol. 399, no. 9, pp. 2885-7.
- McGlinchey, C. 2012, 'Handheld XRF for the examination of paintings: proper use and limitations', in A.N. Shugar & J.L. Mass (eds), *Handheld XRF for Art and Archaeology*, vol. 3, Leuven University Press, Belgium.
- Mills, J.S. & White, R. 1994, *The organic chemistry of museum objects*, Butterworth-Heinemann, Great Britain.
- Mottram, H.R., Dudd, S.N., Lawrence, G., Stott, A.W. & Evershed, R.P. 1999, 'New chromatographic, mass spectrometric and stable isotope approaches to the classification of degraded animal fats preserved in archaeological pottery', *Journal of Chromatography A*, vol. 833, no. 2, pp. 209-21.
- Namowicz, C., Trentelman, K. & McGlinchey, C. 2009, 'XRF of cultural heritage materials: Round-robin IV—paint on canvas', *Powder Diffraction*, vol. 24, no. Special Issue 02, pp. 124-9.
- Nevin, A., Osticioli, I., Anglos, D., Burnstock, A., Cather, S. & Castellucci, E. 2008, 'The analysis of naturally and artificially aged protein-based paint media using Raman spectroscopy combined with Principal Component Analysis', *Journal of Raman Spectroscopy*, vol. 39, no. 8, pp. 993-1000.
- Oakley, L.H., Dinehart, S.A., Svoboda, S.A. & Wustholz, K.L. 2011, 'Identification of organic materials in historic oil paintings using correlated extractionless surface-enhanced

- Raman scattering and fluorescence microscopy', *Analytical chemistry*, vol. 83, no. 11, pp. 3986-9.
- Ormsby, B. & Learner, T. 2009, 'The effects of wet surface cleaning treatments on acrylic emulsion artists' paints—a review of recent scientific research', *Studies in Conservation*, vol. 54, no. sup1, pp. 29-41.
- Osete-Cortina, L., Doménech-Carbó, M., Mateo-Castro, R., Gimeno-Adelantado, J. & Bosch-Reig, F. 2004, 'Identification of diterpenes in canvas painting varnishes by gas chromatography–mass spectrometry with combined derivatisation', *Journal of Chromatography A*, vol. 1024, no. 1, pp. 187-94.
- Osete-Cortina, L. & Doménech-Carbó, M.T. 2006, 'Characterization of acrylic resins used for restoration of artworks by pyrolysis-silylation-gas chromatography/mass spectrometry with hexamethyldisilazane', *Journal of chromatography A*, vol. 1127, no. 1, pp. 228-36.
- Osticioli, I., Zoppi, A. & Castellucci, E.M. 2006, 'Fluorescence and Raman spectra on painting materials: reconstruction of spectra with mathematical methods', *Journal of Raman Spectroscopy*, vol. 37, no. 10, pp. 974-80.
- Pallipurath, A., Vófély, R.V., Skelton, J., Ricciardi, P., Bucklow, S. & Elliott, S. 2014, 'Estimating the concentrations of pigments and binders in lead-based paints using FT-Raman spectroscopy and principal component analysis', *Journal of Raman Spectroscopy*, vol. 45, no. 11-12, pp. 1272-8.
- Pitthard, V. & Finch, P. 2001, 'GC-MS analysis of monosaccharide mixtures as their diethyldithioacetal derivatives: Application to plant gums used in art works', *Chromatographia*, vol. 53, no. 1, pp. S317-S21.
- Pitthard, V., Griesser, M., Stanek, S. & Bayerova, T. 2006, 'Study of complex organic binding media systems on artworks applying GC-MS analysis: selected examples from the Kunsthistorisches Museum, Vienna', *Macromolecular symposia*, vol. 238, Wiley Online Library, pp. 37-45.
- Plater, M.J., De Silva, B., Gelbrich, T., Hursthouse, M.B., Higgitt, C.L. & Saunders, D.R. 2003, 'The characterisation of lead fatty acid soaps in 'protrusions' in aged traditional oil paint', *Polyhedron*, vol. 22, no. 24, pp. 3171-9.
- Ploeger, R., Scalarone, D. & Chiantore, O. 2008, 'The characterization of commercial artists' alkyd paints', *Journal of Cultural Heritage*, vol. 9, no. 4, pp. 412-9.

- Poldi, G. & Caglio, S. 2013, 'Phthalocyanine identification in paintings by reflectance spectroscopy. A laboratory and in situ study', *Optics and Spectroscopy*, vol. 114, no. 6, pp. 929-35.
- Potts, P.J. & West, M. 2008, *Portable X-ray Fluorescence Spectrometry: Capabilities for in Situ Analysis*, The Royal Society of Chemistry, Cambridge, United Kingdom.
- Pouyet, E., Lluveras-Tenorio, A., Nevin, A., Saviello, D., Sette, F. & Cotte, M. 2014, 'Preparation of thin-sections of painting fragments: Classical and innovative strategies', *Analytica Chimica Acta*, vol. 822, no. 0, pp. 51-9.
- Pozzi, F. & Leona, M. 2016, 'Surface-enhanced Raman spectroscopy in art and archaeology', *Journal of Raman Spectroscopy*, vol. 47, no. 1, pp. 67-77.
- Pozzi, F., Porcinai, S., Lombardi, J.R. & Leona, M. 2013, 'Statistical methods and library search approaches for fast and reliable identification of dyes using surface-enhanced Raman spectroscopy (SERS)', *Analytical Methods*, vol. 5, no. 16, pp. 4205-12.
- Pozzi, F., Shibayama, N., Leona, M. & Lombardi, J.R. 2013, 'TLC-SERS study of Syrian rue (*Peganum harmala*) and its main alkaloid constituents', *Journal of Raman Spectroscopy*, vol. 44, no. 1, pp. 102-7.
- Prati, S., Joseph, E., Sciutto, G. & Mazzeo, R. 2010, 'New Advances in the Application of FTIR Microscopy and Spectroscopy for the Characterization of Artistic Materials', *Accounts of Chemical Research*, vol. 43, no. 6, pp. 792-801.
- Prati, S., Sciutto, G., Catelli, E., Ashashina, A. & Mazzeo, R. 2013, 'Development of innovative embedding procedures for the analyses of paint cross sections in ATR FTIR microscopy', *Analytical and Bioanalytical Chemistry*, vol. 405, no. 2-3, pp. 895-905.
- Price, B.A. & Pretzel, B. 2007, 'Infrared and Raman Users Group Spectral Database', 20 June 2014 edn, vol. 1 & 2, Philadelphia.
- Prinsloo, L.C., Tournié, A., Colombari, P., Paris, C. & Bassett, S.T. 2013, 'In search of the optimum Raman/IR signatures of potential ingredients used in San/Bushman rock art paint', *Journal of Archaeological Science*, vol. 40, no. 7, pp. 2981-90.
- Rampazzi, L., Cariati, F., Tanda, G. & Colombini, M.P. 2002, 'Characterisation of wall paintings in the Sos Furrighesos necropolis (Anela, Italy)', *Journal of Cultural Heritage*, vol. 3, no. 3, pp. 237-40.
- Regert, M., Langlois, J. & Colinart, S. 2005, 'Characterisation of wax works of art by gas chromatographic procedures', *Journal of Chromatography A*, vol. 1091, no. 1, pp. 124-36.

- Rizzo, A. 2008, 'Progress in the application of ATR-FTIR microscopy to the study of multi-layered cross-sections from works of art', *Analytical and Bioanalytical Chemistry*, vol. 392, no. 1-2, pp. 47-55.
- Robinet, L. & Corbeil, M.-C. 2003, 'The Characterization of Metal Soaps', *Studies in Conservation*, vol. 48, no. 1, pp. 23-40.
- Rosi, F., Paolantoni, M., Clementi, C., Doherty, B., Miliani, C., Brunetti, B.G. & Sgamellotti, A. 2010, 'Subtracted shifted Raman spectroscopy of organic dyes and lakes', *Journal of Raman Spectroscopy*, vol. 41, no. 4, pp. 452-8.
- Russell, J., Singer, B.W., Perry, J.J. & Bacon, A. 2011, 'The identification of synthetic organic pigments in modern paints and modern paintings using pyrolysis-gas chromatography-mass spectrometry', *Analytical and bioanalytical chemistry*, vol. 400, no. 5, pp. 1473-91.
- Rutherford, J.G. & Stout, G.L. 1966, *Painting Materials: A Short Encyclopedia*, New York: Dover.
- Sarmiento, A., Pérez-Alonso, M., Olivares, M., Castro, K., Martínez-Arkarazo, I., Fernández, L.A. & Madariaga, J.M. 2011, 'Classification and identification of organic binding media in artworks by means of Fourier transform infrared spectroscopy and principal component analysis', *Analytical and Bioanalytical Chemistry*, vol. 399, no. 10, pp. 3601-11.
- Saunders, D. & Kirby, J. 2004, 'The effect of relative humidity on artists' pigments', *National Gallery Technical Bulletin*, vol. 25, pp. 62-72.
- Scalarone, D. & Chiantore, O. 2004, 'Separation techniques for the analysis of artists' acrylic emulsion paints', *Journal of Separation Science*, vol. 27, no. 4, pp. 263-74.
- Scherrer, N.C., Stefan, Z., Françoise, D., Annette, F. & Renate, K. 2009, 'Synthetic organic pigments of the 20th and 21st century relevant to artist's paints: Raman spectra reference collection', *Spectrochimica Acta Part A: Molecular and Biomolecular Spectroscopy*, vol. 73, no. 3, pp. 505-24.
- Schilling, M. 2005, 'Paint media analysis', *Scientific Examination of Art: Modern Techniques in Conservation and Analysis: Proceedings of the National Academy of Sciences (PNAS)*, pp. 186-205.
- Sciutto, G., Prati, S., Bonacini, I., Oliveri, P. & Mazzeo, R. 2014, 'FT-NIR microscopy: An advanced spectroscopic approach for the characterisation of paint cross-sections', *Microchemical Journal*, vol. 112, pp. 87-96.

- Scott, D.A., Warmlander, S., Mazurek, J. & Quirke, S. 2009, 'Examination of some pigments, grounds and media from Egyptian cartonnage fragments in the Petrie Museum, University College London', *Journal of Archaeological Science*, vol. 36, no. 3, pp. 923-32.
- Sessa, C., Bagán, H. & García, J.F. 2013, 'Evaluation of MidIR fibre optic reflectance: Detection limit, reproducibility and binary mixture discrimination', *Spectrochimica Acta Part A: Molecular and Biomolecular Spectroscopy*, vol. 115, pp. 617-28.
- Sessa, C., Bagán, H. & García, J.F. 2014, 'Influence of composition and roughness on the pigment mapping of paintings using mid-infrared fiberoptics reflectance spectroscopy (mid-IR FORS) and multivariate calibration', *Analytical and bioanalytical chemistry*, vol. 406, no. 26, pp. 6735-47.
- Severin, K.P. 2004, *Energy dispersive spectrometry of common rock forming minerals*, Kluwer Academic, Boston; Dordrecht.
- Shackley, M.S. 2010, *X-Ray Fluorescence Spectrometry (XRF) in Geoarchaeology*, Springer New York.
- Shadi, I.T., Chowdhry, B.Z., Snowden, M.J. & Withnall, R. 2004, 'Semi-quantitative analysis of alizarin and purpurin by surface-enhanced resonance Raman spectroscopy (SERRS) using silver colloids', *Journal of Raman Spectroscopy*, vol. 35, no. 8-9, pp. 800-7.
- Shedrinsky, A.M., Wampler, T.P., Indictor, N. & Baer, N.S. 1989, 'Application of analytical pyrolysis to problems in art and archaeology: A review', *Journal of Analytical and Applied Pyrolysis*, vol. 15, pp. 393-412.
- Shugar, A.N. & Mass, J.L. 2012, *Handheld XRF for Art and Archaeology*, vol. 3, Leuven University Press, Belgium.
- Silva, M.F., Doménech-Carbó, M.T., Fuster-Lopéz, L., Martín-Rey, S. & Mecklenburg, M.F. 2009, 'Determination of the plasticizer content in poly (vinyl acetate) paint medium by pyrolysis–silylation–gas chromatography–mass spectrometry', *Journal of Analytical and Applied Pyrolysis*, vol. 85, no. 1, pp. 487-91.
- Singer, B. & McGuigan, R. 2007, 'The simultaneous analysis of proteins, lipids, and diterpenoid resins found in cultural objects', *Annali di chimica*, vol. 97, no. 7, pp. 405-17.
- Smith, B.C. 2011, *Fundamentals of Fourier Transform Infrared Spectroscopy*, Taylor & Francis Inc, Boca Roca, United States.
- Smith, G.D. & Clark, R.J. 2004, 'Raman microscopy in archaeological science', *Journal of Archaeological Science*, vol. 31, no. 8, pp. 1137-60.

- Smith, G.D., Newton, K.E. & Altherr, L. 2015, 'Hydrofluoric acid pre-treatment of matte artists' paints for binding medium analysis by Fourier transform infrared microspectroscopy', *Vibrational Spectroscopy*, vol. 81, pp. 46-52.
- Solé, V., Papillon, E., Cotte, M., Walter, P. & Susini, J. 2007, 'A multiplatform code for the analysis of energy-dispersive X-ray fluorescence spectra', *Spectrochimica Acta Part B: Atomic Spectroscopy*, vol. 62, no. 1, pp. 63-8.
- Sonoda, N. 1999, 'Characterization of organic azo-pigments by pyrolysis–gas chromatography', *Studies in Conservation*, vol. 44, no. 3, pp. 195-208.
- Spring, M., Ricci, C., Peggie, D. & Kazarian, S. 2008, 'ATR-FTIR imaging for the analysis of organic materials in paint cross sections: case studies on paint samples from the National Gallery, London', *Analytical and Bioanalytical Chemistry*, vol. 392, no. 1-2, pp. 37-45.
- Standeven, A.L.H. 2011, *House paints, 1900-1960: history and use*, Getty Conservation Institute, Los Angeles.
- Steele, V.J., Stern, B. & Stott, A.W. 2010, 'Olive oil or lard?: Distinguishing plant oils from animal fats in the archeological record of the eastern Mediterranean using gas chromatography/combustion/isotope ratio mass spectrometry', *Rapid communications in Mass spectrometry*, vol. 24, no. 23, pp. 3478-84.
- Stevanato, R., Rovea, M., Carbini, M., Favretto, D. & Traldi, P. 1997, 'Curie-point Pyrolysis/Gas Chromatography/Mass Spectrometry in the Art Field. Part 3: The Characterization of Some Non-proteinaceous Binders', *Rapid Communications in Mass Spectrometry*, vol. 11, no. 3, pp. 286-94.
- Stuart, B.H. 2007, *Analytical Techniques in Materials Conservation*, John Wiley & Sons Ltd.
- Sutherland, K. 2010, 'Bleached shellac picture varnishes: characterization and case studies', *Journal of the Institute of Conservation*, vol. 33, no. 2, pp. 129-45.
- Tamayo, S.N., Andres, J.V. & Pons, J.O. 2013, 'Applications of reflectance transformation imaging for documentation and surface analysis in conservation', *International Journal of Conservation Science*.
- Tan, H., Tian, H., Verbeeck, J., Monico, L., Janssens, K. & Van Tendeloo, G. 2013, 'Nanoscale Investigation of the Degradation Mechanism of a Historical Chrome Yellow Paint by Quantitative Electron Energy Loss spectroscopy Mapping of Chromium Species', *Angewandte Chemie International Edition*, vol. 52, no. 43, pp. 11360-3.

- Targowski, P. & Iwanicka, M. 2012, 'Optical Coherence Tomography: its role in the non-invasive structural examination and conservation of cultural heritage objects—a review', *Applied Physics A*, vol. 106, no. 2, pp. 265-77.
- Tommaso, P., Chiantore, O., Giovagnoli, A. & Piccirillo, A. 2012, 'FTIR imaging investigation in MIR and in an enlarged MIR–NIR spectral range', *Analytical and Bioanalytical Chemistry*, vol. 402, no. 9, pp. 2977-84.
- Townsend, J. & Boon, J. 2012, 'Research and Instrumental Analysis in the Materials of Easel Paintings', in R. Rushfield & J.H. Stoner (eds), *The Conservation of Easel Paintings*, Routledge: London and New York, pp. 341-65.
- Tumosa, C.S. & Mecklenburg, M.F. 2005, 'The influence of lead ions on the drying of oils', *Studies in Conservation*, vol. 50, no. sup1, pp. 39-47.
- Tuschel, D. 2016, 'Selecting an Excitation Wavelength for Raman Spectroscopy', *Spectroscopy*, vol. 31, no. 3, pp. 14-23.
- Vahur, S., Ulla, K. & Leito, I. 2009, 'ATR-FT-IR spectroscopy in the region of 500–230cm⁻¹ for identification of inorganic red pigments', *Spectrochimica Acta Part A: Molecular and Biomolecular Spectroscopy*, vol. 73, no. 4, pp. 764-71.
- Vallance, S.L., Singer, B., Hitchen, S. & Townsend, J. 1998, 'The development and initial application of a gas chromatographic method for the characterization of gum media', *Journal of the American Institute for Conservation*, vol. 37, no. 3, pp. 294-311.
- Van der Weerd, J., H. B., J. Jaap, B. & Ron M.A., H. 2002, 'Fourier Transform Infrared Microscopic Imaging of an Embedded Paint Cross-Section', *Applied Spectroscopy*, vol. 56, no. 3, pp. 275-83.
- Van der Weerd, J., Heeren, R.M.A. & Boon, J.J. 2004, 'Preparation Methods and Accessories for the Infrared Spectroscopic Analysis of Multi-Layer Paint Films', *Studies in Conservation*, vol. 49, no. 3, pp. 193-210.
- Vandenabeele, P., Castro, K., Hargreaves, M., Moens, L., Madariaga, J.M. & Edwards, H.G.M. 2007, 'Comparative study of mobile Raman instrumentation for art analysis', *Analytica Chimica Acta*, vol. 588, no. 1, pp. 108-16.
- Vandenabeele, P., Edwards, H.G.M. & Moens, L. 2007, 'A Decade of Raman Spectroscopy in Art and Archaeology', *Chemical Reviews*, vol. 107, no. 3, pp. 675-86.
- Vandenabeele, P. & Moens, L. 2003, 'Micro-Raman spectroscopy of natural and synthetic indigo samples', *Analyst*, vol. 128, no. 2, pp. 187-93.

- Vandenabeele, P., Moens, L., Edwards, H.G.M. & Dams, R. 2000, 'Raman spectroscopic database of azo pigments and application to modern art studies', *Journal of Raman Spectroscopy*, vol. 31, no. 6, pp. 509-17.
- Vandenabeele, P., Wehling, B., Moens, L., Edwards, H., De Reu, M. & Van Hooydonk, G. 2000, 'Analysis with micro-Raman spectroscopy of natural organic binding media and varnishes used in art', *Analytica Chimica Acta*, vol. 407, no. 1–2, pp. 261-74.
- Vetter, W. & Schreiner, M. 2011, 'Characterization of Pigment-Binding Media Systems—Comparison of Non-Invasive in-situ Reflection FTIR with Transmission FTIR Microscopy', *e-Preservation Science*, vol. 8, pp. 10-22.
- Von Aderkas, E.L., Barsan, M.M., Gilson, D.F. & Butler, I.S. 2010, 'Application of photoacoustic infrared spectroscopy in the forensic analysis of artists' inorganic pigments', *Spectrochimica Acta Part A: Molecular and Biomolecular Spectroscopy*, vol. 77, no. 5, pp. 954-9.
- Wei, S., Pintus, V. & Schreiner, M. 2012, 'Photochemical degradation study of polyvinyl acetate paints used in artworks by Py–GC/MS', *Journal of Analytical and Applied Pyrolysis*, vol. 97, pp. 158-63.
- Wei, S., Pintus, V. & Schreiner, M. 2013, 'A comparison study of alkyd resin used in art works by Py-GC/MS and GC/MS: The influence of aging', *Journal of Analytical and Applied Pyrolysis*, vol. 104, pp. 441-7.
- White, R.E. 2007, 'Conservation of 19th and early 20th century oil paintings: Studies of pigment discolouration by scanning electron microscopy', PhD thesis, University Technology Sydney.
- Wong, L. & Agnew, N. 2013, *The conservation of Cave 85 at the Mogao Grottoes, Dunhuang : a collaborative project of the Getty Conservation Institute and the Dunhuang Academy*, Getty Conservation Institute, Los Angeles.
- Wustholz, K.L., Brosseau, C.L., Casadio, F. & Van Duyne, R.P. 2009, 'Surface-enhanced Raman spectroscopy of dyes: from single molecules to the artists' canvas', *Physical Chemistry Chemical Physics*, vol. 11, no. 34, pp. 7350-9.
- Yu, J. & Butler, I.S. 2015, 'Recent applications of infrared and Raman spectroscopy in art forensics: A brief overview', *Applied Spectroscopy Reviews*, vol. 50, no. 2, pp. 152-7.

A close-up photograph of a ceremonial object, likely a mask or headdress, featuring vibrant red, blue, and tan pigments. The red pigment is the most prominent, covering the upper right portion of the object. The blue pigment is applied in a more textured, layered fashion, particularly on the left side. The tan pigment is visible at the bottom left, appearing as a rough, fibrous material. The overall texture is highly detailed and intricate.

Chapter 3

Characterisation of paint
materials on ceremonial
objects from the Highlands of
Papua New Guinea

3.1 Background

The heritage of Papua New Guinea (PNG) is one of the world's most culturally diverse. With over 700 different languages, populations were largely isolated from one another, developing distinct cultures. This indigenous group is well-known for their artistic ability to create hand-made cultural objects with unusual motifs, shapes and designs used for their rituals and traditional ceremonies. Their works have captivated collectors worldwide and countless have been actively acquired by foreign museums since the 1880s, continuing to the late 20th century (Hill 2001). Amongst these massive collections, less attention was given to colourfully painted ceremonial objects in the Highlands, where living communities were previously not known to exist until the recent 1930s. A rare collection of elaborate ceremonial objects such as battle shields, figurines, masks and headdresses collected by Australian Stanley Moriarty from various parts of the Highlands between 1961 and 1972, are presently placed in the custody and care of the Art Gallery of New South Wales (AGNSW).

The study of objects in this collection was initiated by the preparation of an exhibition of the Moriarty collection by the AGNSW. Although considerable efforts by curatorial and conservation staff had been carried out while preparing for the exhibition entitled “Plumes and Pearlshells: Art of the New Guinea Highlands” (Wilson 2014), material documentation could only be inferred by eye, oral interviews and past anecdotal research, which may not be considered truly complete without the evidence from scientific analysis. Primarily, little was understood about the nature of materials in this diverse collection and questions relating to the materiality remain unanswered. In particular, the possible inclusion of a rare blue vivianite pigment, an iron phosphate mineral of apparent natural origin, first drew interest to the scientific analysis of blue paints. A visual survey shows that the paints appear to encompass different shades of colours, including a number of brightly coloured paints probably of synthetic origin. However, no scientific study had been devoted to the analysis of the pigments that formed the colour palette of the Highlands. Also, the analysis of binders in

the paints was also of concern, as binders affect the colour appearance, paint adherence and ageing properties, which ultimately affects the permanence and conservation of paint. Some paints appeared to be loosely bound to the substrate, while some others adhered extremely well. For those that are loosely bound, it is questionable if the adherence after decades is based only on the layered structural property of clay, or if a binder does exist but in lesser amounts. A few paints also appeared particularly glossy than others. In the Highlands, the use of pig fat or tigaso oil to impart opacity and sheen to the ceremonial objects has been reported and it may be that the glossy paints observed contain such lipid or resinous binders (Hill 2011; Strathern & Strathern 1971). While most of the works are well-preserved, a few demonstrated extreme degradation such as flaking paint and mould infestation. Objects such as dance banners and headdresses were made without the intention to preserve for long term. After use, they were discarded to degrade in the natural environment. Sometimes, these “used objects” were reused. New coats of paint applied over old paints were believed to contain magical power that revived the object. One of the shields in the AGNSW collection showed similar signs of reuse, as the outer paint layers peeling off reveals other coloured layers beneath.

Facing such a diverse collection of materials that potentially include both natural and synthetic origins, it is beneficial to confirm the identity of these materials from the scientific perspective as well as to relate the findings to the Highlanders’ tradition in making ceremonial objects. This is especially crucial in light that the art of making ceremonial objects is fast disappearing and only some are made for entertainment purposes in the Garoka and Mount Hagen festivals today (Boylan, Moriarty & Wilson 2014). The issue of insufficient or inaccurate documentation has been encountered in museums worldwide, where ceremonial objects extensively acquired from other parts of Papua New Guinea since the 1880s have marked them as artefacts ineligible for museum display (Hill 2001). To prevent this undesirable situation, a conscientious effort in providing an accurate documentation and meaning to the PNG Highlands collections was made at the AGNSW. Documentation of these

Highlands collections is, however, an issue that was found difficult to address at the AGNSW, considering that these objects were collected from a large number of over 300 language groups in the Highlands and names of places have changed. Furthermore, attributing the material on a specific artwork based on its provenance has its uncertainty, as it is possible that the objects shifted in location from where Moriarty collected the work and that past anecdotal research only covered limited areas of the Highlands. By providing scientific analysis as an alternative tool, the results can contribute to accurate documentation. Amongst scientific publications, only two publications contained in-depth technical analysis on two PNG ceremonial masks collected in the early 1930s (Baraldi et al. 2014; Harrison et al. 2005). Yet, these works do not originate from the Highlands and the coverage of materials are limited to PNG masks. Thus, the scientific analysis of paints on the PNG Highlands collections is reported for the first time when a substantial number of objects were analyzed in detail using micro-characterisation techniques.

This study presents the characterization of a range of natural and synthetic pigments, binders and organic degradation products from inherent and biological sources in micro-sized paints extracted from fifty ceremonial objects collected from various parts of the Highlands, by means of FTIR, Raman spectroscopy coupled with microscopy, and in some samples, with SEM-EDS, XRD and GC/MS. Samples are usually analysed directly by the instrumentation, whereas for some heterogeneous samples, a solvent extraction or pretreatment with HF was carried out to remove interferences of inorganic materials, prior to binder identification by FTIR and Raman spectroscopy.

3.2 Materials and Methods

3.2.1 Techniques that eliminate interference for binder identification

3.2.1.1 Solvent extraction

Where only a few grains of samples were available, a solvent extraction method adapted from Teetsov (Teetsov 2006) was applied. A few grains of powder sample (about 100-300 μm) were transferred to a cleaned glass slide using a stereo-microscope. 10-30 μL of solvent was added adjacent to the powder sample. This step may be repeated, depending on the volatility of solvent. After the solvent evaporated, the residue from the periphery of the solvent droplet was scraped off and analysed by FTIR or Raman microscopy. This method is only applicable when substantial amounts of binder is present in the micro-sample. A low binder to pigment ratio may make it difficult to separate the binder from the solid residue. In certain cases, no residue was observed after solvent evaporation. This may mean that the solvent used is not appropriate, or a binder does not exist.

Where more sample is available, the binder was extracted with a solvent method adapted from Sarmiento et al. (Sarmiento et al. 2011), modified to suit even smaller sized samples. The powder sample (about 1 mm) was transferred into a micro-volume glass insert with cone-shaped bottom. 200 μL of solvent was added, vortexed and ultrasonicated to extract the binder into the liquid phase. After centrifugation, 30 μL of the supernatant was dropped onto a cleaned glass slide. When the solvent has evaporated, the residual film was scraped off and analyzed by FTIR or Raman microscopy. After centrifugation, the supernatant may be passed through PVDF filter, but it was found that this step was not always necessary as most samples produce the same spectral bands even without passing through PVDF filter. In some samples, clay particles can be finer than the PVDF filters of 0.45 μm pore size and were not effectively removed.

Hexane, chloroform, methanol, acetone (Honeywell, analytical grade) were used as solvents. As solvents may leave a residue upon evaporation, blank solvent controls were carried out to ensure negligible contamination to the interpretation of binder.

3.2.1.2 HF pretreatment

A few grains of powdered sample (about 100-300 μm) were placed on a Teflon cap liner. Following the procedure from Smith et al. (Smith, Newton & Altherr 2015), a drop of 10 % HF was placed adjacent to the sample and a Teflon lined vial cap was capped over the sample and HF droplet to create a HF chamber. After 2 h, the cap was removed and HF was allowed to evaporate in a fumehood overnight. The sample was then transferred to a diamond cell for FTIR analysis. This method is effective for removing silicates and carbonates, but does not eliminate absorptions due to sulphates and synthetic organic pigments.

3.2.2 Fourier-Transform Infrared Spectroscopy

FTIR spectra in transmission mode were obtained using a Thermo Scientific Nicolet Magna 6700 spectrometer coupled to Nic-Plan IR microscope with a liquid nitrogen-cooled mercury cadmium telluride (MCT) detector. The powder samples were compressed between two diamond half-cells and focused on the microscope stage. The FTIR acquisition was set at 128 scans in the range of 4000–650 cm^{-1} , the resolution being 4 cm^{-1} .

3.2.3 Raman spectroscopy

Raman analyses were carried out with a Renishaw InVia spectrometer system configured with a Leica DMLB microscope, notch filters, and a thermoelectrically cooled charged-coupled device (CCD) detector. Neutral density filters were used to set the laser power at the sample to values between 0.2 mW and 0.38 mW for the 514 nm laser, between 0.075 and 1.5 mW for the 785 nm laser and between 0.1 and 1 mW for the 633 nm laser. The integration times vary from 10 s to 320 s. The sample powders were placed on a clean glass slide or stainless steel and the laser beam was focused on different sample spots using mainly a 50X objective.

3.2.4 Scanning Electron Microscope-Energy Dispersive Spectroscopy

A Zeiss Evo LS15 SEM equipped with a Bruker EDS Quantax 400 with silicon drift detector (SDD) for high speed elemental analysis. The accelerating voltage was set between 10 and 20 kV and the working distance at 10 mm. Analyses of paint samples were carried out under partial vacuum at 120 Pa. Samples were mounted as loose powders on carbon stubs.

3.2.5 X-ray diffraction

The X-ray powder diffraction patterns were obtained using a Siemens D 5000 diffractometer with Cu K α radiation, $\lambda = 1.5406 \text{ \AA}$. The data were recorded from 3° to 70° in 2 θ at a voltage of 40 KV, current of 30 mA, and step length of 0.04°. The identification was performed by comparing the obtained patterns with the patterns established by the International Centre for Diffraction data (ICDD).

3.2.6 Gas Chromatography /Mass Spectrometry

About 0.1 mg of sample was weighed in a 2 mL scintillation glass vial. 240 μL of chloroform was added, vortexed and ultrasonicated to extract the binder. Chloroform solvent was evaporated with a gentle stream of pure nitrogen. The residual sample is derivatised with 50 μL BSTFA (1 % TMCS) for 70°C, 15 min, evaporated to dryness and reconstituted in 60 μL chloroform. 1 μL of derivatised sample is injected into the GC/MS.

A GC 6890 (Agilent) coupled with 5973 quadruple mass spectrometer operated in EI positive mode was used. Chromatograms were obtained at total ion chromatogram (TIC) mode in full scan. A GC non-polar column ZB-5-MS (5% diphenyl-95% dimethylpolysiloxane) 30 m x 0.25 mm x 0.25 μm film thickness was fitted. The carrier gas (purity 99.995%) through the GC is kept at 1.2 mL/min. High purity ethyl acetate is used for pre- and post-washes of autosampler syringe needle. The oven temperature starts at 50°C, held for 2 min, then ramped at 10°C/min to 250°C, held isothermal at 2 min, then ramped at 4°C/min to 290°C and held isothermal for 4 min.

3.3 Results and Discussion

The diversity of materials dealt with in the PNG Highlands collections is categorised according to the chemical nature in Fig. 3.1. In the following sections 3.3.1-3.3.6, the characterisation results are presented by highlighting exemplar data from selected ceremonial objects.

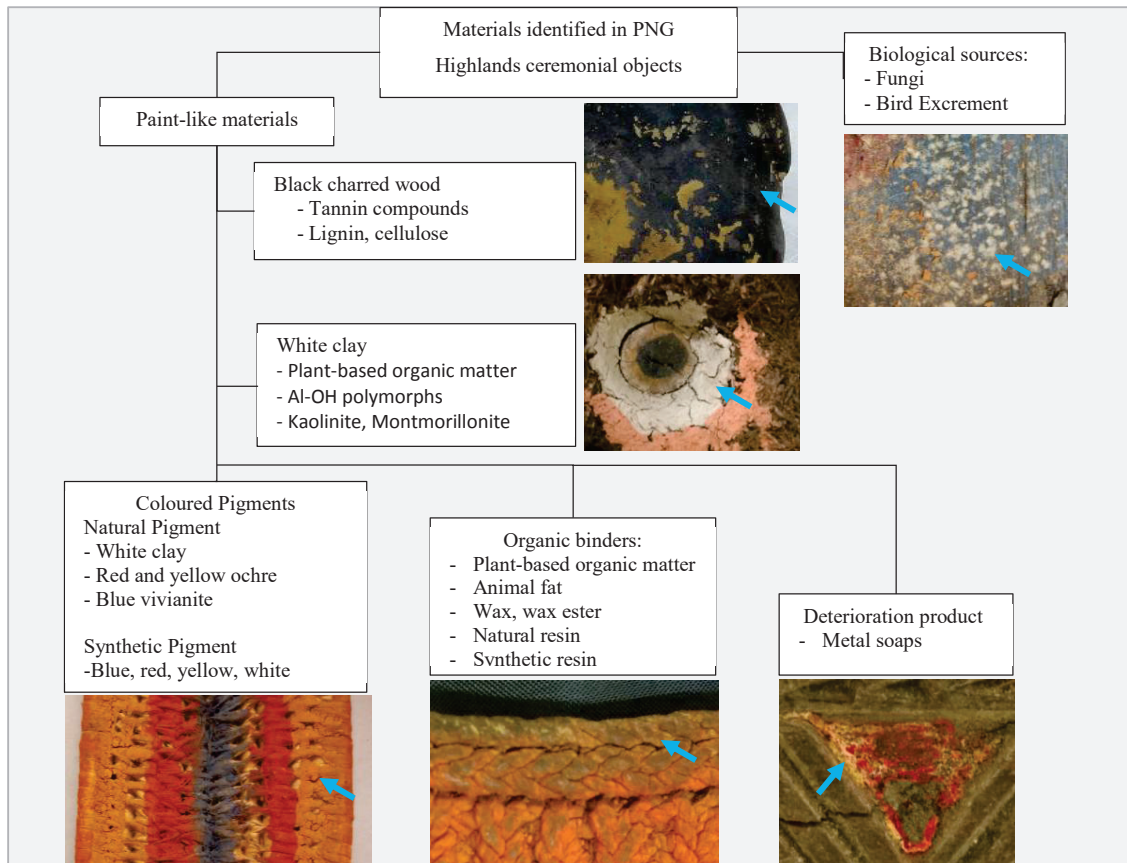


Fig. 3.1 Materials identified in PNG Highlands ceremonial objects.

Photos of sampled areas in these painted objects are shown in Table 3.1 below. Full image photos of the ceremonial objects can be located by searching for the accession number in the AGNSW collections website (*Art Gallery of NSW*).

Table 3.1 Photos of sampled areas of painted ceremonial objects collected from PNG Highlands

#239.1977

Mask

Gourd, human hair, burr seeds, tigaso oil,
plant resin, plant fibres, coix seeds



#18.2005

Timbu wara

Woven vegetable fibre, cane, blue vivianite
and red ochre



#240.1977

Gourd mask

Gourd, clay, charred wood, CaCO₃,
synthetic blue, yellow and red pigments



#242.1977

Female Figure

Wood, blue vivianite, red and yellow ochre,
diterpenoid resin, human hair, cassowary
feathers, gourd, plant fibre, black seeds,
machine-made beads, plastic, mollusk shell,
gold-lipped oyster shell, pig tail, plaited
split rattan, plant resin, bamboo, stone,
sledge grass



#243.1977

Timbu Wara

Coiled plant fibre, cane, blue vivianite, red
and yellow ochre

#245.1977

Ceremonial Hat

Cane, fibre, clay, red ochre and blue
vivianite



#580.1979

Timbu wara

Coiled plant fibre, cane, blue vivianite, red and yellow ochre



#258.1978

Shield with arrows

Wood, red ochre, charred wood, chalk, clay, plant fibre, feathers, split rattan, dried leaves and flowers



#260.1978

Shield

Wood, charred wood, red ochre, clay, ultramarine blue, synthetic red pigment, punctuated designs, plant fibres, rattan sling, remains of arrow



#265.1977

Shield

Wood, bamboo, machine-wove sling, synthetic red pigment, clay, charred wood, acrylic resin (conservation material)



#272.1978

Sacred stone (Front)

Stone, red and yellow ochre, charred wood, clay, pork fats

Sacred stone (Back)



#278.1978

Ceremonial house board

Carved balsa wood, red synthetic pigment, ultramarine blue, green synthetic alkyd, plant fibre

#279.1977

Mortar

Stone, blue vivianite



#283.1978

Yupini

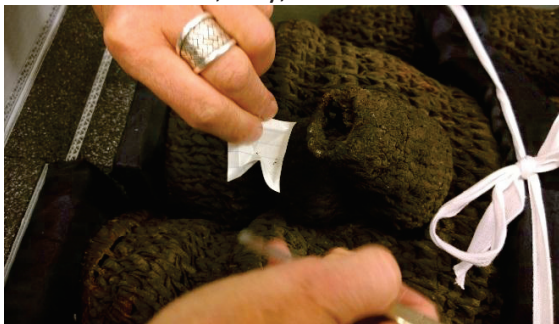
Woven, coiled and plaited plant fibre, black (charred wood), yellow ochre, red ochre, clay, iron nails



#287.1978

Gourd mask with human hair

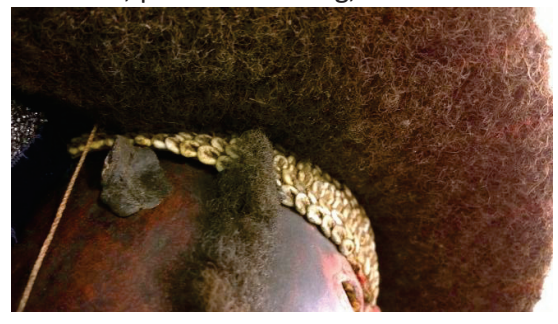
Gourd, synthetic red pigment, wax, human hair, seeds, mammalian teeth, plant resin, wood, plant fibre string, nassa shells



#290.1977

Tree fern head

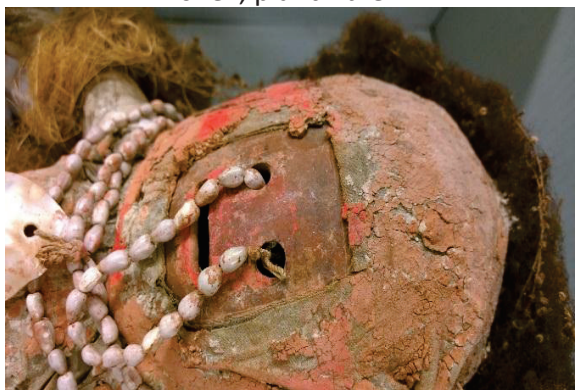
Tree fern, shells, bird feathers, pig tusks, mammalian teeth, clay, red ochre, plant fibre string



#294.1977

Female figure doll

Gourd, synthetic red pigment, clay, human hair, machine-woven cotton fabric, plant fibre string, coix seeds, gold-lipped oyster shell, plant fibre



#302.1978

Shield

Wood, red ochre, clay, bird excrement



#319.1978

Moka kin

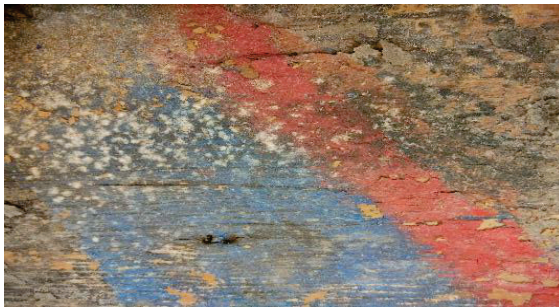
Gold-lipped oyster shell, kilt tree resin, red ochre, bamboo



#490.1979

Shield

White mould, synthetic red pigment, ultramarine blue, plant fibre, dried leaf sheath



#522.1979

Armband

Carved wood, traces of synthetic red and yellow pigment, blue ultramarine and zinc soaps



#533.1979

Bark belt wallet

Incised bark, zinc oleate soaps in white incrustation, synthetic red pigment



#553.1979

Judge's wig

Bark on cane frame, human hair, kilt tree resin, green beetles, plant fibre, synthetic yellow, red pigment and ultramarine blue pigment, clay, bird feathers



#248.1977

Apron adorning

Plant fibre string, synthetic red and yellow pigment, tigaso oil, plaited split-rattan chains, pig tails



#666.1979

Mortar

Stone, calcium & potassium soaps in white incrustation



#818.1979

Effigy

Wood, synthetic red and yellow pigment, cotton, plant fibre, marsupial fur, mammalian skin, coix seeds, feather, gold-lipped oyster shell, cone shell, printed paper



#821.1979

Gourd mask

Gourd, diterpenoid resin, human hair, ultramarine blue, synthetic red and yellow pigment



3.3.1 White clays

The white paint samples collected were found to be mostly composed of a clay matrix applied to contrast the other colours or mixed in with other paint colours. With the microscope, they appear yellowish white, probably due to an impurity from a goethite or organic binder. With FTIR spectroscopy, the white clay matrix is shown to be primarily

composed of kaolinite and quartz, while some contain montmorillonite and Al-OH polymorphs (Fig. 3.2). Samples of white clays and other colours containing clay (e.g. ochres) give a strong fluorescence in Raman spectroscopy. For the white clay samples, this does not appear to minimize even after hours of quenching or with use of a near infrared laser. The poor scattering is likely due to very fine particle size of clay minerals, which were further obscured in the high fluorescence background due to organic impurities present in clay, giving a poor signal acquisition in the Raman spectrum (Wang, Haskin & Jolliff 1998).

Aside from the inorganic silicate vibrations, a number of white clay samples shows two weak, broad C-O or C=C absorption bands at ≈ 1650 and ≈ 1410 - 1435 cm^{-1} , along with methylene stretching at 2920 , 2850 cm^{-1} , that suggests the presence of an organic matter. More details of this organic matter are provided in Section 3.3.4.

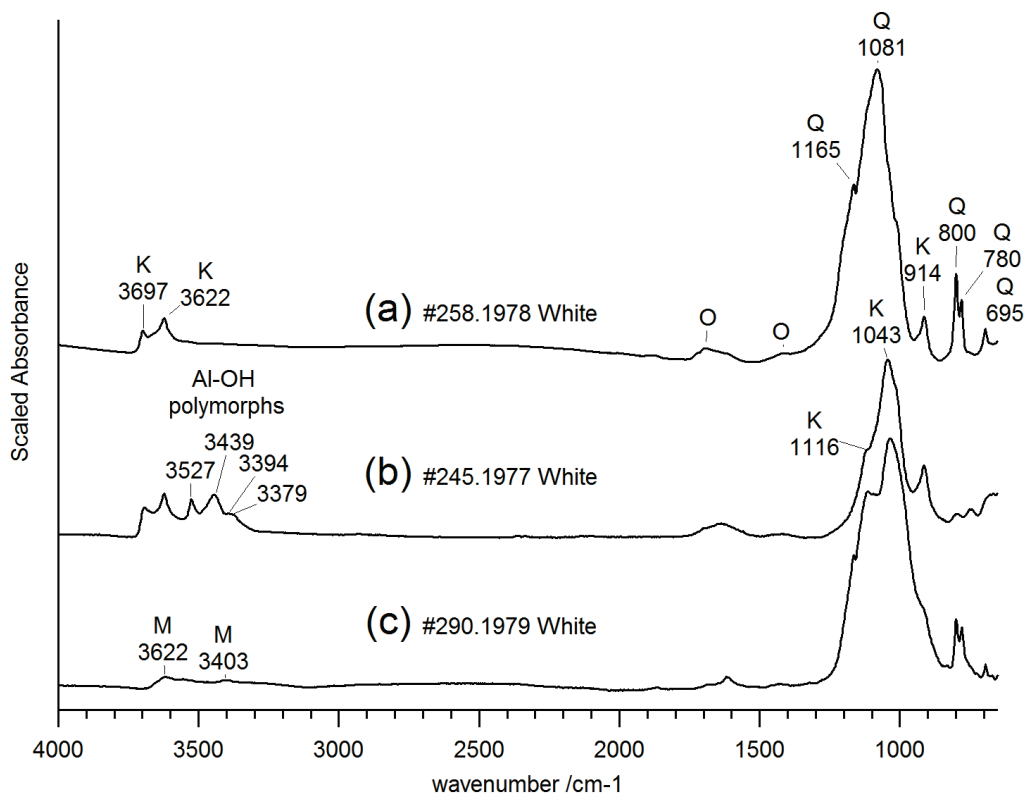


Fig. 3.2 FTIR spectra of white clay samples from (a) #258.1978 shield, (b) #245.1977 ceremonial hat, (c) #290.1979 tree fern head, where K = kaolinite, O = organic matter, Q = quartz, M = montmorillonite.

3.3.2 Black charred wood

The FTIR spectra of the black specimens show mainly charred wood (Fig. 3.3). The FTIR spectrum of a wood fibre that has not been charred is shown as a comparison, where cellulose and lignin band features are indicated (Fig. 3.3a). When wood is charred, subtle differences in the relative intensities between 1705 and 1604 cm^{-1} were observed, possibly due to the differences in the time length of heating and temperature (Fig. 3.3b-d). Although some lignin and cellulose bands are retained after charring, slight spectral shifts are likely attributed to tannin compounds released from heating of wood, which appear at 1604, 1515, 1456, 1215 and 1041 cm^{-1} (Falcão & Araújo 2013). There are an uncountable number of different tannins. Bands possibly due to hydrolysable tannins (polymers containing a polyol sugar core multi-esterified with gallic acid) and condensed tannins (polymeric flavonoids) are also indicated. The charred wood particles are completely soluble in water, giving a yellow brown solution characteristic of tannins. A few black samples gave a completely different spectrum (Fig. 3.3e), where the lignin and cellulose bands disappear and the absorptions coalesce into strong and broad bands, centering around 1596 and 1429 cm^{-1} . Such a phenomenon could be explained by prolonged heating at high temperatures (Rutherford, Wershaw & Cox 2005). Black charred wood particles can also be found as particles contaminating or mixed into other paint colours. Calcium carbonate was also detected in one of the black charred woods from the *shield* (#258.1978), which explains its matte appearance.

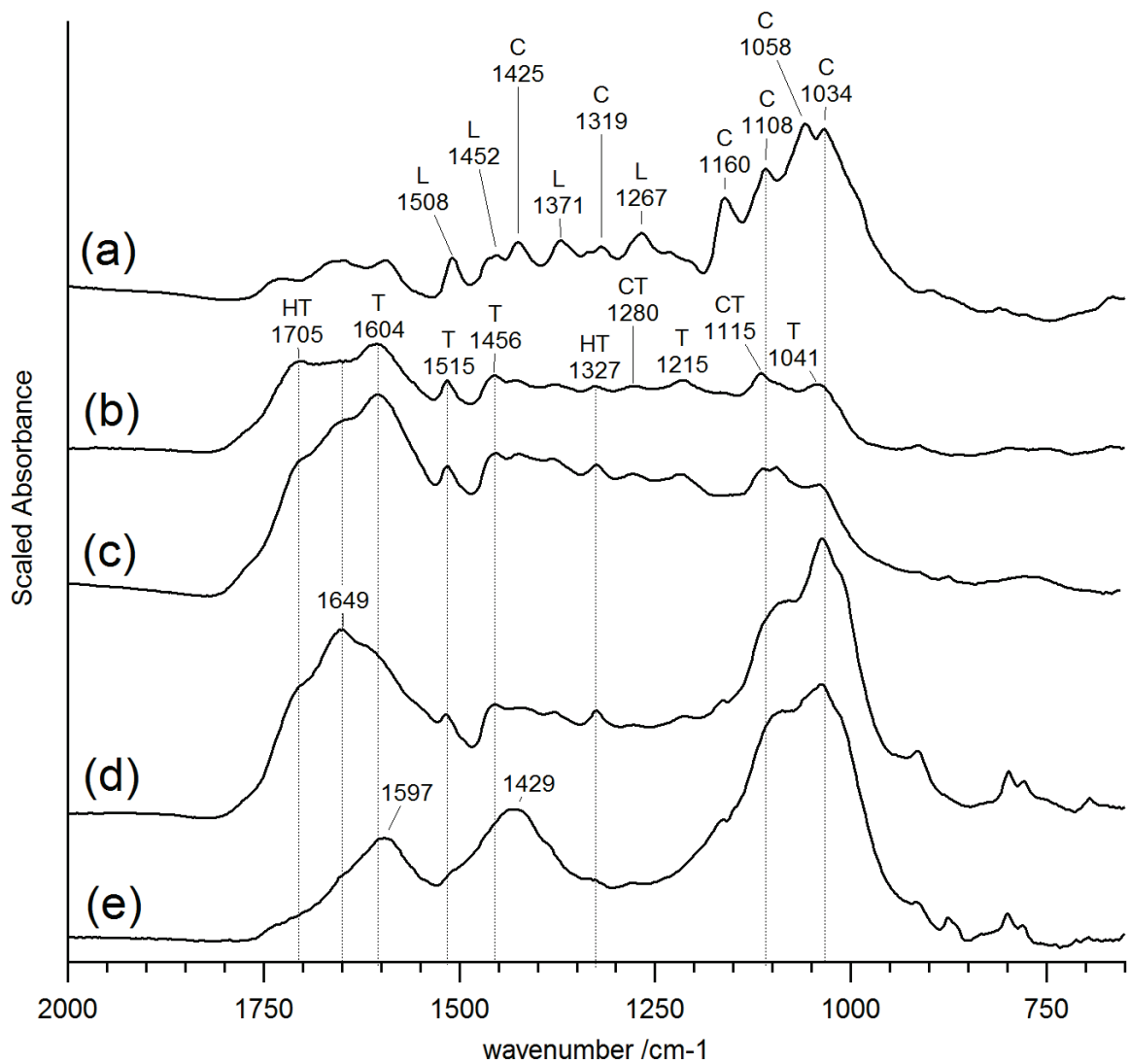
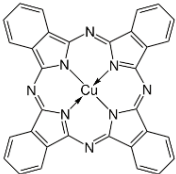
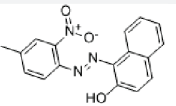
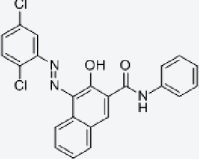
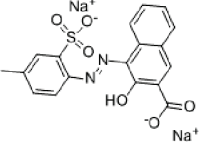
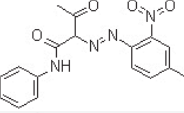
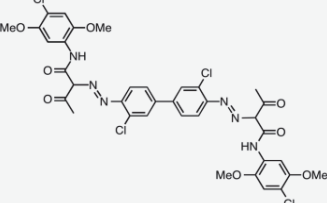


Fig. 3.3 FTIR spectra of (a) fibre obtained from plant substrate of *Shield* (#490.1979) (b) black undercoat obtained from *Shield* (#265.1977), (c) black particles that filled the woven plant fibre, on left arm of *Yupini* (#283.1978), (d) black particles obtained from grey paint on *Shield* (#260.1978) and (e) black particles obtained from the black areas of *Sacred Stone* (#272.1978); L= lignin, C= cellulose, T= tannin, HT= hydrolysable tannin, CT= condensed tannin.

3.3.3. Coloured pigments

A broad range of coloured pigments have been identified on artefacts collected from the Highlands of Papua New Guinea in this study and results are tabulated in Table 3.2.

Table 3.2 Coloured pigments identified in the artefacts collected from the PNG Highlands.

Colour	Pigment	Chemical formula/ structure
Blue	vivianite	$\text{Fe}^{2+}_3(\text{PO}_4)_2 \cdot 8\text{H}_2\text{O}$
	PB29 ultramarine blue	$\text{Na}_2\text{O}8\text{Al}_2\text{O}_3 \cdot \text{SiO}_2$
	PB27 prussian blue	$\text{Fe}_4[\text{Fe}(\text{CN})_6]_3 \cdot n\text{H}_2\text{O}$
	PB15 phthalocyanine blue	
Red	red ochre	Fe_2O_3 + other inorganic oxides (e.g. SiO_2)
	PR3 toluidine red, β -naphthol	
	PR2 naphthol red	
	PR57 calcium salt of BONA (beta-oxynaphthoic acid)	
Yellow	yellow ochre	$\text{FeO}(\text{OH})$ + other inorganic oxides (e.g. SiO_2)
	PY1 monoazo yellow	
	PY83 diarylide yellow	

3.3.3.1 Blue Vivianites

Vivianite is a pale blue iron phosphate mineral ($\text{Fe}^{2+}_3(\text{PO}_4)_2 \cdot 8\text{H}_2\text{O}$) that was known to exist in different colours of blue, grey (due to reaction with oil binder) and yellow (due to photo-induced oxidation to amorphous santabarbarite) (Čermáková et al. 2013). Viana et al. also observed light to dark green with purplish green reflexes (Viana & Prado 2007). The colour shifts can be explained by a change in oxidation state of iron (Scott & Eggert 2007).

Blue vivianites in the PNG samples were characterised using a combination of SEM-EDS, FTIR and Raman spectroscopy techniques. Although vivianite is known to exist in other colours, this has not been observed in non-blue PNG samples analysed, suggesting that the mineral is unlikely altered in chemical composition. Amongst the vivianites detected in this study, the colours range from light to dark shades of blue, where the lighter colours are attributed to higher clay content.

The FTIR spectra of the blue vivianites showed absorption bands that agree with literature values (Frost et al. 2002; Henderson et al. 1984; Rodgers, Kobe & Childs 1993). A shoulder at 3460 cm^{-1} is assigned to the hydroxyl stretching of vivianite, the bands at 1050, 979 and 950 cm^{-1} are characteristic of the phosphate stretches, and a moderately strong band at around 800 cm^{-1} indicates water libration of vivianite. In some samples, the strong Si-O-Si stretching bands of clay can obscure the spectral features of vivianites.

On the other hand, Raman microscopy produced a characteristic fingerprint for all samples containing vivianite. The phosphate stretching bands at 950, 1014 and 1058 cm^{-1} correspond to literature values (Čermáková et al. 2014; Frost & Weier 2004; Piriou & Poullen 1984), but the bands below 700 cm^{-1} do not completely agree (Fig. 3.4a). These bands are attributed to a mix of vivianite, kaolinite, quartz (strong band at 463 cm^{-1}) and possibly other impurities. It was found that vivianites gave a lower fluorescence using the laser at 785 nm. With 633 nm, the power increments either burnt the sample or gave a poor signal. Vivianites are prone to oxidation, and experiments showed that the laser power has to fall below 0.1 mW in order to

avoid burning to yellow. If the laser power was too high, phosphate stretching features were lost, the overall spectral shape became slightly distorted and a large broad band appeared around 1395 cm^{-1} (Fig. 3.4b).

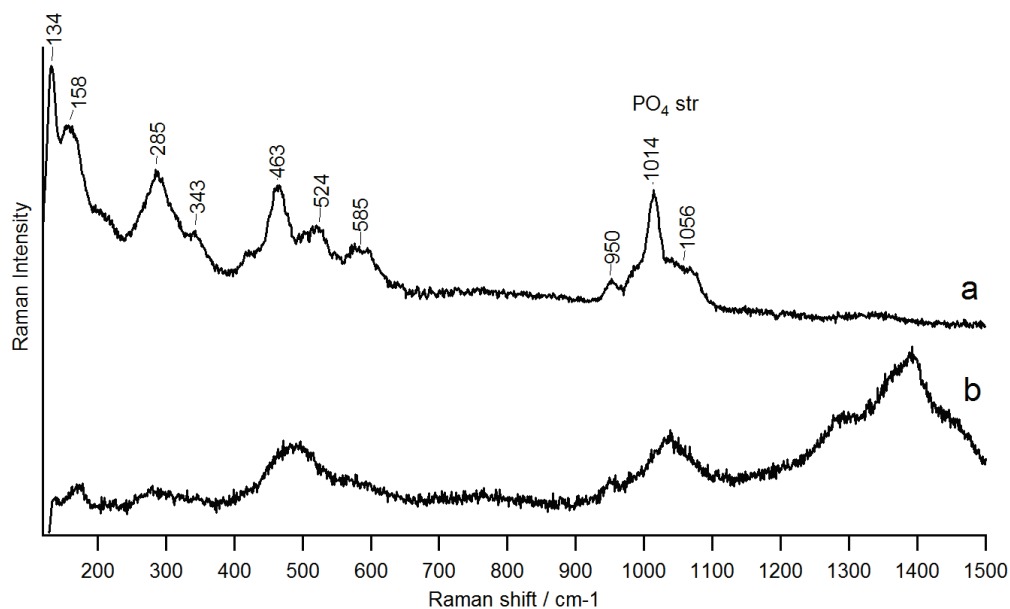


Fig. 3.4 Raman spectra of blue vivianite sample taken from *Timbu wara* (#580.1979), (a) 785 nm, low power < 0.1 mW, no colour change, (b) 785 nm, higher power, discolouration to yellow.

At 785 nm, the scattering above 2700 cm^{-1} is weak and does not provide information about the oxidation state of iron in vivianite. When blue vivianite collected from *Timbu wara* (#18.2005) was analysed with 514 nm, the bands 3077 cm^{-1} and 3494 cm^{-1} appeared (Fig. 3.5a). These two bands also appeared when analyzing vivianite reference from Kremer Inc. (naturally mined from Bolivia, South America). In another blue vivianite sample collected from *Mortar* (#279.1977) (Fig. 3.5b), the hydroxyl stretching band at 3485 cm^{-1} suggests that partial oxidation of Fe^{2+} to Fe^{3+} has occurred (Čermáková et al. 2014). Vivianites can undergo self-oxidation or oxidation by air and the likely form of vivianite samples from the PNG Highlands objects is the mildly oxidized $(\text{Fe}^{2+})_{3-x}(\text{Fe}^{3+})_x(\text{PO}_4)_2(\text{OH})_x \cdot (8-x)\text{H}_2\text{O}$ (where $x < 1.2$) (Chua et al. 2016; Frost & Weier 2004).

It is generally difficult to judge if a pigment is of natural or synthetic origin, as there is no striking spectral difference between the naturally mined pigments and those produced synthetically. However, for the vivianites detected on the PNG Highlands ceremonial objects, there is sufficient evidence to attribute them as natural origin. The amount of vivianite covered substantial areas on moderately sized objects such as *Timbu waras* (around 100 x 100 cm), suggesting that Highlanders had access to a considerable amount of vivianite.

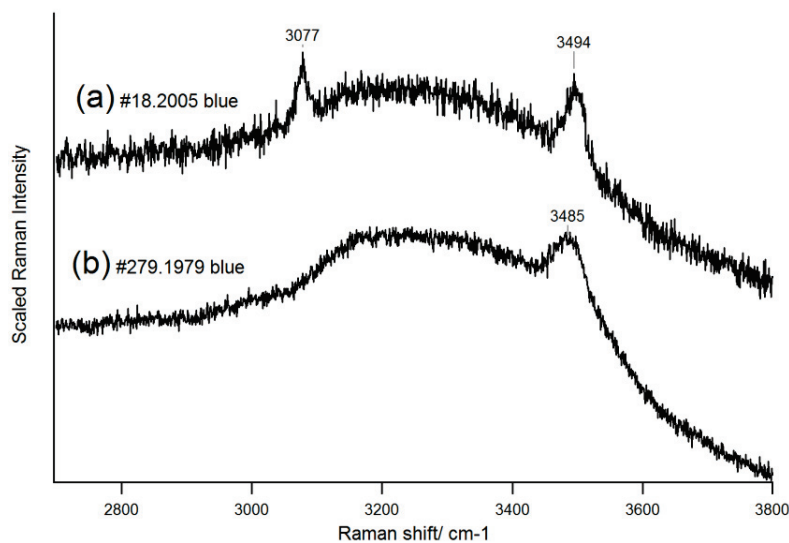


Fig. 3.5 Raman spectra of blue vivianites at 514 nm in the spectral region 2700-3800 cm^{-1} (a) blue vivianite from *Timbu wara* (#18.2005) (b) blue vivianite from *Mortar* (#279.1977), the band at 3485 cm^{-1} suggests partial oxidation of Fe^{2+} to Fe^{3+} .

Due to its rarity and hence value, it is unlikely that vivianite was introduced from foreign sources into the Highlands. According to various historical sources (Hill 2001; Hughes 1977; Strathern & Strathern 1971), natural vivianite was discovered along rivers or swamps in a few regions within the central and southern parts of PNG Highlands (Table 3.3). Even within these regions, vivianites were highly regarded and not widely traded (Hughes 1977). This is evident from the results of this study, where the vivianites identified came only from objects collected in the Southern Highlands, isolated from the other blue pigments (Fig. 3.6). In addition, the vivianites detected showed varying amounts of clay bands and a very weak

broad band between 1400-1430 cm⁻¹ in the FTIR spectrum, probably due to organic matter from groundwater, and the elemental distribution contains traces of Na, Al, Si and S, which

Table 3.3 List of natural vivianite sources in PNG Highlands

Location of source	Description of source	Trading	Trade Name	Use	Type	Source
Waghi region	Da Nigl stream in Chimbu district, Kerowagi sub-district	Yes, area larger than 648km ² , mainly to South of Dom language area	<i>Gambakum</i>	Genar Nogar tribe	Anecdotal	(Hughes 1977)
					XRD analysis (scientific data was not published)	(Hughes 1977)
Waghi region	Swamp contained a good deposit of vivianite 1.5m below ground surface, discovered around 1967-1968	No trade	-	-	Anecdotal	(Hughes 1977)
Poru region	Noiya, South of Poru River (centre of Wiru language area) and Warababe, Iaro Valley	Trade within Poru, 1295km ²	<i>Tumbo</i>	Used to decorate tall poles in ritual spirit houses in Poru. Also used in the Kewa language areas.	Anecdotal	(Hughes 1977)
Around Mount Hagen	Found "in or beside rivers" and along white and yellow clays	-	-	-	Anecdotal	(Strathern & Strathern 1971)
Mendi valley	Kewa speaking area (Poroma sub-district), tiny nodules in brown clays in river banks and creek beds	-	-	-	XRD analysis (scientific data was not published)	(Hill 2001)
-	-	Not traded nor circulated	-	Used by Mendi speakers for face painting	Anecdotal, from Mendi informants in Bela	(Hill 2001)
-	-	-	-	Used by Wiru people in arrowheads and spirit masks	Anecdotal	(Hill 2001)

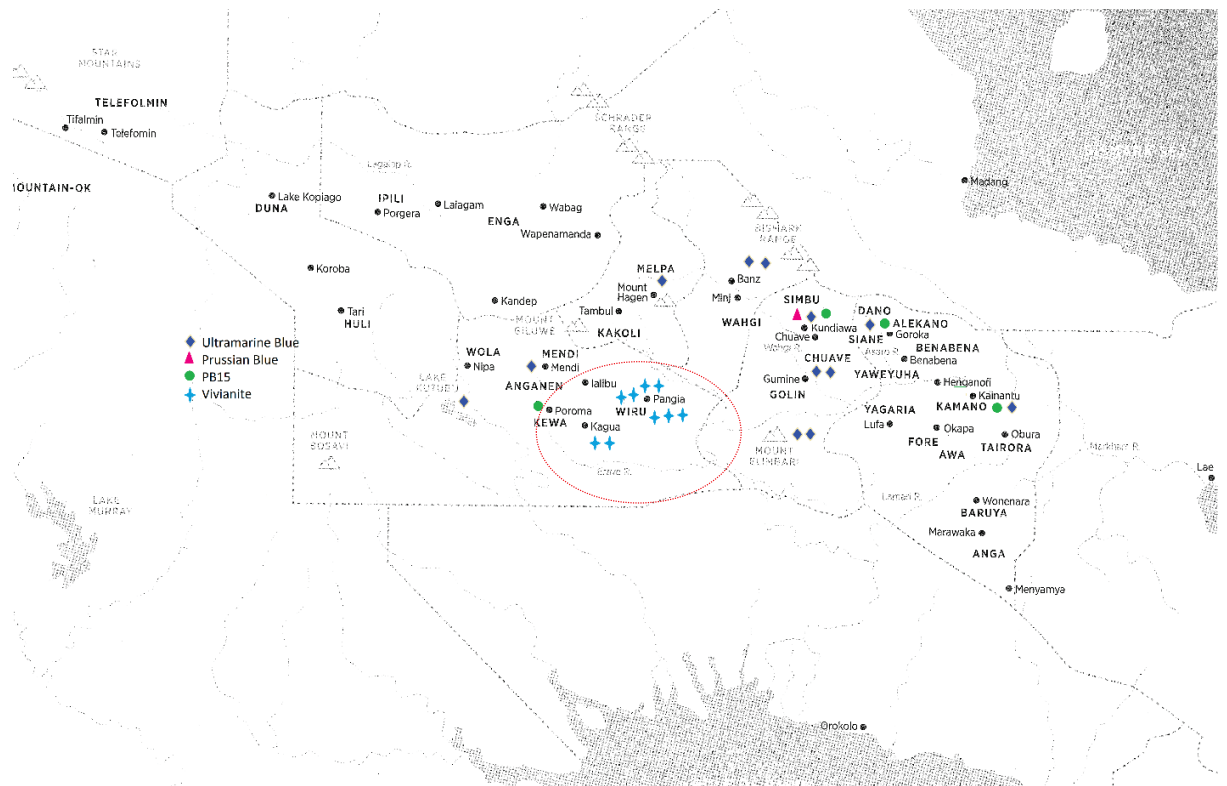


Fig. 3.6 Distribution of blue pigments detected in the ceremonial objects, collected by Moriarty from various regions of the PNG Highlands between 1961 and 1972. Red dotted circle highlights the isolated occurrence of ceremonial objects containing vivianite.

are not observed in a pure synthetic iron phosphate (Luna-Zaragoza, Romero-Guzmán & Reyes-Gutiérrez 2009). With optical microscopy, the varying crystal sizes suggest vivianite is likely of natural origin (Fig. 3.7). The spectral fingerprint of vivianites detected from the PNG Highlands objects generally agree well with vivianite obtained from Kremer Inc. (naturally mined from Bolivia, South America), as well as literature sources of natural vivianite mineral obtained from different localities (Frost et al. 2002; Henderson et al. 1984; Rodgers, Kobe & Childs 1993). However, subtle differences in vibrations below 800 cm^{-1} may be characteristic of the location in which the vivianite was mined (Frost & Weier 2004).

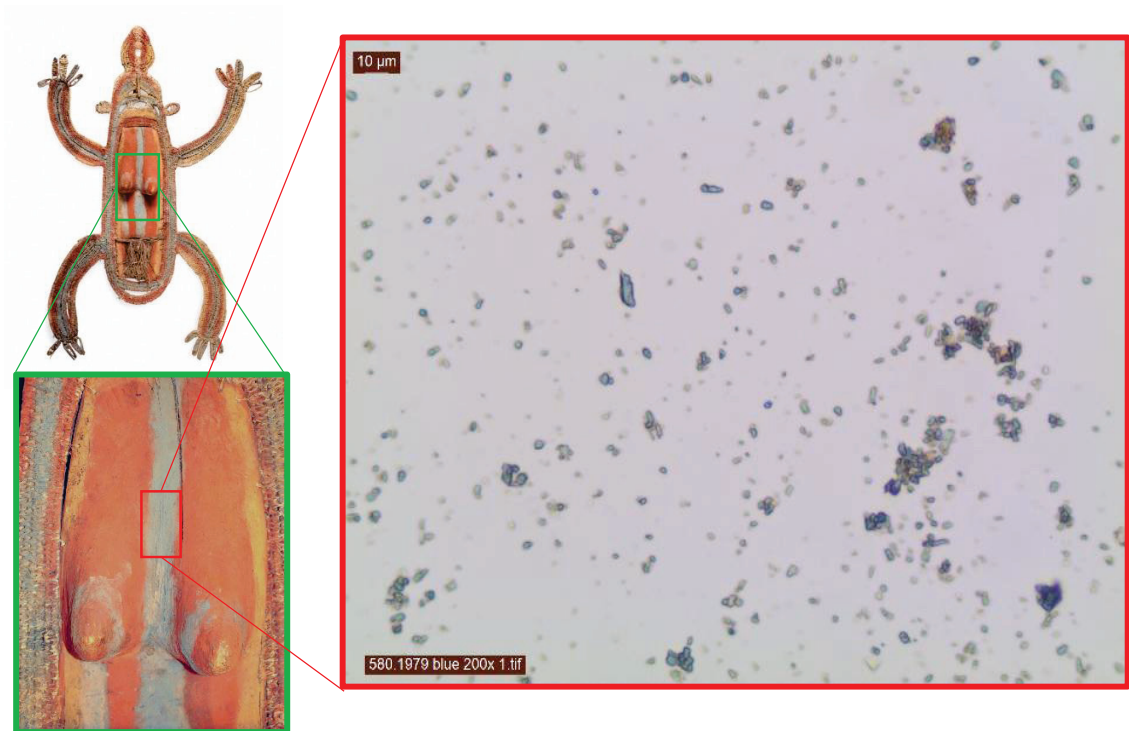


Fig. 3.7 Optical microscopic image of vivianite sample dispersed in glycerine at 200X magnification, collected from *Timbu wara* (#580.1979). Top left photo courtesy of AGNSW.

3.3.3.2 Red and Yellow ochres

Most of the reds and yellow pigments identified are ochres obtained from the natural environment. The natural origin of ochres was deduced based on the variety of clay components (kaolinite, quartz, Al-OH polymorphs) associated with the ochres. In addition, a number of red ochres showed a weak band at 2339 cm^{-1} due to interstitial carbon dioxide, which is unlikely present in a synthetic iron oxide.

To determine the pigments of the ochres, Raman spectroscopy prevails over FTIR spectroscopy. Although FTIR spectroscopy has been used for characterizing pigments in ochres, the characteristic peaks appear below 650 cm^{-1} and is not within the detectable region of the MCT detector using FTIR microscopy. Moreover, infrared bands are broad and the centre maxima of the main absorptions are very similar (≈ 477 and 547 cm^{-1} for hematite,

≈ 466 and 534 cm^{-1} for goethite, ≈ 457 and 510 cm^{-1} for quartz). The hydroxyl deformations of goethite at 900 and 800 cm^{-1} are easily obscured by sharp strong bands from kaolinite and quartz.

When analysing red ochres, the red laser 633 nm was found to give the best signal to noise ratio. It is generally difficult to obtain Raman signals from the red ochres, likely due to the high fluorescence associated with organic matter. However, by manipulating the laser power with sample bleaching and accumulation of scans, the hematite peaks can be detected. In some samples, characteristic Raman bands of hematite shifted to lower wavenumbers. The Raman shifts can be explained by variation in crystallinity and grain size, as well as the laser power used (de Faria, Venâncio Silva & de Oliveira 1997; Wang, Haskin & Jolliff 1998).

The Raman analysis of pigment in yellow ochres was not always successful with 633 or 785 nm laser, likely due to the high amounts of clay content. A yellow ochre reference sample from Kremer Inc. gives an excellent Raman spectrum, but when applied onto the PNG yellow ochre samples, it is generally not possible to obtain a reasonable signal. Power of laser cannot be set too high, as that leads to laser-induced phase transformation to hematite. Nevertheless, limonite in one of the yellow ochres was successfully characterised with Raman spectroscopy using 514 nm while XRD detected lepidocrocite ($\gamma\text{-FeOOH}$) as well as goethite in other yellow ochre samples.

3.3.3.3 Synthetic Pigments

Amongst the synthetic pigment palette, the synthetic organic pigments (SOPs) identified include red (PR3, PR2, PR57), yellow (PY1, PY83), ultramarine blue (PB29) phthalocyanine blue (PB15), Prussian blue (PB27) and rutile. To distinguish the PB15 variants is difficult as their spectra are very similar. Although Scherrer et al. employed specific flow chart markers to differentiate the variants, Fremout and Saverwyns showed that this method has ambiguity (Fremout & Saverwyns 2012; Scherrer et al. 2009). Intensity ratios of characteristic PB15 bands in the Raman spectrum do not compare well with literature values and were unable to

be differentiated (Defeyt et al. 2012). Moreover, differentiating PB15 polymorphs was highlighted as a problematic task when only Raman spectroscopy was used (Centeno 2015). Hence, it is preferred to keep the identification to the class PB15. SOPs show up particularly well with either Raman or FTIR spectroscopy. As some of the SOPs are mixed with gypsum and binders that interfere its identification in the FTIR spectrum, the identification of SOPs are generally confirmed with Raman spectroscopy. When different SOPs are present in the same paint sample, the principle of superposition may not hold and some bands are suppressed while some may be accentuated, making it problematic to characterise the pigments based on comparison to known peaks (Breitman, Ruiz-Moreno & Gil 2007). This may explain why the identification of the red and yellow SOPs in the orange paint of the gourd mask #240.1977 was not affirmative. Amongst the titanium whites, anatase and rutile are identified. The rutile version is commonly encountered in commercial paints and is likely a synthetic origin, whereas anatase could be an impurity from the clay mineral. The inorganic ultramarine blue identified was verified to come from a synthetic origin, based on the uniform and small pigment sizes observed with optical microscopy. The consistent appearance of filler BaSO₄ detected along with ultramarine blue exclude its possibility as 'laundry blue', which is a synthetic ultramarine pigment without BaSO₄ content.

Amongst the synthetic pigments identified, ultramarine blue, PR3 and PY1 dominated the palette. In fact, the frequent occurrence of these pigments identified on numerous objects, especially PR3, suggests its widespread distribution across the Highlands. These pigments are likely obtained from trade stores as powder packets or as gifts from patrol officers for the services rendered (Ballard 1994). At that time, many areas were still designated as restricted zones where patrol officers had access, suggesting that the movement of these synthetic pigments was related to the route of patrol officers. Comparing the distribution map of headquarters, sub-district posts and patrol posts of colonial officers in the Highlands in 1966 (Robson 1954, 1958, 1961, 1964, 1966, 1969), it was found that the widespread identification

of PR3 came from similar regions (Fig. 3.8a and 3.8b), demonstrating the impact of colonialism.

3.3.4 Binders

3.3.4.1 Plant-based organic matter

In some red ochre samples, the FTIR spectra show broad and strong bands at 1653, 1425, 1323 cm^{-1} that indicate the presence of an organic matter. An example FTIR spectrum of these samples is shown in Fig. 3.9a. These broad bands are not likely due to interstitial water as the centre maxima is different from water vibrations and CH vibrations are also observed. The two possible sources are plant saps or soil organic matter.

The use of plant saps to improve adhesion in paints have been reported in the PNG Highlands, whereby the leaves were rubbed against the substrate prior to paint application (Hill 2001). Plant sap is a water-soluble fluid containing a mix of soluble salts, sugars, proteins and carbohydrates. When plant cells break upon rubbing against another substrate, the sap is released in the process and acts as a binder for the pigments.

Some authors have published similar FTIR bands in soil samples, which were attributed to organic matter naturally derived in soils and ground water, broadly termed as soil organic matter (SOM) (Cox et al. 2000; Simkovic et al. 2008), while others suggest the possibility of humic substances (Dick, Santos & Ferranti 2003; Fookan & Liebezeit 2003). SOM refers to all organic fractions present in soil, including plant residues in different decomposition stages, microbial biomass, water-soluble organic matter and humic substances (a mixture of humic acid, fulvic acid and humin, produced from plant and animal decomposition and often a major source of carbon contamination carried by ground water) (Stevenson 1994). The characterisation of SOM and humic substances by mid-IR spectroscopy had been extensively reviewed (Tinti et al. 2015).

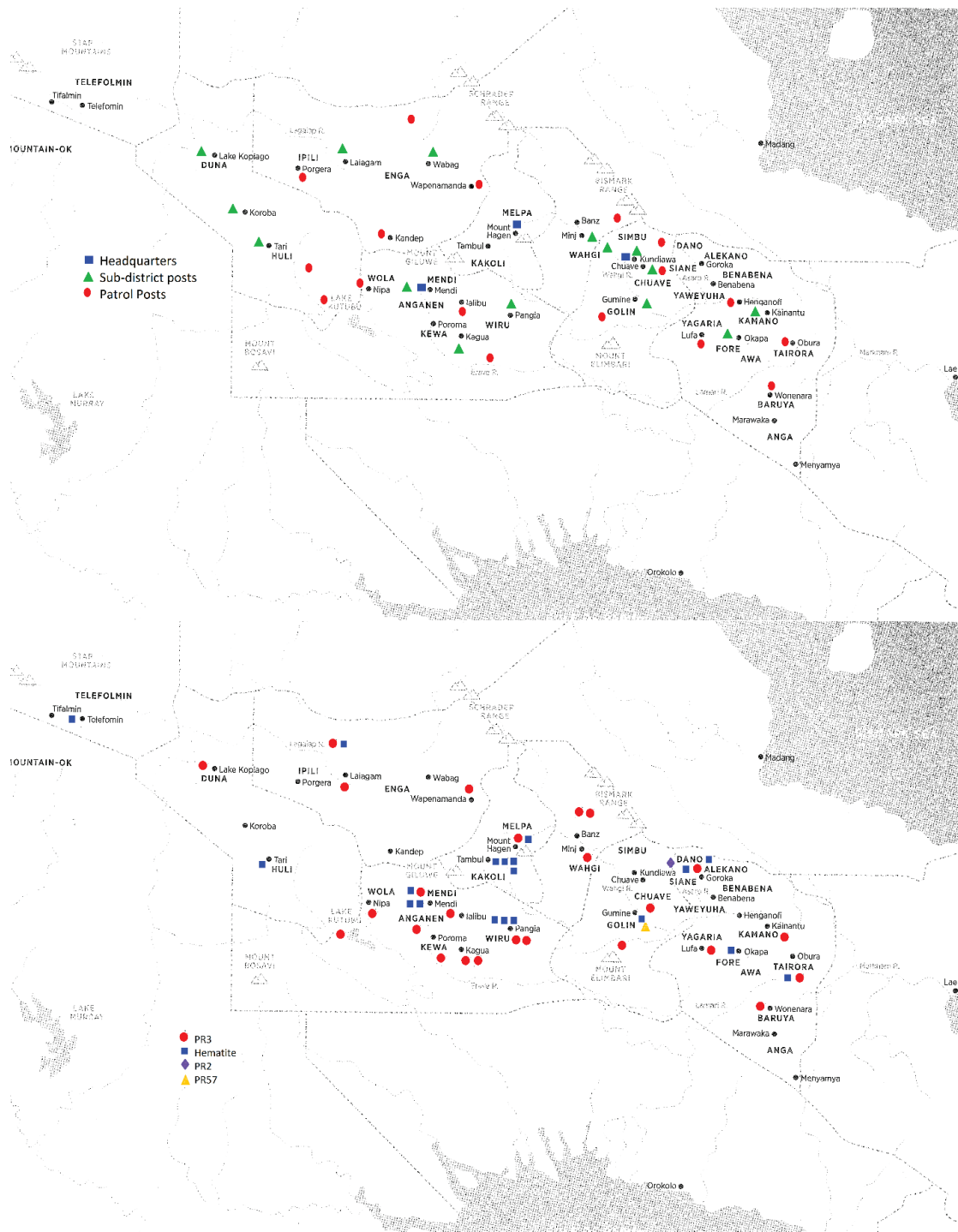


Fig. 3.8 (a) Distribution map of headquarters, sub-district posts and patrol posts recorded in PNG Highlands in 1966 (b) Distribution of red pigments identified on ceremonial objects obtained from different Highlands localities by Moriarty between 1961 and 1972.

As plant saps were reported for use with pigments in the Highlands, the substantial amounts of organic matter observed in Fig. 3.9a may suggest that a plant sap exists on top of the SOM content. On the other hand, the proportion of SOM may vary depending on the condition of soil and area from where it is extracted, hence, it is also possible that the significant IR binder bands arise from a higher proportion of SOM naturally occurring in the red ochre sample.

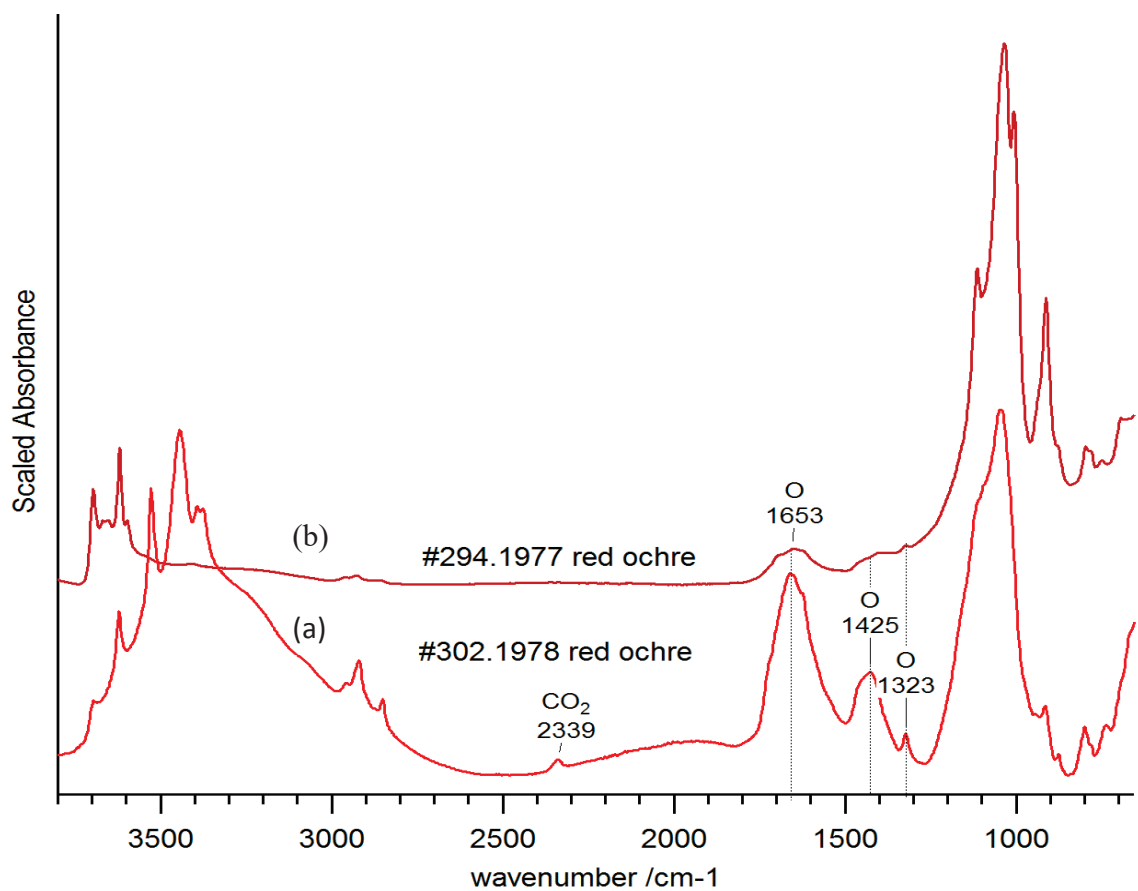


Fig. 3.9 Exemplar FTIR spectra of red ochres containing (a) substantial organic matter (shield #302.1978) and (b) little organic matter (apron adorer #294.1977).

Other coloured paints (i.e. ochres, ultramarine blues) give similar broad bands centering at 1650 cm^{-1} and 1425 cm^{-1} , but appear at weaker intensities due to the interferences from silicates (Fig. 3.10a). These bands are similar to the organic matter observed in the FTIR spectra of some white clays in section 3.3.1.

To clarify the type of organic binder, these samples are extracted with water or treated with HF to eliminate interferences from clay and insoluble pigments in the FTIR spectrum. As shown in Fig. 3.10a, the residue of water extracts of different coloured paints gives spectral vibrations at $1700\text{-}1760\text{ cm}^{-1}$ (C=O stretching), $1350\text{-}1410\text{ cm}^{-1}$ (CH bending), a weak band at 1324 cm^{-1} , $1260\text{-}1265\text{ cm}^{-1}$, strong bands at $1103\text{-}1111\text{ cm}^{-1}$ and $1030\text{-}1050\text{ cm}^{-1}$ (C-O, C-C stretching).

Spectral effects from water at 3400 cm^{-1} (OH stretching from water) and $1641\text{-}1646\text{ cm}^{-1}$ (OH bending from water) are also observed, likely due to hydrogen-bonded water molecules. In Fig. 3.10b, strong bands centering at $1666\text{-}1664$, $1460\text{-}1440\text{ cm}^{-1}$ and other peaks were observed in the FTIR spectrum after the silicate interference was removed with HF treatment. For the ultramarine blue sample, even though sulphate bands are not eliminated with HF, the absence of silicate bands reveals IR bands arising from the organic material.

Although the sample pretreatments provide a clearer spectrum of the organic material, it is difficult to attribute the bands to solely plant sap or SOM. This is partly because of the wide variety of functional groups present in these materials, which are further complicated by different plant species and source. Furthermore, the IR bands of these substances are broad with overlapping functional groups and are poorly resolved. As paints were applied onto plant-based materials, contamination from plant sap possibly existed with the paint agglomerate.

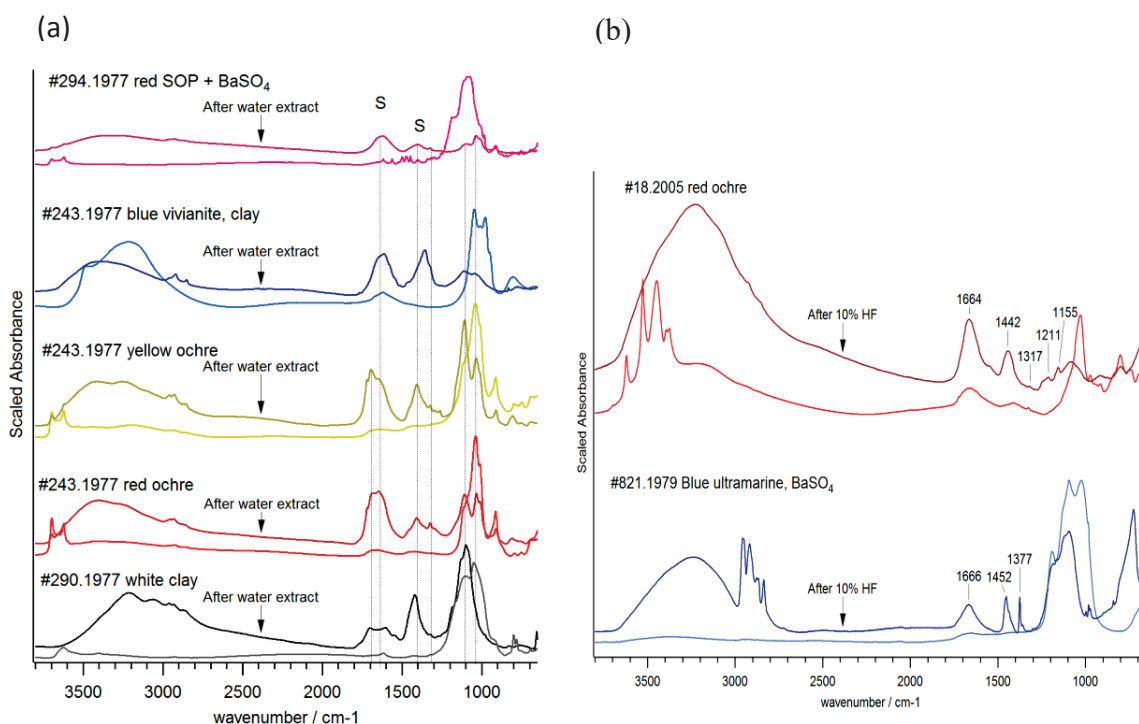


Fig. 3.10 FTIR spectra of various coloured samples of residue (a) after water extraction and (b) after 10% HF pretreatment, S= plant sap or SOM.

3.3.4.2 Lipids

Several paints show the presence of a carbonyl stretch at 1700-1745 cm⁻¹, which suggests the presence of lipids, wax esters or resin. This region is transparent to absorption bands of pigments and often serves as the first indication of non-water-soluble binder. To provide further clarity, these paint powders were subjected to a solvent extraction using chloroform or hexane. The white residue after evaporation of solvent was analyzed by vibrational spectroscopy. The FTIR spectrum reveals a carbonyl stretch (ester, acids) between 1700-1745 cm⁻¹, bands around 1465-1471 cm⁻¹ and 719-729 cm⁻¹ due to CH deformations, a weak CH₃ bending at 1376-1377 cm⁻¹ and intense CH stretching at 2850-2950 cm⁻¹, which are characteristic of long alkyl hydrocarbon chains and in some cases a series of bands with the

highest intensity around 1172-1182 cm^{-1} suggestive of C-O stretching in triglycerides. Based on this spectrum, the possibility of natural resin can be ruled out due to absence of carbonyl stretching band in the region 1695-1715 cm^{-1} (Derrick, Stulik & Landry 1999), and the binder class can belong to a lipid, wax ester or a combination of lipid and wax, as illustrated in Fig. 3.11. The interpretation of such binder classes is further complicated by its origin (plant or animal, natural or synthetic) and degradation processes.

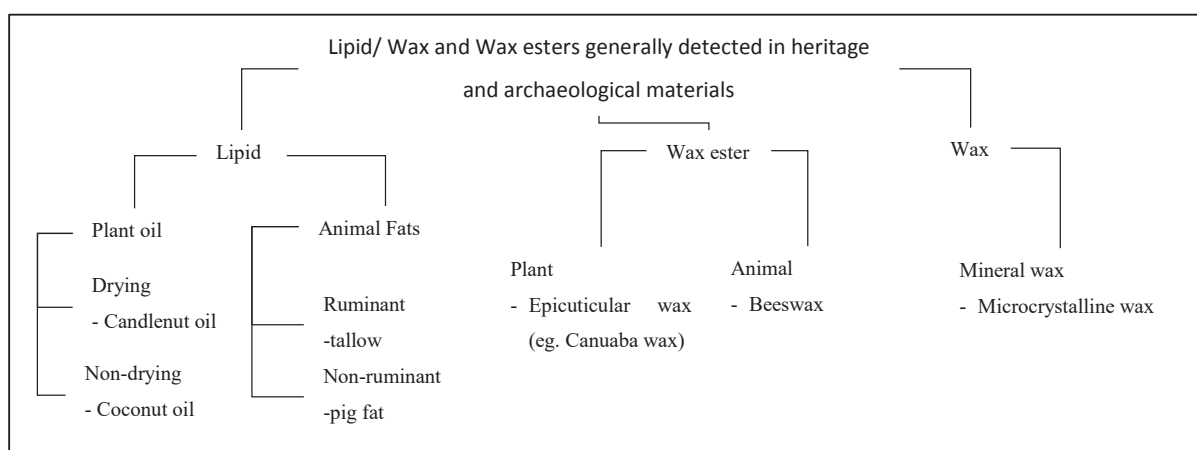


Fig. 3.11 Generic illustration of various binder classes of lipid, wax and wax esters containing long chain alkanes, esters and other functional groups.

A lipid contains triacylglycerols with fatty acid chains extending to about 18 carbons. The degree of unsaturation in these alkyl chains determines its property as a drying or non-drying oil. A non-drying oil such as coconut oil contains a high percentage of saturated fatty acids (C12-C16). Although animal fats such as pig fats also contain a high percentage of saturated fatty acids, the chain lengths are longer (C16-C18) and cholesterol is present in considerable amounts, which explains its solid property at room temperature. Degradation of fats often results in rancidity (producing an unpleasant smell), and this is due to hydrolysis, oxidation or a microbial reaction. The hydrolysis process breaks the ester linkages and results in increased amounts of alcohols and aldehydes, which can further oxidise. The mixture of compounds thus broadens the C=O band at 1740 cm^{-1} with shifting to lower frequencies at 1730-1710

cm^{-1} in the FTIR spectrum. Oxidation involves a free radical reaction of unsaturated C=C bonds, leading to the formation of oxidation products, including hydrocarbons, aldehydes and ketones. This results in a lower intensity C=C stretch in the Raman spectrum. Heat, light and microbial activity increases the rate of degradation.

Wax esters derived from animals (e.g. beeswax) contain saturated hydrocarbon chains (branched or unbranched) extending to C40 and the ester linkages are not solely based on triacylglycerols. While wax and wax esters can be differentiated from lipids by the FTIR spectrum based on the sharp doublets at $1463/1471 \text{ cm}^{-1}$ and $721/729 \text{ cm}^{-1}$, this differentiation becomes difficult when wax esters degrade and the initially sharp bands collapse into one broad band. Hydrolysis of wax esters yields free fatty acids and alcohols that can oxidise to acids, aldehydes and ketones, broadening the carbonyl stretch and lowering the frequencies to $1730\text{-}1710 \text{ cm}^{-1}$. Alkanes and fatty acids in wax esters can also vaporize and sublime, leading to partial or total disappearance for detection. Natural wax esters can also be found on the surface of leaves or fruits of plants, which composes of aliphatic hydrocarbons (both saturated and unsaturated) and various functional groups. The composition of plant wax esters depends on the species of plant, area from which the wax was formed, the season and age of plant.

To interpret such unknown binders based on FTIR alone is not practically achievable, but the identification can be narrowed by referring to anecdotal sources. In the Highlands, pig fat was frequently recorded for use on ceremonial objects and rituals (Hill 2001; Strathern & Strathern 1971; Wilson 2014), while candlenut oil, coconut oil and commercial castor oil were also mentioned for mixing with charcoal in Hill's research (Hill 2001). However, natural wax esters have not previously been reported for use in preparing paints in the PNG Highlands. The closest connection accounted for vegetable wax is the historical use of waxy leaves for storing the prepared paints (Hill 2011). Similarly, the only evidence of beeswax used in PNG was for tuning of drums in the late 1980s (Wanek & Studies 1996), which is not relevant to the Highlands ceremonial objects in this study. Crayons or candles containing

mineral wax could have been introduced to the Highlanders through the colonial officers. Therefore, the possibilities are further narrowed to pig fats or plant oil for lipids and mineral wax or plant wax esters.

In the characterisation of lipid/wax ester binders of the paint samples collected in this study, FTIR and Raman microscopy suitable for sample size of only tens of microns were employed. Although GC/MS is often used as a complementary technique to FTIR, the amount of binder material extractable from the lipid-containing PNG paint samples was too low to give any significant information and was not used.

In the FTIR spectrum of the red ochre paint on *Sacred Stone* (272.1978), intense C-H stretches (from CH₂ and CH₃), a strong carbonyl (ester) absorption at 1741 cm⁻¹, C-H bending at 1465 cm⁻¹, C-O stretch due to triglyceride at 1174 cm⁻¹ and CH₂ rocking at 720 cm⁻¹ agrees well with a pork lard reference (purified form of pig fat). A shoulder at 1728 cm⁻¹ and a slight decrease in intensity of the weak band at 3010 cm⁻¹ in the FTIR spectrum, as well as a lower intensity of C=C stretching at 1656 cm⁻¹ in the Raman spectrum (Fig. 3.12bii) suggests that minor oxidation had occurred. In addition, a few weak bands at 1727, 1103 and 921 cm⁻¹ (labelled asterisk * in Fig. 3.12bii) visible in the red ochre sample are not present in the fresh pork lard reference. A literature search suggests that the weak band at 1103 cm⁻¹ (C-C skeletal stretching) and a sharp weak peak at 607 cm⁻¹ are characteristic of an ozone-aged animal fat (pig suet) that are not present in beeswax nor olive oil (Gamberini et al. 2011). The appearance of 1727 cm⁻¹ may be due to aldehydes or ketones formed from C=C oxidation. The intensity ratio of CH₃ to CH₂ stretching greater than 1 in the region 2800-3000 cm⁻¹, and the C-H bending at 1460 cm⁻¹ and 889 cm⁻¹ are accentuated, suggesting traces of wax are present (Fig. 3.12bii). A microcrystalline wax reference is shown for comparison. The contamination of such waxy material on this artefact is likely transferred from different hands of the Highlanders when preparing other objects during ceremonies. The assignment of the weak band at 921 cm⁻¹ is not affirmative and could arise from pig fat impurity, likely

proline ring from collagen (Frushour & Koenig 1975; Gentleman et al. 2009; Nguyen et al. 2012).

The identification of pork lard on the *Sacred Stone* can be related to its unique purpose of creation. Interestingly, the *Sacred Stone* (a representative of female figure) is used in the *Kepele* or fertility ritual of the *Yupini* (a basketwood figure representing a male figure), whereby pork lard was used as a symbolic transfer for the “copulation process” (Wilson 2014). Some black particles from the male genital organ of the *Yupini* (#283.1978) were subjected to solvent extraction and the resulting binder residue gave FTIR and Raman spectra analogous to degraded pork lard. In the FTIR spectrum, the increased band broadening and shifting of the carbonyl stretch to 1735 cm^{-1} , along with a shoulder at 1716 cm^{-1} (free fatty acids), signify that the triglycerides had undergone considerable hydrolysis and oxidation (Fig. 3.12aiii). The sharp band observed at 1471 cm^{-1} rather than 1465 cm^{-1} in the FTIR spectrum is more prominent than other fats spectra. This band at 1471 cm^{-1} is also shown in the FTIR spectrum of dried fat from wildebeest carcass (Prinsloo, Wadley & Lombard 2014). In the corresponding Raman spectrum in Fig. 3.12biii, the absence of C=C stretching at 1656 cm^{-1} indicates that the unsaturated C=C bonds had largely oxidised (Maier et al. 2005). The broadening of bands also suggests the formation of oxidation products.

The presence of lipids is also observed in other ceremonial objects containing synthetic organic pigments. In the red synthetic paint of *Judge's Wig* (#553.1979), where the red pigment was previously identified as PR3 with BaSO_4 , two weak bands around 1730 and 1710 cm^{-1} suggests the presence of a lipid or wax ester. This time, the hexane extraction shows a different degradation profile in the FTIR spectrum. The majority of the C=O absorption centers at 1710 cm^{-1} , with a shoulder occurring at 1735 cm^{-1} (Fig. 3.12aiv), indicating that the bulk of the binder consists of free fatty acids. Moreover, the C-O stretching bands at 1240 – 1090 cm^{-1} are hardly visible, indicating that the triglyceride esters are almost hydrolysed. Similarly, the corresponding Raman spectrum (Fig. 3.12biv) shows broad bands of oxidation

products, which is comparable to the degraded pork lard identified in #283.1978 (Fig. 3.12biii).

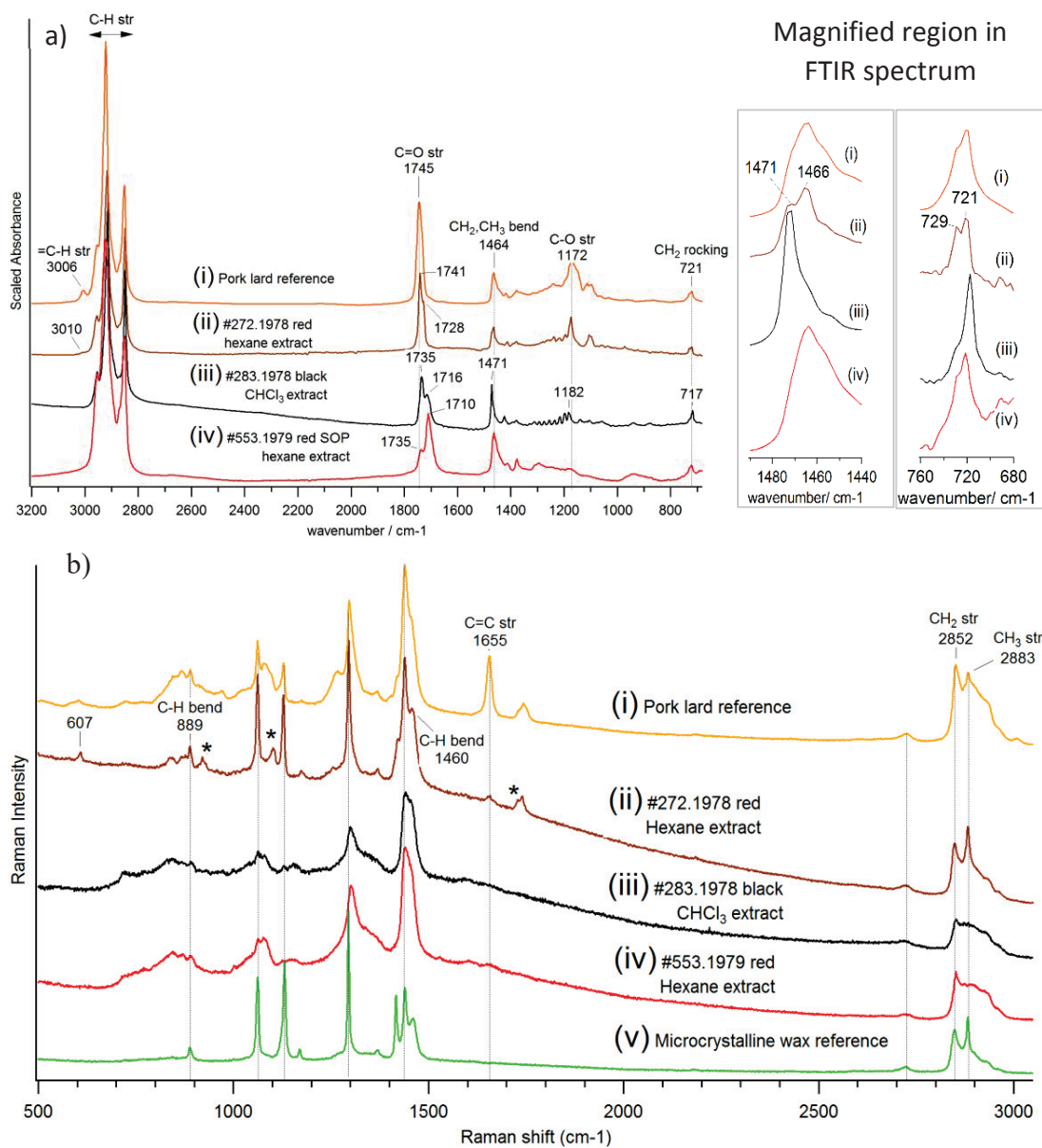


Fig. 3.12 FTIR spectra of (a)(i) unaged pork lard reference (ii) red ochre paint on *Sacred Stone* (#272.1978), (iii) black particles from scrotum of *Yupini* (#283.1978), (iv) red SOP paint on *Judge's Wig* (#553.1979) and (v) Microcrystalline wax reference b) corresponding Raman spectrum of the samples in (a) collected at 785 nm.

3.3.4.3 Wax and wax esters

Wax can be easily differentiated based on the sharp doublets in FTIR spectrum. However, attributing the wax peaks to the source (plant/animal, natural/synthetic origin) is less straightforward. Based on historical records (described in Section 3.3.4.2), the possibility of wax and wax esters is narrowed to plant wax ester or synthetic petroleum-based wax introduced by foreigners.

In two of the artefacts, wax peaks are evident in the FTIR spectra (Fig. 3.13a). Both of them are painted *Gourd Masks* (#240.1977 and #287.1978), which seems to suggest that the wax could come from the natural waxy surface formed on gourds with ageing.

In the *Gourd Mask* (#240.1977), the blue and red paints only show distinctive doublets, suggesting petroleum wax as the source. The FTIR spectra do not show additional bands due to functional groups other than aliphatic hydrocarbons, except for the yellow paint which shows a strong and broad band at 1700 cm^{-1} due to fatty acids with intermolecular bonding. This may indicate that a degraded wax ester is present or the petroleum wax is contaminated with fatty acids. As the Raman spectrum of the hexane extraction of yellow paint gives an exact match to a microcrystalline wax consisting of long chain branched alkanes (Fig. 3.13bi), it suggests the presence of petroleum-based wax. A few bands between 1032 and 914 cm^{-1} not attributable to petroleum-based wax are likely contamination from wax gourd or other sources.

In the *Gourd Mask* (#287.1978), a yellowish brown substance that appears resin-like was extracted from the back of the ear. In addition to the doublets, the C=O stretching bands at 1710 cm^{-1} and 1733 cm^{-1} in the FTIR spectrum were observed (Fig. 3.13a). The C-O stretches give a series of bands with the highest intensity occurring at 1060 cm^{-1} . The Raman spectrum of this substance gives similar spectral vibrations to a wax gourd, beeswax and microcrystalline wax, making it difficult to be differentiated. Noting that the C-C stretching band at 1129 cm^{-1} is lower than the C-C stretching band at 1064 cm^{-1} in the Raman spectrum

(Fig. 3.13b), the brown substance observed in *Gourd Mask* (#287.1978) is likely a waxy material occurring naturally on the gourd.

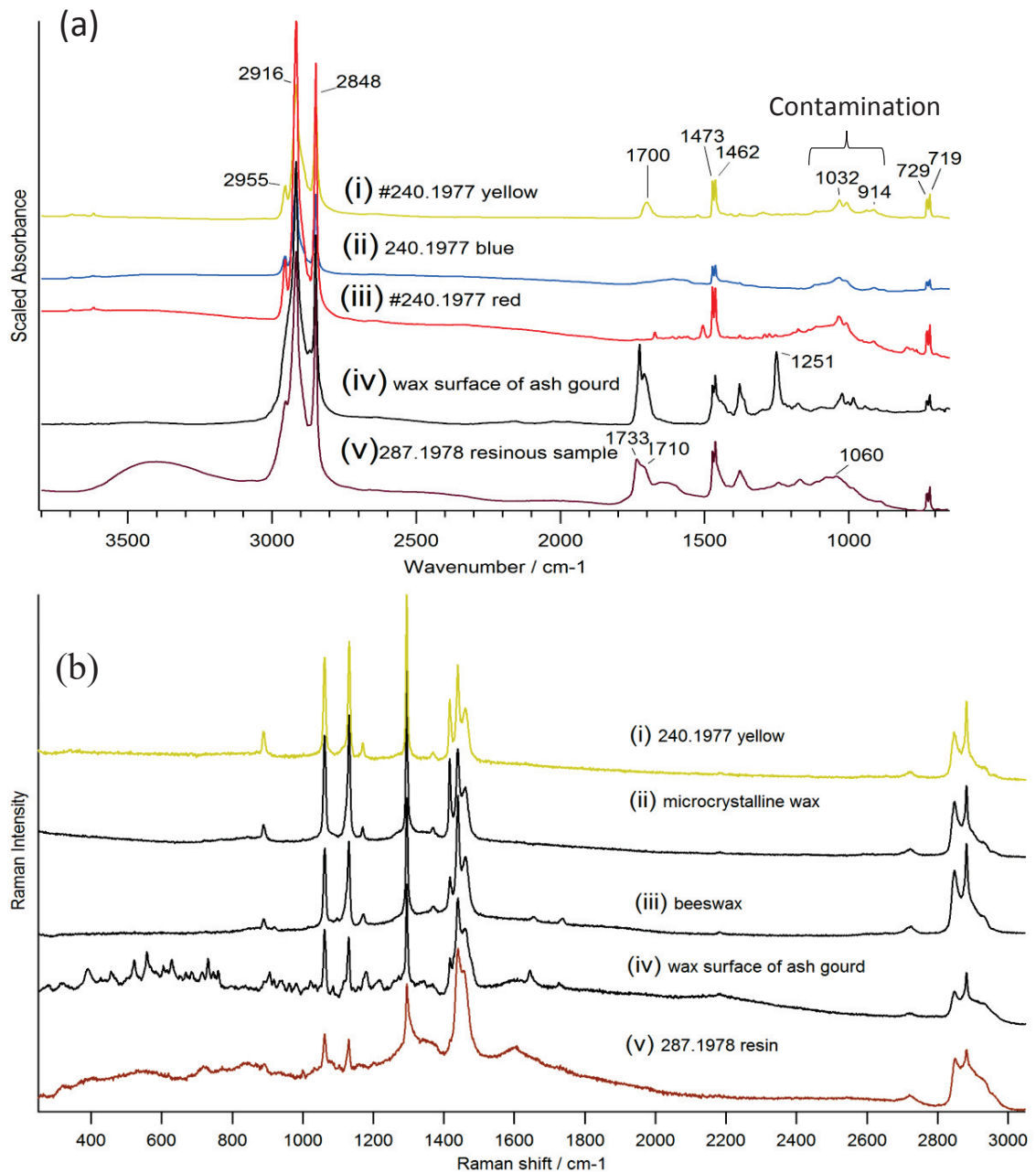


Fig. 3.13 a) FTIR spectra and b) Raman spectra collected at 785 nm, of samples containing wax or wax esters.

3.3.4.4 Natural Resin

A number of resins were found on some objects, either as a transparent coating over another paint layer or applied directly over the substrate. The identification of the resins is mainly based on comparing the fingerprint region of the FTIR spectrum with available references. However, two of the unknown resins give a spectrum that resemble a sandarac or copal, which have very similar composition and it is difficult to affirm the identity based on FTIR alone (Fig. 3.14a). These resins are thus identified as diterpenoid resins. Referencing can also rely on known sources of artefacts containing the suspected material. As shown in Fig. 3.14b, two of the unknown resins were identified as tigaso oil based on comparison with a tigaso oil reference from *Bambe* (A59800), a tigaso oil container from the collection of the South Australian Museum. Where no reference is available, anecdotal sources helped to narrow the identification. In Fig. 3.14c, the kilt tree resins are identified based on historical records that highlighted their use on certain specific ceremonial objects, such as the *Judge's Wig* (#553.1979) and the *Moka Kin* (#319.1978).

To further confirm the chemical components of tigaso oil, GC/MS of the solvent extract of resin from the gourd mask #239.1977 and tigaso oil reference sample were carried out and a comparison shows a high correlation (Fig. 3.15). The appearance of an abundance of benzoic acid and oleic acid (C18:1) is consistent with the oxidative degradation of tigaso oil, which was chemically identified as campospermonol (10hydroxy-3-(nonadec-10¹-en-2¹-onyl)benzene) and 5-hydroxy-5-(nonadec-10¹-en-2¹-onyl)cyclohex-2-enone) in other studies (Colombini & Modugno 2009; Johns et al. 1987). The lower relative intensity of unsaturated oleic acid observed in mask (#239.1977) is probably due to increased oxidation of C=C linkages.

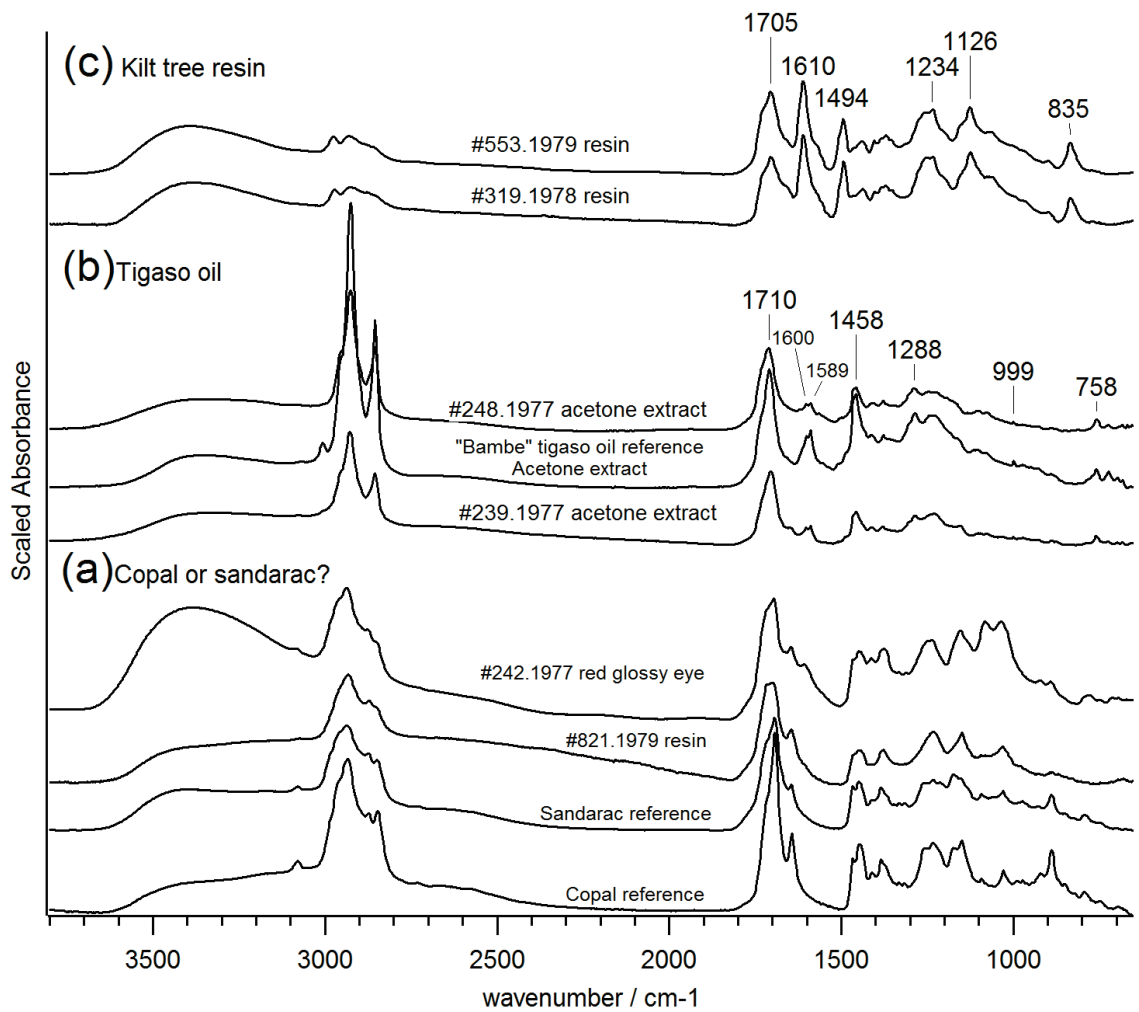


Fig. 3.14 FTIR spectra of various resins identified.

The chemical structure of tigaso oil can be visualised as aromatic phenols or cyclic rings linked to long hydrocarbon chains containing only one unsaturated C=C bond, thereby explaining its non-drying consistency. Tigaso oil is often used to rub the bodies and hands of Highlanders during performances and rituals, which may be transferred to the ceremonial objects in the interactive process.

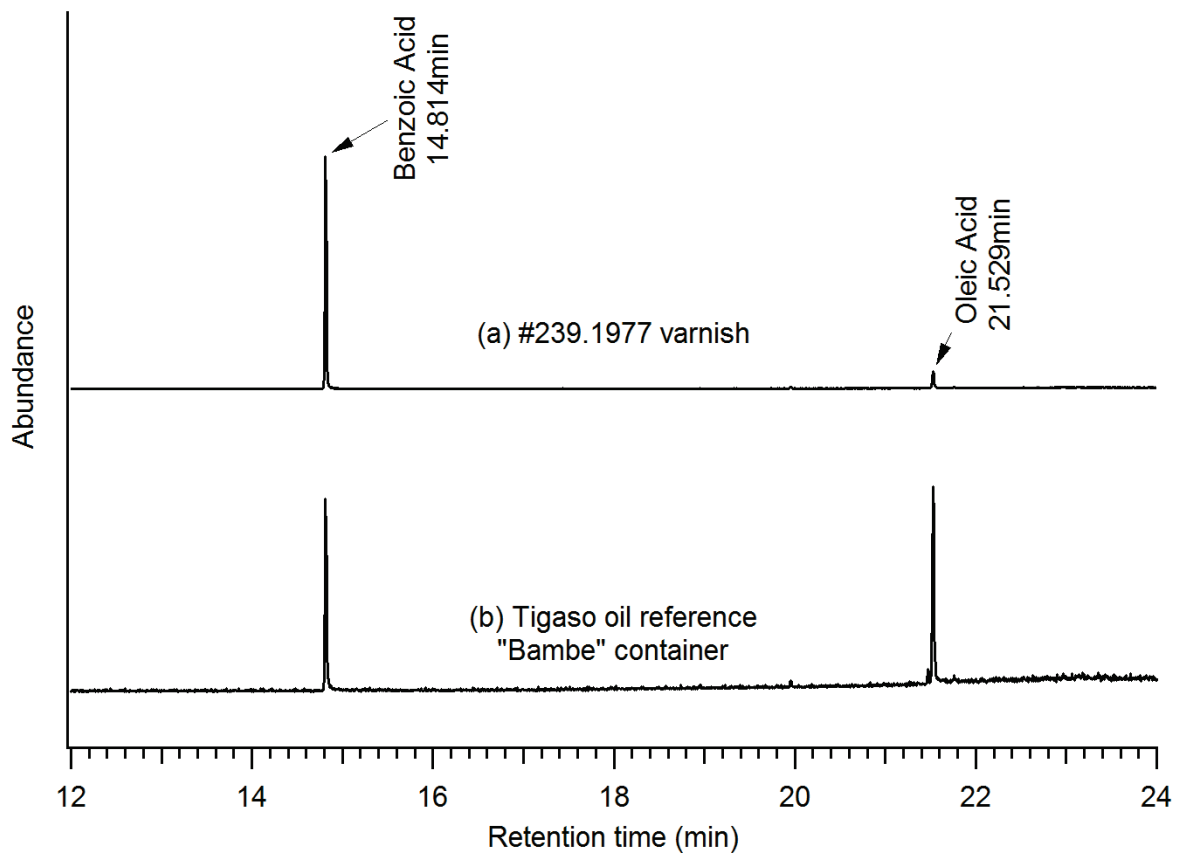


Fig. 3.15 Total ion chromatogram of (a) #239.1977 varnish and (b) Tigaso oil reference.

3.3.4.5 Synthetic Resin

The pale green strips applied over a wooden substrate of *Ceremonial Board* (#278.1978) gives a strong carbonyl stretch at 1730 cm^{-1} , a broad absorption band at 1262 cm^{-1} , along with two strong absorptions at $1122, 1070\text{ cm}^{-1}$ in the FTIR spectrum that are characteristic of alkyd (Learner 2004; Ploeger, Scalarone & Chiantore 2008). Alkyds in house paints were popular from the mid- to late-1950s in Europe and slightly earlier in the USA (Learner 2000) and these cheap paints were likely introduced to the PNG Highlands at that time. Hence, it is not unusual to find alkyd on this object, which was collected much later in the year 1966. However, it is a rather rare find as alkyd is the only definite synthetic binder detected in one

of the fifty ceremonial objects studied. This could imply that accessibility to synthetic house paints was still limited at that time or that such commercially prepared paints were not in favour by the Highlanders, probably due to the lack of bright colour range offered.

Different from the other blacks, the black undercoat on the *Shield* (#265.1977) appeared particularly reflective and it adhered more strongly to the substrate, such that force on the scalpel blade was required to extract the black particles. Initially, it was thought that the strong adherence of black charred wood was due to natural resins released from prolonged fuming of the wood, but this was shown otherwise with FTIR analysis. As seen in Fig. 3.16, the FTIR spectrum of the black charred wood particles was compared before and after solvent extraction to check for the presence of a binder. After evaporation of the solvent, the orange white residue produced bands at 1733 cm^{-1} (C=O stretching), 1465, 1451, 1380, 1295 cm^{-1} (CH bending), 1255, 1178, 1160, 1116, 1094, 1027 cm^{-1} (C-O and C-C stretching) and 852 cm^{-1} (CH_2 rocking) in the FTIR spectrum, which are characteristic of a poly(ethylacrylate) (PEA) resin (Fig. 3.16b) (Learner 2004). A few weak bands at 1606, 1517, 1217 cm^{-1} are due to tannin compounds from the charred wood. According to the past conservation record, this object was previously conserved using Plextol B500, Jun Funori (a polysaccharide seaweed) and Bermocoll EHEC (a non-ionic cellulose ether) as the pigments were friable and poorly bound. The acrylic resin identified by FTIR spectroscopy was attributed to Plextol B500, a ethyl acrylate – methyl methacrylate (EA-MMA) copolymer. It is likely that the proportion of EA is greater than MMA, which explains why the IR bands observed were attributed to EA only. Hence, the exceptional reflectivity and strong bonding observed in this black undercoat is due to the Plextol B500 applied as a consolidant.

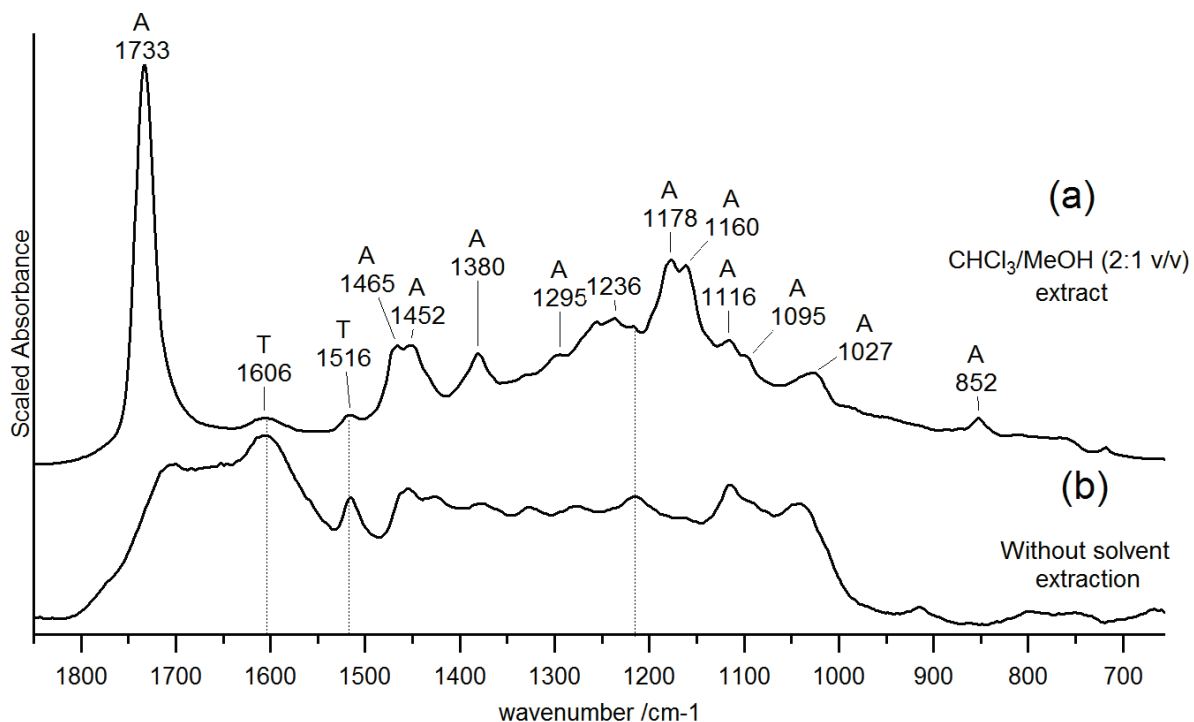


Fig. 3.16 FTIR spectra of black particles obtained from black undercoat of *Shield* (#265.1977) (a) orange residue from $\text{CHCl}_3/\text{MeOH}$ (2:1 v/v) extract (b) raw black particles, without solvent extraction, A = acrylate, T = tannin.

3.3.5 Metal soaps

Some red synthetic paints containing PR3 found namely on *Kund Gale* (#818.1979), *Ceremonial Board* (#278.1978), *Bowman's Wooden Wrist Guard* (#522.1979), show a strong carboxylate peak at 1539 cm^{-1} , indicating presence of zinc stearate. The FTIR spectra of these carboxylate-containing paints showed fatty binder peaks at $\approx 1735\text{--}1710\text{ cm}^{-1}$, $1464\text{--}1471\text{ cm}^{-1}$ and 720 cm^{-1} after solvent extraction, which contributes to the source of carboxylate ions like stearate. Small to trace amounts of Zn were detected with EDS. Interestingly, the EDS mapping of zinc shows that the formation of metal soap is localised (Fig. 3.17), explaining why other synthetic red paints containing wax esters did not give a carboxylate band with FTIR microanalysis, as micro-samples were taken from an area without zinc soap. The appearance of zinc does not overlap with that of Ba and S, and is unlikely contributed

from lithopone, but more likely associated with the red synthetic pigment introduced by colonial officers at that time.

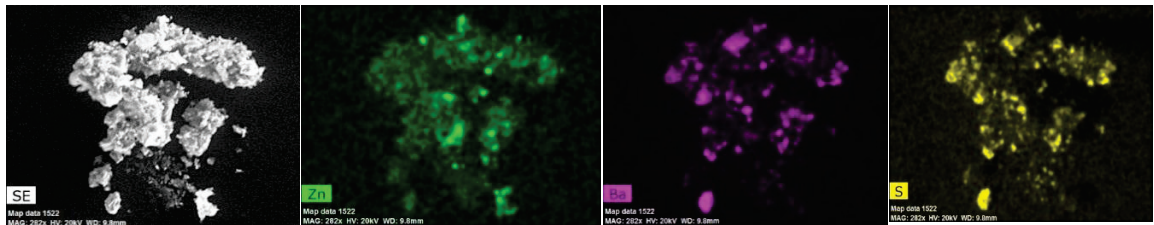


Fig. 3.17 EDS mapping of red synthetic paint containing zinc carboxylate soap from *Effigy* (#818.1979).

A white encrustation was also seen around the magenta paint in *Bark Belt* (#533.1979). In this case, the EDS mapping of the white paint shows a widespread distribution of zinc as the major element. As seen in Fig. 3.18a, strong absorption bands at 1550, 1527 cm^{-1} and a doublet at 1465, 1457, and 1405 cm^{-1} , as well as a weak peak at 3005 cm^{-1} in the FTIR spectrum indicate the presence of zinc oleate (Otero et al. 2014). A sharp absorption at 1399 cm^{-1} is attributed to zinc palmitate or stearate (Otero et al. 2014). Noting the primary abundance of oleate and secondary amounts of palmitate and stearate suggests that the carboxylate source could be non-drying fat such as pork lard (Rohman et al. 2012).

In another instance, significant amounts of metal soaps were identified in the grey paint in *Mortar* (#666.1979), an object used to grind and prepare paint. Majority of K and Ca sporadically distributed throughout the paint sample is seen with EDS mapping. In the FTIR spectrum seen in Fig. 3.18b, vibrational bands at 1576, 1540, 1471, 1416 cm^{-1} and 1556, 1471, 1416 cm^{-1} are characteristic of calcium palmitate and potassium stearate, respectively (Gasgnier 2001; Hénichart et al. 1982). Palmitates and stearates are stable saturated fatty acids that can come from drying oils or waxes.

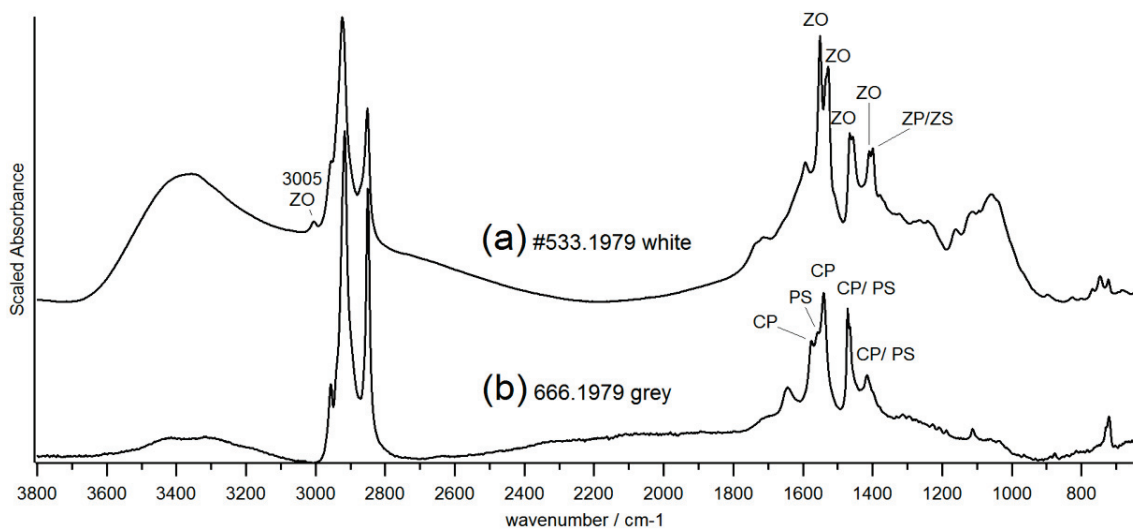


Fig. 3.18 FTIR spectra of a) #533.1979 bark belt- white sample at the periphery of the red synthetic paint shows an abundance of zinc oleate (ZO) and zinc palmitate or zinc stearate (ZP/ ZS) b) #666.1979 mortar-grey sample shows an abundance of calcium palmitate (CP) and potassium stearate (PS).

3.3.6 Extraneous organic materials

During the sampling of the *Shield* (#302.1978), minute white paint was observed dotted in random locations on the surface of the wood, raising the question as to whether it belongs to part of the decoration or a splash contamination from another painting process. The white paint appears 'wet' to the scalpel, which is unusual for paints aged after decades. A further examination with SEM showed an interesting morphology of spherical globules, which does not appear to be paint (Fig. 3.19a). As seen in the FTIR spectrum of Fig. 3.19b, two strong bands at 1120, 987 cm^{-1} and three distinct sharp peaks at 786 (CH_2 rocking), 752 (mixture of C-C stretch, N-H out-of-plane bending and C-N stretch of aromatic) and 705 cm^{-1} (libration of water) correlate to a uric acid reference. In the corresponding Raman spectrum in Fig. 3.19c, the bands at 1650, 1423, 1038 and 631 cm^{-1} are characteristic markers of uric acid in the bird excrement, with slight deviation from the markers highlighted in a raptor faeces (Prinsloo et al. 2013).

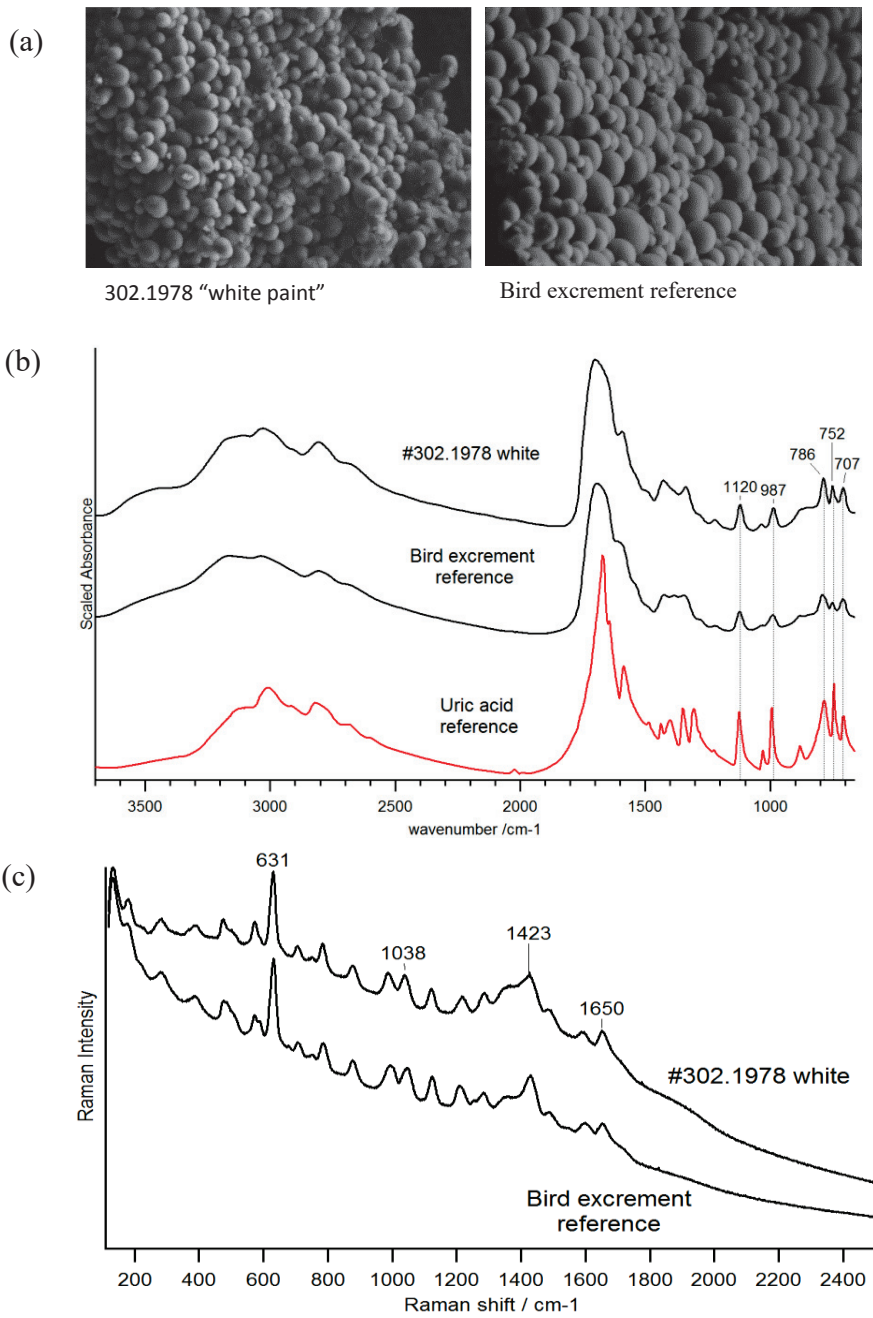


Fig. 3.19 a) SEM image at around 2000 X magnification c) FTIR spectrum and d) Raman spectrum collected at 785 nm, of the "white paint" on *shield* (#302.1978) in comparison with a bird excrement reference

In another instance, white efflorescence suggestive of biological infestation is apparent on the *Shield* (#490.1979). This object is in an almost unrecognizable state, where the poor condition and unknown provenance renders it unsuitable for display. During sampling of the white efflorescence particles, they powder immediately with the touch of a scalpel blade. If it were fungi, filamental hyphae would be expected to be observed with the optical microscope, but this was not the case. To ascertain the identity of the white efflorescence, FTIR spectra were collected over multiple spots. A few spots show the presence of chalk (Fig. 3.20a) and the majority of the spots gave the same FTIR spectrum that resembles a gum-like binder (Fig. 3.20b), whereas only one spectrum reveals more detailed features where some of the bands can be attributed to a fungus (Fig. 3.20c). IR bands at 1647, 1548 cm^{-1} are assigned to amide I and II bands of proteins, respectively, while a shoulder at 1155 cm^{-1} with peaks at 1074 cm^{-1} and 1045 cm^{-1} represent various absorptions of chitin and glucan (Koestler & Art 2003). A 1438 cm^{-1} band is assigned to CH_2 bending. However, the weak carbonyl (lipid ester) stretch at 1735-1750 cm^{-1} that is usually seen in fungi was not observed in the acquired FTIR spectrum. The SEM image sheds more light into the ambiguity observed (Fig. 3.20d), where the white efflorescence sample shows fungal filaments enveloping only at the surface of the gum, which explains why the majority of the spots previously analysed by FTIR fail to show distinctive spectral features of fungi. The broad absorption bands seen in the majority of the spectra (Fig 3.20b) could be contributed from a mixture of largely gum and minor fungal absorptions. The difficulty of identifying filamentous fungi based on optical microscopy is due to optical aberration from a heterogeneous mix of materials, including contamination from brown wood substrate, white clay silicates and blue ultramarine paint in the agglomerate sample mass.

Blooming has been encountered in a number of PNG artefacts containing pig fat (Hill 2001), but so far, this was not observed in ceremonial objects identified as pig fat at the AGNSW collection. In this example, the fungal growth is shown to feed on a substrate, likely gums or

plant saps, aided by other environmental factors like relative humidity and temperature of the PNG Highlands climate.

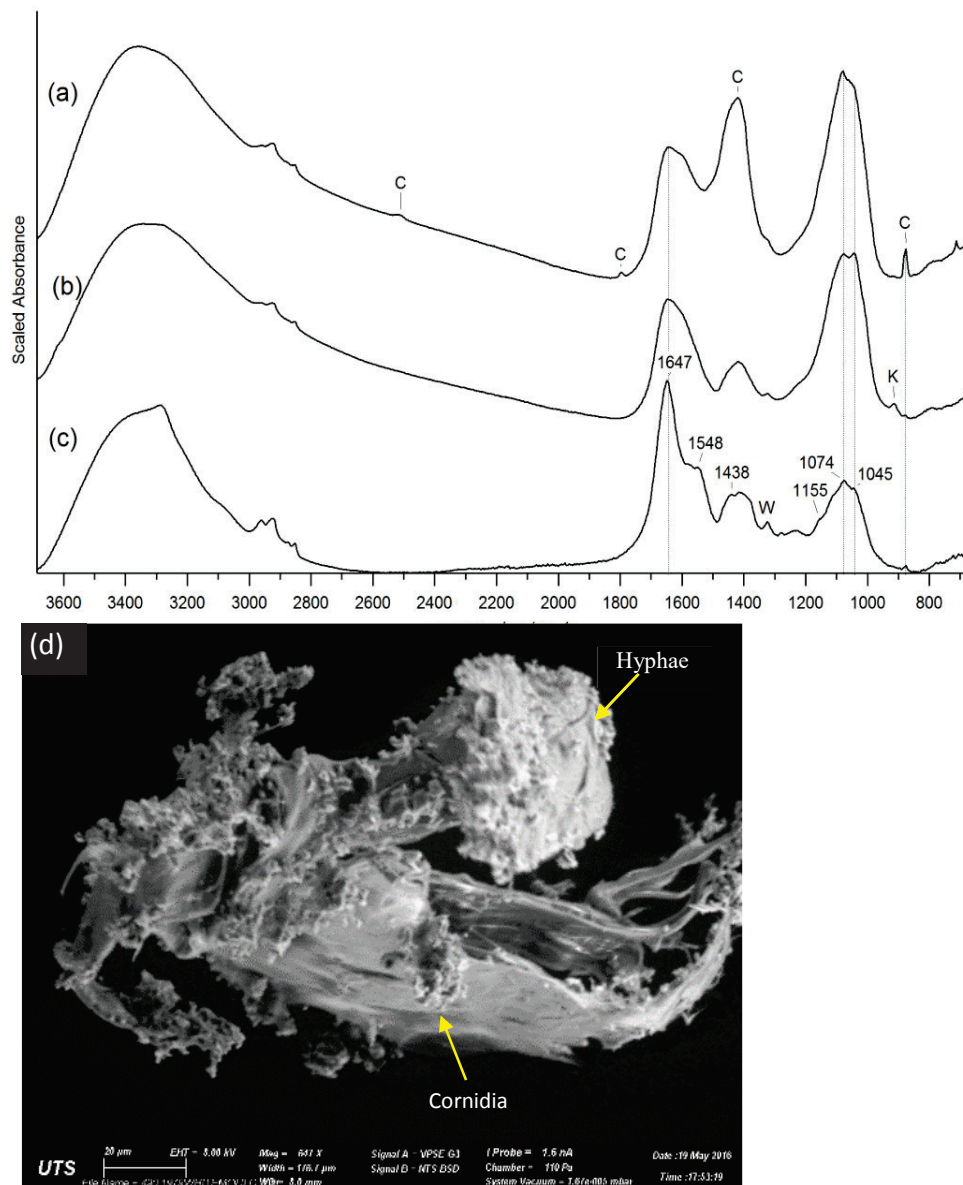


Fig. 3.20 Photo of white efflorescence (indicated by black arrows) on *Shield* (#490.1979). FTIR spectrum of multiple spots on the white efflorescence sample shows a) C-chalk, b) possible gum-like binder or unresolved features of fungi, c) fungi features; d) SEM image of white efflorescence details fungal morphology residing at the surface of a substrate.

3.4 Conclusions

The coloured pigments constituting the Highlands palette are characterised as natural blue vivianites, red ochres (hematite), yellow ochres (goethite, limonite, lepidocrocite) and synthetic ultramarine blue, PR3 and PY1, mixed with BaSO₄. Other synthetic pigments identified are phthalocyanine blue, Prussian blue, PY83, PR2, PR57 and rutile. A few synthetic organic pigments remain unidentified as spectral bands can be suppressed when more than one SOP coexist in the same sample. White clays containing kaolinite, quartz and Al–OH polymorphs were characterised. The black paints consist of charred wood that were exposed to different temperature and time length of heating, as shown by the variation of band absorptions in the FTIR spectrum.

Attributing the pigment source to natural or synthetic can be attained by micro-structural analysis, in conjunction with historical evidence. For example, ultramarine mixed with barium sulphate observed as regular small sized particles are attributed to a synthetic origin, whereas red ochres containing a mix of iron oxide grain sizes, clay minerals and interstitial carbon dioxide suggest a natural origin. The blue vivianite phases characterised contain varying proportions of clay minerals, oxidation phases, non-uniform crystal sizes and traces of soil elements, suggesting a natural source. Furthermore, natural vivianite mines were reported to have existed in selected areas of PNG Highlands with limited trading.

On the other hand, the identification of binders demonstrated a challenging task when facing such heterogeneous micro-sized samples obtained from the natural environment. Substrates such as hair, wood and cellulosic fibres can be found as remnants naturally occurring in some samples and are potential sources of contamination to the identification of binders. Black charred wood releases water-soluble tannins that are yellowish brown and may explain the brown gradation observed when white clays were applied over the black undercoat of a shield. White clays obtained from the ground contain traces of organic matter, which can come from soil organic matter. Such organic matter is also likely to be present in a number of

coloured samples. For some of the ochre and ultramarine blue samples, the elimination of clay peaks by HF treatment revealed bands due to a gum-like binder, suggesting the presence of a plant sap added for increased binding ability. The combination of evidences from FTIR spectroscopy, GC/MS and anecdotal records have narrowed the identification to kilt tree resin and tigaso oil, which are natural products specific to the fauna of the PNG Highlands. Differentiation of animal fats from other lipids and wax esters is not straightforward. However, the characterisation of pork lard at different levels of degradation has been successfully applied to some paint samples, using IR and Raman signatures, supported by anecdotal sources. Although waxes are identified in two gourd masks, it is difficult to attribute the source as natural or synthetic. The components identified consist of a majority of aliphatic branched and linear hydrocarbon chains that may suggest synthetic paraffin or microcrystalline wax. However, small amounts of stearic acids that are also detected could arise from hydrolysis of natural wax esters or contamination from other sources. Only one object was found to contain a synthetic alkyd resin commonly found in house paints or architectural paints. The low popularity of synthetic ready-made house paints could be due to the low availability of bright colour range at that time.

Degradation materials including metal soaps, bird excrement and fungi have been characterised. While characterisation of zinc soaps is not unusual on paintings, it is less commonly found on painted ethnographical objects. Although the presence of bird excrements and fungi are expected on such plant-based materials, the characterisation by scientific means is not direct. As revealed by SEM, the fungal mycelium was found as a thin film on the surface of the white binder matrix, making it difficult to characterise by FTIR microscopy.

This rigorous micro-analysis of the materials constituting the paint samples in the PNG Highlands resulted in several outcomes beneficial towards conservation documentation and technical art history. Pigment results have rectified 27% of blues and 33% of 52 reds analysed, whereas the ambiguous identity of organic binders were confirmed. Results also

show the widespread distribution of PR3, PY1 and ultramarine blues across the Highlands, suggesting that these compounds represented the trade store pigments made available by colonial officers at that time. As these synthetic pigments were given to Highlanders for services rendered, it is possible to deduce from the widespread distribution of PR3, that the synthetic red pigment played a crucial role for colonialists to diffuse easily into the Highlands. As can be seen, the scientific results demonstrated the far-reaching colonial influences that transformed the culture of Highlands art. The blue vivianites detected from 9 objects collected in Kewa and Wiru speaking region were all located in close proximity to a vivianite source. The limited trading of the vivianite pigment suggests that it can be used to trace the provenance of an object.

The characterisation of organic binders and accompanying deterioration products are important knowledge for conservation and explains for the visual appearance and condition of an object. In all coloured paints, relative proportions of plant-based organic matter are present, which can either occur naturally in the soil with the clays or derived from plant sap. While non-water-soluble binders provide sufficient binding ability, they can lead to other conservation issues. Pig fats can cause darkening of red ochre, formation of metal soaps and attraction of dirt and fungal growth. Tigaso oil is non-drying and may also attract dirt. This scientific study complements past anecdotal research and contributes to the knowledge gap in technical art history and conservation knowledge of PNG highlands ceremonial objects.

3.5 References

Art Gallery of NSW, viewed 20 June 2016, <<http://www.artgallery.nsw.gov.au/search/>>.

Ballard, C. 1994, 'The Centre Cannot Hold. Trade Networks and Sacred Geography in the Papua New Guinea Highlands', *Archaeology in Oceania*, vol. 29, no. 3, pp. 130-48.

Baraldi, P., Lo Monaco, A., Ortenzi, F., Pelosi, C., Quarato, F. & Rossi, L. 2014, 'Study of the Technique and of the Materials of a 19th-Century Polychrome Wood Mask from Papua New Guinea', *Archaeometry*, vol. 56, no. 2, pp. 313-30.

- Boylan, C., Moriarty, S. & Wilson, N. 2014, 'The Moriarty legacy: collecting New Guinea Highlands art', in N. Wilson (ed.), *Plumes and Pearlshells: Art of the New Guinea Highlands*, Art Gallery of New South Wales, Sydney, pp. 19-21.
- Breitman, M., Ruiz-Moreno, S. & Gil, A.L. 2007, 'Experimental problems in Raman spectroscopy applied to pigment identification in mixtures', *Spectrochimica Acta Part A: Molecular and Biomolecular Spectroscopy*, vol. 68, no. 4, pp. 1114-9.
- Centeno, S.A. 2015, 'Identification of artistic materials in paintings and drawings by Raman spectroscopy: some challenges and future outlook', *Journal of Raman Spectroscopy*, vol. 47, no. 1, pp. 9-15.
- Čermáková, Z., Hradilová, J., Jehlička, J., Osterrothová, K., Massanek, A., Bezdička, P. & Hradil, D. 2014, 'Identification of Vivianite in Painted Works of Art and Its Significance for Provenance and Authorship Studies', *Archaeometry*, vol. 56, pp. 148-67.
- Čermáková, Z., Švarcová, S., Hradil, D., Bauerová, P., Hradilová, J. & Bezdička, P. 2013, 'Vivianite: A historic blue pigment and its degradation under scrutiny', in M.A. Rogerio-Candelera, M. Lazzari & E. Cano (eds), *Science and technology for the conservation of cultural heritage*, CRC press, Florida, pp. 75-8.
- Chua, L., Maynard-Casely, H.E., Thomas, P.S., Head, K. & Stuart, B.H. 2016, 'Characterisation of blue pigments from ceremonial objects of the Southern Highlands in Papua New Guinea using vibrational spectroscopy and X-ray diffraction', *Vibrational Spectroscopy*, vol. 85, pp. 43-7.
- Colombini, M.P. & Modugno, F. 2009, *Organic Mass Spectrometry in Art and Archaeology*, Wiley, Chichester.
- Cox, R.J., Peterson, H.L., Young, J., Cusik, C. & Espinoza, E.O. 2000, 'The forensic analysis of soil organic by FTIR', *Forensic Science International*, vol. 108, no. 2, pp. 107-16.
- de Faria, D.L.A., Venâncio Silva, S. & de Oliveira, M.T. 1997, 'Raman microspectroscopy of some iron oxides and oxyhydroxides', *Journal of Raman Spectroscopy*, vol. 28, no. 11, pp. 873-8.

- Defeyt, C., Vandenabeele, P., Gilbert, B., Van Pevenage, J., Cloots, R. & Strivay, D. 2012, 'Contribution to the identification of α -, β - and ϵ -copper phthalocyanine blue pigments in modern artists' paints by X-ray powder diffraction, attenuated total reflectance micro-fourier transform infrared spectroscopy and micro-Raman spectroscopy', *Journal of Raman Spectroscopy*, vol. 43, no. 11, pp. 1772-80.
- Derrick, M.R., Stulik, D. & Landry, J.M. 1999, *Infrared Spectroscopy in Conservation Science*, The Getty Conservation Institute, USA.
- Dick, D.P., Santos, J.H.Z. & Ferranti, E.M. 2003, 'Chemical characterization and infrared spectroscopy of soil organic matter from two southern brazilian soils', *Revista Brasileira de Ciência do Solo*, vol. 27, pp. 29-39.
- Falcão, L. & Araújo, M.E.M. 2013, 'Tannins characterization in historic leathers by complementary analytical techniques ATR-FTIR, UV-Vis and chemical tests', *Journal of Cultural Heritage*, vol. 14, no. 6, pp. 499-508.
- Fooker, U. & Liebezeit, G. 2003, 'An IR study of humic acids isolated from sediments and soils', *Senckenbergiana maritima*, vol. 32, no. 1, pp. 183-9.
- Fremout, W. & Saverwyns, S. 2012, 'Identification of synthetic organic pigments: the role of a comprehensive digital Raman spectral library', *Journal of Raman Spectroscopy*, vol. 43, no. 11, pp. 1536-44.
- Frost, R.L., Martens, W., Williams, P.A. & Kloprogge, J.T. 2002, 'Raman and infrared spectroscopic study of the vivianite-group phosphates vivianite, baricite and bobierite', *Mineralogical Magazine*, vol. 66, no. 6, pp. 1063-73.
- Frost, R.L. & Weier, M.L. 2004, 'Raman spectroscopic study of vivianites of different origins', *Neues Jahrbuch fuer Mineralogie, Monatshefte*, vol. 10, pp. 445-63.
- Frushour, B.G. & Koenig, J.L. 1975, 'Raman scattering of collagen, gelatin, and elastin', *Biopolymers*, vol. 14, no. 2, pp. 379-91.
- Gamberini, M.C., Baraldi, C., Freguglia, G. & Baraldi, P. 2011, 'Spectral analysis of pharmaceutical formulations prepared according to ancient recipes in comparison

- with old museum remains', *Analytical and Bioanalytical Chemistry*, vol. 401, no. 6, pp. 1839-46.
- Gasgnier, M. 2001, 'IR spectra of some potassium carboxylates', *Journal of Materials Science Letters*, vol. 20, no. 13, pp. 1259-62.
- Gentleman, E., Swain, R.J., Evans, N.D., Boonrungsiman, S., Jell, G., Ball, M.D., Shean, T.A.V., Oyen, M.L., Porter, A. & Stevens, M.M. 2009, 'Comparative materials differences revealed in engineered bone as a function of cell-specific differentiation', *Nature Materials*, vol. 8, no. 9, pp. 763-70.
- Harrison, S.M., Kaml, I., Rainer, F. & Kenndler, E. 2005, 'Identification of drying oils in mixtures of natural binding media used for artistic and historic works by capillary electrophoresis', *Journal of Separation Science*, vol. 28, no. 13, pp. 1587-94.
- Henderson, G.S., Black, P.M., Rodgers, K.A. & Rankin, P.C. 1984, 'New data on New Zealand vivianite and metavivianite', *New Zealand Journal of Geology and Geophysics*, vol. 27, no. 3, pp. 367-78.
- Hénichart, J.-P., Bernier, J.-L., Roman, M. & Roussel, P. 1982, 'Identification of calcium palmitate in gallstones by infra-red spectroscopy', *Clinica Chimica Acta*, vol. 118, no. 2, pp. 279-87.
- Hill, R. 2001, 'Traditional Paint From Papua New Guinea: Context, Materials and Techniques, and their implications for conservation', *Journal of the Institute of Conservation*, vol. 35, no. 2, pp. 115-6.
- Hill, R. 2011, *Colour and Ceremony: the role of paints among the Mendi and Sulka peoples of Papua New Guinea*, Durham University, Durham E-Theses, viewed April 10 2015, <<http://etheses.dur.ac.uk/3562/>>.
- Hughes, I. 1977, *New Guinea Stone Age Trade: The Geography and Ecology of Traffic in the Interior*, Department of Prehistory, Research School of Pacific Studies, The Australian National University.
- Johns, S., Lambertson, J., Morton, T., Soares, H. & Willing, R. 1987, 'Camnosperma Exudates. The Optically Active Long Chain 5-Hydroxycyclohex-2-Enones and Long-Chain

- Bicyclo[3.3.1]Nonane-3,7-Diones', *Australian Journal of Chemistry*, vol. 40, no. 1, pp. 79-96.
- Koestler, R.J. & Art, M.M.o. 2003, *Art, Biology, and Conservation: Biodeterioration of Works of Art*, Metropolitan Museum of Art.
- Learner, T. 2000, 'A review of synthetic binding media in twentieth - century paints', *The Conservator*, vol. 24, no. 1, pp. 96-103.
- Learner, T. 2004, *Analysis of modern paints*, Getty Conservation Institute, Los Angeles.
- Luna-Zaragoza, D., Romero-Guzmán, E. & Reyes-Gutiérrez, L. 2009, 'Surface and physicochemical characterization of phosphates vivianite, $\text{Fe}_2(\text{PO}_4)_3$ and hydroxyapatite, $\text{Ca}_5(\text{PO}_4)_3(\text{OH})$ ', *Journal of Minerals and Materials Characterization and Engineering*, vol. 8, no. 08, p. 591.
- Maier, M.S., de Faria, D.L.A., Boschin, M.T. & Parera, S.D. 2005, 'Characterization of reference lipids and their degradation products by Raman spectroscopy, nuclear magnetic resonance and gas chromatography-mass spectrometry', *Archive for organic chemistry*, no. 12, pp. 311-8.
- Nguyen, T.T., Gobinet, C., Feru, J., -Pasco, S.B., Manfait, M. & Piot, O. 2012, 'Characterisation of Type I and IV Collagens by Raman Microspectroscopy: Identification of Spectral Markers of the Dermo-Epidermal Junction', *Spectroscopy: An International Journal*, vol. 27, no. 5-6, p. 7.
- Otero, V., Sanches, D., Montagner, C., Vilarigues, M., Carlyle, L., Lopes, J.A. & Melo, M.J. 2014, 'Characterisation of metal carboxylates by Raman and infrared spectroscopy in works of art', *Journal of Raman Spectroscopy*, vol. 45, no. 11-12, pp. 1197-206.
- Piriou, B. & Poullen, J.F. 1984, 'Raman study of vivianite', *Journal of Raman Spectroscopy*, vol. 15, no. 5, pp. 343-6.
- Ploeger, R., Scalarone, D. & Chiantore, O. 2008, 'The characterization of commercial artists' alkyd paints', *Journal of Cultural Heritage*, vol. 9, no. 4, pp. 412-9.

- Prinsloo, L.C., Tournié, A., Colomban, P., Paris, C. & Bassett, S.T. 2013, 'In search of the optimum Raman/IR signatures of potential ingredients used in San/Bushman rock art paint', *Journal of Archaeological Science*, vol. 40, no. 7, pp. 2981-90.
- Prinsloo, L.C., Wadley, L. & Lombard, M. 2014, 'Infrared reflectance spectroscopy as an analytical technique for the study of residues on stone tools: potential and challenges', *Journal of Archaeological Science*, vol. 41, pp. 732-9.
- Robson, R.W. 1954, 1958, 1961, 1964, 1966, 1969, *The handbook of Papua and New Guinea*, Ed1- Ed6 edn, Pacific Publications, Sydney.
- Rodgers, K.A., Kobe, H.W. & Childs, C.W. 1993, 'Characterization of vivianite from Catavi, Llallagua Bolivia', *Mineralogy and Petrology*, vol. 47, no. 2-4, pp. 193-208.
- Rohman, A., Kuwat, T., Retno, S., Yuny, E. & Tridjoko, W. 2012, 'Fourier transform infrared spectroscopy applied for rapid analysis of lard in palm oil', *International Food Research Journal*, vol. 19, no. 3, pp. 1161-5.
- Rutherford, D.W., Wershaw, R.L. & Cox, L.G. 2005, *Changes in composition and porosity occurring during the thermal degradation of wood and wood components*, U.S. Dept. of the Interior, U.S. Geological Survey, Reston, Virginia.
- Sarmiento, A., Pérez-Alonso, M., Olivares, M., Castro, K., Martínez-Arkarazo, I., Fernández, L.A. & Madariaga, J.M. 2011, 'Classification and identification of organic binding media in artworks by means of Fourier transform infrared spectroscopy and principal component analysis', *Analytical and Bioanalytical Chemistry*, vol. 399, no. 10, pp. 3601-11.
- Scherrer, N.C., Stefan, Z., Françoise, D., Annette, F. & Renate, K. 2009, 'Synthetic organic pigments of the 20th and 21st century relevant to artist's paints: Raman spectra reference collection', *Spectrochimica Acta Part A: Molecular and Biomolecular Spectroscopy*, vol. 73, no. 3, pp. 505-24.
- Scott, D.A. & Eggert, G. 2007, 'The vicissitudes of vivianite as pigment and corrosion product', *Studies in Conservation*, vol. 52, no. Supplement-1, pp. 3-13.

- Simkovic, I., Dlapa, P., Doerr, S.H., Mataix-Solera, J. & Sasinkova, V. 2008, 'Thermal destruction of soil water repellency and associated changes to soil organic matter as observed by FTIR spectroscopy', *CATENA*, vol. 74, no. 3, pp. 205-11.
- Smith, G.D., Newton, K.E. & Altherr, L. 2015, 'Hydrofluoric acid pre-treatment of matte artists' paints for binding medium analysis by Fourier transform infrared microspectroscopy', *Vibrational Spectroscopy*, vol. 81, pp. 46-52.
- Stevenson, F.J. 1994, *Humus Chemistry: Genesis, Composition, Reactions*, Wiley.
- Strathern, A. & Strathern, M. 1971, *Self-decoration in Mount Hagen*, Gerald Duckworth & Co. Ltd, London.
- Teetsov, S.A. 2006, 'Prep School : Micro-Extraction of Soluble Components from Small Particles for Infrared Analysis ', *Modern Microscopy Journal*.
- Tinti, A.T., Tugnoli, V.T., Bonora, S.B. & Francisco, O.F. 2015, 'Recent applications of vibrational mid-Infrared (IR) spectroscopy for studying soil components: a review ', *Journal of Central European Agriculture*, vol. 16, no. 1, pp. 1-22.
- Viana, R.R. & Prado, R.J. 2007, 'Mineralogical and chemical characterization of vivianite occurrence in pegmatites from the Eastern Brazilian pegmatite province', *Unpaginated abstract in: Granitic Pegmatites: the State of the Art (T. Martins and R. Vieira, editors). Memórias*, vol. 8.
- Wanek, A. & Studies, N.I.o.A. 1996, *The State and Its Enemies in Papua New Guinea*, Curzon.
- Wang, A., Haskin, L.A. & Jolliff, B.L. 1998, 'Characterization of Mineral products of oxidation and hydration by laser raman spectroscopy- Implications for in situ prtrological investigation on the surface of Mars', paper presented to the *Lunar and Planetary Science XXIX*, Houston.
- Wilson, N. 2014, 'Plumes and pearlshells: the shows of the New Guinea Highlands', in N. Wilson (ed.), *Plumes and Pearlshells: Art of the New Guinea Highlands*, Art Gallery of New South Wales, Sydney, pp. 11-6.



Chapter 4

NON-INVASIVE ANALYSIS OF
PIGMENTS AND LIGHTFASTNESS OF
“*POEM*” SERIES OF PRINTS BY
JAPANESE ARTIST HAKU MAKI

4.1 BACKGROUND

Maejima Tadaaki (1924-2000), known since 1950 as Haku Maki, established himself in the canon of Japanese printmakers by producing prints of modified Chinese characters (kanji) in brilliant, contrasting colours using an unusual embossing technique (Tretiak 2007). A small collection of 24 prints was gifted to the Indianapolis Museum of Art (IMA) in 2013. Recently, four of his works from the “Poem” series (Fig. 4.1) were investigated to understand their state of preservation and to learn more about the materials of this innovative artist.

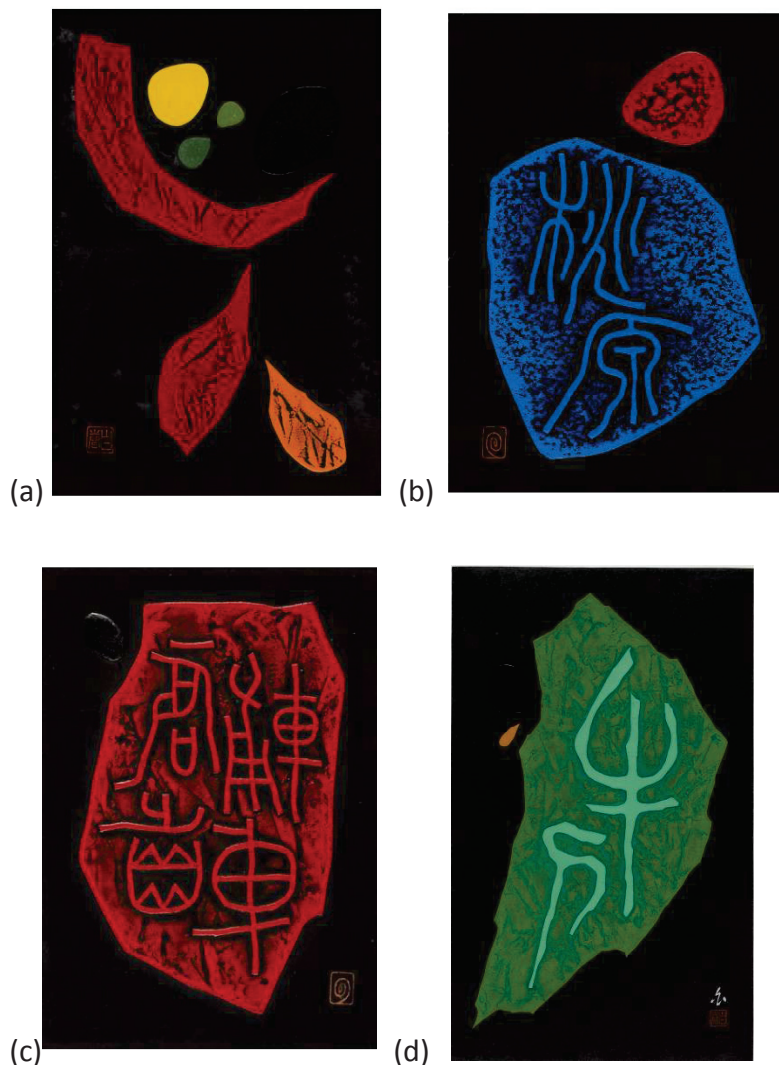


Fig. 4.1 Prints by Haku Maki. (a) Poem 71-29, 1970, IMA#2013.419, 10.5”x7.25”, (b) Poem 70-90, 1970 IMA#2013.418, 6.5”x4.75”, (c) Poem 70-70, 1970, IMA#2013.417, 6.5”x4.5”, and (d) Poem 71-61, 1971, IMA#2013.420, 17.24”x10.5”. Gifts of Donald A. and Loryne M. Coffin. White efflorescence is visible in the black fields of (a). Photos courtesy of IMA.

Initiated by the paper conservator, the analysis was held in an attempt to comprehend the artwork's condition prior to an upcoming exhibition. At the time of accessioning, some prints were observed to have unknown white efflorescence on their surface, most easily seen in the velvety black regions (Fig. 4.1a). On closer look, the exceptionally bright colours are deemed unusual for printing inks and the conservator is concerned if these colours have a potential to fade. Yet, very little information is available on the paint materials used by Haku Maki. In the scant contemporary literature on Maki's printmaking (Petit & Arboleda 1977; Tretiak 2007), he is reported to have relied on Portland cement modified with a chemical bond additive to create his hard textural surfaces and a coating of shellac to prevent water penetration. His colours were comprised of poster paints, oil paints thinned with turpentine, and full-bodied offset printing inks diluted with a thinner spread ink to prevent the paper from sticking to the block or to create a glossier appearance. These generic information, however, do not express more about his choices of pigments or media.

As a result, it became desirable to learn more about Maki's choice of printing inks and paints as well as to assess the stability of these intensely luminous colourants to light prior to their exhibition.

4.2 MATERIALS AND METHODS

4.2.1 REFERENCE SAMPLES

Pigment reference samples were acquired in order to confirm spectral characterizations and to construct model samples of paint mixtures. Aniline black (Paliotol L0080, PBk1) was acquired from BASF, chrome yellow medium (PY34) and toluidine red (PR3) from Kremer Pigments, and molybdate orange (PR104) from Rublev. A reference for lamp black (PBk6) was acquired in the form of a commercial Winsor & Newton watercolour tube paint. Model paints were prepared by mulling the pure pigment or 4p:1p (aniline black: lamp black) pigment mixtures with Kremer gum arabic prepared as a thick watercolour paste according to an artist's recipe (Mayer 1950) and spread to dry on white paper or glass slides.

4.2.2 OPTICAL MICROSCOPY

Stereomicroscopy was performed at low magnification (7.5 X to 150 X) on a Zeiss Discovery V20 microscope while inspection at higher magnification was performed in transmission mode on a Zeiss AxioImager M2m compound microscope. Microsamples of the white haze were acquired for transmission optical microscopy using a tungsten needle and then transferring the sample to transparent adhesive tape that was adhered to a glass microscope slide. Photomicrographs were taken using a Zeiss ERc5 digital camera on the stereomicroscope and a Zeiss MRc5 on the compound microscope.

4.2.3 FTIR MICROSCOPY

Fourier transform infrared (FTIR) microspectroscopy was performed on a Continuum microscope with an MCT A detector coupled to a Nicolet 6700 spectrometer purged with dry, CO₂-free air. The spectra are the sum of 64 co-additions at 4 cm⁻¹ spectral resolution. Microsamples were crushed on a diamond compression cell and held on a single diamond window during the analysis. Sample identification was performed using the Infrared and Raman Users Group (IRUG) reference spectral library.

4.2.4 RAMAN MICROSCOPY

Raman spectra were acquired using a Bruker Senterra microspectrometer on a Z-axis gantry. The spectrometer utilizes 3 selectable excitation lasers (532, 633, and 785 nm), an Andor Peltier-cooled CCD detector, and a 50 μm confocal pinhole. Laser power at the surface of the print was below 5 mW. The spectra are the result of 10 s integrations with 10-30 co-additions. A 50 X ultra-long working distance objective was used to focus on select pigment particles directly on the prints. The analysis spot size was on the order of 1 μm, and the spectral resolution was in the range of 3-5 cm⁻¹ or 9-18 cm⁻¹. OPUS software allowed for automated cosmic spike removal, peak shape correction, and spectral calibration.

4.2.5 MICROFOCUS X-RAY SPECTROSCOPY (XRF)

A Bruker Artax microfocus XRF with rhodium tube, silicon-drift detector, and polycapillary focusing lens (≈100 μm spot) was used in the analysis. Experimental parameters included

50 keV tube voltage, 600 μ A current, and 600 s live time acquisitions. A helium purge gas allowed for light element detection. Elemental survey spectra were collected in the energy range from 0 to 50 keV.

4.2.6 MICROFADE TESTING (MFT)

In situ accelerated lightfastness testing was achieved with a Newport-Oriel style microfademeter previously described by Whitmore et al (Whitmore, Pan & Bailie 1999). The xenon arc lamp source was filtered to emit only visible light in the wavelength range of 400-700 nm. The luminous flux was measured at \approx 0.72 lumens using an ILT1700 radiometer with SPD024Y probe from International Light Technologies. Spectral reflectance data were acquired from an approximately 400 μ m spot every minute over the period of 10 min. The time period of 10 min is sufficient to show the different rate of fading. Colour difference was calculated using the CIE Lab* colour difference equation from 1976.

Triplicate analyses of fading curves for ISO Blue Wool Standards 1, 2, and 3 (BWS1-3, Talas) were run prior to the analysis of the artwork. Single in situ measurements were made of each prominent colour observed in the print under study. A lightfastness equivalency for each paint or ink was assigned based on the sample's similarity to fading curves for BWS1-3.

4.3 RESULTS & DISCUSSION

4.3.1 WHITE HAZE

The white hazy patches were examined with optical stereo-microscopy, using fibre optic light illuminating at an angle at magnifications up to 100 X. The white film was seen as a soft, fibrous network of filaments enveloping the surface of the black ink layer. The areas of occurrences appear to be random, where some areas appear thicker than others. Under UVa illumination using a black light lamp, there is no clear fluorescence from the white film. These prints had been previously framed under glass, and it was thought that the white haze might be a fatty acid bloom arising from the printing ink's interaction with the storage environment (Ordonez & Twilley 1997; Puglieri et al. 2016). To investigate further, a microsample of the white haze had to be removed for FTIR transmission microscopy, which

was selected as the mode of analysis. Placing the print directly under the micro-ATR tip was avoided, lest it left any accidental mark on the print.

Removing these particles as a microsample without disrupting the black ink layer was difficult, especially in the areas with a thin sheen (Fig. 4.2a). The ease of dislodging the black ink particles suggests the paint is highly underbound. The white filaments also appear to penetrate into the black layer. However, a thicker agglomerate of white filaments, shown in Fig. 4.2b, allowed the lifting of a microsample of the white material without interferences from the underlying black paint. Examined in transmission mode using a compound microscope, the sample in Fig. 4.2c shows a similarity to dehydrated fungal hyphae, suggestive of biological growth. However, no characteristic conidia were observed.

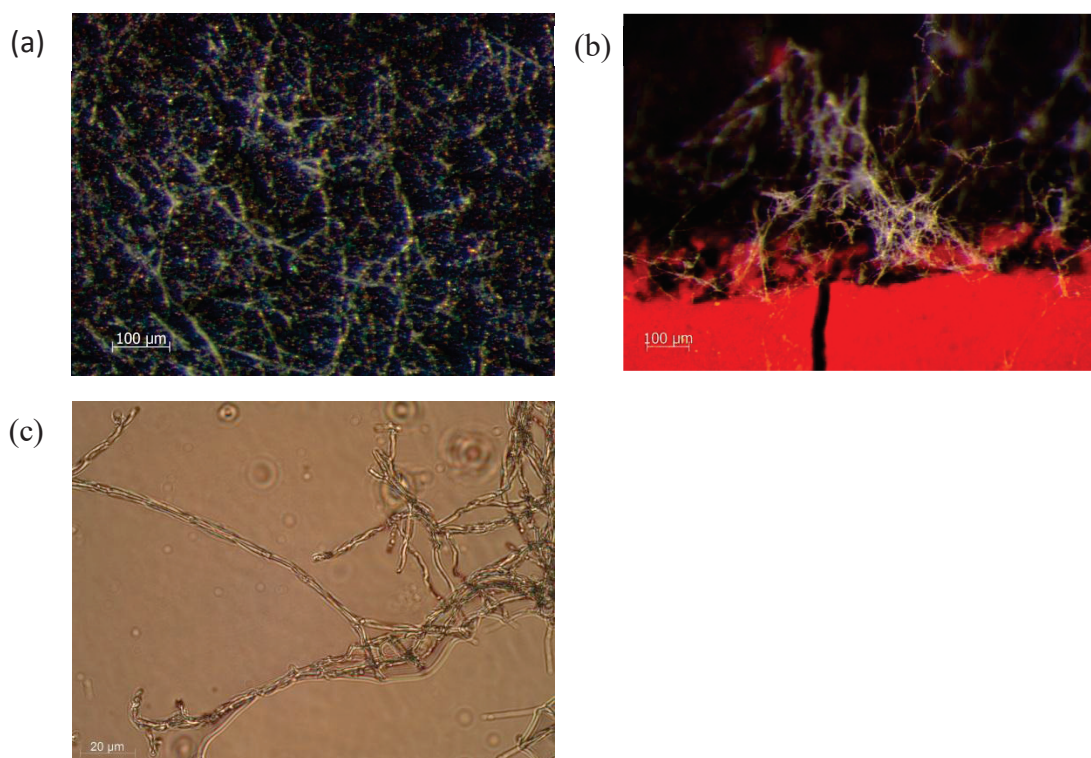


Fig. 4.2 Photomicrographs of the white efflorescence on *Poem 71-29*: (a) thin and soft web-like layer, (b) thicker clump of white filaments, and (c) transmission optical image of the fungal hyphae.

To confirm the biological nature of the white surface material, an infrared spectrum of the filaments was obtained (Fig. 4.3a). The spectral features did not appear similar to cotton fibres from the paper (Fig. 4.3b), ruling out a disruption of the printing support that could

have resulted from the repeated pressing typical of Maki's technique. The spectrum of the white filaments reveals glycoprotein bands comparable to previous studies reported for fungal mycelia (Dixit et al. 2014; Erukhimovitch et al. 2005; Gupta, Jelle & Gao 2015). The wavenumbers at 1643, 1545 and 1452 cm^{-1} were attributed to protein amide I, II and III bands. It should be noted that Maki has not been reported to use any proteinaceous glue based sizing or adhesive for laminating - only rice starch paste (Petit & Arboleda 1977) - so contamination is unlikely. The shoulder at around 1720 cm^{-1} can be attributed to lipid C=O stretching, and the remaining C-O and C-H vibrations between 1420-1030 cm^{-1} can arise from cell carbohydrate and phospholipid moieties. The assignment of the spectrum to mould was further confirmed by its close comparison in the lab to a white mould sample obtained from decaying vegetable skins (not shown).

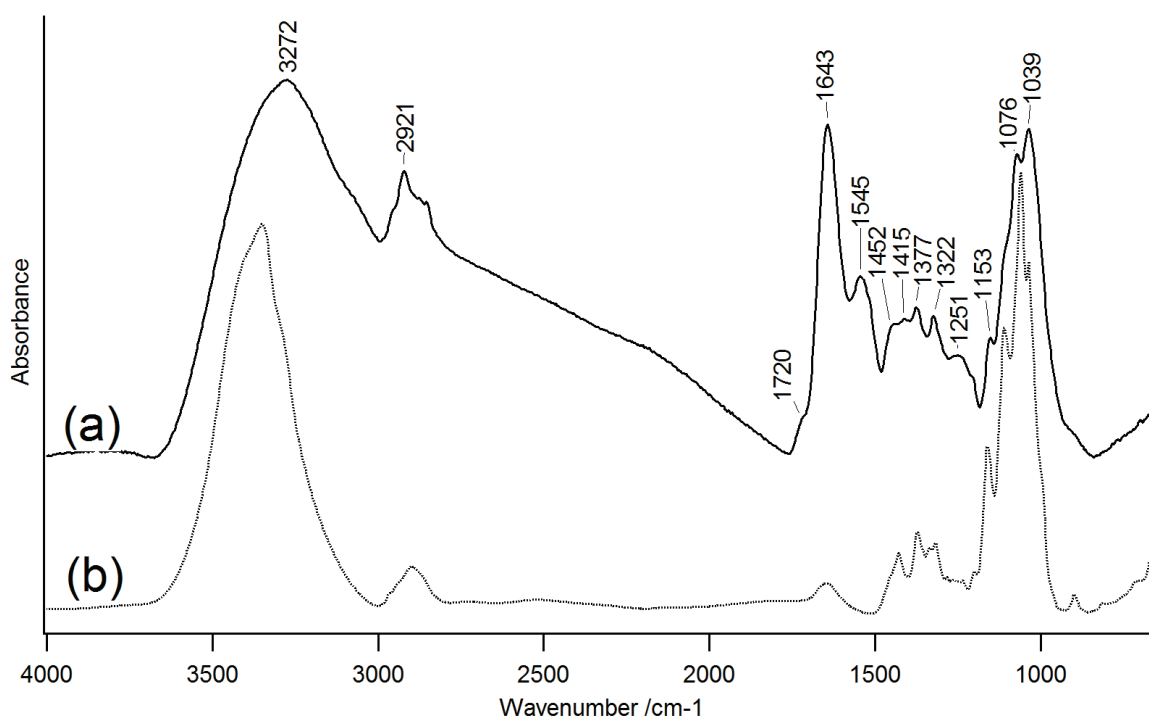


Fig. 4.3 FTIR spectrum of (a) the white filaments shown in Fig. 4.2b and (b) a paper fiber taken from the print Poem71-29.

4.3.2 PIGMENT IDENTIFICATION

Although the nature of the disfiguring white haze was quickly resolved using light microscopy and infrared spectroscopy, the nature of the pigments, especially the matte black pigment on which the mycelia were concentrated, was also of interest.

To preserve the original artwork, every effort was made to conduct only non-destructive, in situ analyses of the artist's palette. However, when sampling the white filaments from the prints, microsamples of the underbound black matte paint were also dislodged and became available for transmission FTIR spectroscopy. The structure of this synthetic organic black pigment is shown in the inset of Fig 4.4. Its strong visible absorption arises from its highly conjugated polymeric structure. The strong bands at 1590 and 1508 cm^{-1} in the FTIR spectrum are attributed to quinonoid and benzene ring stretching whereas the sharp features at 829, 754 and 696 cm^{-1} arise from the di- and mono-substitutions of the benzene rings (Trchová & Stejskal 2011). Although a clear indication of the black pigment was obtained, no evidence of the binding medium was seen in the FTIR spectrum, again hinting at a largely underbound matte black paint used on the prints.

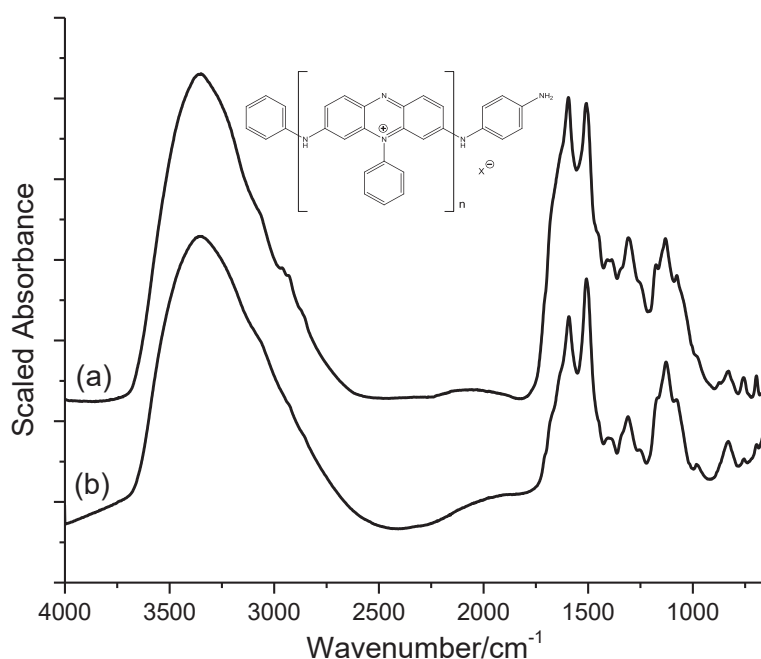


Fig. 4.4 FTIR spectral comparison of (a) the black paint in Poem 71-29 and (b) an aniline black reference pigment whose structure is shown in the inset ($n \approx 3$, $X^- = \text{HCrO}_4^-, \text{Cl}^-$).

Aniline black, also known as chrome black, is perhaps the earliest of the synthetic organic pigments, being discovered between 1860 and 1863 (Eastaugh 2013). It is known for its matte finish (Herbst & Hunger 2002), which Maki uses to contrast with the glossier, high key pigments of the coloured subjects. Although aniline black is known to have been widely used in the printing and dyeing industries since 1863, it has only previously been specifically

identified in the cultural heritage literature as an ink in a 1930s printed book (Doncea & Ion 2014). In that work, Doncea and Ion published a diffuse reflectance infrared spectrum (DRIFTS) for the pigment, but the dependence of the DRIFTS technique on the optical properties of the sample makes it insufficient to serve as a general reference for further identifications. It should be noted that the popular Infrared and Raman Users Group (IRUG) spectral database does not contain a reference spectrum of aniline black (Price & Pretzel 2007), which may have contributed to the lack of observed occurrences for this historically important pigment. To the authors' knowledge, the aniline black reported here for three of Haku Maki's "Poem" series prints is the pigment's first discovery on a work of fine art. The use of aniline black has declined since the mid-1930s when other synthetic blacks that were safer and easier to apply emerged onto the market (Travis 1994). It is worth noting, however, that the pigment is still included in several commercial artists' paint lines, such as Winsor & Newton's Designers Gouache Jet Black (#50947171) and Holbein's Artists' Watercolour Tube Peach Black (#W137W337), where it is mixed in the latter with lamp black. As such, it would not be surprising to find other examples of the use of aniline black, even in contemporary artworks.

The remainder of the inks were analysed non-destructively on the four prints using Raman microspectroscopy and XRF. These results are summarized in

Table 4.1. By casual observation of Maki's prints, it might seem that Haku Maki used a fairly simple and consistent range of pigments for the "Poem" series, but these results prove otherwise with a rather large range of pigments identified, including for instance three different pigment mixtures for green colours in *Poem 71-61*. Interestingly, the only pigment previously reported to have been used by the artist, cobalt blue (Petit & Arboleda 1977), in fact does not appear in these works. The only vibrant blue in this study that fits that description appears in *Poem 70-90* (Fig. 4.1b) where the paint is in fact comprised of phthalocyanine blue (PB15) with a small amount of Prussian blue (PB27) and ultramarine (PB29). It could be that the previous reference to "cobalt blue" was merely describing a deep vibrant blue coloured paint and not the actual pigment.

The previous identification of aniline black by FTIR in the background of *Poem 71-29* was confirmed using Raman spectroscopy on three of the artworks analysed. The 532 nm

excitation laser was preferred over 633 nm and 785 nm for its stronger scattering efficiency, while a very low power of less than 0.1 mW was necessary to avoid thermal degradation of the black pigment. Fig. 4.5a shows the Raman spectrum of the black background in *Poem 70-70* compared to a reference sample of aniline black, Fig. 4.5b, collected as a watercolour preparation under identical instrumental parameters.

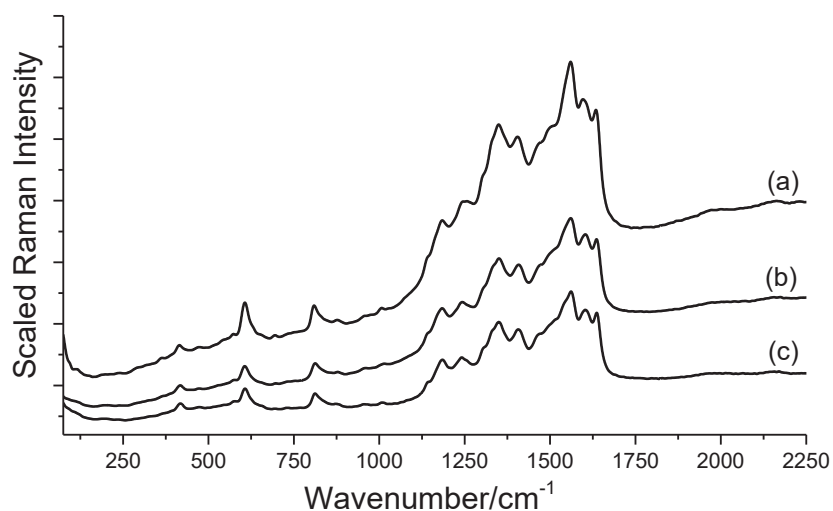


Fig. 4.5 Raman spectrum collected at 532 nm, of the black background in (a) *Poem 70-70* compared to (b) a reference sample of aniline black watercolour. A similar match is obtained when (c) aniline black is diluted in a 4:1 ratio with lamp black in watercolour medium.

The bands arising from the black background, namely at 1634, 1596, 1561 (vs), 1403 (s), 1351 (s), 1243, 1185, 810s, 606 (s) and 415 cm⁻¹, gave a close match to the aniline black reference. While the usual practice is to assign the black background as solely aniline black, in this case, the presence of carbon black was suspected, since aniline black is often admixed with a carbonaceous black pigment in commercial paint preparations. The Raman spectrum obtained did not show bands attributable to carbon black, likely because the Raman peaks for carbon black at ~ 1325 and 1580 cm⁻¹ are broad and they fall under the similarly broad features in the pure aniline black reference pigment. Fig. 4.5c shows a reference mixture of aniline black and lamp black in a 4:1 ratio prepared as a watercolour paint. Based on the similarity of the three spectra, the poster paint used in the Haku Maki background could possibly be a mixture of both aniline black and carbon-based black pigments.

Table 4.1 Summary of the results from Raman and XRF analyses of pigments on selected Haku Maki prints from the “Poem” series.

“Poem” Print	Colour	Raman results	XRF*	Remark
70-70 (1970)	Paper	-	Ti, Ca, (Fe, S)	Likely titanium white and chalk filler
	Black	aniline black, carbon black?	Cr, Cu, Ca, Ti, (S, Cl, Fe)	Black layer underlies all other colours
	Glossy black	strong fluorescence	Cr, Cu, Ca, Ti, (S, Cl, Fe, Co)	Co appears characteristic of glossy black
	Red	PR3, BaSO ₄	Pb, Cr, Ba, S, Mn, Cu, Ca, (K, Fe, Al)	Mn and Pb may indicate use of siccativ
	Red seal	molybdate orange, PR22, CaCO ₃ , PR48:3?	Pb, Cr, Cu, Ca, Ti, (K, Fe, Mo, Cl)	PR48:3 features appear as trace Raman signal
70-90 (1970)	Paper	-	Ti, Ca, (Fe)	Likely titanium white and chalk filler
	Black	aniline black, carbon black?	Cr, Cu, Ca, Fe, Cl, S, Ti	Black layer underlies all other colours
	Blue	phthalocyanine, Prussian, and ultramarine blues	Zn, (Fe, Cu, Cr, Al, Si, Ti, Ca, S)	Zinc white may be present, although not detected by Raman
	Red	PR3, BaSO ₄	Pb, Cr, Ba, S, Mn, Cu, Ca, (Al, K, Fe)	Mn and Pb may indicate use of siccativ
	Red seal	molybdate orange, PR48:3	Cr, Pb, Cu, Ba, Ca, (Fe, Cl, Mo, Cd)	-
71-29 (1970)	Paper	-	Ca, Ti, (Fe, Cu)	Likely titanium white and chalk filler
	Black	aniline black, carbon black?	Cr, Cu, Fe, Ca, K, Cl, S, Ti, (Al, Si, Pb)	Black layer underlies all other colours
	Dark green	chrome yellow, Prussian blue	Pb, Cr, Fe, (Cu, Ti, Ca, Al)	Common mixture known as chrome green
	Light green	chrome yellow, Prussian blue	Pb, Cr, Fe, (Cu, Ti, Ca, Al, Zn)	Common mixture known as chrome green
	Yellow	chrome yellow	Pb, Cr, (Cu, Ba, Ca, Al, Fe)	-
	Orange	chrome yellow	Pb, Cr, (Cu, Ca, Ba, Al, Fe, Mo)	Predominantly monoclinic phase PY34, Mo indicates presence of molybdate orange
	Red	PR3, BaSO ₄	Cr, Cu, Ba, S, Ca, Pb, Fe, (Al, K)	-

	Red seal	molybdate orange, PR48:3, iron oxide?	Pb, Cr, Cu, Ca, Ba, (Fe, Mo, Cd, Cl)	possible traces of iron oxide
71-61 (1971)	Paper	-	Ca, Ti, (Fe)	Likely titanium white and chalk filler
	Black	carbon black, Prussian blue	Ca, Ti, Fe, Zn, (S)	Black layer underlies all other colours
	Glossy black	strong fluorescence	Cr, Cu, Ca, Ti, (Fe, Co, Cl, S)	Co appears characteristic of glossy black
	Light green	barium chromate, viridian	Ba, Cr, Pb, (Ca, Fe, Cu, Al)	Possible Pb drier or lead white underneath the green paint
	Medium green	chrome yellow, Prussian blue	Pb, Cr, Fe, (Cu, Ca, Ti, Al)	Common mixture known as chrome green
	Dark green	chrome yellow, phthalocyanine blue	Pb, Cr, Cu, Fe, Ba, Si, (Al, K, Ca)	-
	Silvery white	strong fluorescence	Ca, Ti, Fe, Zn, (Al)	Possibly titanium white with chalk and zinc white
	Brown	strong fluorescence	Fe, Cu, Cr, (Ca, Ti, Si, S, K)	Possibly iron oxide pigment
	Red seal	molybdate orange, PR48:3	Ca, Ti, Ba, Cr, Fe, Pb, Zn, (Mo, Cd)	-

***Major**, minor, (trace) intensities.

The occurrence of Cr, Cu, S and Cl in the elemental spectrum of these black areas in *Poem 70-70*, *Poem 70-90*, and *Poem 71-29* (Table 4.1) is characteristic of aniline black and is consistent with the manufacture of the pigment (Herbst & Hunger 2002). The black paint underlying the other coloured areas contributes a strong chromium XRF signal to other colours even if chrome yellow is not present in them. Interestingly, the black background in *Poem 71-61*, made a year later than the other three prints, is characterised as a mixture of carbonaceous black and Prussian blue (PB27). The black background in this print appears visually less intense when compared with the other three prints. The identification of Prussian blue in these blacks has important conservation implications for future treatment strategies; for instance, strong alkaline treatments and anoxic environments would not be desirable.

Another striking colour, the orange in *Poem 71-29*, proved similarly interesting. As seen in Fig. 4.6a, the Raman spectrum of the orange paint showed only strong bands similar to those of yellow lead chromate (Fig. 4.6b) and no other bands indicative of a red or orange

pigment contributing to the orange hue observed in the print. A Raman spectrum of chrome orange (PO21: $\text{PbO}\cdot\text{PbCrO}_4$) is shown in Fig. 4.6c to rule out the presence of this orange variant of chrome yellow. A tiny sample was extracted and analysed by FTIR microspectroscopy (not shown) to test for the presence of any red or orange synthetic organic pigment. However, only strong chromate stretching bands and bands due to an oil medium were observed, with no features suggestive of a synthetic organic pigment.

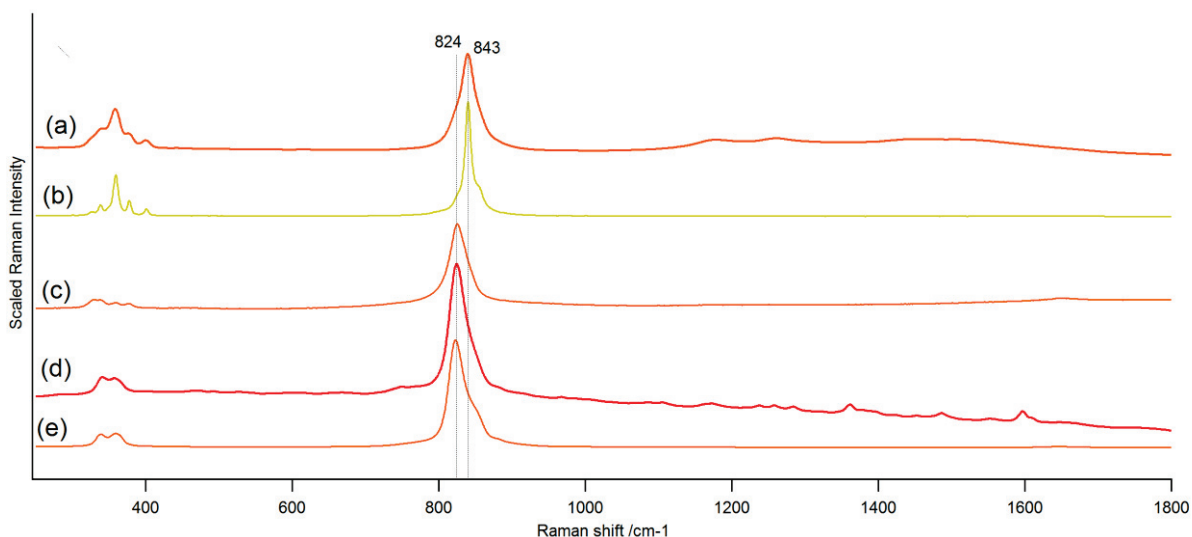


Fig. 4.6 Raman spectra of (a) the orange paint in Poem 71-29 at 785 nm, (b) chrome yellow (PY34) at 633 nm, (c) chrome orange (PO21) at 633 nm, (d) the red artist's seal in Poem 70-90 at 633 nm and (e) molybdate orange (PR104) at 633 nm.

XRF analysis was undertaken to check for the possible presence of an inorganic component that was not observed with Raman analysis. The XRF analysis of the orange paint indicated the unusual presence of (Mo) molybdenum (Fig. 4.7a), suggesting that the orange paint could in fact include molybdate orange (PR104), a solid solution of $\text{PbCrO}_4\cdot\text{PbMoO}_4\cdot\text{PbSO}_4$ in varied proportions, combined with the dominant chrome yellow. It was reported that blending molybdate orange and chrome yellow matches the colour of chrome orange at lower cost and better gloss (Gardner & Sward 1922) and such pigment combination was reported as existing in one of the commercial watercolour paint tubes (Wilcox 1991). The presence of Mo in the orange paint is evident as a distinctive peak in Fig. 4.7a, whereas this is not seen in the underlying black paint (Fig. 4.7b) or in the yellow paint (Fig. 4.7c). Molybdate orange has been a common industrial pigment since its commercialization in 1934-35 (Eastaugh 2013), but to date no published identifications have appeared in the

conservation literature. Among unpublished sources, molybdate orange was previously detected in the IMA's 1967 Donald Judd sculpture *Untitled* (IMA#1992.362), and a poster presented at the 2015 American Institute for Conservation's annual meeting in Miami reported its use in admixture with lead chromate yellow in Robert Murray's *Duet* owned by California State University, Long Beach.

As a mixed salt, molybdate orange generally contains only about 10 % lead molybdate (Buxbaum & Pfaff 2005). Because the tinting strength of molybdate orange is strong, the proportion of this colourant added to the paint also appears to be low, hence the weak intensity of the Mo peak in the XRF spectrum when the pigment is admixed with another lead containing pigment. Additionally, the distinctive Raman signature of molybdate orange does not show up when in the presence of the strongly scattering chrome yellow, preventing its detection solely by Raman analysis.

Molybdate orange appears again in the red artist's seals on all four prints. The Raman spectrum of the red artist's mark in *Poem 70-90* (Fig. 4.6d) matches the spectrum of a molybdate orange reference pigment (Fig. 4.6e), and Mo appears again in the XRF analysis for all of the artist's seals (Table 1). All of the Raman spectra taken from the seals also include a series of weak bands in the region of 1000-1600 cm^{-1} . Molybdate orange is often blended with synthetic organic pigments to produce a red shade (Buxbaum & Pfaff 2005), particularly toluidine red (PR3) (Eastaugh 2013), but in this case, the spectral match with PR3 is poor. The Raman spectral bands for three of the red signatures, however, match those of the BONA pigment lake PR48:3, in which *Poem 71-29* shows an additional small peak at 289 cm^{-1} , which is one of the strongest shifts characteristic of an iron oxide pigment. Unlike the other prints, the organic pigment in the red seal on *Poem 70-70* matches the Naphthol AS pigment PR22, and calcium carbonate is also observed. This suggests the use of a similarly coloured, but slightly modified paint formulation. An additional peak shoulder at 1598 cm^{-1} indicates the presence of what is likely another synthetic organic pigment. While this pigment could not be identified with confidence based on one shoulder peak, this spectral feature could be the strongest Raman band of PR48:3, the synthetic organic pigment found in the other red seals.

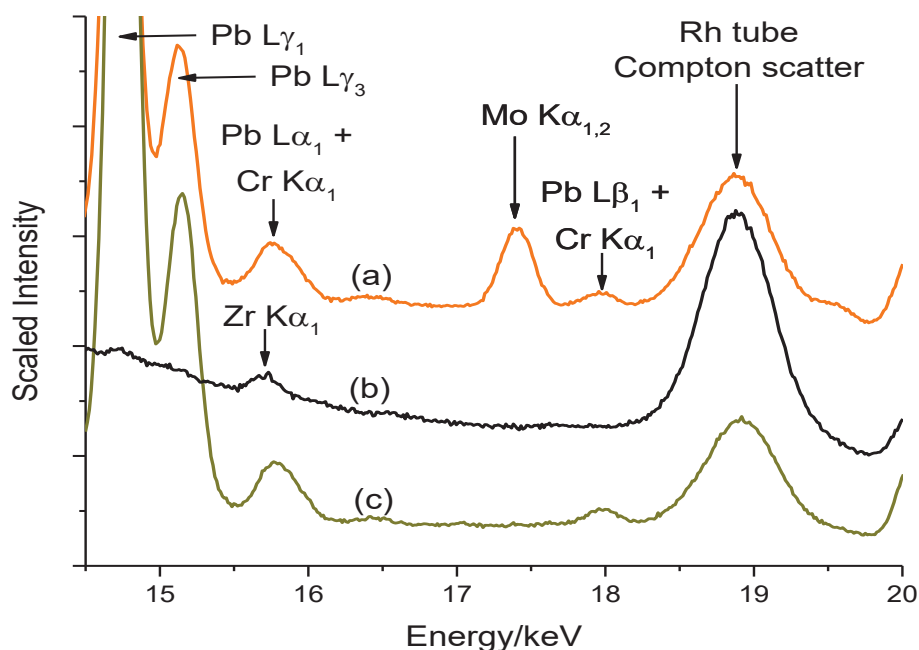


Fig. 4.7 Detail of the XRF elemental spectra of *Poem 71-29* (a) orange paint, (b) black paint, and (c) yellow paint.

4.3.3 MICROFADE TESTING

The vibrancy of the contrasting colours in the Haku Maki prints and the potential for lengthy or repeated exhibition raised concerns over the stability of the inks to light. Chrome based pigments are known to darken upon exposure to light, and the lightfastness of aniline black is variously reported as either good or questionable. Herbst and Hunger's authoritative industrial textbook describes the lightfastness of aniline black as good in the masstone, but weaker when admixed with titanium white (Herbst & Hunger 2002). However, several artists' websites and watercolour manuals list the pigment in commercial paints as being of only moderate lightfastness or fugitive unless mixed with carbon black (McEvoy 2015; Myers 2013; Wilcox 1991). Molybdate orange in particular is considered to have only modest lightfastness (Buxbaum & Pfaff 2005; Wilcox 1991).

One print, *Poem 71-29*, was chosen for in situ lightfastness testing as it has a wide ranging palette including the pigments of particular concern. Fig. 4.8 shows the total colour change (ΔE) of the artwork's paint colours in comparison to BWS 2 and 3 upon exposure to visible light. Any colour change faster than the fading curve of BWS 3 is considered fugitive (Whitmore, Pan & Bailie 1999) and careful consideration is required when planning

exhibition lighting and duration. For this particular print, only the orange and yellow colours are considered fugitive, whereby the orange colour showed a more dramatic change in lightfastness (Fig. 4.8). All other colours of black, green and red performed better than BWS 3 and were not considered fugitive.

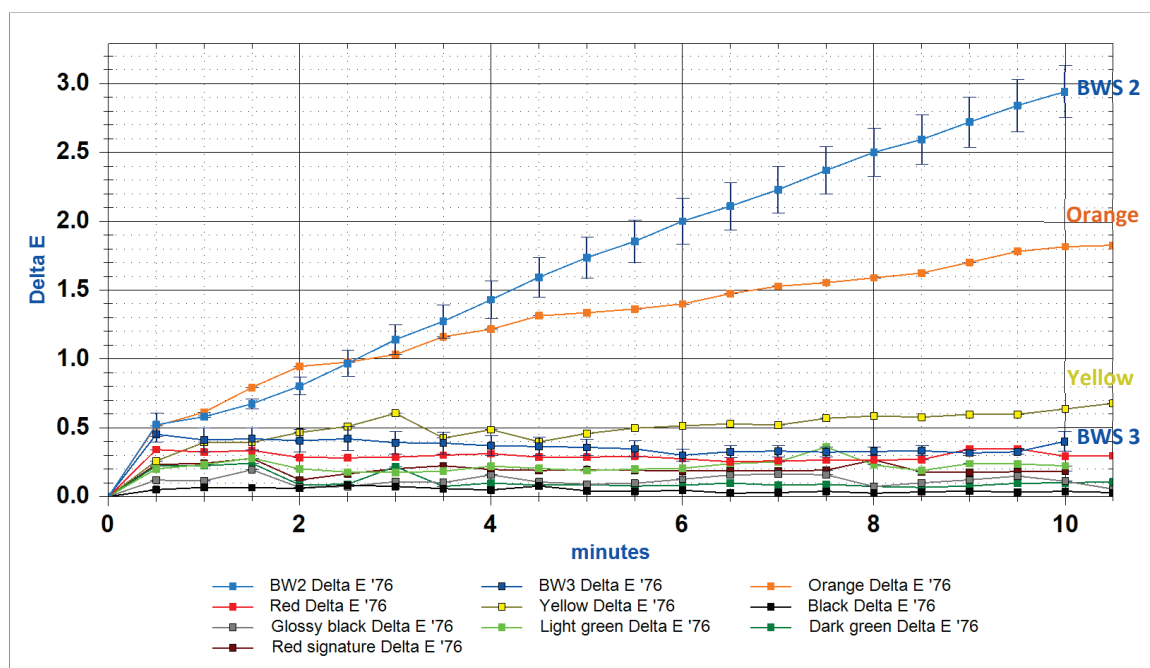


Fig. 4.8 ΔE fading curves for the coloured areas of Poem 71-29. The colours being analysed are as indicated in the data traces, and the blue lines indicate average fading (with error bars) for the triplicate analyses of BWS 2 (upper) and BWS 3 (lower).

In this print, the aniline black paint did not show rapid colour change. Due to mixed reviews on its lightfastness, the fading of the pure pigment, as well as in an equal mixture with lamp black prepared as watercolour samples, were studied (Fig. 4.9). The MFT results show that aniline black is in fact particularly susceptible to fading on its own, fading at a rate greater than BWS 3. Analysis of the individual colour coordinates indicates that the aniline black pigment shifted to become lighter and slightly more yellow. However, when mixed with a carbonaceous black pigment, the colourant demonstrates suitable lightfastness with a fading rate slower than BWS 3. Analysis of the individual colour coordinates showed that the aniline black and carbon black mixture shifted to become only very slightly lighter. These results reveal that mixing carbon black with aniline black improves the lightfastness of the organic colourant. Based on this observation of a better-than-expected lightfastness

of the black background, it is likely that the black background in the Haku Maki print is a combination of the two pigments.

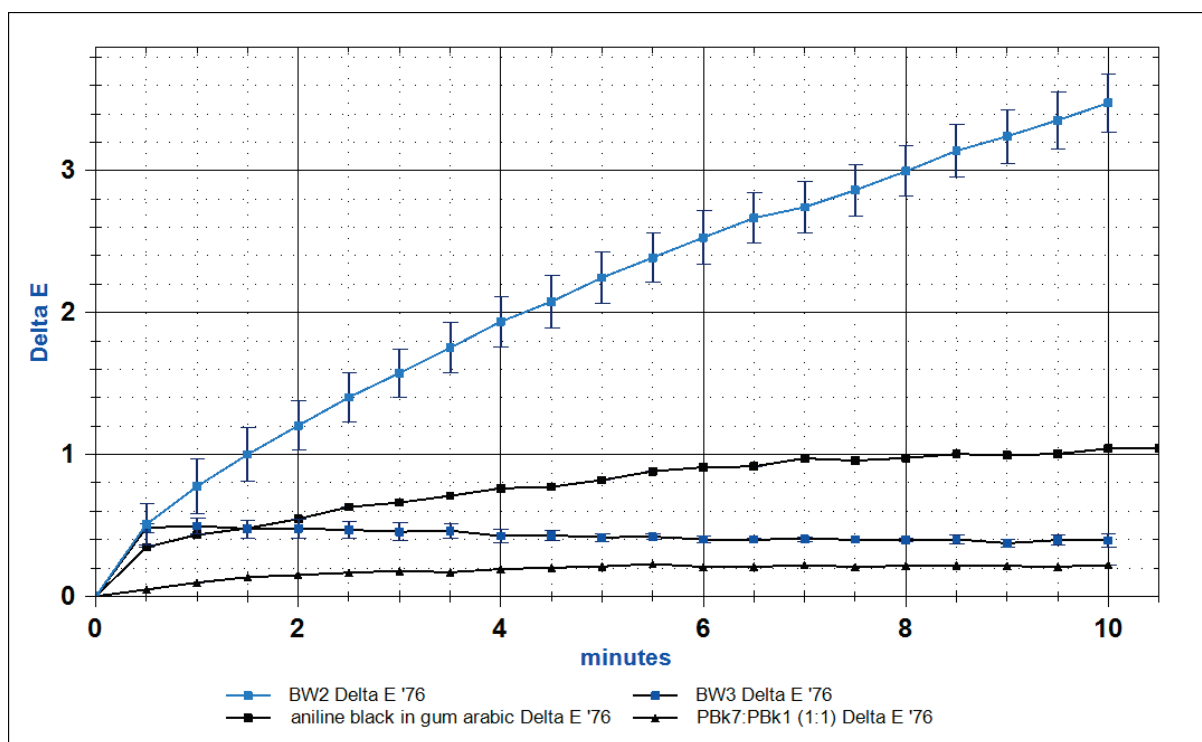


Fig. 4.9 ΔE fading curves for pure BASF aniline black (black squares) and in equal admixture with carbon black (black triangles) prepared as watercolour paints. These curves are compared to BWS 2 and 3.

Multiple studies have demonstrated the darkening of chrome yellow pigments and have attributed this phenomenon to the reduction of Cr^{6+} to Cr^{3+} (Pichon 2013). The reaction is accelerated by sunlight and the action of sulfurous pollutants, leading to a colour shift from yellow to brown. The colour change observed in Fig. 4.8 for the chrome yellow paint used in the Haku Maki prints, changing slightly faster than BWS 3, is therefore not surprising. The orange paint characterised as a mixture of chrome yellow and molybdate orange, however, altered even faster than pure chrome yellow, showing a rate of colour change approximately halfway between BWS 2 and 3. This result raises concerns regarding its exposure to exhibition lighting. Analysis of the individual colour coordinates indicated that the orange paint shifted to become darker, less red, and less yellow.

To explain this difference, we examined the sulphur content of the yellow and orange paints as revealed by Raman spectroscopy. Recent investigations have found that the

darkening of chrome yellows also depends on the chemical composition ($\text{PbCr}_{1-x}\text{S}_x\text{O}_4$) and crystalline structure (monoclinic or orthorhombic) of the material (Monico et al. 2015; Monico, Janssens, Vanmeert, et al. 2014; Tan et al. 2013). Sulphur-rich orthorhombic forms are more susceptible to browning. It has been postulated that PbCrO_4 and $\text{PbCr}_{1-x}\text{S}_x\text{O}_4$ are more soluble when in the orthorhombic phase than their monoclinic equivalents, and thus more chromate ions are available for redox reactions (Monico et al. 2013). Using Raman spectroscopic analysis with 785 nm laser excitation, Monico et al. were able to discriminate to an extent among the different chrome yellow variants based on $\text{PbCr}_{1-x}\text{S}_x\text{O}_4$ (Monico, Janssens, Hendriks, et al. 2014). When the sulfate concentration increases (as x increases), the $\nu_1(\text{CrO}_4^{2-})$ mode at 841 cm^{-1} changes to 845 cm^{-1} and the $\nu_1(\text{SO}_4^{2-})$ mode moves from 971 cm^{-1} ($x \approx 0.1$) to 978 cm^{-1} ($x \approx 0.75$). For the monoclinic structure, the $\nu_2/\nu_4(\text{CrO}_4^{2-})$ modes are located at 400, 377, 358, 336, and 323 cm^{-1} , whereas peaks at 411, 384, 362 and 341 cm^{-1} are characteristic of the orthorhombic phase (Monico, Janssens, Hendriks, et al. 2014).

These spectral markers were compared to the Raman spectrum of the Haku Maki yellow paint, in which the bands at 840, 400, 377, 358, 337 and 325 cm^{-1} , along with a weak sulfate band at 970 cm^{-1} , all suggest a monoclinic phase with low sulfur content of $x \leq 0.1$. However, it is possible that mixtures of different phases exist in the paint. Where the orthorhombic and sulphur-rich ($x > 0.4$) phase is mixed in substantial amounts with the monoclinic phase, the peaks appear at 841, 402 and 359 cm^{-1} , resembling monoclinic features due to a higher Raman scattering coefficient of the monoclinic phase, whereas the sulphate peak occurs at 978 cm^{-1} (Monico, Janssens, Hendriks, et al. 2014). Noting that the yellow pigment in Haku Maki's print gives a weak sulfate peak at 970 cm^{-1} , it can be deduced that it is predominantly monoclinic with low sulphur content ($x < 0.25$). This may explain why the MFT results show only slight darkening of the yellow paint with accelerated light aging.

Interestingly, the Raman features of the orange paint matched that of the yellow paint, attributing the primary pigment to chrome yellow in its predominantly monoclinic phase (Monico, Janssens, Hendriks, et al. 2014). Considering that both the orange and yellow paints were applied at the same time and aged together in the same environment over the same period, it is surprising that the orange paint darkens much faster than the yellow

paint. Since the orange paint has an additional component of molybdate orange, it would be interesting in the future to consider the role that this pigment mixture plays in the rate of the color change reaction.

4.4 CONCLUSIONS

The study of Haku Maki “Poem” prints provides an interesting example that demonstrates the role of light in appreciating both the beauty and defects of an artwork, and ironically, its potential to cause damage to an artwork. At the same time, light-based techniques were used to characterise the paint materials, in which the results helped explain for what was visually observed.

The attribution of the white efflorescence to biological mould was affirmed from a combination of FTIR spectroscopy and transmission optical microscopy. Now that its identity is revealed, it was possible to attribute the cause to improper environmental conditions during the glazing process. However, at this stage, removal of the fungi without impacting the underbound matte black paint remains a conservation challenge.

Through analysis of the pigments, this study provides the opportunity to positively characterise molybdate orange and aniline black for the first time on works of fine art. It also addresses the close relationship in interpreting the data to the visually observed colour and the importance for using complementary techniques. For instance, molybdate orange might not be detected in the orange paint if XRF was not carried out in conjunction with Raman microscopy. In another instance, the detection of carbon black with aniline black would have been easily missed if the MFT study was not carried out.

The observance of these pigments has also led to a study of the lightfastness of Maki’s palette on one of the prints. Through a combination of Raman microscopy and microfadeometry, the orange paint characterised as molybdate orange with chrome yellow was found to be more susceptible to loss of hue intensity and darkening upon exposure to light, than if the paint comprises of just chrome yellow alone. In addition, it demonstrated surprisingly that blending carbon black to a fugitive aniline black results in a relatively lightfast colour.

This study highlights the importance of light in the appreciation of these vibrant modern woodblock prints, the utility of light-based analyses in understanding the artist's material choices, the role of light in the degradation of these same artworks, and the importance of identifying artist's materials for customising stewardship practices.

4.5 REFERENCES

- Buxbaum, G. & Pfaff, G. 2005, *Industrial Inorganic Pigments*, 3 edn, Wiley-VCH, Germany.
- Dixit, V., Cho, B.K., Obendorf, K. & Tewari, J. 2014, 'Identifications of household's spores using mid infrared spectroscopy', *Spectrochimica Acta Part A: Molecular and Biomolecular Spectroscopy*, vol. 123, pp. 490-6.
- Doncea, S.-M. & Ion, R.-M. 2014, 'FTIR (DRIFT) analysis of some printing inks from the 19th and 20th centuries', *Revue Roumaine de Chimie* vol. 59, no. 3-4, pp. 173-83.
- Eastaugh, N. 2013, *The pigment compendium : a dictionary and optical microscopy of historical pigments*, Routledge, New York.
- Erukhimovitch, V., Pavlov, V., Talyshinsky, M., Souprun, Y. & Huleihel, M. 2005, 'FTIR microscopy as a method for identification of bacterial and fungal infections', *Journal of Pharmaceutical and Biomedical Analysis*, vol. 37, no. 5, pp. 1105-8.
- Gardner, H.A. & Sward, G.G. 1922, *Paint testing manual*, American Society for Testing and Materials., Philadelphia.
- Gupta, B.S., Jelle, B.P. & Gao, T. 2015, 'Application of ATR-FTIR Spectroscopy to Compare the Cell Materials of Wood Decay Fungi with Wood Mould Fungi', *International Journal of Spectroscopy*, vol. 2015, p. 7.
- Herbst, W. & Hunger, K. 2002, *Industrial Organic Pigments: Production, Properties, Applications*, Wiley-VCH, Germany.
- Mayer, R. 1950, *The artist's handbook of materials and techniques*, The Viking Press, New York.
- McEvoy, B. 2015, *Handprint Guide to Watercolor Paints*, viewed 6 March 2016, <<http://www.handprint.com/HP/WCL/waterw.html>>.
- Monico, L., Janssens, K., Hendriks, E., Brunetti, B.G. & Miliani, C. 2014, 'Raman study of different crystalline forms of PbCrO₄ and PbCr_{1-x}S_xO₄ solid solutions for the

- noninvasive identification of chrome yellows in paintings: a focus on works by Vincent van Gogh', *Journal of Raman Spectroscopy*, vol. 45, no. 11-12, pp. 1034-45.
- Monico, L., Janssens, K., Hendriks, E., Vanmeert, F., Van der Snickt, G., Cotte, M., Falkenberg, G., Brunetti, B.G. & Miliani, C. 2015, 'Evidence for Degradation of the Chrome Yellows in Van Gogh's Sunflowers: A Study Using Noninvasive In Situ Methods and Synchrotron-Radiation-Based X-ray Techniques', *Angewandte Chemie International Edition*, vol. 54, no. 47, pp. 13923-7.
- Monico, L., Janssens, K., Miliani, C., Van der Snickt, G., Brunetti, B.G., Cestelli Guidi, M., Radepon, M. & Cotte, M. 2013, 'Degradation Process of Lead Chromate in Paintings by Vincent van Gogh Studied by Means of Spectromicroscopic Methods. 4. Artificial Aging of Model Samples of Co-Precipitates of Lead Chromate and Lead Sulfate', *Analytical Chemistry*, vol. 85, no. 2, pp. 860-7.
- Monico, L., Janssens, K., Vanmeert, F., Cotte, M., Brunetti, B.G., Van der Snickt, G., Leeuwestein, M., Salvant Plisson, J., Menu, M. & Miliani, C. 2014, 'Degradation Process of Lead Chromate in Paintings by Vincent van Gogh Studied by Means of Spectromicroscopic Methods. Part 5. Effects of Nonoriginal Surface Coatings into the Nature and Distribution of Chromium and Sulfur Species in Chrome Yellow Paints', *Analytical Chemistry*, vol. 86, no. 21, pp. 10804-11.
- Myers, D. 2013, *The Color of Art Pigment Database: Pigment Black*, viewed 6 March 2016, <<http://www.artiscreation.com/black.html#PBk1>>.
- Ordonez, E. & Twilley, J. 1997, 'Peer Reviewed: Clarifying the Haze: Efflorescence on Works of Art', *Analytical Chemistry*, vol. 69, no. 13, pp. 416A-22A.
- Petit, G. & Arboleda, A. 1977, *Evolving techniques in Japanese woodblock prints*, Kodansha International, Tokyo.
- Pichon, A. 2013, 'Pigment degradation: Chrome yellow's darker side', *Nat Chem*, vol. 5, no. 11, p. 897.
- Price, B.A. & Pretzel, B. 2007, 'Infrared and Raman Users Group Spectral Database', 20 June 2014 edn, vol. 1 & 2, Philadelphia.
- Puglieri, T.S., Lavezzo, A.S., Santos, I.F.S.d. & de Faria, D.L.A. 2016, 'Investigation on the hazing of a Brazilian contemporary painting', *Spectrochimica Acta Part A: Molecular and Biomolecular Spectroscopy*, vol. 159, pp. 117-22.

- Tan, H., Tian, H., Verbeeck, J., Monico, L., Janssens, K. & Van Tendeloo, G. 2013, 'Nanoscale investigation of the degradation mechanism of a historical chrome yellow paint by quantitative electron energy loss spectroscopy mapping of chromium species', *Angewandte Chemie International Edition*, vol. 52, no. 43, pp. 11360-3.
- Travis, A.S. 1994, 'From Manchester to Massachusetts via Mulhouse: The Transatlantic Voyage of Aniline Black', *Technology and Culture*, vol. 35, no. 1, pp. 70-99.
- Trchová, M. & Stejskal, J. 2011, 'Polyaniline: The infrared spectroscopy of conducting polymer nanotubes (IUPAC Technical Report)', *Pure and applied chemistry*, vol. 83, no. 10, pp. 1803-17.
- Tretiak, D. 2007, *The life and works of Haku Maki*, Outskirts Press, USA.
- Whitmore, P.M., Pan, X. & Bailie, C. 1999, 'Predicting The Fading of Objects: Identification of Fugitive Colorants Through Direct Nondestructive Lightfastness Measurements', *Journal of the American Institute for Conservation*, vol. 38, no. 3, pp. 395-409.
- Wilcox, M. 1991, *The Wilcox guide to the best watercolor paints*, Artways, Cloverdale, Perth, Western Australia.



Chapter 5

INVESTIGATING CAUSES FOR
POLYURETHANE PAINT
FAILURE ON MODERN
OUTDOOR SCULPTURES
“NUMBERS 0-9”

5.1 BACKGROUND

'Numbers 0-9' is a significant outdoor sculpture by American artist Robert Indiana (b. 1928) that has garnered international recognition. The idea was first conceived in two dimensional (2D) prints, which later led to the creation of three dimensional (3D) sculptures. These sculptures were made on multiple occasions and displayed all over the world, but the set of *Numbers* donated to the Indianapolis Museum of Art (IMA) in 1989 is the first and oldest, being fabricated in 1980-1983 by the Lippincott foundry (1966-1994). Constructed from welded sheets of aluminum, each *Number* was applied with distinctive two-toned industrial polyurethane paints, which have failed overtime and were newly restored in 2011 (Fig. 5.1). Unlike most conservation projects of painted artworks, outdoor sculptures like *Numbers* present a unique case in that the work itself is not always physically painted by the artist, nor physically treated by the conservator, but by workers hired at a fabrication company to perform the task. The choice of paint materials, paint application technique and welding of the metal substrate is largely coordinated by the fabrication company (Lippincott 2010).

Before Restoration



After Restoration



Fig. 5.1 Image of “Numbers 0-9”, Robert Indiana, 1988.241-250, automotive paint on aluminum, Top: Before restoration in 2011, first displayed at IMA in 1992; Bottom: 4 years after restoration in 2011. Photos Courtesy of IMA.

By the mid-1960s, it was popular to commission artists to produce public art sculptures that accentuates a commercial building or surrounding landscape (Lippincott 2010). When artists were commissioned to make works of a large size, they had to source and work with industrial manufacturers, usually steel fabricators or boat builders. The idea of the artist is communicated to several workers who will then physically fabricate the work. At the time when *Numbers* was fabricated in the 1980s, Lippincott was already well-established in the field, having worked with many other notable artists such as Lichtenstein, Oldenburg, Murray, Morris and Sugarman. To ensure consistent performance, the team of trained workers performing the fabrication was kept smaller than 16. Considerable thought also went into the process of fabrication, as aptly described by Donald Lippincott (Lippincott 2010):

“...the artist and I, usually with Eddie, work out the general problems of fabrication, which are the selection of material and the way it’s going to be put together. The fabrication process involves three stages. First is layout. We have two people who pretty much do nothing but layout work all the time. In the typical situation, the material is laid out and cut by them. Then it goes to a welding group in which there are four or five people. This group is headed by Bob Giza, who joined Lippincott in 1967 and is second in command to Eddie. He determines who takes on the job based on the specific issues of the piece. Then the finishing of the sculpture- sandblasting and painting- is a third department.”

Problems with paint adhesion had been recounted in many sculptures fabricated in the 1960s-1980s, with many being returned for restorative work. For *Numbers* and many other painted aluminum sculptures with odd curvatures and flat surfaces, achieving a pristine finish with proper paint adherence is not easy and demands a substantial level of skills. Just before applying the paint, any protruding metal from the welding process has to be ground down to flatness and commercial fairing compounds (filler) are used to patch up any localized imperfections. It should be noted that a smooth surface like

aluminum metal does not provide enough grip to hold onto the paint film and requires addition of a primer. Furthermore, the instantaneous buildup of oxides on aluminum upon exposure to air is an obstruction to paint adherence (Wolfe 2013), and this process can happen starting from the first hour, depending on the alloy grade. To resolve these issues, the standard practice in original equipment manufacture (OEM) of automotive painted parts is to first pretreat bare aluminum with a conversion coating, followed by application of primer, primer surfacer, topcoat and lastly a clearcoat for protection (McIntee 2008). Industrially, the choices for primer and primer surfacers are too extensive and such a discussion is outside of the scope of this study, but the ones used for metal adhesion can be broadly categorised into two types: non-etching primer and self-etch primer. According to Paul Amaral, an experienced fabricator/restorer in painted outdoor sculptures, only one type of primer works on aluminum, which was described as being “pea green” in colour (Amaral 2013).

For the first five years after *Numbers* was displayed in 1992, conservators had been grappling with the problem of paint instability on these aluminum sculptures. At that time, the top concave parts of *Numbers 5* and *7* inadvertently became potential sites for collecting rainwater while the downward slope on *Number 4* was often treated as a slide by children, resulting in scratches at the edges. Abrasions cut through the paint into the metal substrate and increased the likelihood of rusting. Subjected to weather and vandalism incidents, damage to the paint frequently called for conservation retouching. The treatment, however, was not straightforward. Retouching was found to be unstable after 2-6 months and adjustments in colour were constantly required. Overtime, the paints have suffered from extreme discolouration from strong sunlight, so much so that the colours appeared strikingly different compared to when first fabricated.

To re-establish the original aesthetic colours, the conservation process resorted to an expensive undertaking and radical treatment; the original paint was sandblasted down to the bare metal and the *Numbers* were newly coated with contemporary polyurethane paint. At the time of repainting in 2011, Lippincott had already closed its fabrication space in North Haven, and so the job was allocated to a local steel fabricator

instead. Based on paint purchase records from the Lippincott foundry and partial inputs from Robert Indiana's recollection, the same brand and colour codes (i.e. Imron 5.0 VOC polyurethane enamel paints, manufactured by DuPont) as the original paints were used for the repainting. Since the repainting of *Numbers* was carried out in 2011, signs of paint delamination were already apparent at an early stage in the first few years, such that the paint could be lifted off easily with the fingernail. In addition, the surface provided evidence of recoating and incomplete sandblasting of the original paint suggested haphazardness in the repainting process (Fig. 5.2). These observations suggest that the cause(s) for paint failure are likely inherent, probably relating to the restoration technique, choice of materials or change in paint formulation over a 30 year time gap. This scientific investigation was prompted by a desire to understand Robert Indiana's original paint choices and to explore the reason(s) for paint failure in the polyurethane coatings.

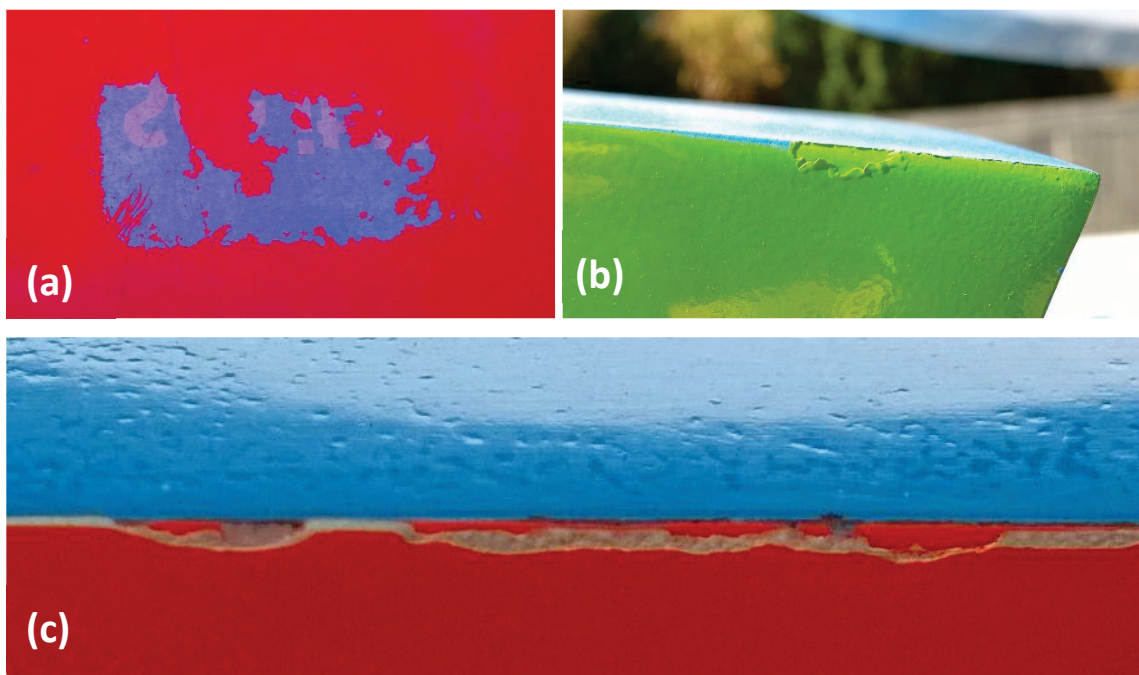


Fig. 5.2 Close-up photos of some damages seen in "*Numbers 0-9*", Robert Indiana, 1988.241-250, taken 4 years after restoration: (a) paint delamination over a significant area revealing the aluminum surface in *Number 8* (b) paint delamination in *Number 2* reveals original paint that has not been properly removed. (c) paint loss along edge in *Number 7* reveals primer layer and signs of repainting.

The inclusion of scientific data is perceived as an important piece of information in the conservation file of *'Numbers'*, particularly when the original paint had been stripped off, so any material information could only be preserved from analysing the fragments of original paint samples collected prior to restoration. In the wider realm of contemporary art, conservators are often compelled to understand industrial paints and its associated fabrication technology. Yet, knowledge of industrial synthetic paints on artworks is scant in the conservation literature, although polyurethane was briefly mentioned in the modern paints research by Learner (Learner 2004). The only related scientific analysis seems to be the technical analysis carried out at the GCI on Roy Lichtenstein's "Three Brushstrokes", which was fabricated in 1984 by the Tallix Fine Arts Foundry (Considine et al. 2010), with a colour scheme limited to yellow, blue and red. On the other hand, *Numbers* presents a quintessential case for scientific study, presenting questions on the materials used and painting process from two different fabricators, over a wide colour palette of 20 colours from the same paint manufacturer, complemented with conservation observations over a 25 year long period.

In this chapter, a comparison of the paint composition and application technique between the first fabricator in 1980-1983 and the second fabricator in 2011 forms the main focus. The layer stratigraphy of the original paints and new restoration paints were discriminated by optical and electron microscopy, whereas primer and pigment/binder paint composition were determined with XRF, EDS, FTIR spectroscopy and Raman microscopy as well as Py-GC/MS. Colourimetric studies were additionally carried out to ascertain the colour match of the restoration paints to the artist's approved colours from the early 1980s as evidenced by sample book.

5.2 MATERIALS AND METHODS

5.2.1 PAINT SAMPLES

Original paint fragments that had spalled from the artworks were collected prior to repainting of *Numbers 0-9*. For comparison, a scalpel was used to extract small-sized paint chips from the broken paint edges of each restored *Number*. Care was taken to remove as much water-soluble dirt as possible from the paint surface of each dried

chip. In addition, paint drips from the exterior of the Imron 5.0 polyurethane enamel tin cans used in the restoration were available for analysis. These two-part paints were still soft and flexible at the time of analysis, as they were not previously combined with the activator. Care was taken to remove as much dirt as possible from the paint surface. This data was used to verify the composition of Imron 5.0 paints purchased in 2011.

5.2.2 UV-VIS MICROSCOPY COMBINED WITH STEREOMICROSCOPY AND VISUAL OBSERVATION

A visual observation of the sculptures using an optivisor revealed the order of paint applications in both the original and restored paints colour. When the same paint fragments were examined at higher magnification using a stereomicroscope, the number of foundation layers beneath the topcoat became clearer, but similar colours were not easily distinguished and the existence of thin layers of around 20 μm were often overlooked. A cross-section examined at even higher magnification under a compound microscope provided clarity to the thickness and differentiation of similarly-coloured layers. These three examination techniques were necessary to obtain a complete picture of each paint sample.

Paint samples were embedded in epoxy resin, followed by manual polishing using a metal holder and Micro-mesh cloths at successive grades of 1800, 2400, 3200, 4000, 6000, 8000 and 12000, to obtain a polished cross-section. The prepared cross-sections were then examined at 20 X objective magnification using dark field (DF) illumination with a Zeiss M2m Axio Imager compound microscope. UV-induced visible fluorescence images were acquired on the same microscope using a Lumen Dynamics X-cite 120Q mercury vapor lamp source. A 4',6-diamidino-2-phenylindole (DAPI) filter cube set allowed narrowband excitation between 325 and 375 nm with observation throughout the visible spectrum ($\lambda > 412 \text{ nm}$). Images were recorded with a 5 megapixel AxioCam MRc5 digital camera.

5.2.3 SCANNING ELECTRON MICROSCOPY WITH ENERGY DISPERSIVE SPECTROMETRY (SEM-EDS)

Electron micrographs of cross-sections were collected using a Zeiss EVO MA15 scanning electron microscope operated in variable air pressure mode at 50-80 Pa. A pressure limiting Beam Sleeve aperture was attached to the pole piece to reduce beam scatter in the chamber. A five segment backscattered electron (BSE) detector, a variable pressure secondary electron (VSPE) detector and a Bruker Quantax 200 energy dispersive spectrometer (EDS) were used to acquire images. Electron accelerating voltage was set at 20 keV to ensure generation of x-rays for all heavy metals in the sample while a beam current of 3 nA yielded > 10 kcps detector signal with a few percent dead time. When imaging fine lines that distinguish two coats of applied paint, the beam current was further reduced to about 1.8 nA. A sample working distance of 8.5 mm optimized EDS detection. Hypermapping for 30 min was carried out to show the distribution of elements and to detect elements that a point analysis may have missed.

5.2.4 RAMAN MICROSPECTROMETRY

Raman spectra were acquired using a Bruker Senterra microspectrometer on a Z-axis gantry. The spectrometer utilized 3 selectable excitation lasers (532, 633 and 785 nm), Peltier-cooled CCD detector and a 50 μm confocal pinhole. Laser power at the sample was generally below 5 mW. The spectra were the result of 10 s integrations with 16-65 co-additions. The spectral resolution was in the range of 9-18 cm^{-1} and 3-5 cm^{-1} . OPUS software allowed for automated cosmic spike removal, peak shape correction and spectral calibration.

For most of the coloured samples, 532 nm and 633 nm produced high fluorescence that overwhelmed the signals. Hence, the paint samples were analyzed mainly with 785 nm. However, 532 nm was particularly suitable for analysing the green paints as it detected additional synthetic organic pigments due to an enhanced resonance effect and larger Raman scattering efficiency (ν^4 dependence).

5.2.5 FOURIER TRANSFORM INFRARED (FTIR) SPECTROSCOPY

FTIR microspectroscopy was performed on a Continuum microscope with an MCT A detector coupled to a Nicolet 6700 spectrometer purged with dry, CO_2 -free air. The spectra are the sum of 32 co-additions at 4 cm^{-1} spectral resolution. Microsamples

were crushed on a diamond compression cell and held on a single diamond window during the analysis. ATR-FTIR spectroscopy was performed using a SpectraTech Smart Orbit diamond ATR attachment coupled to a Nicolet 6700 spectrometer with a mid-IR DTGS detector. The instrument was purged with dry, CO₂-free air. The spectra were the sum of 32 co-additions at 4 cm⁻¹ spectral resolution. Sample identification was performed using the Infrared and Raman Users Group (IRUG) reference spectral library.

5.2.6 PYROLYSIS - GAS CHROMATOGRAPHY – MASS SPECTROMETRY (PY-GC-MS)

The samples were analyzed using a Frontier Lab Py-2020D double-shot pyrolyzer system with a 320°C interface to a Thermo Trace gas chromatograph and an ISQ single quadrupole mass spectrometer. A Thermo TG-5MS capillary column (30 m x 0.25 mm x 0.25 µm) was used for the separation with 1 mL/min of He as the carrier gas. The split injector was set to 220°C with a split ratio of 20:1. The GC oven temperature program was 40°C for 2 min, held for 5 min, ramped to 150°C at 8°C/min, then to 210°C at 3°C/min, followed by a 10 min isothermal period. The MS transfer line was at 250°C, the source at 250°C, and the MS quadrupole at 150°C. The mass spectrometer was scanned from 25-650 amu at a dwell time of 0.3 s with no solvent delay. Samples were pyrolyzed using a single-shot method at 600°C for 0.2 min. Sample identification was aided by searching the NIST MS library.

5.2.7 COLOURIMETRIC MEASUREMENTS

Tristimulus chromaticity and gloss data were obtained from the *Numbers* after restoration and on the paint swatches in a DuPont Imron catalogue dated 1979, which served as a good representation of the original colour scheme. Chromaticity changes of the original paint fragments after more than 30 years of ageing were also recorded. Surfaces of the paint were cleaned with a damp cloth prior to analysis.

5.3 RESULTS AND DISCUSSION

5.3.1 LAYER STRATIGRAPHY

The microscopic results of the industrial paint cross-sections revealed an interesting layer stratigraphy that is interpreted differently from easel paint cross-sections. Being an industrial paint system, the layer stratigraphy of *Numbers* resembles automobile paint cross-sections or original equipment manufacturer (OEM) (Fig. 5.3). Topcoat refers to the topmost layer that provides colour and gloss. Surfacer, primer surfacer, undercoat or primer sealer is a highly filler layer that is easily sanded to remove dirt and provide a polished surface for adhesion to topcoat. Primer (epoxy primer, etch primer, direct to metal primer) is the first layer in contact with the aluminum substrate, hence it contains corrosion resistant properties and should adhere well to the metal. Filler or body filler or fairing compound or “Bondo” is used in localized areas to patch up imperfections of the metal substrate. However, unlike automobile coating systems, no clear coat or thin pre-treatment conversion layer (if any) was found in the samples from *Numbers*.

The thicknesses of a layer depended on the number of passes made by the spray application over an area, which was roughly gauged by the worker’s judgement at the time of application. It was found that a single paint layer could actually be formed from up to 4 coats or passes of paint application. Topcoats ranged from 40-115 μm per layer, while the primers/surfacers ranged from 5-123 μm . This thickness range deviates from mean conventional standards of 35-45 μm in OEM, where paint application is machine operated. The variable thickness of the primer can be a cause for paint failure. Applying the primer too thickly can cause cracks to appear (Fig. 5.3), while a primer that is too thin has less filling power and topcoat holdout.

A corresponding SEM image is able to reveal more about the paint condition otherwise not shown in visible microscopy. In this case (Fig. 5.3), the cracks extending into the primer suggests primer breakdown and loss of adhesion between topcoat/surfacer and primer. As seen in Fig. 5.4, different microscopy techniques in analysing such paint systems on *Numbers* are required to compare the front/ back and side topcoats. The original paints were collected as larger sized pieces that had delaminated from the middle areas of each colored face of the artwork. In contrast, the restoration paints allowed only micro-sized pieces to be cut along exposed edges of each color. Noting the

location of the paint sample is of paramount importance in analyzing these data. For example, in Fig. 5.4, the blue topcoat mottled with reddish brown primer in restored *Number 2* is interpreted as contamination from the side blue topcoat, which is expected along the edge.

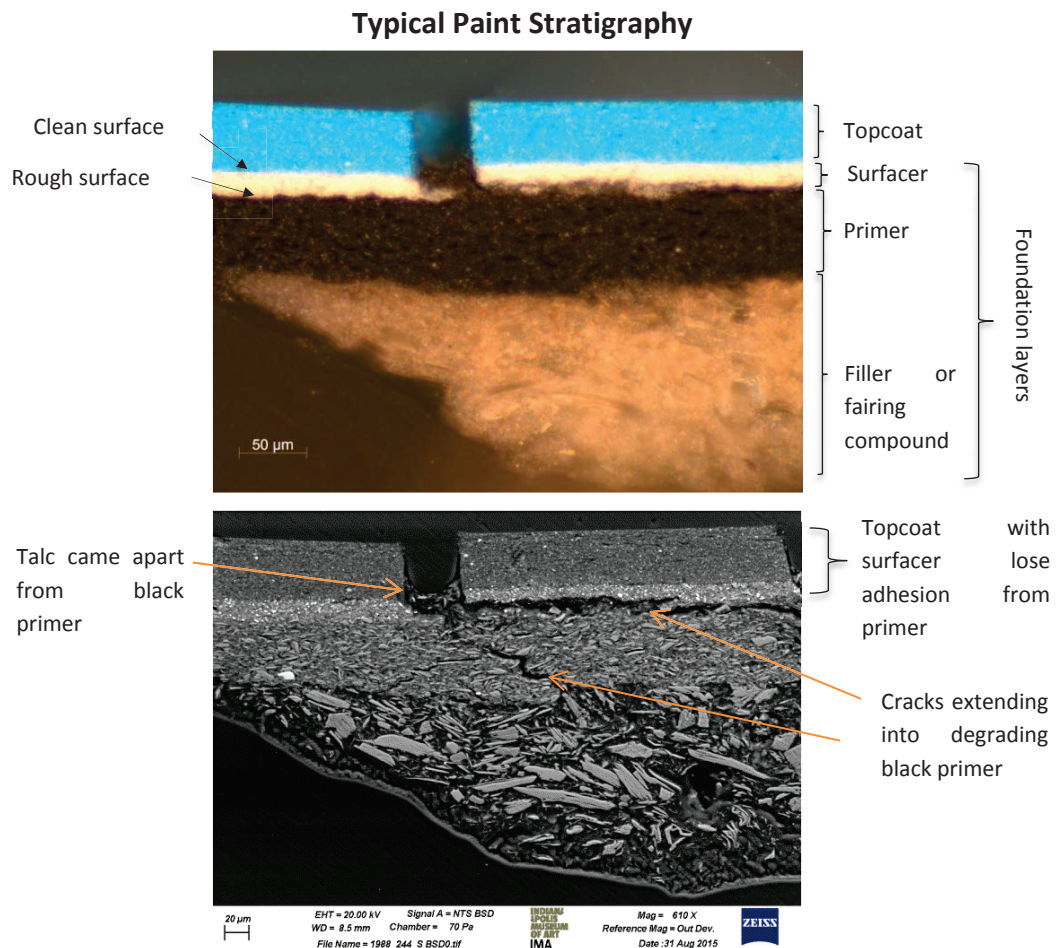


Fig. 5.3 Example of the original paint system fabricated by Lippincott from *Number 2*. using terms based on original equipment manufacture (OEM).

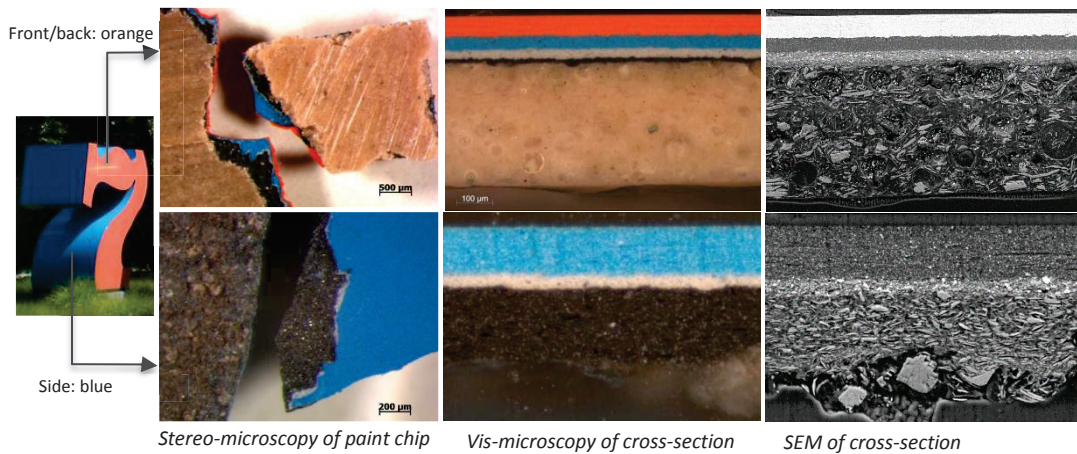
One striking difference of the restoration paints compared to the original paint stratigraphy is the paint sequence. In the original paints, all samples showed that the side topcoat was applied before the front/ back topcoats. In contrast, the restoration stratigraphy did not show particular preference on which topcoat was painted first¹. It

¹ *Numbers 1,2,3,4,5,8,9,0 (restored)*: Front/back faces are applied with paint first before sides;

Numbers 6,7 (restored): Sides are applied with paint first before front/back faces

is unknown why the original fabricator, Lippincott Foundry, chose to coat the entire surface of each of Indiana's sculptures prior to working on the front/ back surfaces, although one might guess that the curved surfaces of the sides of the sculptures may have presented a more challenging paint application. By coating the entire surface first, any mistakes could be corrected without potentially compromising a completed finish on the front/ back surfaces.

Original paints



Restoration paints

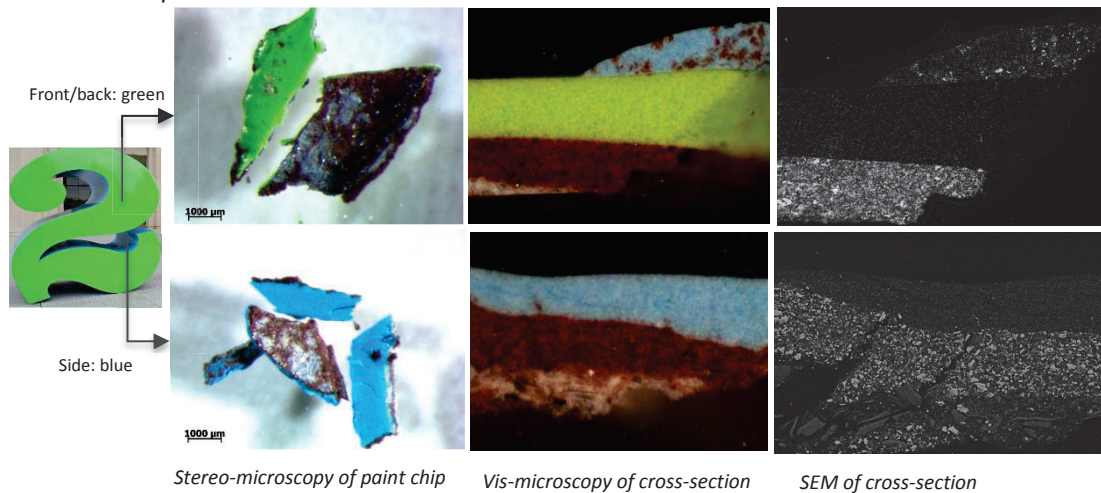


Fig. 5.4 Front/back facings and side colours of *Number 7* original vs *Number 2* restored.

The consistency of stratigraphy (Table S1) in all original paint samples implies that the whole sculpture was first prepared with a black primer, followed by a white surfacer and subsequent side and front/ back topcoats. This application approach can be viewed as somewhat wasteful, as the side topcoat covers the sculpture completely, even in

areas that do not directly expose its colour (e.g. front/ back areas). In some *Numbers*, the white surfacer was omitted as the topcoat is seen directly on top of the black primer. The fairing compound may or may not appear, depending on whether it was extracted together with the paint chip, but it always appears below the black primer if present.

In the restored paints, however, the lack of consistency across the *Numbers* does not allow the painting procedure to be deduced. The reddish brown and white foundation layers do not show a standard application sequence, making it difficult to attribute either as primer or surfacer. In some of the restored *Numbers*, the topcoat is painted directly on top of the priming layer without any contact in between topcoats, while some others show direct contact between topcoats, where the front/ back topcoat is applied before the side topcoat². Two such examples are highlighted in Fig. 5.5. These observations suggest that the restoration paint application process lacks standardization, possibly carried out by different workers.

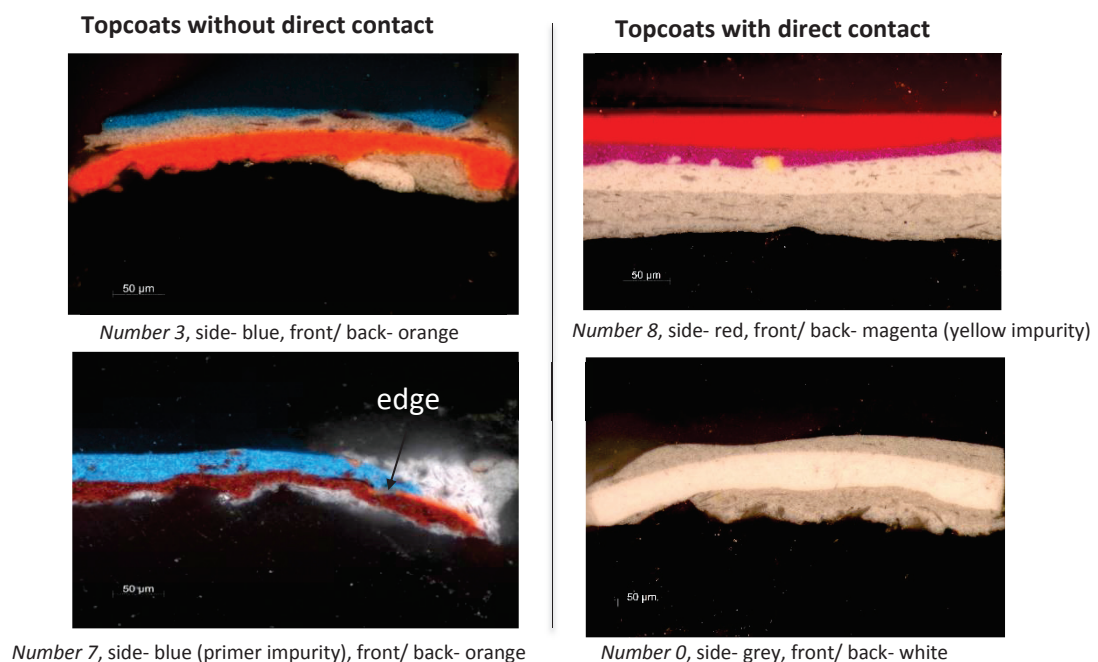


Fig. 5.5 Some examples of restored paint cross-sections demonstrating inconsistency in layer stratigraphy.

² *Numbers 6, 8, 9, 0 (restored)*: Front/ back paint is applied over the entire sculpture surface, followed by side paint; *Numbers 1, 2, 3, 4, 5, 7 (restored)*: Front/ back and side paint is applied directly on primer, without contact between the topcoats.

While evidence of reapplication of the paints at the foundry was observed in one original paint application system, it was not found in the restoration paint samples. An example of repainting can be seen in the white front/ back area of the original paints in *Number 5*, in which the first blue layer was made up of 2 coats (Fig. 5.6). Interestingly, the strict regime of a side-front/ back sequence was persisted even when repainting the front/ back white topcoat, suggesting a conscientious effort by the Lippincott workers.

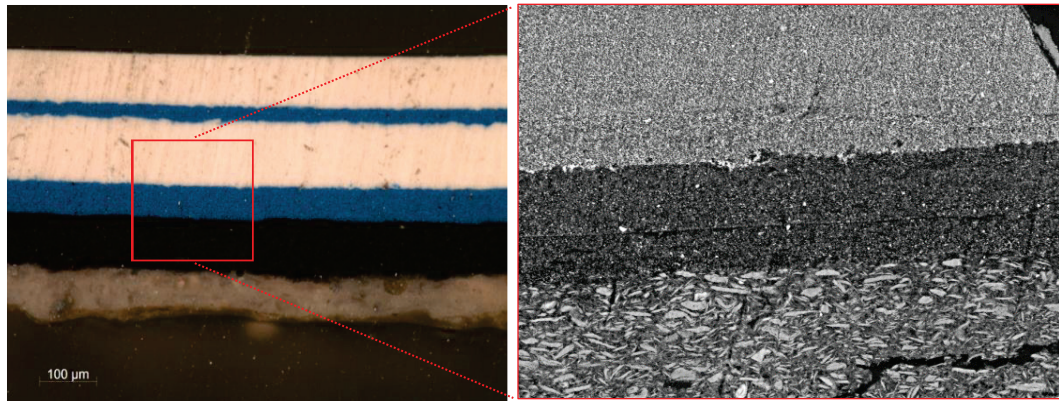


Fig. 5.6 Left: Front/ back paint cross-section of original *Number 5* with vis-microscopy. Right: SEM image shows that the first blue layer was formed by two coats, as seen by a distinct line in the middle.

Paint loss can arise from aluminum oxides acting as a barrier to proper adhesion (Wolfe 2013) and this inevitable phenomenon has been portrayed in one of the original paint cross-sections (Fig. 5.7), demonstrating the difficulty in painting aluminum.

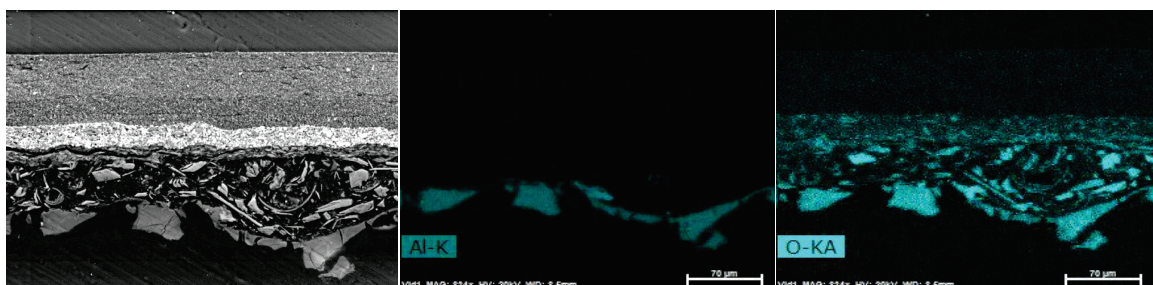


Fig. 5.7 SEM image of *Number 0* paint cross-section taken from front/ back area, where aluminum (Al) and oxygen (O) represents aluminum oxides below the fairing layer.

5.3.2 FOUNDATION LAYERS

Primers and surfacers characterised by a polyester backbone with high abundance of inorganic extenders play an important role in the overall appearance of the final topcoats (Streitberger & Dossel 2008). However, differentiating the priming layers by compositional analysis is not straightforward, which can be highly variable due to the vast variety of commercial primer recipes available in the market. As encountered in the *Numbers*, at least three types of primer/surfacers exist in the original finishes, which are different from the four types identified in the restoration treatment.

5.3.2.1 INORGANIC EXTENDERS

In both original and restoration paint primer/surfacers, the extenders characterised by FTIR spectroscopy include a combination of talc (670, 1020, 3677 cm^{-1}), magnesite (3655, 1818, 1450, 884, 747 cm^{-1}) and/or kaolinite (3696, 3621, 1033, 1012, 914 cm^{-1}). For white primer/ surfacers, EDS revealed localized spots of barium sulphate with small amounts of Ti, attributed to titanium white. The black original primer is mainly carbon while the reddish brown restoration primer contains iron oxide. Interestingly, the majority of white surfacers in the original paint scheme contain particles that fluoresce yellow in UV, which are analogous to the elemental distribution of Zn, suggesting the presence of zinc white. Attribution to lithopone is discounted as the distributions of Zn and S do not overlap in the hypermap images (Fig. 5.8). These inorganic extenders and pigments are consistent with raw materials used in primer surfacers of OEM, which are selected due to their hardness, chemical inertness and UV resistance (Streitberger & Dossel 2008).

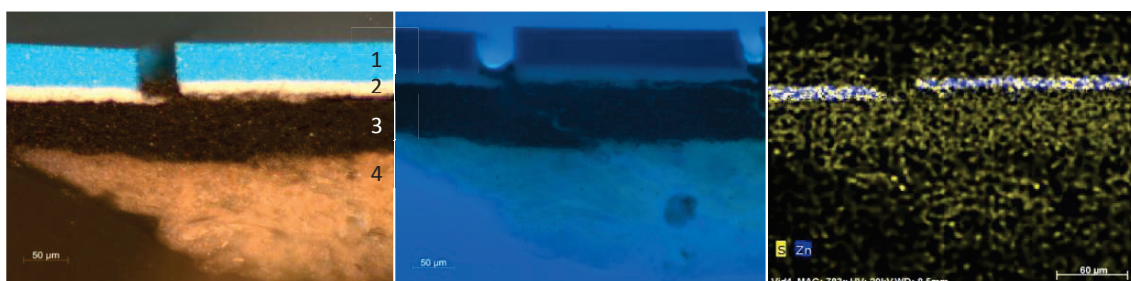


Fig. 5.8 White surfacer (layer 2) in cross-section of *Number 3* fluoresces yellow and is analogous to the distribution of Zn (zinc) in the EDS Hypermap image. Similar distribution of Zn is observed in white primer/surfacers in original *Numbers 0, 3, 4, 6, 7, 8 and 9* and Restored *Numbers 3, 5, 8 and 9*.

5.3.2.2 BINDER

By means of spectral markers in the FTIR spectrum, the type of primer/surfacer can be differentiated (Fig. 5.9). Epoxy is a common constituent and can be identified by the narrow bands at 1606, 1510, 1182 and 829 cm^{-1} (Fig. 5.9a and 9g). This is confirmed with Py-GC/MS, where 4-isopropenyl phenol, benzene and phenol pyrolyzates were detected. Acrylate shows a strong carbonyl absorption at $\approx 1730 \text{ cm}^{-1}$, along with moderate bands at 1450, 1242 and 1149 cm^{-1} (Fig. 5.9b and 9e). The type of acrylate in Fig. 5.9b is identified as a methyl methacrylate (MMA) – ethyl acrylate (EA) copolymer, as substantiated by an abundance of MMA) and small amounts of benzene and EA in Py-GC/MS. In industrial paints, acrylates are often modified with urethane, which is observed as a distinct absorption at 1690 cm^{-1} and a weaker broad band at 1521 cm^{-1} (Fig. 5.9d). Nitrocellulose-based primer is also identified at 1644-1655 and 1278 cm^{-1} corresponding to nitrate and phthalate, respectively (Fig. 5.9c and 9f), which may be modified with alkyd or acrylate polyesters to counteract its brittleness, giving additional bands around 1728, 1452-1465 and 1379-1386 cm^{-1} .

In the original paint systems, the white surfacers were characterised as either epoxy or acrylate while the black primer is nitrocellulose-based (Fig. 5.9a-c). Epoxy resins provide efficient corrosion protection and adheres well to metal surfaces, but the aromatic epoxy types as detected herein are prone to UV degradation (Streitberger & Dossel 2008). UV may have penetrated the topcoat to the surfacer layer, leading to degradation of epoxy resin, chalking, reduced adhesion of topcoat and eventually delamination. As shown in Fig. 5.10, the cracks along the epoxy white surfacer demonstrate partial loss of topcoat adherence. The black nitrocellulose primer is also unstable, as seen by the cracks in this layer. Nitrocellulose primers were used in old formulations for early automotive paint because they were easy to apply, fast-drying and recoatable at any time. However, their poor UV resistance, low gloss and brittleness led to the use of more durable acrylics and alkyds still in use today (Lambourne & Strivens 1999).

In the restoration paint systems, the white primer/surfacers were characterised as urethane-modified acrylates or nitrocellulose alkyd, whilst the reddish brown

FTIR	Py-GC/MS	Numbers
Original Paint Primers/ Surfacer		
<p>(a) White surfacer, epoxy-based</p>	<p>Benzene, phenol, 1-iso propenylphenol</p>	<p>#0, 8 and 9</p>
<p>(b) White surfacer, acrylate-based</p>	<p>Methyl methacrylate (MMA), styrene, benzene EA</p>	<p>#3, 4, 6 and 7</p>
<p>(c) Black primer, Nitrocellulose-based</p>	<p>Benzene, styrene, dibutyl phthalate</p>	<p>All</p>
Restoration Paint Primers/ Surfacer		
<p>(d) White primer/surfacer, urethane acrylate</p>	<p>Not tested</p>	<p>#, 5, 6, 8, 9, 0</p>
<p>(e) White primer/surfacer: Acrylate</p>	<p>Not tested</p>	<p>#2,4 and 7</p>
<p>(f) White primer/surfacer: Nitrocellulose-based</p>	<p>Not tested</p>	<p>#0</p>
<p>(g) Red brown primer/surfacer: Epoxy-based</p>	<p>Phenol, isopropenyl phenol</p>	<p>4- #1, 2, 4 and 7</p>

Figure 5.9 Column 1- FTIR spectra of primer/surfacers in original (a-c) and restored (d-g) paints, where T - talc, K - kaolinite, M -magnesite, A - acrylate, NC - nitrocellulose, E - epoxy, U - urethane; Column 2- corresponding Py-GC/MS pyrolyzates; Column 3- the Numbers that contain the exemplar primer/surfacers.

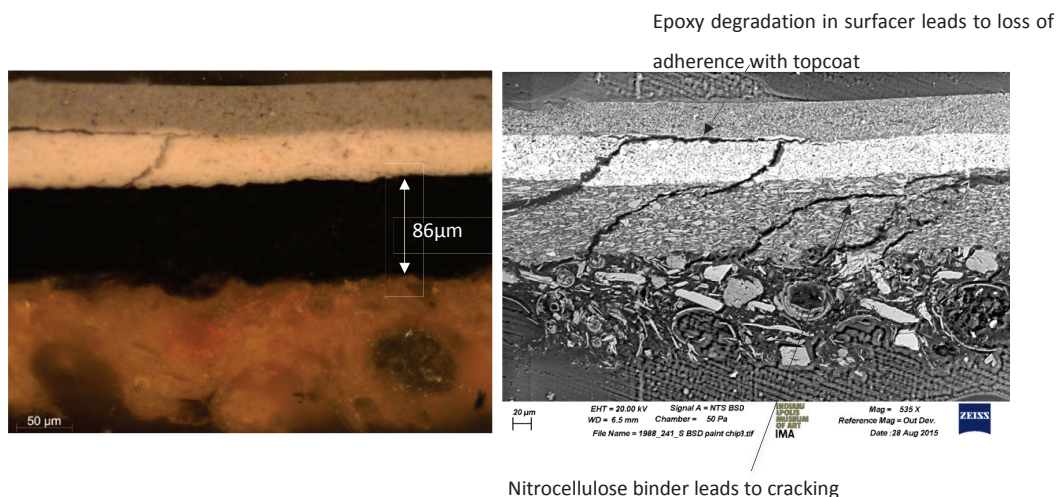


Fig. 5.10 Images of cross-section in Original *Number 0* Grey reveal paint failure. Left: Optical microscopic image; Right: SEM image.

primer/surfacer contains mainly epoxy (Fig. 5.8 d-g). Similarly, epoxy and nitrocellulose-based binders are not UV resistant and are prone to degradation from strong sunlight. An example of crack formation in the reddish brown epoxy primer/surfacer can be seen in the SEM image of *Number 2* (Fig. 5.4).

5.3.3 TOPCOAT BINDER

The results of the binder composition of the topcoats in original and restoration paints are summarised in Supplementary Data, Table S2.

The binder in the original topcoats was characterised as a styrene-MMA copolymer modified urethane, where the urethane component is hexane 1,6-diisocyanate (HDI), the hard segment that is known to produce extremely durable and weather-resistant polyurethane coatings (Learner 2001). This result is characteristic of DuPont Imron 5.0 VOC polyurethane enamel paints used in the early 1980s, which was documented as applied to the *Numbers* according to past Lippincott purchase records. In another study of outdoor paint sculptures, the high abundance of styrene and HDI were also previously characterised in Imron type polyurethane enamel paints (Considine et al. 2010).

For the restoration topcoats, the paint drips that were partially dried on the exterior of the tin cans purchased in 2011 were tested since microsamples from the restored artworks do not provide sufficient material for Py-GC/MS analysis. In this instance, Py-GC/MS detected several additional acrylates other than PMMA and no phthalate was detected. The replacement of phthalate in the restored paints with copolymerization of mixed acrylates enhanced paint flexibility without the degradative effects commonly experienced with migrating plasticisers, suggesting an improvement in the formulation from DuPont over this 30 year period (Fig. 5.11). As the paints tested were not mixed with the urethane-containing activator, the resulting pyrogram did not show any urethane component. It is worthwhile to point out that styrene was left out of the ingredients listed on the paint cans despite large amounts being detected in the analysis.

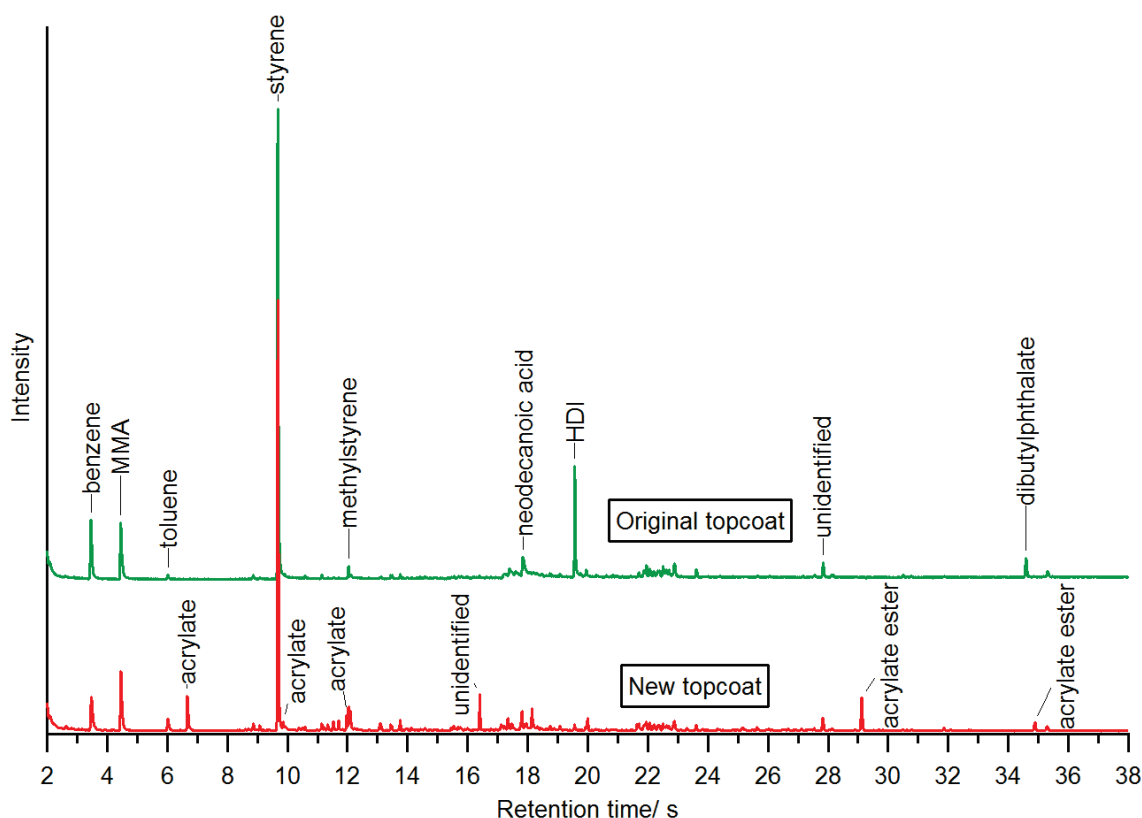


Fig. 5.11 Pyrogram of restored paint (*Number 6* red) vs original paint (*Number 2* green)

Aside from the identification of polyurethane, a greater interest lies in the condition of the topcoat, which can be determined using FTIR spectroscopy. As seen in Fig. 5.12, the

carbonyl stretching band of urethane at 1690 cm^{-1} is prominent in the restored paints (Fig. 5.12c), but its intensity is markedly reduced in the original paints (Fig. 5.12a, b). This is more evident at the surface of some original paints, where the urethane absorption is completely hidden by the acrylate band at 1730 cm^{-1} (Fig. 5.12b). The loss of urethane vibrations suggests the breakdown of polyurethane with ageing, which explains for the lower gloss in the original paints (Farcas 2013), although physical abrasion and weathering almost certainly also play a role after 30 years of outdoor exposure.

Interestingly, all the original paints shows a loss of the urethane band, except for *Numbers 0, 8 and 9*. As noted in Fig. 5.8a, *Numbers 0, 8 and 9* contain the same white surfacer composed of epoxy resin. This resistance to polyurethane breakdown is probably due to a sacrificial degradation of the epoxy surfacer. However, more research is needed to support this hypothesis.

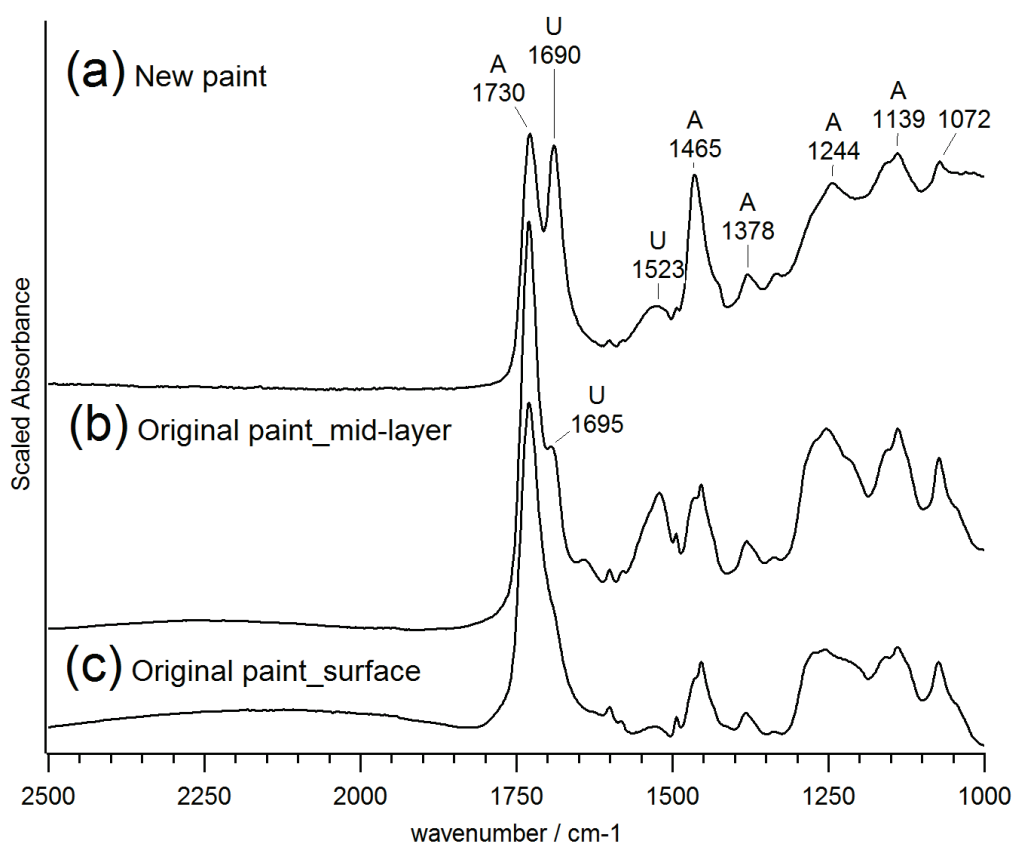


Fig. 5.12 FTIR spectrum (a) at surface of topcoat original paint and (b) deeper within the topcoat original paint (c) restored paint after 3 years curing.

5.3.4 TOPCOAT PIGMENTS

As seen in Table 5.1, the pigments constituting the original and restoration paints are largely similar, except for the greens (*Numbers 1, 2 and 6*) and one of the yellows (*Number 9*). The lead chromate (PY34) in these colours was partially or totally replaced by PY154, a benzimidazolone yellow pigment that is characterised by a distinctive strong band at 1697 cm^{-1} in the FTIR spectrum and the presence of fluorine in the EDS results. PY154 was introduced in the mid-1970s as one of the most weather-fast organic yellow pigments recommended for high-grade industrial paints (Herbst & Hunger 2002), which explains why it is detected in the restored paints purchased in 2011 and not in the original paints from the early 1980s. However, chrome yellow remains the preferential colour capable of achieving the desired strong yellow hue, as seen in *Number 4* yellow and *Number 3* orange, and is not superseded by newer synthetic organic pigments.

Warm colours (magenta, red, orange, yellow) in the *Numbers* mainly consist of a blend of inorganic pigments from the lead chromate family of pigments (PR104, PY34) and a red synthetic organic pigment PR122. The characterisation process is fairly complex and requires a combination of spectral markers, solvent extractions and data processing to differentiate these pigments, which are highlighted in detail in section 5.3.4.1.

5.3.4.1 CHARACTERISATION OF LEAD CHROMATE FAMILY PIGMENTS IN MAGENTA, RED, ORANGE AND YELLOW TOPCOATS

A first analysis undertaken with EDS showed that the red, orange and yellow topcoats contain significant amounts of Pb and Cr. If the sample belonged to an easel painting before the 20th century, it is fairly straightforward to attribute Pb and Cr to either chrome yellow or orange. However, since late 1934 -early 1935, the commercialisation of molybdate orange (PR104) was added to the family of lead chromate pigments available for use in paints (Huckle & Lalor 1955). Being a solid solution of $\text{PbCrO}_4\text{PbMo}_4\text{PbSO}_4$, the reddish pigment is highly tinted and is often present in low concentrations in the paint, posing a difficulty for its detection.

Table 5.1 Summary of pigment results identified in original and restoration paints

	Original			Restored	
Sample	EDS (only prominent elements were listed)	XRF(only prominent elements were listed)	Raman	EDS (only prominent elements were listed)	Raman
White/ Grey/ Black					
Number 0 white	Ti	Ti	rutile	Ti	rutile
Number 5 white	Ti	Ti	rutile	Ti	rutile
Number 0 grey	Ti, (S)	Ti	rutile+ carbon	Ti	rutile+ carbon
Number 9 black	C	NA	carbon	C	carbon
Blue					
Number 2 blue	Ti, Cl, (Cu)	Ti, Cu	rutile+ PB15+PG7	Ti, Cl, (Cu)	rutile+ PB15+PG7
Number 3 blue	Ti, Cl, (Cu)	Ti, Cu	PB15+ PG7	Ti, Cl, (Cu)	PB15+ PG7
Number 5 blue	Ti, Cl, (Cu), (Fe)	Ti, Cu	PB15	Ti, Cl, (Cu)	PB15
Number 7 blue	Ti, Cl, (Cu)	Ti, Cu	PB15	Ti, Cl, (Cu)	PB15
Green					
Number 1 green	Ti, Cl, (Cu), (Ni), Mg, Si, Ba, S	Ni, Cu, Ti, Cl	PG7, rutile, traces of PY34	Ti, Cl, (Cu), (F)	rutile, PY154, PG7
Number 6 green	Pb, Cr, Ti, Cl	Pb, Cr, Ti, Cu, (Sb)	PY34, PG7, traces of rutile	Ti, Pb, Cr, Cl, F	PY34, PY154, PG7
Number 2 green	Pb, Cr, Ti, Cl, (Sb)	Pb, Cr, Ti, (Cu), (Sb)	PY34, rutile, PG7	Ti, Cl, F	rutile, PY154, PG7
Red					
Number 1 red	Pb, Cr, Ti	Pb, Cr, (Mo)	PR122+ PR104	Pb, Cr, Ti	PR122+ PR104
Number 4 red	Pb, Cr, Ti	Pb, Cr, (Mo)	PR122+ PR104	Pb, Cr, Ti	PR122+ PR104
Number 6 red	Pb, Cr, Ti	Pb, Cr, (Mo)	PR122+ PR104+ PY34	Pb, Cr, Ti	PR122+ PR104+PY34
Number 8 red	Pb, Cr, Ti	Pb, Cr, Mo	PR104+ traces of rutile	Pb, Cr, Ti	PR104+ traces of rutile

	Original			Restored	
Sample	EDS (only prominent elements were listed)	XRF(only prominent elements were listed)	Raman	EDS (only prominent elements were listed)	Raman
Magenta					
Number 8 magenta	Ti, Pb, Cr, Fe	Ti, Pb, Cr, (Mo), (Fe)	rutile+ PR104+ PR122+ PB15	Ti, Pb, Cr, (Fe)	rutile+ PR104+ PR122+ PB15
Orange					
Number 3 orange	Pb, Cr, Ti	Pb, Cr, (Mo)	PY34+ PR104 (less)	Pb, Cr, Ti	PY34+ PR104 (less)
Number 7 orange	Pb, Cr, Ti	Pb, Cr, Mo	rutile+ PR104	Pb, Cr, Ti	rutile+ PR104
Yellow					
Number 4 yellow	Pb, Cr, Ti	Pb, Cr, (Mo)	PY34	Pb, Cr, Ti	PY34
Number 9 yellow	Ti, Pb, Cr, (Sb)	Ti, Pb, Cr, (Mo)	rutile+ PY34	Ti, Pb, Cr, (F)	rutile+ PY34+ PY154
Note: The detection of trace amounts of Sb or Fe was inconsistent, probably due to contamination from fabrication environment.					

Previously, it has been shown that detection of traces of Mo by XRF could be attributed to a molybdate orange pigment (Chapter 4). However, EDS is less promising in detecting molybdate orange pigment as the Mo X-rays obtained from the surface of paint sample is too low to generate a visible signal. As such, XRF was applied to the original *Numbers* to test for the presence of Mo. Although Mo was detected in all the red and orange topcoats, traces of Mo were also detected in the black priming layers and the yellow topcoat (probably additive or contaminant), making it difficult to ascertain the presence of molybdate orange using this technique.

Although elemental analyses for these samples do not fully resolve their identification, Raman spectroscopy prevails in distinguishing molybdate orange (PR104: $\text{PbCrO}_4 \cdot \text{PbMo}_4 \cdot \text{PbSO}_4$) from chrome orange (PO21: $\text{PbO} \cdot \text{PbCrO}_4$) and chrome yellow (PY34: PbCrO_4). Molybdate and chrome orange can first be differentiated from chrome yellow by noting the strong Cr-O stretching band, where 825 cm^{-1} can be attributed to molybdate orange or chrome orange while a higher shift at 838 cm^{-1} suggest chrome yellow. The lower Raman shifts in the $250\text{-}430 \text{ cm}^{-1}$ region allows further

discrimination: a doublet at 340 and 358 cm^{-1} is characteristic of molybdate orange while chrome yellow can be identified by a series of bands centering at 358 cm^{-1} , alongside bands at 137, 358, 378 and 400 cm^{-1} . Raman bands for chrome orange in this region vary, but often shows up as non-uniform series of bands around 324, 341, 380 cm^{-1} or 377, 359, 338, 329 cm^{-1} .

While it may seem straightforward using these Raman spectral markers to differentiate pigments in the lead chromate family, the interpretation can be more complex when dealing with heterogeneous paint samples from the *Numbers*, as presented in Fig. 5.13. For example, the band shape in *Number 1* red shows only one broad band at 340 cm^{-1} and the resolution of the doublet in *Number 8* red is poor. After performing a binder extraction using acetone, the solid residue produces a clearer doublet attributable to molybdate orange, which is shown in the dark red trace below the original Raman spectrum (red trace). Interestingly, the molybdate orange doublet in *Number 6* red appears lopsided, and a shoulder next to the strong band at 825 cm^{-1} shows up at 839 cm^{-1} , suggesting that PY34 could be present. After taking a high resolution spectrum, the strong band was resolved into two peaks at 838 and 822 cm^{-1} , confirming that chrome yellow was admixed into the orange molybdate paint. In another instance, *Number 3* orange appears to contain only chrome yellow, but a deconvolution makes it clearer that the strong band at 838 cm^{-1} contains a shoulder at 824 cm^{-1} and the series of bands is asymmetrical with a shoulder at 339 cm^{-1} , confirming that orange molybdate was admixed into chrome yellow to produce the orange hue in *Number 3*.

At the same time, it is interesting to highlight the corresponding FTIR spectra in the chromate stretching region (750-950 cm^{-1}), which indicates the relative proportion of pigment in the paint (Fig. 5.13). When chromate from PR104 is present as the major pigment component, a strong doublet (poorly resolved) appears (#7 orange, #8 red), while chromate from PY34 generates a strong triplet (#3 orange, #4 yellow). However, when synthetic organic pigment (SOP) is present, the strong chromate band disappears and is overtaken by the weakest bands of the SOP. This happens because the relative amount of SOP is much higher than PR104. As SOPs have a lower hiding power compared to inorganic PR104 or PY34, they were often added in larger amounts to

provide the opacity needed in paints (Herbst & Hunger 2002). Knowing the relative proportion is significant in conservation as lead chromates are prone to discolouration from sunlight and acid (i.e. acid rain). By introducing SOPs into the paint formulation, the effect of discolouration is expected to be reduced.

The identification of the type of SOP was difficult due to interfering bands from the styrene-acrylate-urethane binder. Removal of the polymeric binder in polyurethane cured paints using solvent extraction does not work well as the molecular weight is too high. However, this is feasible for uncured paints obtained from the tin cans. After extraction of binder with acetone, the residue that remained after acetone evaporation revealed sharp and intense peaks in the FTIR spectrum that are due to the organic pigment. As seen in Fig. 5.14, most of the peaks initially present due to the acrylate binder had disappeared and the pigment could be identified confidently as PR122. Due to the weak Raman scattering of PR122, the FTIR spectrum provides more information than the Raman spectrum. Furthermore, published Raman shifts for PR122 vary, which was found to depend on the laser and matrix conditions (Massonnet & Stoecklein ; Scherrer et al. 2009; Schulte et al. 2008). The combination of quinacridones such as PR122 with molybdate orange is frequently employed in automotive paints for a greater hiding power. Addition of synthetic organic pigments to expensive inorganic pigments not only lowers costs, but also achieves the desired bright colour (Suzuki & Marshall 1998).

5.3.5 COLOUR MEASUREMENTS

Although the paint swatches in the Dupont paint catalogue (1979) are nitrocellulose-based, their colour appearances serve as the closest piece of evidence matching to Robert Indiana's choice of colours at the time of fabrication. As such, colourimetric data collected from these swatches are considered representative of the original colour scheme of the *Numbers* in the 1980s. The results comparing the restoration paints to these historic paint swatches generates dE values within 6 ± 0.8 , which is considered low, especially when compared to the dE of 24.33 observed between the weathered original paints and the paint swatches. In this case, dE refers to the colour difference between two colours. The results also show that the restored surfaces of *Numbers* have

a much higher gloss than the historic paint swatches, which is expected since the polyurethane paint binder is still relatively young (less than 4 years old). The lower gloss in the paint swatches is attributed to degradation of the nitrocellulose binder.

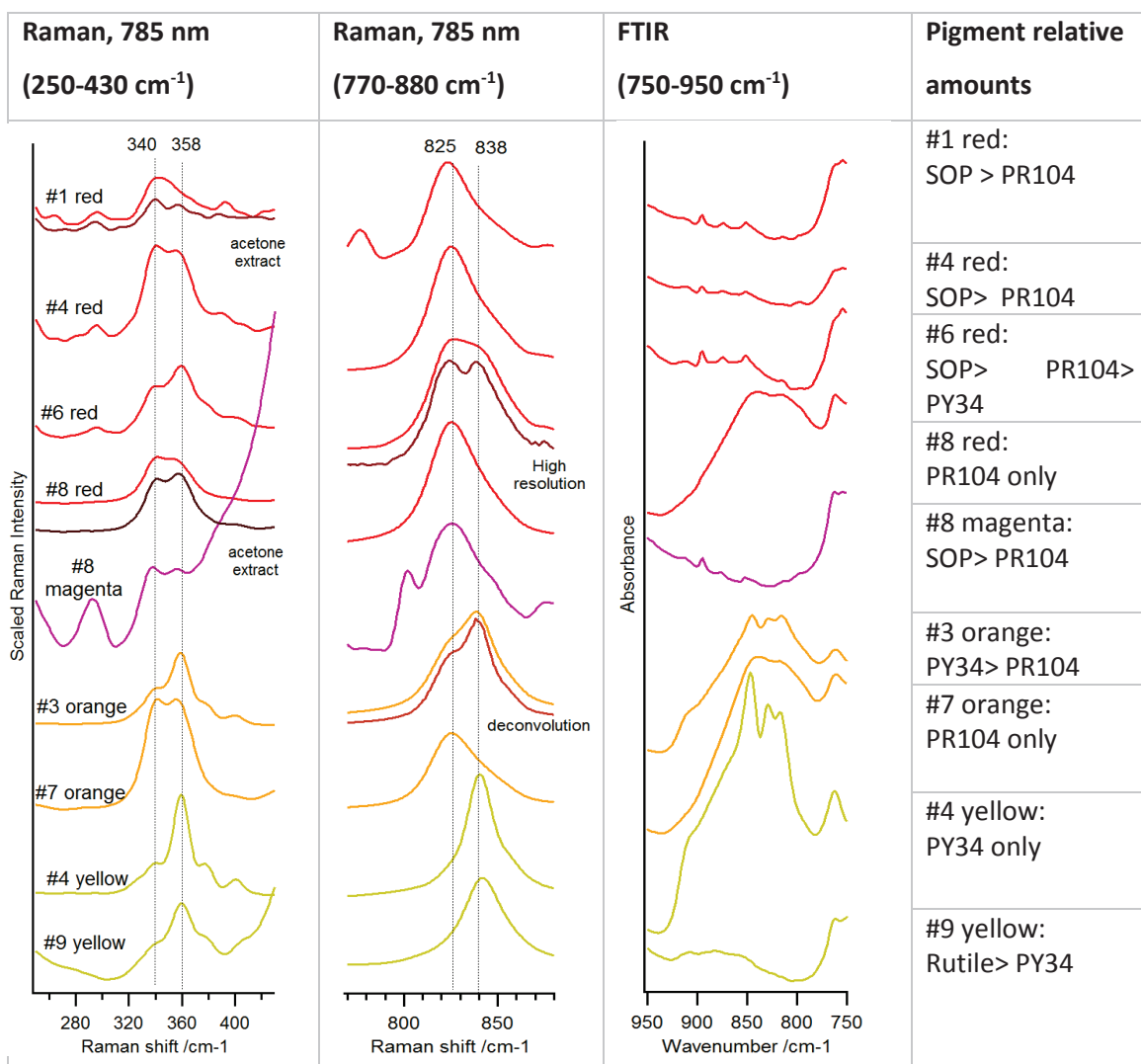


Fig. 5.13 Raman spectra (collected at 785 nm) and FTIR spectra of magenta, red, orange and yellow original topcoats. Selective spectral regions enable discrimination of molybdate orange (PR104) and chrome yellow (PY34), and allow relative pigment proportions in the paint mixture to be determined. 825, 340, 358 cm^{-1} are characteristic peaks for PR104, whereas 838 cm^{-1} and a fountain series of peaks centering at 340 cm^{-1} are characteristic of PY34.

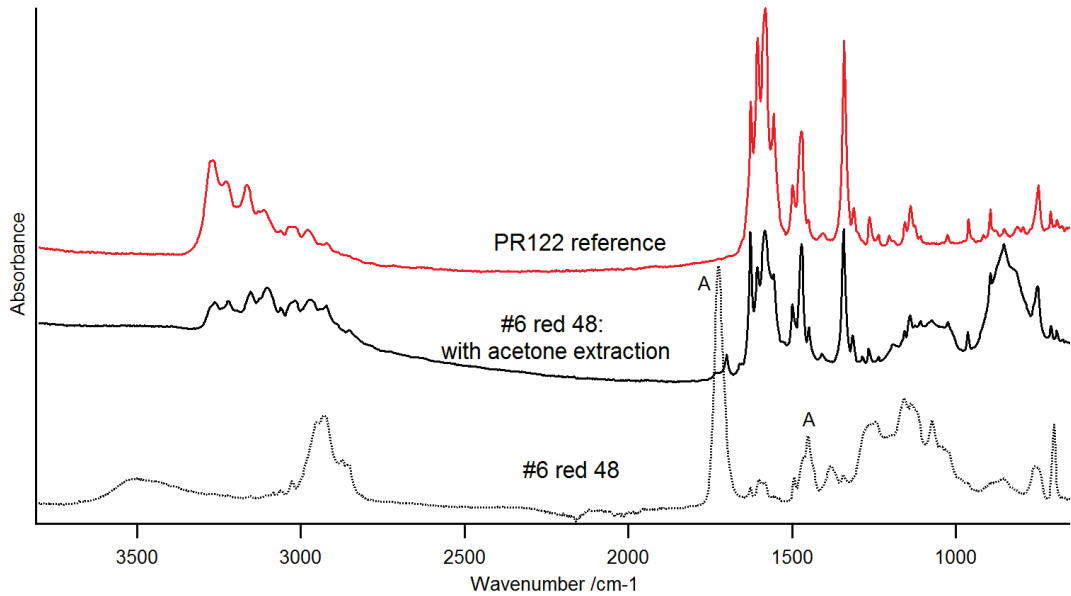


Fig. 5.14. FTIR spectra of (a) Pigment reference PR122; (b) #48 red paint from uncured tin for *Number 6*, after extraction of binder with acetone; (c) the same paint as (b) without acetone extraction, where A : acrylate.

5.4 CONCLUSIONS

Focusing on Robert Indiana’s *Numbers 0-9* as an example, this technical study provided a detailed characterisation of painted aluminum outdoor sculptures at a micro-level. By comparing the paint application techniques between Lippincott and a local steel fabricator, as well as Imron polyurethane enamel paint composition purchased from DuPont in 1980-1983 and 2011, causes for paint failure were deduced at a micro-level.

The study of paint-cross sections from the *Numbers* showed that the layer stratigraphy is more complex than initially assumed for industrial paint systems, including wide-ranging coating thicknesses, multiple recoatings and variable types of primers and surfacers. Eventual paint loss can be attributed to the use of UV sensitive epoxy-based and nitrocellulose-based primers/surfacers used, as well as the inevitable difficulty in eliminating aluminum oxides formation. Loss of gloss could result from the breakdown of urethane component in the topcoat, which was found in all the original *Numbers* except *Numbers 0, 8* and *9*.

Regarding the paint formulation over time, a few minor changes in the composition between 1980 and 2011 generally improved the paint properties and permanency. A more weather-fast organic yellow pigment PY154 has been substituted for lead chromate in some of the colours whereas phthalate plasticisers that impart flexibility had been replaced with mixed acrylates, avoiding problems associated with plasticiser migrations.

The scientific results have shown that the restoration of *Numbers* in 2011 used a much improved topcoat formulation that generated the same colour scheme as in the 1980s, but the use of primer/surfacers containing epoxy and nitrocellulose may be a concern for paint adhesion. Relating these choices in restoration treatments to the permanency of the paints remains to be tested with time.

5.5 SUPPLEMENTARY DATA

Table S1: Layer stratigraphy of original and restoration paints, from outer to inner.

	Original, Face	Original, Side	Original, Sequence	Restored, Face	Restored, Side	Restored, Sequence
#1	Red - Green - (Blk)	Green-(Blk)	Red-green	Red - (RBrn)	Green - (RBrn-Bondo)	Green-red
#2	Green - Blue - (Blk)	Blue- (Blk)	Green-blue	"Blue"-Green-(RBrn-W5)	Blue-RBrn-(W5-RBrn)	Blue-green
#3	Orange - Blue - (W2 - Blk - Brn)	Blue - (W2 - Blk - Brn)	Orange-blue	Orange-(W4-W4(Zn))	Blue - (W4)-Orange-(W4-W4(Zn))	Blue-orange
	Original, Face	Original, Side	Original, Sequence	Restored, Face	Restored, Side	Restored, Sequence
#4	Yellow - Red - (W2)	Red - (W2)	Yellow-red	Yellow - (RBrn - W5)	Red - (RBrn-W5)	Red - yellow
#5	White - Blue - White - Blue - (Blk - Brn)	Blue - (Blk - Brn)	White-blue	White - (W4(Zn) - W4- Bondo)	Blue - (W4)	Blue-white
#6	Green - Red - (W3 - Blk - Brn)	Red - (W3 - Blk - Brn)	Green-red	Green - Red - (W4)	Red - (W4)	Green-red
#7	Orange - Blue - (W2 - Blk - Brn)	Blue - (W2 - Blk - Brn)	Orange-blue	Orange - (W5)	Blue - (RBrn - W5)	Orange - blue

#8	Magenta - Red - (W1 - Blk)	Red - (W1 - Blk)	Magenta- red	Magenta - (W4(Zn)-W4)	Red - Magenta - (W4(Zn)- W4)	Red - magenta
#9	Yellow - Black -(W1 - Blk - Brn)	Black -(W1 - Blk - Brn)	Yellow- black	Yellow - (W4 (Zn)-W4)	Black - Yellow - (W4(Zn)- W4)	Black- yellow
#0	White - Grey - (W1 - Blk - Brn)	Grey - (W1 - Blk - Brn)	White- grey	White - (W4)	Grey - White-(W4)	Grey - White

Blk: black primer (nitrocelullose based) – fig. 5.9c
 RBrn: reddish brown primer/ surfacer (epoxy based)- fig. 5.9g
 W1: white surfacer (epoxy-based)- fig. 5.9a
 W2: white surfacer (acrylate-based)- fig. 5.9b
 W3: white primer/ surfacer (urethane acrylate)- fig. 5.9d
 W4: white primer/ surfacer (acrylate); W4 (Zn): W4 with Zn identified by EDS- fig. 5.9e
 W5: white primer/ surfacer (nitrocellulose-based)- fig. 5.9f
 Brn: brown fairing compound (i.e. Bondo)

Table S2: Binder comparison of DuPont Imron polyurethane paints applied on Numbers in 1980-1982 vs 2011.

Topcoat	Consistency	FTIR	Py-GCMS	Components
Original topcoat (applied 1980-1982)	Hard	styrene, acrylate only; Urethane band is only seen in Numbers 0, 8 and 9	styrene, HDI, MMA, phthalate	P(styrene-MMA) copolymer with urethane, phthalate
Restoration topcoat (applied 2011)	Soft	styrene, acrylate, urethane	styrene, HDI, various acrylates, ethylbenzene (solvent)	P(styrene-acrylate) copolymer with traces of solvents

HDI: 1,6-hexamethylene diisocyanate
 MMA: methyl methacrylate

5.6 REFERENCES

Amaral, P. 2013, *Robert Indiana LOVE sculpture*, Youtube, Date accessed: 01 Jan 2016, <https://www.youtube.com/watch?v=nvRYkGAI_m8>.

Considine, B.B., Wolfe, J., Posner, K. & Bouchard, M. 2010, 'Scientific Investigations', *Conserving outdoor sculpture : the Stark collection at the Getty Center*, Getty Conservation Institute, Los Angeles, pp. 53-82.

- Farcas, F. 2013, 'Characterization of Organic Materials used in Civil Engineering by Chemical and Physico-chemical Methods', *Organic Materials for Sustainable Construction*, John Wiley & Sons, Inc., pp. 553-82.
- Herbst, W. & Hunger, K. 2002, *Industrial Organic Pigments: Production, Properties, Applications*, Wiley-VCH, Germany.
- Huckle, W.G. & Lalor, E. 1955, 'Inorganic Pigments', *Industrial & Engineering Chemistry*, vol. 47, no. 8, pp. 1501-6.
- Lambourne, R. & Strivens, T.A. 1999, *Paint and Surface Coatings: Theory and Practice*, William Andrew Pub.
- Learner, T. 2001, 'The Analysis of Synthetic Paints by Pyrolysis-Gas Chromatography-Mass Spectrometry (PyGCMS)', *Studies in Conservation*, vol. 46, no. 4, pp. 225-41.
- Learner, T. 2004, *Analysis of modern paints*, Getty Conservation Institute, Los Angeles.
- Lippincott, J.D. 2010, *Large scale fabricating sculpture in the 1960s and 1970s*, Princeton Architectural Press, New York, N.Y.
- Massonnet, G. & Stoecklein, W., 'Identification of organic pigments in coatings: applications to red automotive topcoats', *Science and Justice*, vol. 39, no. 3, pp. 181-7.
- McIntee, E. 2008, 'Forensic Analysis Of Automobile Paints By Atomic And Molecular Spectroscopic Methods And Statistical Data Analyses', University of Central Florida, Orlando.
- Scherrer, N.C., Stefan, Z., Françoise, D., Annette, F. & Renate, K. 2009, 'Synthetic organic pigments of the 20th and 21st century relevant to artist's paints: Raman spectra reference collection', *Spectrochimica Acta Part A: Molecular and Biomolecular Spectroscopy*, vol. 73, no. 3, pp. 505-24.
- Schulte, F., Brzezinka, K.-W., Lutzenberger, K., Stege, H. & Panne, U. 2008, 'Raman spectroscopy of synthetic organic pigments used in 20th century works of art', *Journal of Raman Spectroscopy*, vol. 39, no. 10, pp. 1455-63.

- Streitberger, H.J. & Dossel, K.F. 2008, *Automotive Paints and Coatings*, Wiley.
- Suzuki, E.M. & Marshall, W. 1998, 'Infrared spectra of U.S. automobile original topcoats (1974-1989): IV. Identification of some organic pigments used in red and brown nonmetallic and metallic monocoats - quinacridones', *Journal of Forensic Sciences*, vol. 43, no. 3, pp. 514-42.
- Wolfe, J. 2013, 'Three Brushstrokes: Re-creating Roy Lichtenstein's Early Techniques for Outdoor Painted Sculpture', *Conserving outdoor painted sculpture : proceedings from the interim meeting of the Modern Materials and Contemporary Art Working Group of ICOM-CC*, eds L. Beerkens & T. Learner, The Getty Conservation Institute, Kröller-Müller Museum, Otterlo, the Netherlands.



Chapter 6

ANALYSIS OF “ESTES PARK,
COLORADO” PREPARATORY SKETCH,
BY ARTIST GUSTAVE BAUMANN

6.1 INTRODUCTION

The IMA holds a complete set of prints by Gustave Baumann, made during the early days of his career in the Brown County art colony and it has been a continual desire to understand the artist's home-made paint recipes. He is said to have mixed his own paints according to his own personal recipe, one that he would not even divulge to close colleagues. Baumann's studio was filled with jars of colored powder and liquid, which provided material evidence of his paint recipe (See Fig. 6.1). Vaguely labeled as "pigments" and "varnishes", this information is not descriptive enough to understand the materials he used. Interestingly, no material suggestive of a binder was found in his studio, an important constituent of paint, which makes its identity questionable. Documented as "tempera sketches" at the time of acquisition, it is possible that gum or egg yolk might have constituted the binder used, but scientific analysis is necessary to confirm this. Knowing the binder used to constitute the artist's safeguarded paint recipe is valuable information for Baumann prints art enthusiasts, and more importantly, for the conservation of this significant yet severely flaking collection.



Fig. 6.1 Colored pigments and varnishes in Baumann's studio

This case-study highlights an in-depth examination of the painting, "Estes Park, Colorado", created by Baumann in 1926 (Fig. 6.2), that has not been analyzed before. Prepared as a sketch, the painting was intended to help the artist finalize the image for a woodblock print. This paint sketch displays one of the worst conditions so far, where the paint was delaminating across the entire surface. Other sketches in the collection are less severe, showing localized paint lifting and cracking.

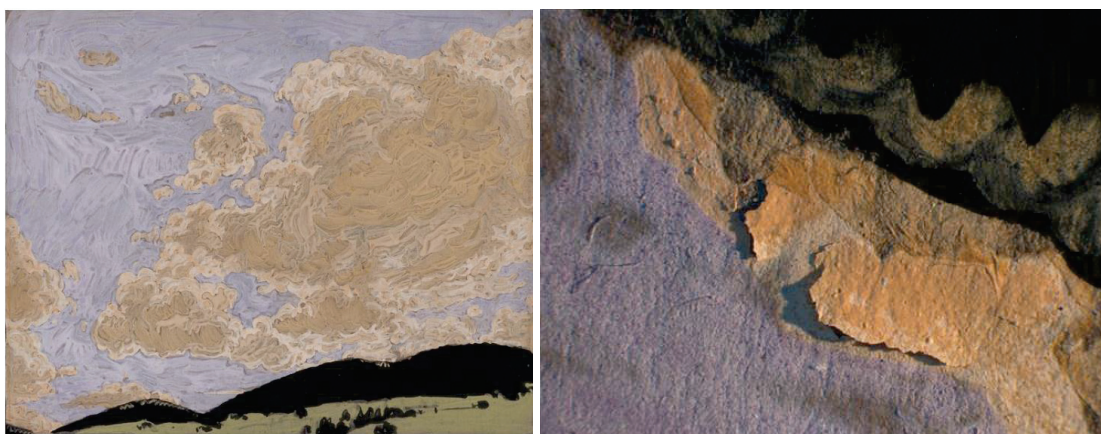


Fig. 6.2 Left: *Estes Park, Colorado, 1926*, Gustav Baumann, IMA# 2008.54, tempera over graphite on brown paper. Loose paint flakes available for analysis were purple, beige and white (Original location of paint is unknown). Purple sample: Sky area, Beige sample: Cloud area, White sample: White margin that borders the painting. Gift of Ann Baumann. Photo Courtesy of IMA. Right: A photomicrograph showing severe delamination of the paint.

6.2 MATERIALS AND METHODS

Due to its unstable condition, some loose paints that fell out of the painting were made available for scientific analysis. With the aid of a stereomicroscope, they were then separated into glass vials of individual colors of beige, purple and white for subsequent instrumental analysis. A clean brush was used for the transfer as the paint chips were light, very brittle and easily fractured.

6.2.1 FTIR MICRO-SPECTROSCOPY

Micro-amounts of the purple, beige and white samples were separately analysed by FTIR micro-spectroscopy on a Continuum microscope with an MCT detector coupled to a Nicolet 6700 spectrometer purged with dry, CO₂-free air. The spectra are the sum of 32 co-additions at 4 cm⁻¹ spectral resolution. Microsamples were crushed on a diamond compression cell and held on a single diamond window during the analysis.

6.2.2 GC/MS

As the GC/MS analytical procedure required a typical sample size of ≈ 0.5 mg, only the beige paint flakes with sufficient quantity was analyzed. The total weight of the beige paint flakes in this analysis was 0.748 mg. The analytical procedure separated the organic binder classes into three organic fractions of lipid/resin, protein and polysaccharide. Each fraction was hydrolysed, cleaned-up and derivatised before injection into the GC/MS. More details of the procedure are described in Appendix.

6.3 RESULTS AND DISCUSSION

6.3.1 FTIR MICRO-SPECTROSCOPY RESULTS

The FTIR spectra of the beige, purple and white paint samples all show a common feature (Fig. 6.3), a very strong and broad band centering around 1590 cm^{-1} and a weak band observed at 1726 cm^{-1} , assigned to carboxylates and metal coordinated fatty acids, respectively (Kaszowska et al. 2013). Since Zn is present as the only major element in the EDS of all three colors, the metal soaps likely occur in the form of zinc carboxylates. However, the broad band around 1590 cm^{-1} cannot be assigned to any specific carboxylate reported in the literature. A band at 1540 cm^{-1} is characteristic of zinc stearate (Robinet & Corbeil 2003) and zinc palmitate (Otero et al. 2014), while zinc azelate and zinc oleate produce doublets at $1556/1535\text{ cm}^{-1}$ and $1547/1527\text{ cm}^{-1}$, respectively (Otero et al. 2014), all of which do not contribute strongly to the 1590 cm^{-1} band in the FTIR spectrum. Although copper palmitate produces a strong band at 1584 cm^{-1} (Mazzeo et al. 2008), no Cu was detected in the EDS and so this possibility was disregarded. In two other instances, the broad band at 1590 cm^{-1} also occurs in zinc-based paints and it was assigned to zinc lactate. This assignment was substantiated with the detection of lactic acid (2-hydroxypropanoic acid) in Py-GC/MS (Helwig et al. 2014) and the presence of other sharp bands at 1367 , 1321 , 1273 cm^{-1} and 866 cm^{-1} in the FTIR spectrum (Osmond, Ebert & Drennan 2015). However, lactic acid was not detected in the FTIR spectrum (Fig. 6.3). Other studies have also reported a broad band at 1590 cm^{-1} for oil paints containing zinc oxide, but the assignment of this band remained ambiguous and was hypothesised as a mixture of zinc carboxylates (Izzo 2010; Kaszowska et al. 2013; Mazzeo et al. 2008). Therefore, the strong band at 1590 cm^{-1} in Fig. 6.3 may be assigned

to a mixture of zinc carboxylates, taking into account of its broad band width of 1650-1520 cm^{-1} (Kaszowska et al. 2013; Van Der Weerd 2002).

The sharp carbonate peak at 1398 cm^{-1} could arise from the mineralisation of zinc carbonate inside zinc soap aggregates upon contact with atmospheric CO_2 (Keune 2005). The C-H stretches (2928 and 2855 cm^{-1}) and C-H bending (1465 and 1379 cm^{-1}) observed in the FTIR spectrum are attributed to long hydrocarbon fatty acids chains. The absence of a band at 1710 cm^{-1} which is indicative of free fatty acids, implied that the fatty acids were either coordinated with metal ions or cross-linked. It is difficult to relate the band occurring at 1354 cm^{-1} to a specific compound, though it seems to match one of the smaller peaks in zinc azelate (Helwig et al. 2014).

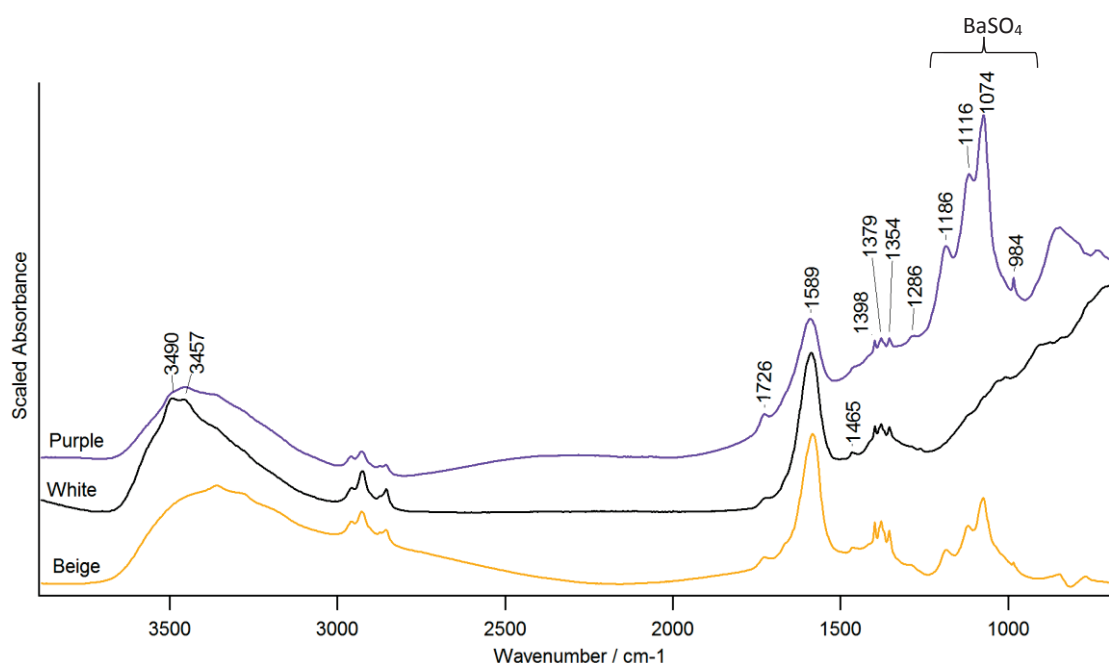


Fig. 6.3 FTIR spectra of purple, beige and white paint samples, indicating the presence of metal carboxylates.

The detection of zinc soaps in the Baumann paint flakes is significant as it explains its brittleness. Reported in a number of other studies, zinc white in oil paint films are particularly stiff and prone to fracture compared to other white pigments used in ground layers (Osmond 2014; Pratali 2013; Rogala et al. 2010; Shimadzu, Keune & Van Den Berg 2008; Van Der Weerd 2002). The brittleness of zinc-containing oil paint can be explained by the fact that after hydrolysis of oil triglycerides, the free fatty acids do not go through

an extensive cross-linking process as it would in a normally oxidised drying oil. Instead, the dicarboxylic and monocarboxylic acids become coordinated with nearby zinc ions, which then crystallise into a highly ordered lamellar network, making it more difficult for the unsaturated double bonds in the fatty hydrocarbon chains to cross-link. As a result, the low degree of cross-linking and high amounts of planar-fracturing sites generates a paint film that is prematurely harder and more brittle (Boon, Hoogland & Keune 2006; Pratali 2013).

6.3.2 GC/MS RESULTS

While FTIR spectroscopy has identified the presence of metal soaps in the paint samples, the attribution of the binder is less certain. Some of the IR bands suggest oil as binder, but it is possible that other binder classes are present and not detected by FTIR spectroscopy. To further confirm the binder identification, the beige sample was subjected to the analytical procedure for GC/MS described in Appendix.

6.3.2.1 FATTY ACID FRACTION

As seen in Fig. 6.4, the TIC of the neutral lipid/resin fraction indicates comparable amounts of dicarboxylic azelaic acid (A), monocarboxylic stearic acid (S) and palmitic acid (P), together with dehydroabietic acid (DHA), an oxidation product from a diterpenoid resin. A significant amount of lauric acid and small amounts of myristic acid are also detected. These fatty acids of different molecular weights may account for the broad FTIR carboxylate band at 1590 cm^{-1} (Kaszowska et al. 2013).

The A/P ratio is 0.5, suggesting the presence of tempera grassa (mixed binder containing oil and egg components). Using another indicator, the sum of dicarboxylic acid is less than 30 % of total fatty acids and more than 10 % total fatty acids, suggesting that the binder is not a pure drying oil (Colombini & Modugno 2009; Colombini et al. 1999).

Saturated fatty acids, being less reactive, do not change significantly with age and, hence, the P/S ratio has been used to distinguish the type of oil binder. The P/S ratio obtained in this beige sample is 2.0, which may imply linseed oil or walnut oil. However, P/S ratio is not always reliable. It was previously reported that P/S ratio changes with the concentration of pigments and the final concentration of fatty acids injected (i.e. sample

dilution) (Colombini & Modugno 2009; Tsakalof, Bairachtari & Chrissyoulakis 2006). P/S ratio is also not valid when comparing mixtures with more than one binder (e.g. egg and oil in “tempera grassa”), when wax is present or when other sources such as microorganisms contribute and alter the level of fatty acids (Colombini & Modugno 2009).

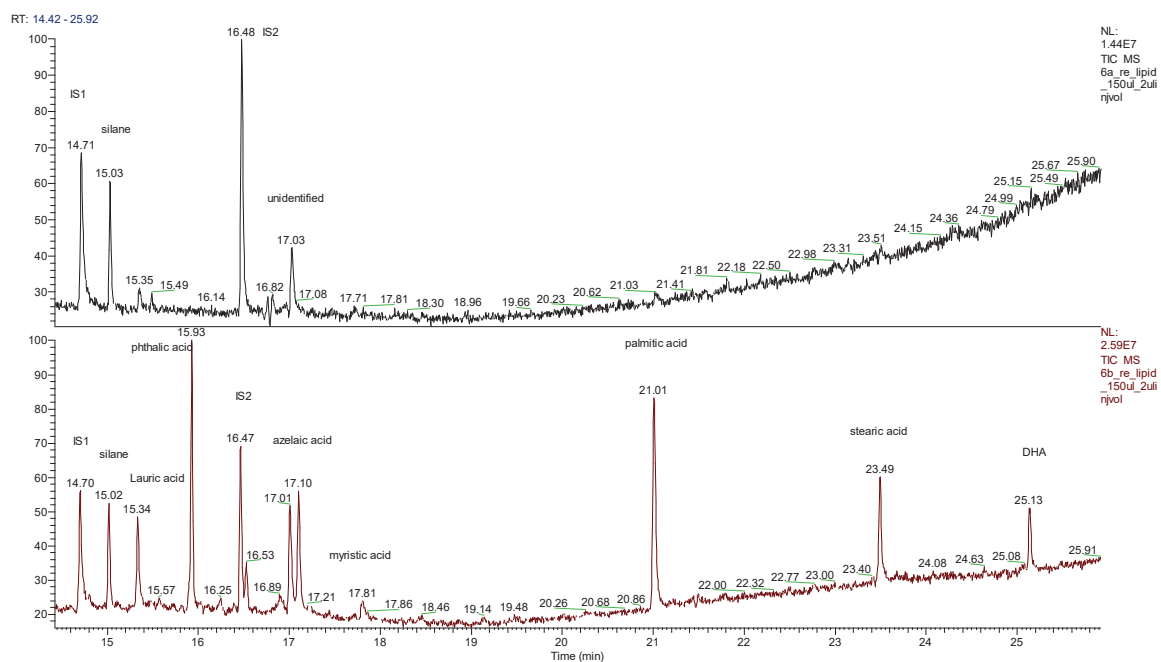


Fig. 6.4 Fatty acid profile of blank (top) and beige sample (Bottom). The phthalic acid in the sample is attributed to contamination from the vial cap.

6.3.2.2 AMINO ACID FRACTION

The beige sample shows trace amounts of amino acids that also appear in an egg yolk reference (Fig. 6.5). Although the S/N ratio is low, these amino acids exist only in the beige sample and not in the blank, ruling out the possibility of procedural contamination.

The recovery of amino acids in egg yolks tends to be lower than other proteinaceous binder (i.e. animal glue and casein) encountered in art samples. When egg yolk is mixed with linseed oil, the yield can be even lower. While it may be ideal to quantify the % amino acid composition and correlate that with an egg yolk reference, the amounts detected are too low for accurate quantitation. Moreover, the coefficient correlations are

not comparable for samples containing egg yolk. For example, the correlation coefficient for egg yolk tempera (both aged and unaged) compared to an unaged unpigmented egg yolk is as low as 0.78, indicating that composition changes for egg yolk are affected by ageing and associated oil binder or pigments (Schilling, Khanjian & Luiz 1996). Therefore, the results suggest that egg yolk is present from a qualitative perspective, but this is not ascertained from a quantitative perspective.

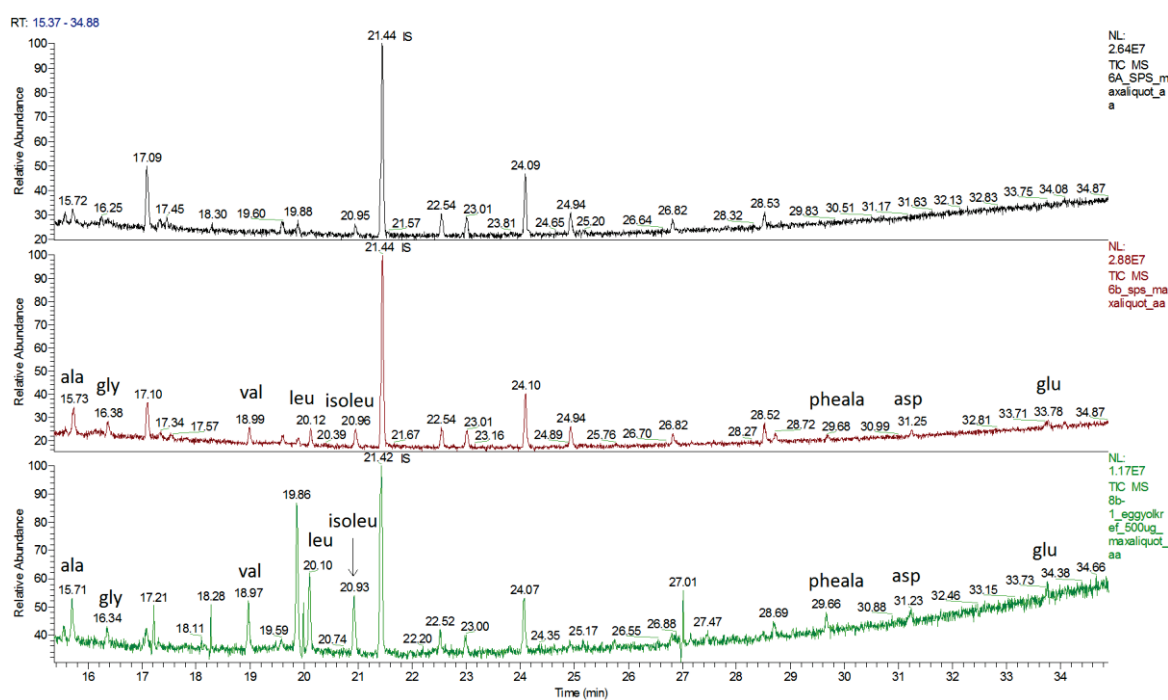


Fig. 6.5 Amino acid profile of blank (top), beige sample (middle) and egg yolk reference (bottom).

6.3.2.3 MONOSACCHARIDE FRACTION

The gum fraction did not show any profile attributable to known gums (Fig. 6.6), based on the decision scheme of gum identification presented by Lluveras et al. (Lluveras et al. 2010). The detection of xylose and galactose could possibly come from the paint substrate or the egg yolk. Detection of xylose has been associated with organic plant tissues such as wood, paper and straw, used to support the paint or preparation layers (Lluveras-Tenorio et al. 2012) whereas the gum fraction of egg yolk reference subjected to the same procedure has shown trace amounts of glucose and galactose.

FTIR and GC/MS results have provided evidence for the presence of fatty acids. The organic analyses of the individual fractions by GC/MS revealed the presence of drying oil,

dehydroabiatic acid and traces of amino acids that likely derived from egg yolk. These results suggest the presence of a *tempera grassa* binder.

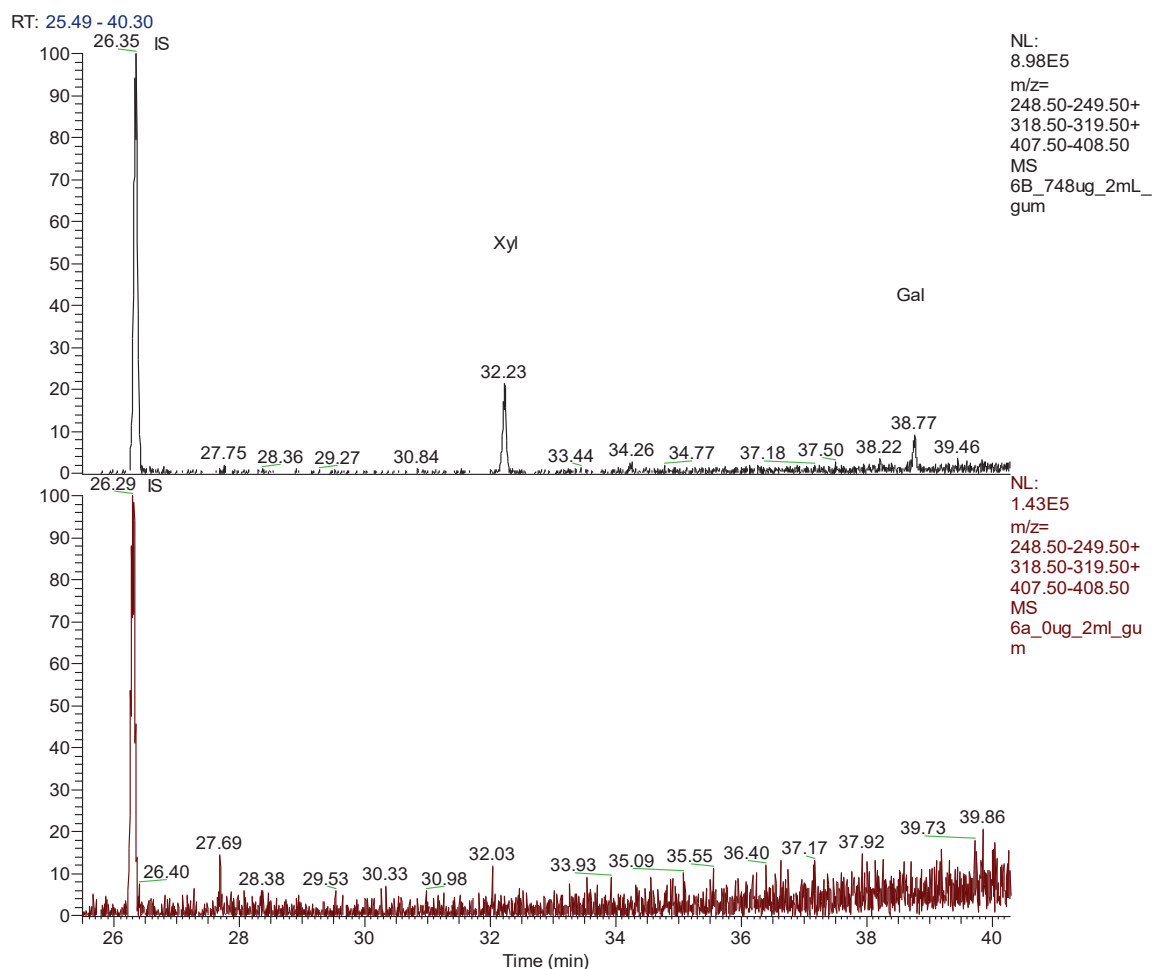


Fig. 6.6 Monosaccharide profile of beige sample (top) and blank (bottom). Ions are extracted at $m/z = 249, 319, 408$.

6.4 CONCLUSIONS

One of Baumann's preparatory paint sketches, "Estes Park, Colorado", was analysed for the first time to determine the identity of the binder and causes for flaking paint. This painting displays a poor condition compared to the rest of Baumann's works, showing severe paint delamination and embrittlement. The FTIR results show that the paint contains metal soaps, notably in the form of mixed molecular weights zinc carboxylates. While this result may explain for its associated fragility, no binder information, other than the possibility of oil, could be revealed in the FTIR spectrum. By applying the developed GC/MS analytical procedure, the presence of drying oil and dehydroabiatic acid, as well as

egg yolk, were detected, suggesting that the binder is a *tempera grassa*. The results from this study demonstrated the benefits of performing a multi-binder analytical procedure for GC/MS, in combination with FTIR spectroscopy, for binding media characterisation. Some of the extant questions remaining to be explored include the binder constituents in other Baumann “tempera” sketches, and whether zinc filled paints are causing fragility in his other works. Further characterisation studies can contribute to the long-term goals in revealing Gustave Baumann’s choice of paint materials and his mysterious home-made paint recipes.

6.5 References

- Boon, J.J., Hoogland, F. & Keune, K. 2006, 'Chemical processes in aged oil paints affecting metal soap migration and aggregation', paper presented to the *34th annual meeting of the AIC of Historic & Artistic Works providence*, Rhode Island, June 16-19.
- Colombini, M.P. & Modugno, F. 2009, *Organic Mass Spectrometry in Art and Archaeology*, Wiley, Chichester.
- Colombini, M.P., Modugno, F., Giacomelli, M. & Francesconi, S. 1999, 'Characterisation of proteinaceous binders and drying oils in wall painting samples by gas chromatography–mass spectrometry', *Journal of Chromatography A*, vol. 846, no. 1–2, pp. 113-24.
- Helwig, K., Poulin, J., Corbeil, M.-C., Moffatt, E. & Duguay, D. 2014, 'Conservation Issues in Several Twentieth-Century Canadian Oil Paintings: The Role of Zinc Carboxylate Reaction Products', in J.K. van den Berg, A. Burnstock, M. de Keijzer, J. Krueger, T. Learner, A. de Tagle & G. Heydenreich (eds), *Issues in Contemporary Oil Paint*, Springer International Publishing, Cham, Switzerland, pp. 167-84.
- Izzo, F.C. 2010, '20th century artists' oil paints: A chemical-physical survey', PhD thesis, University Ca Foscari, Venice.
- Kaszowska, Z., Malek, K., Pańczyk, M. & Mikołajska, A. 2013, 'A joint application of ATR-FTIR and SEM imaging with high spatial resolution: Identification and distribution of painting materials and their degradation products in paint cross sections', *Vibrational Spectroscopy*, vol. 65, pp. 1-11.

- Keune, K. 2005, 'Binding medium, pigments and metal soaps characterised and localised in paint cross-sections', PhD thesis, University of Amsterdam, Netherlands.
- Lluveras-Tenorio, A., Mazurek, J., Restivo, A., Colombini, M.P. & Bonaduce, I. 2012, 'The Development of a New Analytical Model for the Identification of Saccharide Binders in Paint Samples', *PLoS ONE*, vol. 7, no. 11, p. e49383.
- Lluveras, A., Bonaduce, I., Andreotti, A. & Colombini, M.P. 2010, 'GC/MS Analytical Procedure for the Characterization of Glycerolipids, Natural Waxes, Terpenoid Resins, Proteinaceous and Polysaccharide Materials in the Same Paint Microsample Avoiding Interferences from Inorganic Media', *Analytical Chemistry*, vol. 82, no. 1, pp. 376-86.
- Mazzeo, R., Prati, S., Quaranta, M., Joseph, E., Kendix, E. & Galeotti, M. 2008, 'Attenuated total reflection micro FTIR characterisation of pigment–binder interaction in reconstructed paint films', *Analytical and Bioanalytical Chemistry*, vol. 392, no. 1, pp. 65-76.
- Osmond, G. 2014, 'Zinc White and the Influence of Paint Composition for Stability in Oil Based Media', in J.K. van den Berg, A. Burnstock, M. de Keijzer, J. Krueger, T. Learner, A. de Tagle & G. Heydenreich (eds), *Issues in Contemporary Oil Paint*, Springer International Publishing, Cham, Switzerland, pp. 263-81.
- Osmond, G., Ebert, B. & Drennan, J. 2015, 'Zinc oxide-centred deterioration in 20th century Vietnamese paintings by Nguyễn Trọng Kiệm (1933–1991)', *AICCM bulletin*, vol. 34, no. 1, pp. 4-14.
- Otero, V., Sanches, D., Montagner, C., Vilarigues, M., Carlyle, L., Lopes, J.A. & Melo, M.J. 2014, 'Characterisation of metal carboxylates by Raman and infrared spectroscopy in works of art', *Journal of Raman Spectroscopy*, vol. 45, no. 11-12, pp. 1197-206.
- Pratali, E. 2013, 'Zinc oxide grounds in 19th and 20th century oil paintings and their role in picture degradation processes ', *CeROArt [En ligne]*, vol. 3.
- Robinet, L. & Corbeil, M.-C. 2003, 'The Characterization of Metal Soaps', *Studies in Conservation*, vol. 48, no. 1, pp. 23-40.
- Rogala, D., Lake, S., Maines, C. & Mecklenburg, M. 2010, 'Condition problems related to zinc oxide underlayers: Examination of selected abstract expressionist paintings

from the collection of the Hirshhorn museum and sculpture garden, Smithsonian Institution', *Journal of the American Institute for Conservation*, vol. 49, no. 2, pp. 96-113.

Schilling, M.R., Khanjian, H.P. & Luiz, A.C.S. 1996, 'Gas Chromatographic Analysis of Amino Acids as Ethyl Chloroformate Derivatives. Part 1, Composition of Proteins Associated with Art Objects and Monuments', *Journal of the American Institute for Conservation*, vol. 35, no. 1, pp. 45-59.

Shimadzu, Y., Keune, K. & Van Den Berg, J.K. 2008, 'The effects of lead and zinc white saponification on surface appearance of paints', *15th Triennial Conference*, Allied Publishers, New Delhi, pp. 626-32.

Tsakalof, A.K., Bairachtari, K.A. & Chryssoulakis, I.D. 2006, 'Pitfalls in drying oils identification in art objects by gas chromatography', *Journal of separation science*, vol. 29, pp. 1642-6.

Van Der Weerd, J. 2002, 'Microspectroscopic analysis of traditional oil paint', PhD thesis, University of Amsterdam, Netherlands.

Chapter 7

Conclusions

The four case-studies (Chapters 3-6) demonstrated the application of multiple instrumental techniques that addressed specific museum curatorial and conservation concerns. In addition, Chapter 6 demonstrates a technique validation before applying it onto painted artwork samples. Through a detailed micro-characterisation of the pigments, binders and associated deterioration products (Table 7.1), it is possible to draw a few conclusions from the case-studies presented.

Table 7.1 Summary of case-study results

	Chapter 3 Ethnographical objects	Chapter 4 Prints	Chapter 5 Modern Outdoor sculptures	Chapter 6 Preparatory Painting
Motivation	Curatorial concerns, technical art history	Exhibition concern for lightfastness	Conservation concerns, causes of paint failure	Conservation concerns, causes of paint failure
Paint matrix	Paint on plant-based materials	Paint on embossed paper	Paint on aluminum	Paint on paper
Dating	Around mid-20 th century, collected 1961-1972	1970-1971	1980-1982	1926
Pigments	Vivianite, yellow ochre (goethite, lepidocrocite), red ochre (hematite), PY1, PR3, PB15, ultramarine blue	Chrome yellow, Prussian blue, aniline black, carbon black, molybdate orange PR104, PB15, PR3, PR22, PR48:3	Rutile, PB15, PG7, PY34, PY154, PR122, PR104	Zinc white
Binders	Animal fat (pork lard), gum (plant sap), resin (tree), alkyd, wax	Likely oil	Polyurethane acrylate topcoat, epoxy, nitrocellulose, acrylate, urethane-acrylate primer/ surfacer	Drying oil, egg yolk, diterpenoid resin
Other materials	Metal soaps, bird excrement, fungi, charred wood	Fungi, paper	Phthalate	Metal soaps
Technique	Optical microscopy, FTIR, Raman, SEM-EDS, GC/MS, XRD	Optical microscopy, FTIR, Raman, XRF, Microfadeometer	Optical microscopy, FTIR, SEM-EDS, Raman, Py-GC/MS, colorimeter	Optical microscopy, FTIR, SEM-EDS, GC-MS

7.1 Choice of instrumentation technique

All four case-studies shared similarity in the sample of interest, namely pigments and binders that constitute the paint colouration in the 20th century. Consequently, the selection of instrumentation techniques revolved around mainstay techniques used for paint characterization, namely FTIR and Raman spectroscopy, elemental analysis and GC/MS. However, the differences in these paint samples' physical and chemical nature affect the complementary instrumental technique(s) used.

7.1.1 Physical nature

In the PNG Highlands case-study (Chapter 3), the collected paint samples contained a high pigment to binder ratio that could be contaminated by other assorted materials such as plant fibres, wood, hair and clay. For such samples, solvent extraction with filtration or pre-treatment with HF helped to remove the inorganic interferences for binder identification. Similarly, the use of photobleaching and longer excitation wavelengths in Raman spectroscopy reduced the fluorescence effects and improved the identification of certain pigments. In the Numbers outdoor sculptures case-study (Chapter 5), the layers of sprayed-on paint coatings, primers and aluminum substrate present samples with interesting layer stratigraphy that would benefit from observing a polished cross-section with SEM-EDS elemental mapping. In the Haku Maki print case-study (Chapter 4), the prints were in such pristine condition that sampling is avoided as far as possible, and non-invasive analysis using Raman spectroscopy mounted on a gantry and portable XRF were selected.

7.1.2 Chemical nature

When analyzing polyurethane paints in the Numbers outdoors sculptures case-study (Chapter 5), the use of pyrolyser at high temperature was necessary to break down the long polymer to fragments suitable for GC/MS analysis. This is in contrast to smaller molecular weight compounds (i.e. lipids, carbohydrates, wax, resins and proteins) that occur in natural binding medium, which can be extracted with wet chemistry methods and analysed with

GC/MS, as presented in the tempera paint samples in Baumann case-study (Chapter 6). As FTIR spectrum was dominated by absorption bands arising from zinc soap and fatty acids, it was essential to carry out GC/MS analysis to provide more information that could have been missed with FTIR spectroscopy alone. The GC/MS technique validation in Appendix was able to detect protein (egg yolk) and drying oil that ascertain the paint media as a tempera. Paint samples also occur in layers, as seen in the Numbers case-study (Chapter 5).

7.2 Data interpretation

Attributing an unknown material to one that is known can be fairly challenging, considering the myriad of materials that could be available to the artisan and that spectral libraries of reference materials are not always available. The results from the four case-studies could be largely interpreted, owing to literature from similar studies and availability of reference samples to serve as comparison.

The interpretation of results from painted artwork samples share a few similar points. Firstly, different materials used in painted artworks may be similar in chemical composition, giving a similar fingerprint that makes it easy to fall into the trap of over-assumption. For example, the FTIR and Raman fingerprint spectrum of sandarac and copal are highly correlated and should be interpreted in a broader sense as diterpenoid resin (Chapter 3). Secondly, contextual information on the artist background, history of artwork, source(s) of paint, approximate dating, documentation of conservation treatment, often helps narrow the identification of the paint ingredients, associated deterioration product or contamination. Most importantly, having this information ensures that the interpretation is logical and acceptable. For example, the detection of modern synthetic pigments on ethnographical ceremonial objects from the PNG Highlands is logical, considering that trade store pigments were made available to the locals in the same time period (Chapter 3). Lastly, it is important to recognize that samples from artworks are likely to have undergone natural ageing, heating or other forms of conservation treatment. With regards to natural binders, pigment interferences, hydrolysis or oxidation of fats and drying oils, denaturation of proteinaceous

binders are possible issues encountered. Similarly, weathering of modern paints such as polyurethane paints can be observed with the decreasing intensity of the urethane absorption band in the FTIR spectrum (Chapter 5).

7.3 Outcomes

The material results of these artworks have shown to benefit knowledge on technical art history, exhibition concerns and explaining causes for the paint deterioration, all of which informs conservation practices.

Firstly, unusual visual observations during the conservation documentation process can be explained and properly documented. In the PNG case-study (Chapter 3), a visual survey of the collections showed a wide range of color shades in black, blue, red and yellow, despite being a rather simple palette dominated by the same few pigments. The pigment hue can change due to effects from different binder, clay and charred wood. For example, red ochre identified in the sacred stone was dark brown (unlike other red ochres in the collections) due to the presence of pork fats, whereas vivianite in some *Timbu waras* are visually lighter due to a larger clay proportion. In the Haku Maki case-study (Chapter 4), the exceptional pop-up effect is not only attributed to the embossed printing technique, but also due to the choice of pigments- an intense dark aniline black and bright lead chromate pigments.

Secondly, vague or lack of technical documentation of museum collection can cause an incomplete understanding and inaccurate interpretation of an artwork. Having detailed scientific information on the original practice in making the artwork and the resources available to the artist at that time improves conservation and curatorial understanding and interpretations. In the PNG case-study (Chapter 3), the scientific results showed the widespread distribution of synthetic pigments or trade store colors playing an important role in influencing the extensiveness of colonialism in the Highlands. The localized identification of rare blue pigment vivianite also demonstrated limited trading at that time. In the Haku Maki prints case-study (Chapter 6), very little information was recorded on the artist's materials and the generic literature could not represent properly on the palette of bright

colours used by Haku Maki. Through a detailed study of the pigments identified, the importance of identifying artist's materials for customising stewardship practices was highlighted.

Thirdly, the scientific results helped assess the paint condition and predict future stability. From analysis of PNG samples (Chapter 3), many non-drying binders such as tigas oil and pork lard identified remain uncured after decades and these have a potential for attracting dust or dirt. In the Baumann case-study (Chapter 6), the detection of metal soaps, especially zinc carboxylates explain for the fragility and delamination of paint. For the Haku Maki prints (Chapter 4), the microfideometry experiments predicted the poor lightfastness of yellow (chrome yellow) and orange (chrome yellow mixed with molybdate orange) paints, that falls between BW2 and BW3, and poses a concern for exhibition lighting. In the Numbers case-study (Chapter 5), the unstable epoxy based primers used in the new paint systems after conservation is predicted to lead to paint loss, whereas the improved topcoat formulation suggests that the gloss is likely to persist longer in outdoor conditions.

7.4 Future Studies

Although substantial results have been achieved in each case-study, the process of investigation also highlighted potential areas of research that can be explored in future studies. While the PNG case-study (Chapter 3) has identified an eclectic range of binding media, the chemical composition of raw materials (i.e. specific resins and plant saps) from the PNG Highlands has not been investigated. In the Haku Maki print (Chapter 4), the microfideometry study reveals that the darkening of chrome yellow when combined with molybdate orange is much accelerated, through which more research is required to determine the reason(s). In the Numbers case-study (Chapter 5), the reasons postulated for paint failure due to epoxy and nitrocellulose primers/ surfacers remains to be attested with time and mock-up studies will be beneficial in investigating paint failure on aluminum welded outdoor sculptures. In the Baumann case-study (Chapter 6), only one sample was analysed,

but it would take more analysis of other prints to obtain representative data of Baumann's home-made recipe and the presences of metal soaps.

Technical analysis forms the foundation of conservation science, where questions build on questions, leading onto other research areas in greater depth or scope. Museum conservation, with the mission to preserve and care for the collections, can greatly benefit from having a deeper understanding of the material composition and condition of paint, generated from technical analysis. However, the variety of sample matrices encountered in artworks remains an analytical challenge. A non-exhaustive list of materials that can be encountered in works of art, restricted sample size from valuable artefacts, as well as accessibility to aged and heterogeneous references, remain a universal challenge in technical analysis. Nevertheless, improvements in instrumental design and sensitivity and ongoing research on different genre artworks and painting styles can potentially narrow the knowledge gap in data interpretation.

APPENDIX

Validation of analytical procedure for multi-class binders characterisation in the same paint sample with GC/MS

A.1 INTRODUCTION

Organic binders in works of fine art often pose challenges in their characterisation. For example, more than one binder class can exist in one paint sample (e.g. resin, wax, lipids, proteins, gums); pigments and inorganic fillers can interfere with binder analysis; the chemical composition of binder changes with ageing in different environments; or the substrate to which the paint is applied (e.g. cellulose, silk) is chemically similar to the organic binder (gum, proteins) and can appear as contamination. From the analytical viewpoint, the most straightforward identification approach is to compare an unknown to a suitable reference sample. However, reference samples of the appropriate age, ingredients and % composition are not always readily available. Hence in binder analysis of an aged heterogeneous paint chip, the challenges often require separation of organic binder classes prior to identification.

Binder characterisation by means of FTIR spectroscopy is often the most straightforward, yet limited in its specificity to a member of an organic binder class (Derrick, Stulik & Landry 1999). While its use has been fairly successful in identifying synthetic binders such as acrylic, polyurethane and alkyd, its application to traditional binders such as proteins, drying oils, gums and resins has proved less straightforward. This is partly because traditional binders are largely obtained from natural sources (plants and animals) where the chemical compositions are highly complex, species-dependent and vary with ageing. The confidence in “fingerprinting” the FTIR spectrum of an unknown to a reference often presents problems. Firstly, organic binders tend to have weaker and broader band features than pigments, putting them at a lower advantage in being detected. For instance, interference from clay, chalk, barium sulphate and synthetic organic pigments easily masks off the peaks from the binder, especially when analysing highly underbound paints. Though HF has been successfully used to remove interferences from chalk and

clay, this is not successful with barytes and gypsum (Smith, Newton & Altherr 2015). Secondly, binders within the same chemical class are not easily differentiated based on FTIR alone. For example, animal glues such as hide glue, bone glue and rabbit skin glue have very similar FTIR spectra and the differentiating peaks are weak or may not be evident. Thirdly, the tendency for binders to degrade, rearrange and form new bonds with ageing can complicate the FTIR interpretation, such as the formation of metal soaps in drying oils (Robinet & Corbeil 2003). In other instances, the ambiguity stems from a lack of suitable reference, especially when the binder is not well-known in the conservation science field.

Secondary ionisation mass spectrometry (SIMS) has been applied to binder characterisation of micro-paint samples (Dowsett & Adriaens 2004; Spoto 2000). The main advantage is its ability to obtain organic material information at submicron level within a layer or particle in a paint cross-section. Coupled with imaging ability, the distribution of the organic material of interest can be visualised in the cross-section. Despite this advantage, the number of papers published is relatively limited for two primary reasons: (1) the extremely high cost of the requisite instrumentation limits its accessibility to only a few research laboratories, and (2) the mass spectra generated from SIMS are generally complex. Due to a different fragmentation/ionisation process employed, the interpretation of data is different from other mass spectrometric techniques (Colombini & Modugno 2009). As such, information obtained from SIMS tends to stay limited to the organic binder class (Edwards & Vandenabeele 2012) and may still require GC/MS to complement its results. It is a relatively new technique that is still in the exploratory stage in the conservation science field (Voras et al. 2016).

Py-GC/MS is favored for its minimal sample size (about 0.1- 0.5 mm in diameter or 10 µg) with no need for time-consuming sample pretreatment. The operation involves flash heating the sample in a pyrolyser at high temperature of 550-600°C, often with the aid of a derivatising agent. Because of the harsh fragmentation, the pyrogram is often complex and difficult to interpret. Secondary pyrolysates formed produce peaks that may be unidentified, and it can be difficult to correlate the pyrolysed organic fragments to the original structure in the sample. Synthetic organic pigments, if present, can also interfere with the binder analysis. While Py-GC/MS is more applicable to analysis of synthetic

polymeric binders, it is generally problematic when characterising traditional binders, as previously described in Chapter 1.

However, GC/MS analysis is widely applied in binder characterisation in the heritage field. GC/MS instrumentation is commonly available in university labs and the instrumentation cost is reasonable to be incorporated in museum science labs. Although variable cost for chemical consumables can be high and is sample-dependent, it is generally easier to justify than fixed costs. Presently, GC/MS combined with a suitable sample pretreatment is the only standard analytical method that can positively identify gums in a sample containing mixed binder/ pigment classes. The main drawbacks of the GC/MS technique are (1) the time-consuming process involved when treating the paint sample to obtain a suitable matrix for GC/MS analysis, (2) laborious accumulation of data sets for multivariate analyses, (3) a relatively larger sample size of 0.5-1 mg is needed, implying more precious samples will be sacrificed and (4) unsuitable for compounds that are too large in molecular weight with polymeric fractions. In this respect, sandarac, amber and other synthetic polymers will give better results with Py-GC/MS.

GC/MS methods have a long history in paint binder analyses, but most procedural methods have been designed to analyse for one organic class from one microsample. Practically, art samples presented to the analyst are often unknown. The samples may contain other binder classes, pigments or degradation products, which can alter the binder's GC profile. Hence testing for only one organic class does not give enough data for a holistic interpretation. One can opt to repeat the test for another organic class, but this would mean sacrificing double the sample size needed. As such, having a method that can simultaneously identify more than one binder class in the same microsample is considered a very valuable technique in the heritage field.

Amongst such research, the most comprehensive method was developed from Colombini and co-workers in Pisa. The group published several papers building up on past procedures that characterise more than one binder class in the same microsample (Andreotti et al. 2006; Bonaduce, Cito & Colombini 2009; Colombini et al. 1999). The protocol illustrated by Lluveras et al. is probably the most recently elaborated, designed to characterise natural wax, terpenoid resin, glycerolipids, proteins and polysaccharides

in the same microsample (Lliveras et al. 2010). The sample size required for this analysis is 0.2-1.2mg, which is comparable to the amount usually needed for a single class analysis. This procedure includes multiple treatments to extract the organic classes into individual aliquots, each of which undergoes hydrolysis, clean-up and derivatisation, before injection into GC-MS. The group has also built up relevant databases of naturally aged, artificially aged, unaged binders and binder-pigment mixtures that assist in data interpretation (Lliveras-Tenorio et al. 2012a, 2012b).

As the amount of published literature on this method has been tested and proven suitable for heritage art samples, it was chosen for application to the case-study on Baumann paints in Chapter 6. The validation process is divided into three phases: (1) validate data obtained from binder references (e.g. gum Arabic, gum tragacanth, cherry gum, egg yolk, linseed oil) to pure standards (e.g. monosaccharide and uronic acids, amino acids and fatty acid methyl esters) (2) validate the procedural method to mockup pigment/ binder mixtures, and (3) apply the method to real samples obtained from Gustave Baumann's paint studio with comparison of the GC/MS data against FTIR and Py-GC/MS data previously tested on these samples.

A.2 MATERIALS AND METHOD

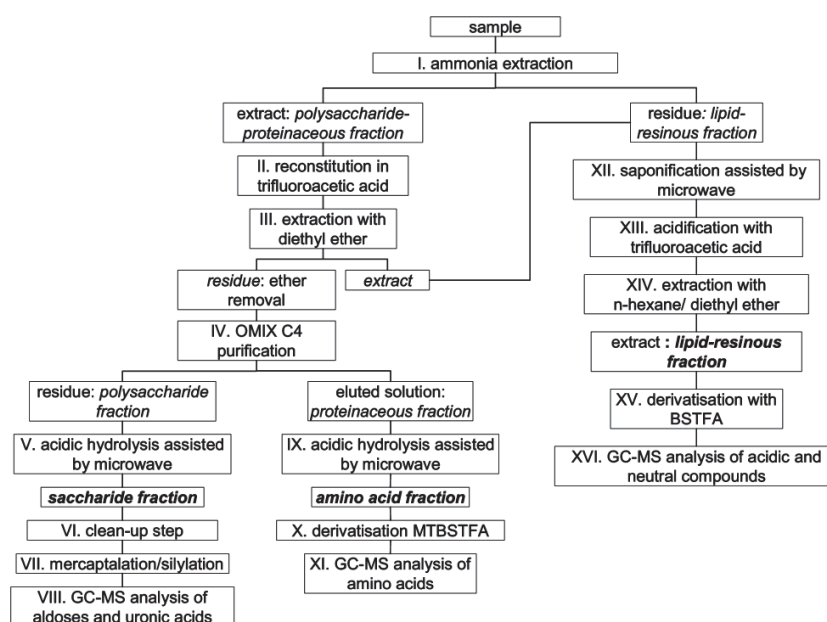


Fig. A.1 Summary of GC/MS combined analytical procedure (Lliveras et al. 2010).

The wet chemistry procedure follows closely to the method developed by Lluveras et al (Fig. A.1), with the differences outlined below.

A.2.1 REAGENTS

1. BSTFA (10% TMCS) was used instead of BSTFA (1% TMCS) due to availability, where BSTFA is N,O-Bis(trimethylsilyl)trifluoroacetamide and TMCS is trimethylchlorosilane

A.2.2 METHOD

1. The microwave oven (Discover, Model No: 510500, CEM Corporation, US) was used for the hydrolysis of proteins only. For saponification of lipids, conventional heating at 60°C for 2 h was carried out following an earlier procedure (Colombini et al. 2002). For carbohydrate hydrolysis, conventional heating at 125°C for 1 h was carried out, adapting from the procedure at the GCI (Lluveras-Tenorio et al. 2012a).
2. Solutions requiring drying in the intermediate steps were carried out under a stream of N₂, instead of using a rotary evaporator, which was not available at the IMA. This is a slow process especially when water is the solvent. As a general rule of thumb, it takes 2-2.5 h to evaporate dry 0.5 mL of aqueous solution using the nitrogen stream, though ammonia solution takes slightly lesser time.
3. The prescribed double exchange resins by the trade name of Zerolit are no longer available from BDH Chemicals. Therefore, the clean-up step uses Amberlite MB20, purchased from Sigma Aldrich, US, which does not have a color indicator like the Zerolit resins.
4. In the protein derivatisation step, hexadecane is not added into the amino acid hydrolysate. Hexadecane has a poor solubility in pyridine and the likelihood of it being detected by MS is low to none. This means that hexadecane in this pyridine solvent system fails to serve its purpose as a volumetric internal standard.
5. A GC trace ultra (Thermo Scientific) is coupled to an ISQ single quadrupole mass spectrometer operated in EI positive ion mode (70 eV). Chromatograms were obtained as total ion chromatogram (TIC) mode in full scan. A GC non-polar column TG-5-MS (5% diphenyl- 95% dimethylpolysiloxane) 30 m x 0.25 mm x 0.25

μm film thickness was used to effect the separation. He carrier gas (purity 99.995%) through the GC is kept in constant flow mode at the specified flow rate. A gas saver option is included to lower the split flow to 20 mL/min after sample injection. Sample is injected with a Triplus autosampler through a split liner into the column. High purity acetone is used for 3x pre and 10x post washes of the autosampler syringe needle. The parameters for analysing the different fractions are as follows:

- Lipid/resin fraction: Method: Inlet T: 300°C, Mass transfer T: 270°C, Ion source T: 220°C, Oven ramp: 90°C hold 5 min, 10°C /min to 200°C, hold 3 min, 10°C /min to 300°C, hold 30 min. Solvent delay: 7 min, 0.3 scan/s, scan 40-700, split 25:1, He Flow 1.2 mL/min, injection vol: 2 μL
- Amino acid fraction: Method: Inlet T: 220°C, Mass transfer T: 250°C, Ion source T: 200°C, Oven ramp: 100°C hold 5 min, 4°C /min to 280°C. Solvent delay: 7 min, 0.3scan/s, scan 40-700, split 25, Flow 1.2 mL/min, injection vol: 2 μL
- Monosaccharide fraction: Method: Inlet T: 250°C, Mass transfer T: 250°C, Ion source T: 200°C, Oven ramp: 50°C hold 5 min, 10°C /min to 190°C, hold 10 min, 5°C /min to 280°C, hold 15 min. Solvent delay: 15 min, 0.3scan/s, scan 40-700, split 25, Flow 1.0 mL/min, injection vol: 2 μL

A.2.3 SAMPLES

1. Pure standards: monosaccharides and fatty acids were self-prepared at a concentration of 100 ppm (0.1 mg/g) in water and isooctane respectively. The amino acid standard was purchased from Sigma Aldrich, occurring as 1 mL ampules of 0.1 M HCl. The derivatisation internal standard for amino acids was norleucine, for lipids was tridecanoic acid and for gums was mannitol.
2. Raw materials: gum arabic, gum tragacanth and cherry gum were purchased from Kremer, with the gum sample wrapped in cheese cloth and immersed in water overnight to dissolve. The gum solution was applied to glass microscopic slides previously cleaned with acetone, then left in an oven to dry at 60°C for 20 min. Egg was obtained from a general supermarket and separated into yolk and egg white, with the membrane removed. Casein, hide glue and bone glue were purchased from Kremer Inc., immersed in water and left in a 60°C water bath for a

few minutes, then left to stand overnight. Linseed oil was obtained from Winsor and Newton and Manilla copal resin was obtained from Kremer Inc.

3. Mock-ups: Combinations of different gum, egg, protein, oil and resin binders were prepared using a glass muller on frosted glass support, then applied to glass microscope slides and left to dry naturally for about 1-2 months before analysis. The combination mock-ups prepared are: (1) linseed oil/ egg yolk, (2) gum arabic*/ egg yolk. Pigments were also added to simulate heavily pigmented paints¹: (3) gum tragacanth, gum arabic*, zinc white and BaSO₄. Inorganic pigments/ fillers were also mixed with water only to simulate paints without a purposefully added binder as a control sample²: (4) Kaolin: mars yellow and some water.

* The gum arabic used for reference mock-ups was prepared according to an artist's recipe (Mayer 1950). 28.35 g of gum arabic was mixed with 56.7 g deionised water, 9.35 g pure glycerin, 10.6 g glucose sugar syrup, 2-5 g oxgall liquid (Winsor and Newton).

4. Paint samples: Pigment powders and semi-liquid varnishes were collected from Gustave Baumann's painting studio (1881-1971). These were previously analysed with FTIR microscopy and Py-GC/MS, which showed the presence of gums, drying oils, resins and wax. Selected samples of 5 pigments and 3 varnishes were subjected to this GC/MS technique. 0.5 – 1 mg of each sample was analysed.

A.3 RESULTS: METHOD VALIDATION

A.3.1 PHASE 1: VALIDATION WITH PURE STANDARDS AND RAW MATERIALS

Testing pure standards is important to determine the retention times of various marker compounds and to ensure the effectiveness of the derivatisation step. Table A.1 shows the organic classes present in common art binders selected as raw materials in this study.

¹ This paint mixture is carried out to mimic that of "Estes Park, Colorado" Case-study, where zinc, barium cations and sulphate anions are present. Gum was chosen as the binding medium because these cations and anions are known to influence the gum profile obtained by GC.

² This paint mixture is carried out to mimic that of "PNG Highlands paints" Case-study. The Highlanders were reported to mix paints using only water or plant saps, with iron-based ochres and clay from their natural environment.

Table A.1 Binder class in raw materials

Binder References	Gum	Protein	Lipid/resin
Gum Arabic	X		
Gum Tragacanth	X		
Cherry gum	X		
Egg yolk		X	X
Hide glue		X	
Bone glue		X	
Casein		X	
Linseed oil			X
Manilla copal			X

A.3.1.1 MONOSACCHARIDE FRACTION

MONOSACCHARIDE DERIVATISATION AND DATA INTERPRETATION

Monosaccharides are derivatised based on a three step procedure (1) mercaptalation of the anomeric carbon with EtSH:TFA of ethanethiol: trifluoroacetic acid (2:1), (2) quenching the reaction using BSTFA to remove excess EtSH and TFA, and (3) derivatisation of mercaptalated monosaccharides with BSTFA (10% trimethylchlorosilane or TMCS) in pyridine. A typical reaction pathway in this derivatisation process is illustrated in Fig. A.2. By mercaptalating the anomeric carbon, the skeletal chain is prevented from returning into its cyclic conformation so one analyte produces one peak, simplifying the data interpretation. This method was also employed using HMDS or hexamethyldisilazane as derivatising agent (Dhakal & Armitage 2013; Pitthard & Finch), but BSTFA was chosen over HMDS for its higher yield. MTBSTFA or N-Methyl-N-tert-butyltrimethylsilyltrifluoroacetamide is not suitable for sugar derivatisation due to sterically hindered sites (Schummer et al. 2009). When using BSTFA, the solvent pyridine has to be used to ensure completeness of the silylation. As TFA and pyridine can react to form a white solid (pyridine trifluoroacetate), the quenching step with BSTFA is necessary

to remove excess TFA prior to adding pyridine and derivatising agent. This ensures a high yield of derivatised monosaccharides. Practically, the white solid can clog the glass syringe used to transfer these reagents, hence a separate glass syringe for transferring TFA and pyridine is recommended.

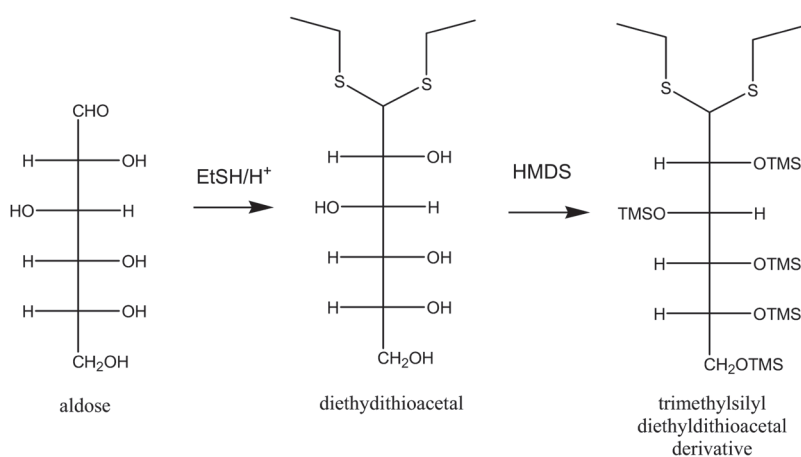


Fig. A.2 Schematic pathway of mercaptalation and derivatisation of carbohydrates (Dhakal & Armitage 2013).

Both the Thermo Scientific and NIST mass spectral libraries do not contain mass spectra of trimethylsilyl diethyldithioacetal derivatives of carbohydrates, hence an automated peak search was not able to identify the peaks of interest in these experiments. As such, it is useful to know the derivatised chemical structure and identify the peak based on the mass fragmentation pattern for each analyte. However, this is not straightforward as mass spectra of aldose and uronic acid peaks are quasi-similar. Vaclav resolved this by matching relative intensities of the mass fragments to identify the monosaccharide peak (Pitthard & Finch). However, the results obtained in this study do not work well with this method; the % mass fragments do not correlate well with literature due to a different derivatising agent used. Furthermore, the relative % of mass fragments remains similar and could not distinguish two closely eluted peaks, such as xylose and arabinose. Hence, different solutions, each containing a trio of known monosaccharides, were analysed to obtain characteristic retention times of each analyte. This allows for the unambiguous assignment of the retention times for all monosaccharides of interest.

MONOSACCHARIDE PURE STANDARD

As shown in Fig. A.3, each monosaccharide can be detected based on one peak. Retention times may change due to a difference in sample concentration. Peak identification by matching the retention times should also be supported by the mass fragmentation pattern of the analyte. If the S/N ratio is too low such that the mass spectrum does not match to an analyte, the peak is considered below the detection limit.

GUM REFERENCES

As shown in Fig. A.4, gum arabic, gum tragacanth and cherry gum produce three different characteristic GC profiles. The % monosaccharide composition is mostly comparable with literature values of unpigmented unaged gums (Table A.2). Differentiating unaged unpigmented gum references may appear straightforward in this case, but in most cases, sugar profiles of pigmented gum samples do not correspond quantitatively to those obtained from reference materials and careful interpretation is needed (Lliveras-Tenorio et al. 2012a).

GUM: UNKNOWN PEAKS

Some unidentified peaks that do not correspond to known aldoses and uronic acids appeared in the TIC of gum samples at $R_t = 23.46, 33.87$ and 37.91 min. These peaks were not observed in a blank control and hence they are not due to procedural contamination. They were not seen in pure standards, indicating that it is unlikely due to the derivatisation process. The reason could, however, be related to the amount of gum samples (i.e. When the gum concentration is high, these peaks appear negligible. If the gum concentration is too low, these peaks appear to dominate the chromatogram). Due to the variable uncertainty that can happen in this long procedure, it is difficult to pinpoint the cause(s) for these unknown peaks. However, it is possible to reduce the intensities of these unknown peaks by extracting ions at $m/z = 248, 304, 319, 407$. Fig. A.5 shows the effects in reducing spurious peaks after applying this filtering method.

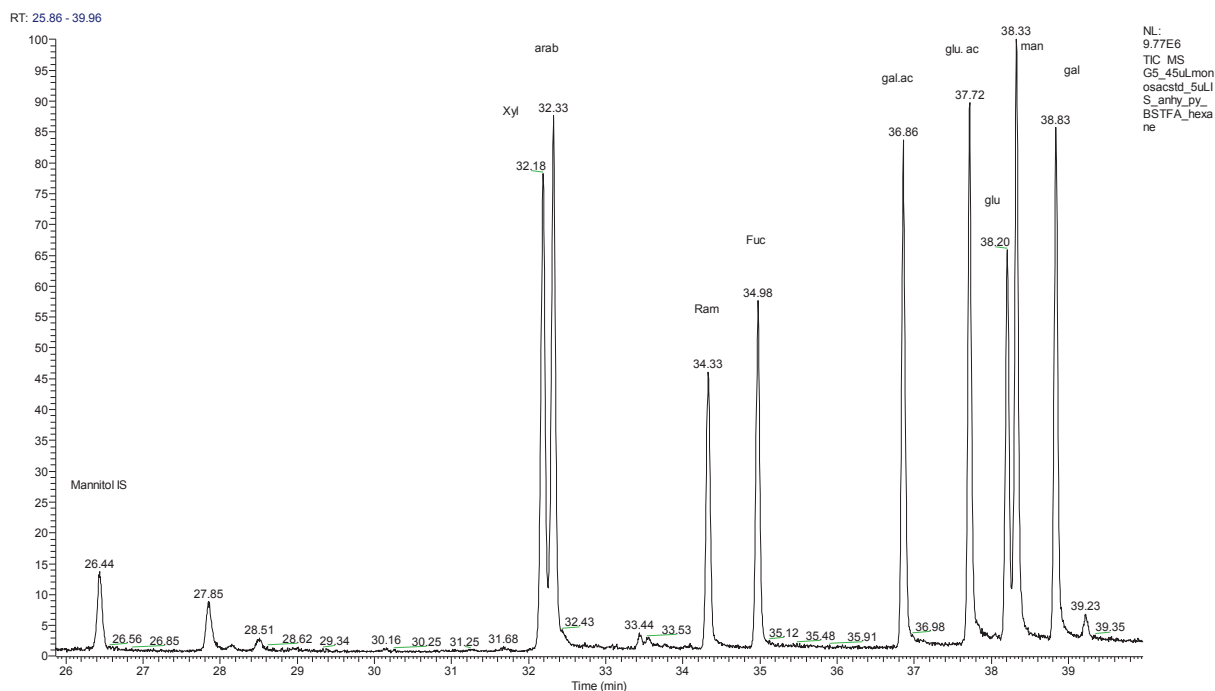


Fig. A.3 TIC of IS (mannitol), aldoses and uronic acids in a monosaccharide standard solution, whereby one peak represents one monosaccharide. Unidentified peak at Rt = 27.85 min also occurs in blanks.

Abbreviation: xyl – xylose, arab – arabinose, ram – ramnose, fuc – fucose, gal.ac – galacturonic acid, glu.ac – glucuronic acid, glu – glucose, man – mannose, galac – galactose

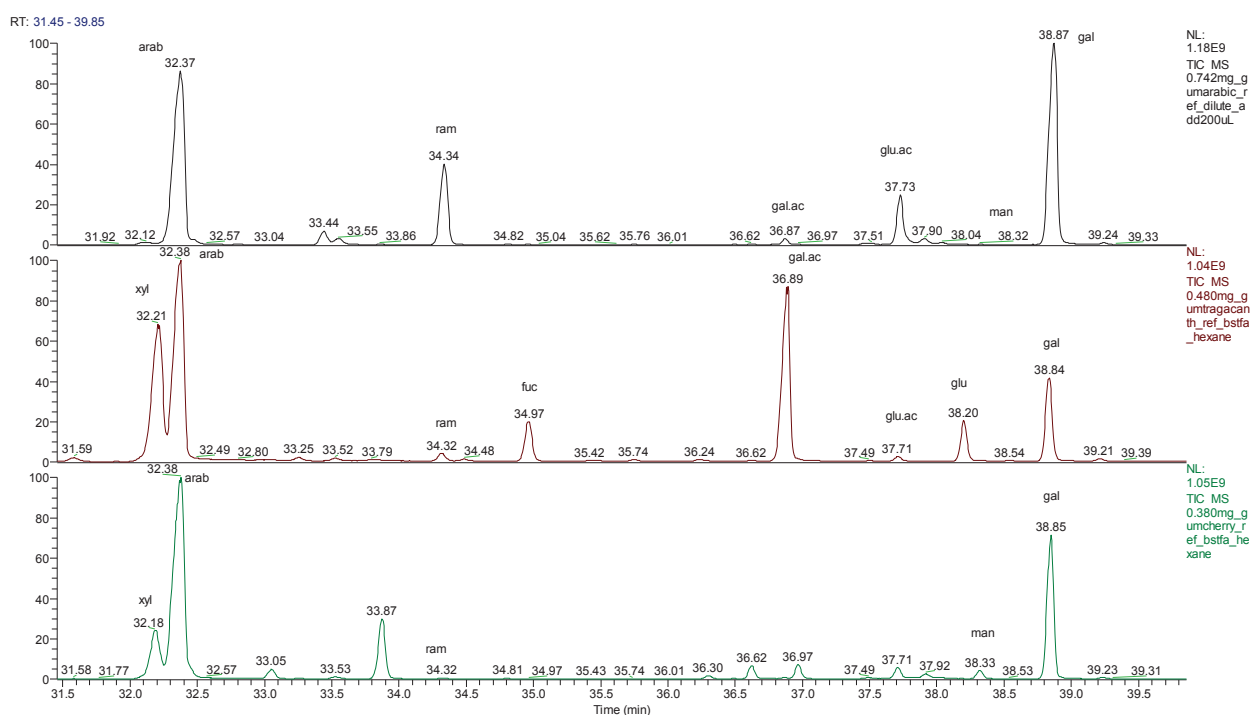


Fig. A.4 TIC of gum arabic (top), gum tragacanth (middle) and cherry gum (bottom).

Table A.2 Percentage (%) monosaccharides composition in gum references

	xyf	arab	ram	fuc	gal.ac	glu.ac	glu	man	galac	Source
Gum arabic	0	42	14	0	0	7	0	0	37	IMA
	0	28±4	14±2	0	0	12±3	0	0	45±5	DCCI
	0	37±3	18±3	0	-	-	0	0	44±5	GCI
Gum tragacanth	23	34	1	5	23	0.5	4	0	10	IMA
	22±5	34±6	2±1	8±2	8±9	1±1	12±6	0	12±2	DCCI
	24±3	45±5	1±0	11±3	-	-	8±3	0	9±2	GCI
Cherry gum	11	58	0.2	0	0	2	0	2	26	IMA
	6±3	46±10	1±1	0	0	7±7	0	3±2	34±14	DCCI
	11±1	50±6	2±1	0	-	-	0	2±2	34±6	GCI

Abbreviation:

IMA: Indianapolis Museum of Art (results obtained in current study)

GCI: Getty Conservation Institute in Los Angeles, USA (Llueras-Tenorio et al. 2012b)

DCCI: Department of Chemistry and Industrial Chemistry of the University of Pisa, Italy (Llueras-Tenorio et al. 2012b)

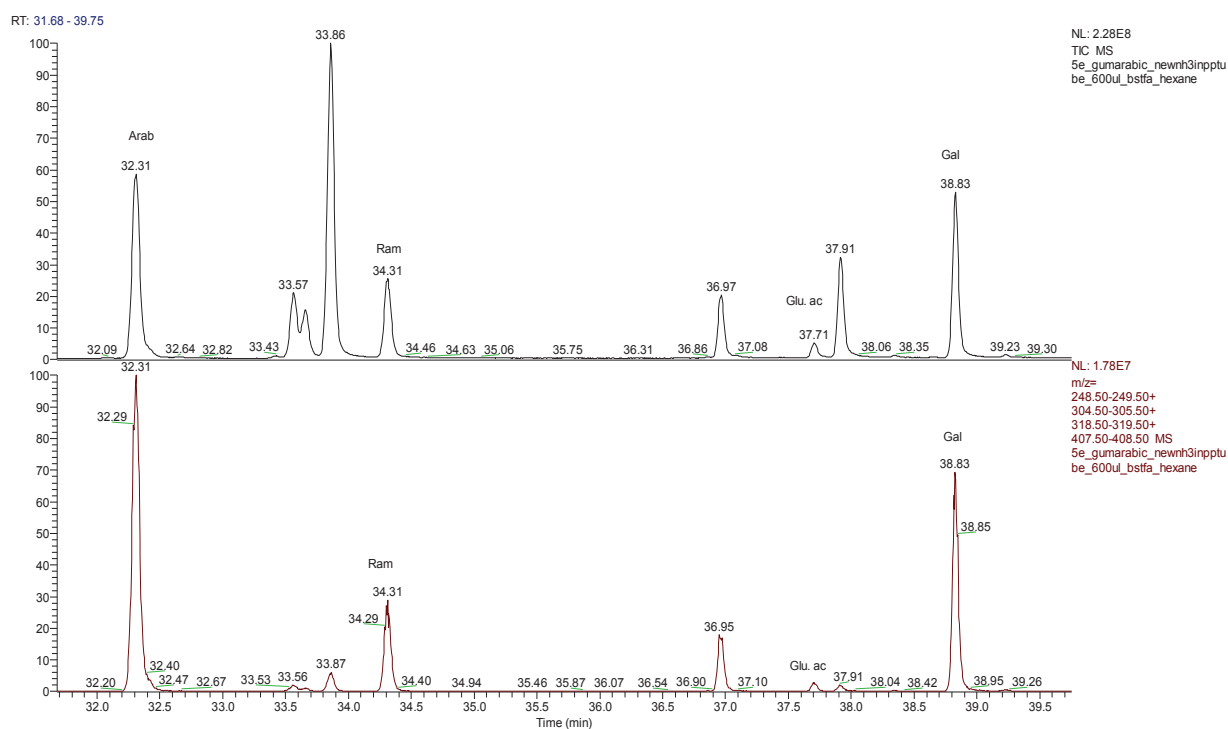


Fig. A.5 TIC of gum arabic (top trace) compared to the same sample with an extracted ion profile at 248, 304, 319 and 407 (bottom trace).

A.3.1.2 AMINO ACID FRACTION

AMINO ACID DERIVATISATION AND DATA INTERPRETATION

Amino acids are derivatised with MTBSTFA in pyridine at 60°C for 30 min, with TEA added as catalyst. When MTBSTFA is used, a small amount of tris(trimethylsilane)borate ($m/z=73, 221, 263$) at 9.71 min is evident in the TIC and this probably results from silylation of borosilicate glass. In blanks and samples with low concentrations of amino acids, a peak at 11.35 min representing *t*-butyl-[2-(*t*-butyldimethylsilyl)oxyethoxy]dimethylsilane ($m/z=73, 147, 173$) is intense, suggesting that MTBSTFA is in excess, and the level of derivatisation is low to none. This compound is likely a by-product from unreacted MTBSTFA and TEA. In pure standards where significant amounts of amino acids are present, the peak at 11.35 min decreases significantly, and additionally, a peak at 7.34 min representing silanamine ($m/z=73, 130, 146, 188$) shows up in the chromatogram. Silanamine is probably a by-product from reacted MTBSTFA, indicating a high level of derivatisation. Using these compounds as markers (Fig. A.6), the level of derivatisation and amount of amino acids in the aliquot can be gauged.

AMINO ACID PURE STANDARD

All amino acids in the standard, with the exception of arginine, appear in the chromatogram with high intensity (signal intensity $\approx E8$) and can be confidently assigned using the library database (Fig.6.6). The total ion counts for the peak representing arginine at $R_t = 38.27$ min ($m/z = 340, 442$) is relatively much lower ($\approx E6$), which means it is easy to miss the detection of arginine even though present. To clarify that the low yield of arginine is not due to a low arginine concentration in the ampule, 100 ppm of arginine solution was prepared separately and analysed. The intensity of the resulting peak at 38.27 min remains low again at $E6$, which suggests that the derivatisation of arginine is poorer compared to other amino acids. Different reasons have been postulated for the poor derivatisation response of arginine. Studies reported that derivatisation of arginine needs a high temperature of at least 95°C (Biermann et al. 1986; Blackburn 1989) and the

arginine molecule after derivatisation is considered thermally unstable because of the presence of the guanidine group in the side chain (Hyotylainen & Wiedmer 2013).

PROTEIN: MICROWAVE HYDROLYSIS

Traditionally, protein hydrolysis has been performed using anoxic heating for 24 h at 110°C with 6 M HCl. This method is time-consuming, which is a critical disadvantage considering that the experimental procedure described here is already very long. Furthermore, it requires a day's use of the heater block and nitrogen stream, which means analysis of other fractions cannot be performed during this time period. A second disadvantage for this method is that the reaction proceeds in a liquid phase, leading to a higher risk of contamination from organic residues or stable amino acids that might be contained in impure HCl, thereby lowering the yield and purity. Residual oxygen in the reaction headspace can also lower the hydrolytic yield. These are good reasons why many protein analysts turn to the use of vapor-phase microwave-assisted hydrolysis, which not only shortens the time of reaction dramatically but also generates a higher yield under inert and anaerobic conditions (Chen et al. 1987; Gilman & Woodward 2012). Amino acids, polypeptides and proteins, being polar and charged, respond well to the oscillating electric and magnetic fields of microwave radiation. This electromagnetic energy is conceived to increase the rotational force on the amino acid moieties, thereby reducing the energy required to break the peptide bonds and decreasing the time needed to propagate the hydrolytic process (Margolis, Jassie & Kingston 1991).

The "CEM Discover" microwave hydrolysis hardware available at the IMA is designed with three different operating modes, namely (1) Standard Control: The power maintains a constant temperature and pressure over a time period, but the power decreases during the hydrolysis, (2) Power-Time control: The system ramps up to the desired power and once the temperature is reached, the system stops and starts cooling, and (3) SPS (Solid phase peptide synthesis) Control: The power cycles on and off to keep the temperature and pressure constant over a time period. The Power-time control is not practically useful as the programme stops as soon as the temperature is reached, rendering insufficient time for reaction and is not considered. Both Standard and SPS control modes could be used, but the SPS control is preferred for a higher yield and therefore used for all subsequent analyses.

The microwave settings applied were taken from the adapted protocol at 250 W, 160°C, 40 min, 6 M HCl (Lliveras et al. 2010), from microwave hydrolysis optimisation studies of rabbit skin glue at 240 W, 90 min, 10 M HCl (Jurado-López & Luque de Castro 2005), and from recommended parameters by CEM manufacturer at 150 W, 150°C, 15 min, 6 M HCl. Lopex et al. concluded that power and time are the most influential parameters in affecting yield. A higher power gives a positive effect up to 270 W, beyond which it starts to give a negative and non-significant effect whereas the irradiation time always has a positive effect and is most significant in phenylalanine and glycine yields (Jurado-López & Luque de Castro 2005). So far, protein samples subjected to the parameters of 240 W, 160°C, 40 min and 6 M HCl in this system gave an adequate yield and were used for all subsequent analyses. However, it would be useful to fully optimise the parameters to ensure the highest yield possible.

PROTEIN REFERENCES

As shown in Fig. A.7 and Table A.3, animal glues (bone glue and hide glue) can be easily differentiated from casein by relying on certain amino acid markers. In this example, leucine, valine and glutamic acid are the major constituents identified in casein while hydroxyproline is the only unique amino acid that is characteristic of animal glues (Colombini & Modugno 2004; Gimeno-Adelantado et al. 2002). Between hide glue and bone glue, a qualitative distinction is more difficult, as they contain predominantly gelatin with frequently repeating glycine-proline-hydroxyproline sequence. Quantitative assay also present difficulties in differentiating animal glues due to the close similarities in the relative distribution of amino acids (Table 3), hence a principal component analysis with more data will provide a clearer distinction between bone glue and hide glue (not carried out in this study).

PROTEIN: UNKNOWN PEAK

Interestingly, a strong fronting peak appears at $R_t = 20$ min in the protein chromatograms. The mass fragmentation pattern ($m/z = 73$ (71%), 115 (12%), 347 (1%)) does not give a confident library match. This peak appears exceptionally strong in proteinaceous samples, blank controls starting from microwave hydrolysis step and self-prepared solutions of amino acids in 0.1 N

HCl, but its amount is low and negligible in blank controls starting from the derivatisation step and amino acid pure standards, which did not pass through microwave hydrolysis. This suggests that the cause of the peak stems from the microwave hydrolysis step.

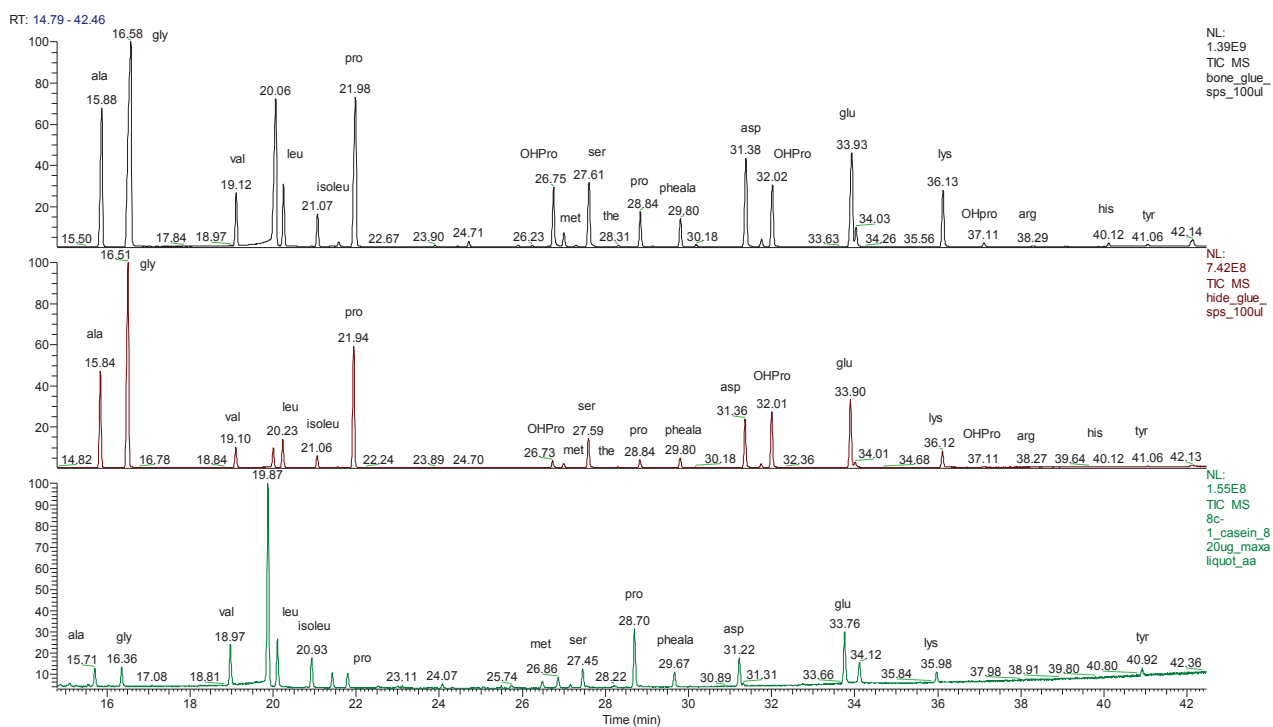


Fig. A.7 Comparison of amino acid fractions: TIC of bone glue, hide glue and casein.

A series of tests was conducted to test for the origin of this spurious peak. It was found that the peak appears strongly in blank controls with HCl liquid condensation than those without. To clarify if the peak is due to HCl, 50 μ L of 6 M HCl reagent (prepared from 37% HCl) was added to a blank vial and analysed. Indeed, the TIC shows one strong peak around 20 min (Fig. A.8) with the same mass fragmentation pattern. It should be highlighted that this peak does not come from impurities possibly present in the 37% HCl reagent, because conventional heating with high purity 6 M HCl (first opened from ampule) also shows this spurious peak. To ascertain that HCl is the main culprit, the same bone glue sample with high purity 6 M HCl was evaporated dry with a stream of nitrogen and rinsed with deionised water. This cycle of drying and rinsing was repeated 5 times, with a final rinsing using 100 μ L EtOH and drying, prior to derivatisation.

Indeed, the peak at Rt= 20 min remarkably reduces after repeated washing and drying, indicating that effects of HCl are reduced (Fig. A.8).

Table A.3: Percentage (%) amino acid composition of protein references.

	bone glue (%)	hide glue (%)	casein %)
ala	11.42	11.91	5.03
gly	25.90	30.72	4.55
val	3.71	2.59	10.56
leu	4.18	3.48	11.85
isoleu	2.18	1.58	7.85
pro	16.86	17.52	3.75
met	0.91	0.53	3.22
ser	5.25	3.90	4.91
the	0.15	0.10	0.00
pheala	2.14	1.33	4.11
asp	7.82	6.56	7.80
OHpro	5.38	7.78	0.00
glu	9.27	9.54	15.30
lys	4.41	2.20	2.88
arg	0.06	0.06	0.00
his	0.24	0.12	0.00
tyr	0.14	0.09	2.75

Abbreviations: ala – alanine, gly – glycine, val – valine, leu – leucine, isoleu – isoleucine, pro – proline, met – methionine, ser – serine, the – threonine, pheala – phenylalanine, asp – aspartic acid, OHpro – hydroxyproline, glu – glutamic acid, lys – lysine, arg – arginine, his – histidine, tyr – tyrosine

Evaporation dry with nitrogen stream does not totally eliminate the water content and associated water-soluble compounds such as HCl. The typical way of removing HCl using repeated cycles of drying and solvent rinsing is too laborious and not time-effective. Instead, by applying an extracted ion profile at m/z 147, the strong peak at 20 min can be reduced while preserving the amino acid peaks. Alternatively, drying the amino acid hydrolysate using a speed vacuum may be beneficial in removing the HCl interference.

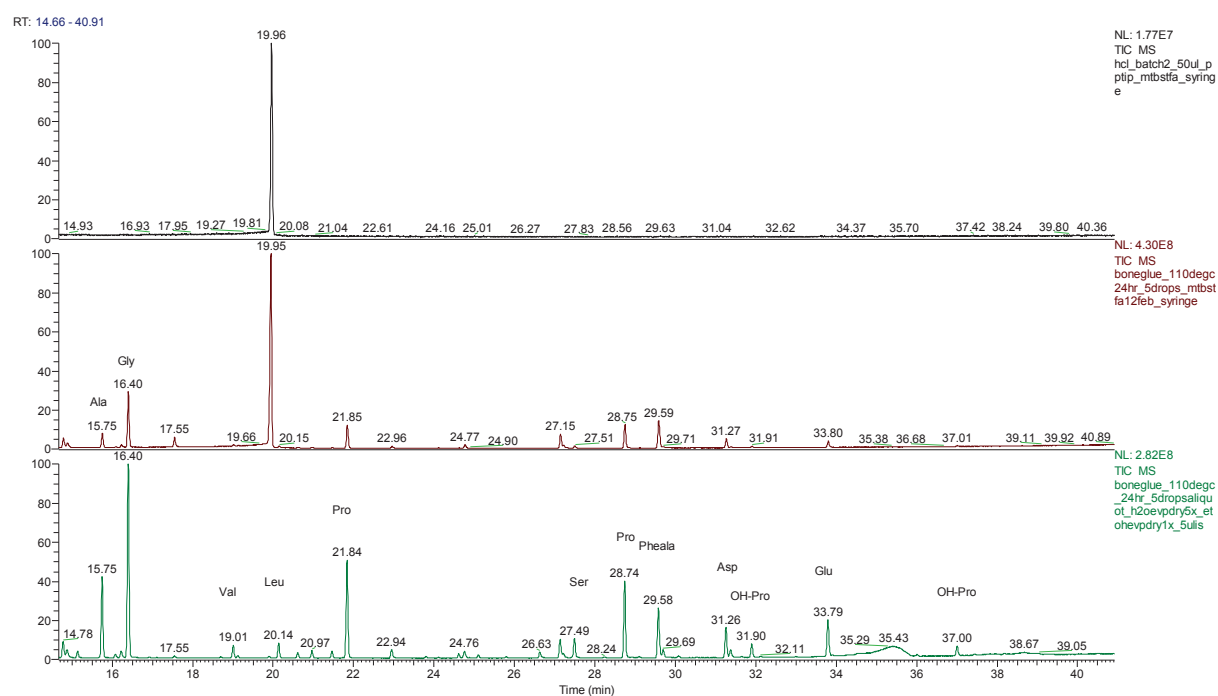


Fig A.8 (a) TIC of HCl, (b) TIC of bone glue with conventional heating in 6 M pure HCl, (c) TIC of an aliquot of the same bone glue hydrolysate in (b) after 5 cycles of rinsing with deionised water, EtOH and evaporation dry with N₂ stream.

A.3.1.3 FATTY ACID/ TERPENOID FRACTION

FATTY ACID PURE STANDARD

As seen in Fig. A.9, all fatty acids derivatised by BSTFA are well separated and assignment of peaks can be achieved with the available library.

LIPID/RESIN REFERENCE

Compared to gum and protein fractions, the fatty acid/terpenoid fractions tend to give higher yields. This is likely because the procedure for obtaining this fraction is the shortest and recovery is expected to be highest. As such the volume of aliquot taken for derivatisation can be lower, requiring only about 1/3 of the initial amount (100 μ L out of 300 μ L). In Fig. A.10, the TIC of the linseed oil/manila copal sample shows the distinction between fatty acids (lipids) and terpenoid (resin) peaks in the same neutral fraction. To ensure the elution of higher MW terpenoids, the temperature was held isothermally at 300°C for 30 min. Ramping up the temperature further may shorten the time needed, but is not possible in this case as the maximum allowable temperature of the column is 350°C.

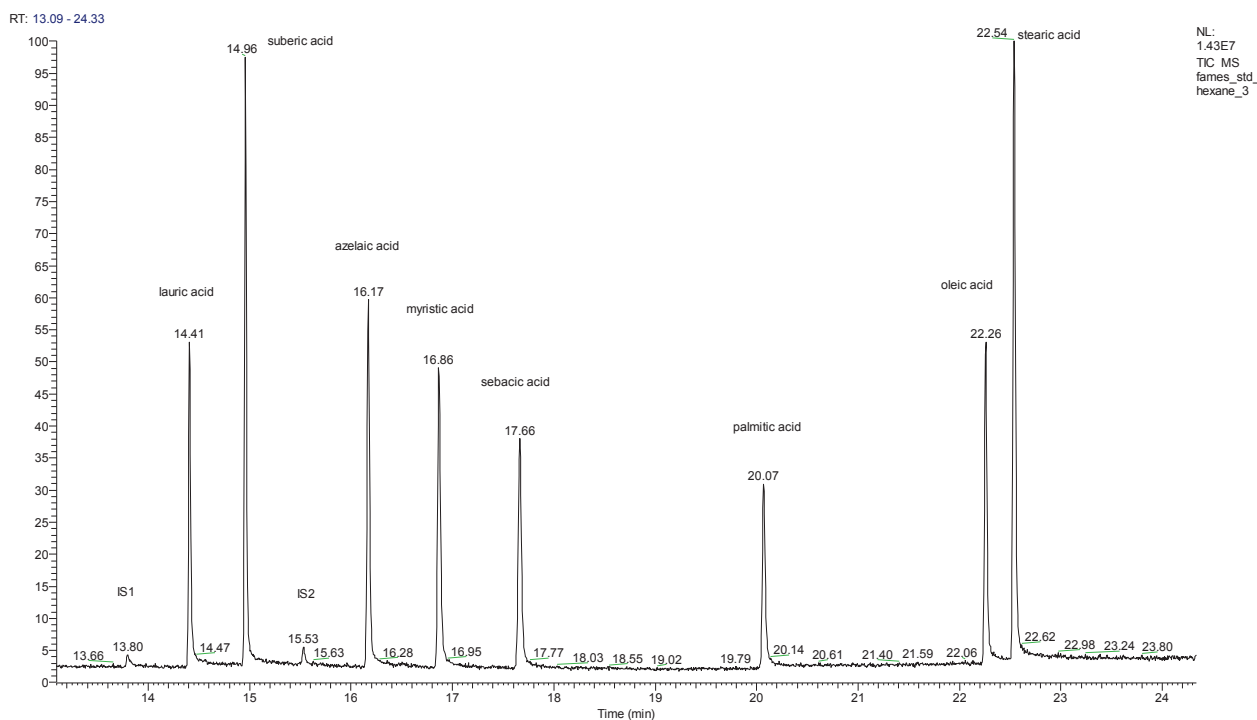


Fig. A.9 Fatty acid profile of pure standard.

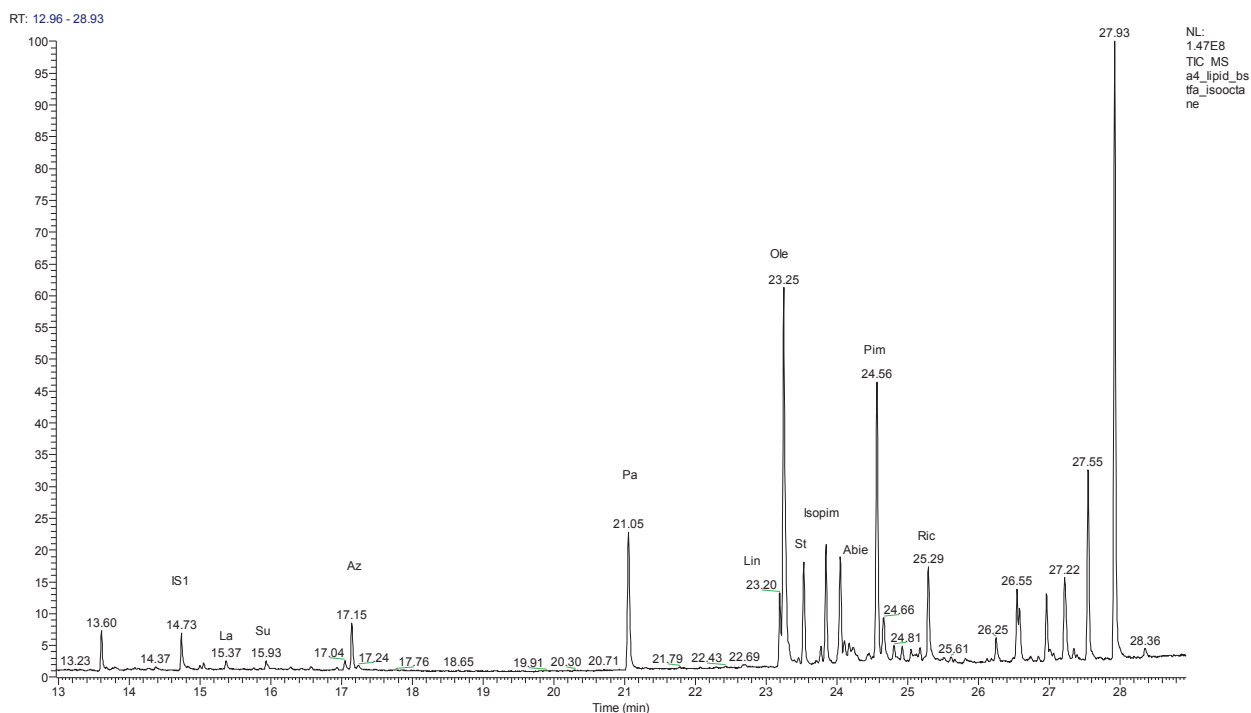


Fig. A.10 TIC of linseed oil/ manila copal fatty acid/terpenoid fraction.

A.3.2 PHASE 2: VALIDATION WITH MOCKUP PIGMENT/BINDER MIXTURES

A few sample mock-ups were tested to determine if the analytes can be positively identified in the individual fractions.

A.3.2.1 EGG YOLK

Although egg yolk itself is one material entity, it contains the three organic classes of compounds (lipid and amino acids, as well as small amounts of carbohydrate) that are of interest in this protocol, so egg yolk is considered as a mixture of different binder classes.

Fatty acid present? The presence of unsaturated fatty acids (oleic acid, linolenic acid and linolenic acid) and absence of dicarboxylic acid indicates that the lipid portion is still very fresh with a low degree of polymerisation. The presence of cholesterol is distinctive, indicating the presence of egg yolk. However, cholesterol can degrade overtime and may not be detectable in aged paints, therefore it is not a reliable marker for egg yolk.

Amino acid present? The results at present show lower amino acid yield from egg yolk than other protein samples like hide glue, bone glue and casein, despite the same procedure being employed. It is not uncommon to get a low recovery of amino acids in egg yolks, which was calculated to be 25% lower than other proteins observed (Schilling, Khanjian & Luiz 1996). This is partly due to the low proportion of protein in egg yolks at 16%, as most of the protein content resides in the egg white. Proteins can also undergo cross-linking with lipids in egg yolks overtime, thus exhibiting reduced solubility in aqueous basic or acidic media used in their extraction (Colombini & Modugno 2004).

Nevertheless, it is still possible to obtain the amino acid profile from egg yolks using GC/MS. A respectable amino acid yield can be obtained from egg yolk reference using the maximum sample aliquot and larger volume of injection at 2 μ L (Fig. A.11). However, the yield of amino acids in egg yolk references was found to be inconsistent. In another instance, the same egg yolk reference with a similar weight gave low intensity amino acid peaks, despite subjecting to the same experimental conditions (Fig. A.11). The decreased yield of amino acids is unlikely due to ageing or pigment interference since the egg yolk sample is young and no pigment is added. It is also unlikely to arise from incomplete derivatisation since the internal standard norleucine gives a peak of reasonable S/N ratio.

A likely cause for the inconsistent amino acid yield in egg yolk could be the uncontrolled temperature in the first ammonia extraction step, limited by the design of the ultrasonicator. Above 45°C, most proteins start to denature and unfold from their three-dimensional configurations, releasing single strands of polypeptide chains. This is desirable as the OMIX tips bind more efficiently to the short chain polypeptides. However, at the onset of about 65°C, the polypeptide strands can start to form new bonds that render a poorer solubility in water, giving a lower yield. It is possible that the temperature fluctuating between 45 and 75°C in the ultrasonicator limits the amount of proteins that can be extracted in egg yolks, thereby giving a yield that is lower than expected.

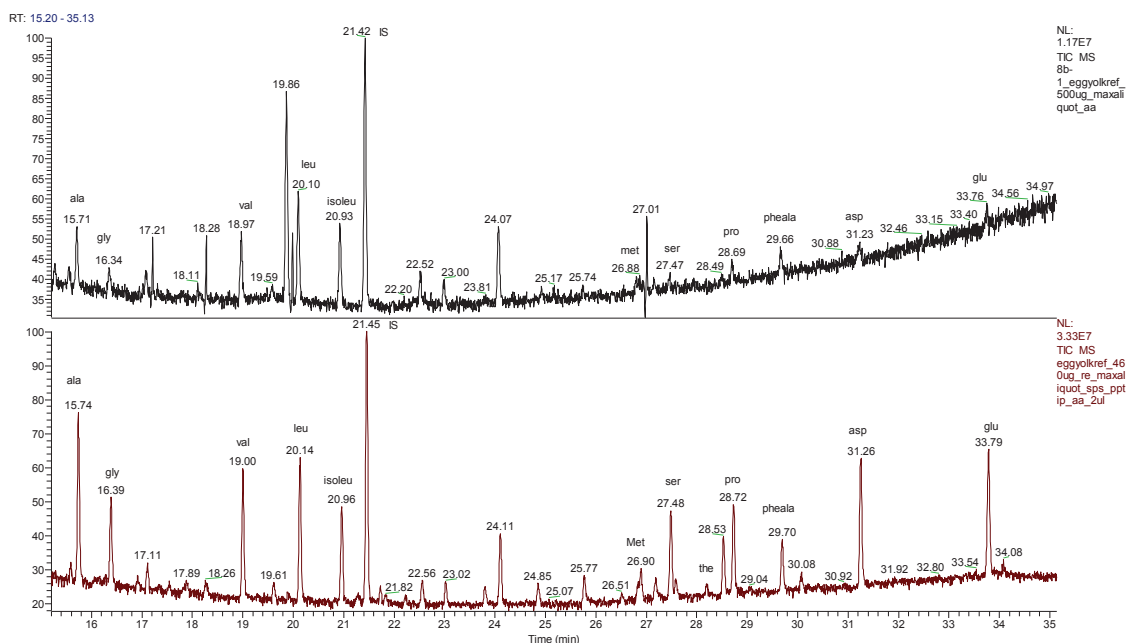


Fig. A.11 TIC of amino acid fractions from an unpigmented, unaged, dried egg yolk sample (top) 500µg and (bottom) 460µg, subjected to the same analytical procedure.

Gum present? The gum fraction of egg yolk shows a strong peak at $R_t = 32.27$ min that coincides with the retention time of xylose. However, the mass fragmentation pattern ($m/z = 73, 147, 191, 217, 305, 318, 432$) is different from xylose and remains unidentified. Two smaller peaks representing glucose and galactose are also observed. This is different from literature results, which indicate mannose as the saccharide content in egg (Lliveras-Tenorio et al. 2012b).

A.3.2.2 EGG YOLK/ LINSEED OIL (3P:1P)

Can fatty acid from egg yolk and linseed oil be differentiated? As seen in Fig. A.12, the lack of discriminating markers prevents the differentiation between egg yolk/ linseed oil mixture from purely egg yolk or linseed oil. This is because the paint tested is young, whereas aged paints with sufficient cross-linking can give a different GC profile that allows differentiation. As a guiding principle, A/P ratio < 0.3 indicates egg lipids (egg & non-drying oil) while an A/P ratio > 1 indicates drying oil. A value in between 0.3 and 1 indicates *tempera grassa* (egg & drying oil) (Colombini & Modugno 2009).

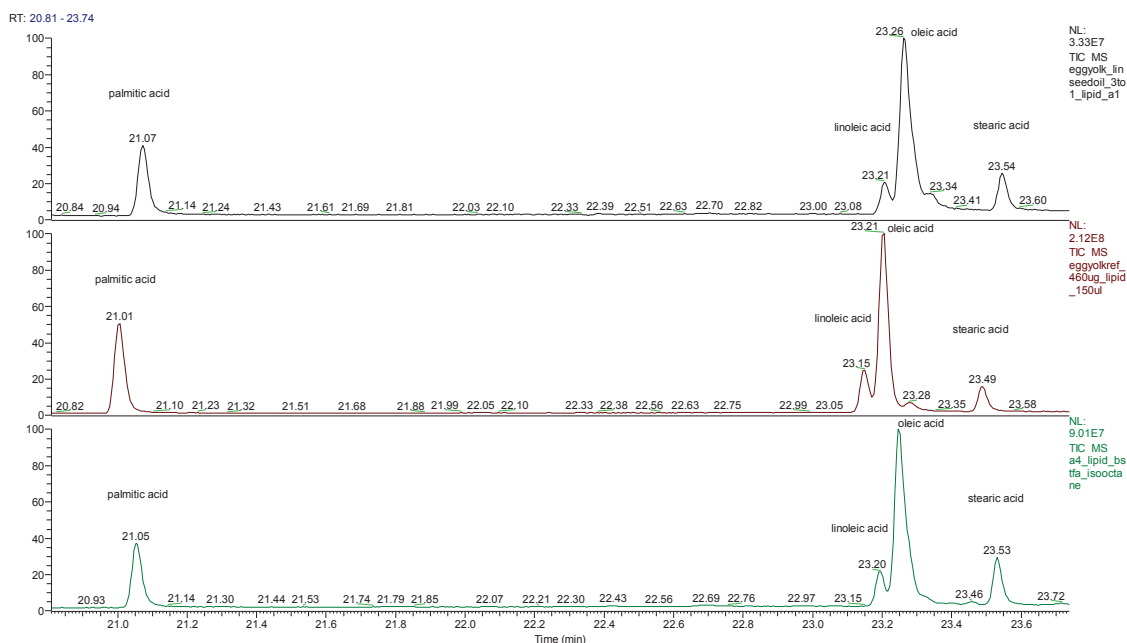


Fig. A.12 Fatty acid profile of (a) egg yolk:linseed oil (3:1), (b) egg yolk only and (c) linseed oil only. Samples are unpigmented and unaged. Retention times vary due to concentration difference.

Amino acid present in egg yolk? Very low yield of aspartic acid and glutamic acid was obtained in the egg yolk/linseed oil mixture. As highlighted above, the probability of detecting amino acids from egg yolks tends to be low. When the egg yolk is mixed with linseed oil as in this case, the concentration of detectable amino acids is even lower. This is because the additional fatty acid content from linseed oil reacts with amine functional groups on proteins, leading to increasing cross-linking, lower solubility and hence a lower amino acid yield.

A.3.2.3 GUM ARABIC:EGG YOLK (2P:1P)

Does egg yolk influence the gum profile? As shown in Fig. A.13, the gum fraction of a composite of gum arabic and egg yolk shows mainly the monosaccharides profile of gum arabic. Glucose from the egg yolk is also detected. The relative amount of galactose is lower, about half that of pure gum arabic reference (Table 4). This clearly shows that the saccharide content in egg yolk (about 1%) is not negligible and can contribute to the GC profile of gum when mixed in

a similar proportion. It also highlights the importance in testing for different organic binder classes in the same sample, especially when egg yolk is suspected.

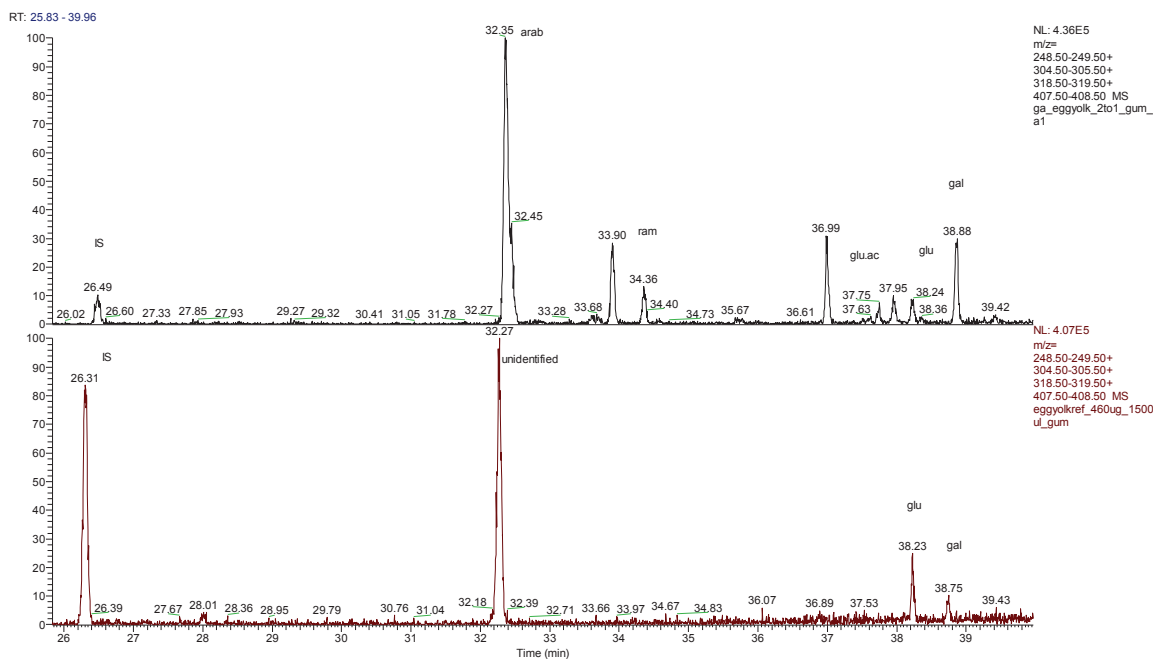


Fig. A.13: Extracted ion profile ($m/z = 249, 305, 319, 408$) of gum fraction in gum arabic/ egg yolk mix (top) and egg yolk reference (bottom).

A.3.2.4 GUM ARABIC: GUM TRAGACANTH (1P:1P), ZINC WHITE AND BaSO_4 :

Interference from Zn^{2+} and SO_4^{2-} ? The presence of derivatised monosaccharide peaks shows that the clean-up step is capable of removing the zinc and sulphate ions.

Can both gums be detected? Analysis of the GC profile could only indicate the presence of gum arabic, whereas the identification of gum tragacanth is ambiguous. The % monosaccharide composition of the gum arabic/gum tragacanth mixture agrees well with other gum arabic samples undertaken in this study (Table 4). Fucose is used as an indicator to differentiate gum tragacanth from gum arabic (Lliveras-Tenorio et al. 2012b), but the relative amount of 0.29% in the gum arabic/gum tragacanth mixture appears to be too low to be confidently assigned to gum tragacanth. According to the method at University of Pisa (DCCI), the recovery of unaged

gums is 65% for gum arabic, 23% for tragacanth gum and 62% for fruit tree gum (Lliveras-Tenorio et al. 2012b).

Table A.4 Percentage (%) aldose and uronic acid composition for single binders: gum arabic references and gum tragacanth reference, in comparison with mixed binders: gum arabic/ gum tragacanth and gum arabic/ egg yolk. Values in bold distinguishes a mixed binder from a single binder.

	<i>Single binder</i>				<i>Mixed binder</i>	
	Gum arabic (GA) (%)			Gum tragacanth (%)	Gum arabic / gum tragacanth (%)	Gum arabic/ egg yolk (%)
	GA1	GA2	GA3			
<i>xyl</i>	0.00	0.00	0.00	23.39	0.00	0.00
<i>arab</i>	41.92	51.53	47.30	33.62	44.05	50.46
<i>ram</i>	13.80	12.40	17.74	1.01	13.20	11.67
<i>fuc</i>	0.00	0.10	0.10	4.93	0.29	0.96
<i>gal.ac</i>	0.00	0.18	0.12	22.69	0.24	1.40
<i>glu.ac</i>	6.87	1.89	2.98	0.52	1.77	5.41
<i>glu</i>	0.00	0.00	0.00	4.24	0.00	9.47
<i>man</i>	0.00	0.01	0.31	0.00	0.00	1.80
<i>galac</i>	37.41	33.90	31.44	9.59	40.45	18.83

A.3.2.5 KAOLIN: MARS YELLOW (1P:1P) AND DI WATER

The FTIR spectrum of clay-based ochres shows non-silicate spectral features that appear to associate with organic matter (Chapter 3). They appear in two weak, broad bands ≈ 1650 and 1410 cm^{-1} , along with a broad hump around 3400 cm^{-1} characteristic of hydrogen bonding hydroxyl groups, methyl and methylene stretching at 2920 and 2850 cm^{-1} . If a binder is present, these peaks suggest gum as the closest class of compound. Hence, it is of interest to find out if a gum exists in these ochres. The GC/MS result shows an absence of monosaccharide,

indicating that the organic matter is likely due to other substances. A literature search suggests the possible presence of humic substances, which are a mixture of humic acid, fulvic acid and humin produced from plant and animal decomposition in soil (Yang & Wang 1997). The negative presence of gum by GC/MS suggests that the organic fraction in the ochres is more likely to be humic substances, where more details are given in Chapter 3.

A.3.3 PHASE 3: VALIDATION WITH BAUMANN STUDIO MATERIALS, COMPARING AGAINST PY-GC/MS AND FTIR DATA

Five powdered artists' materials taken from Baumann's painting studio (Chapter 6) were previously tested with FTIR spectroscopy, and 3 semi-liquid "printing varnish" samples were previously tested with Py-GC/MS. These samples were subjected to the GC/MS protocol developed herein, and the results were compared side by side in Table A.5. The analyses of the powder samples show that FTIR spectroscopy and GC/MS are complementary in the characterisation of binders. Being more sensitive to trace amounts, GC/MS can detect small amounts of gums in addition to starch that would otherwise not be detected if FTIR spectroscopy alone is used. Similarly, the detection of an intense glucose peak by GC/MS does not attribute to any known gum, but with FTIR spectroscopy, it can be identified as starch.

The results of the semi-liquid samples also compare well with Py-GC/MS results, with the exception of sample H-S3-13 (Fig. A.14). For this sample, wax is detected in Py-GC/MS, but not in the GC/MS analytical procedure described herein. Studies have reported that hydrolysis of wax esters is particularly problematic with conventional saponification, hence microwave hydrolysis was subsequently used to improve the detection of wax esters (Andreotti et al. 2006; Bonaduce & Colombini 2004). However, the hydrolysis of the lipid/resin/wax fraction was carried out in the conventional way, which may explain why wax was not detected in sample H-S3-13.

Table A.5. Results of powder and varnish samples obtained from Baumann's painting studio.

<i>Powder Sample</i>	<i>FTIR result</i>	<i>GC/MS result</i>	<i>Interpretation</i>
4B_S3-10 off color hard clump 0.876mg	Gum tragacanth	Xylose, arabinose, fucose, galactose	Valid
4C_C-9 beige powder 1.052mg	Starch	Glucose	Valid
4D_S1-12 white powder_0.478mg	Starch	A lot of glucose with traces of xylose and arabinose	GC/MS shows that there are gum traces in addition to starch, but the yield was too low to be quantitated.
4E_S3-18 off-white powder_1.248mg	Starch	A lot of glucose with traces of xylose, arabinose and galactose	GC/MS show that there are gum traces in addition to starch. A qualitative comparison suggests cherry gum or perhaps another type of fruit gum.
4F_S3-6 brown powder_0.450mg	Unidentified	No positive monosaccharide peak	Valid. Gum binder is absent.
<i>Semi-liquid Sample</i>	<i>Py-GC/MS result</i>	<i>GC/MS result</i>	<i>Interpretation</i>
A-S2-33	Linseed oil	Pa, St, Ole, Az, Se, Su, La suggests linseed oil that is still in the process of ageing	Valid, GC/MS indicates linseed oil.
D-S3-18	Linseed oil, resin	Same fatty acid profile as in A-S2-33, with DHA and 7-oxo-DHA oxidative products from diterpenoid (Pinaceae) resin	Valid, GC/MS indicates a diterpenoid (Pinaceae) resin with linseed oil.
H-S3-13	Linseed oil, resin, wax	DHA and 7-oxo-DHA oxidative products from diterpenoid resin, minor amounts of Az, Su, Pa, Ole and St	Invalid, wax was identified with Py-GC/MS, but not identified in GC/MS result.

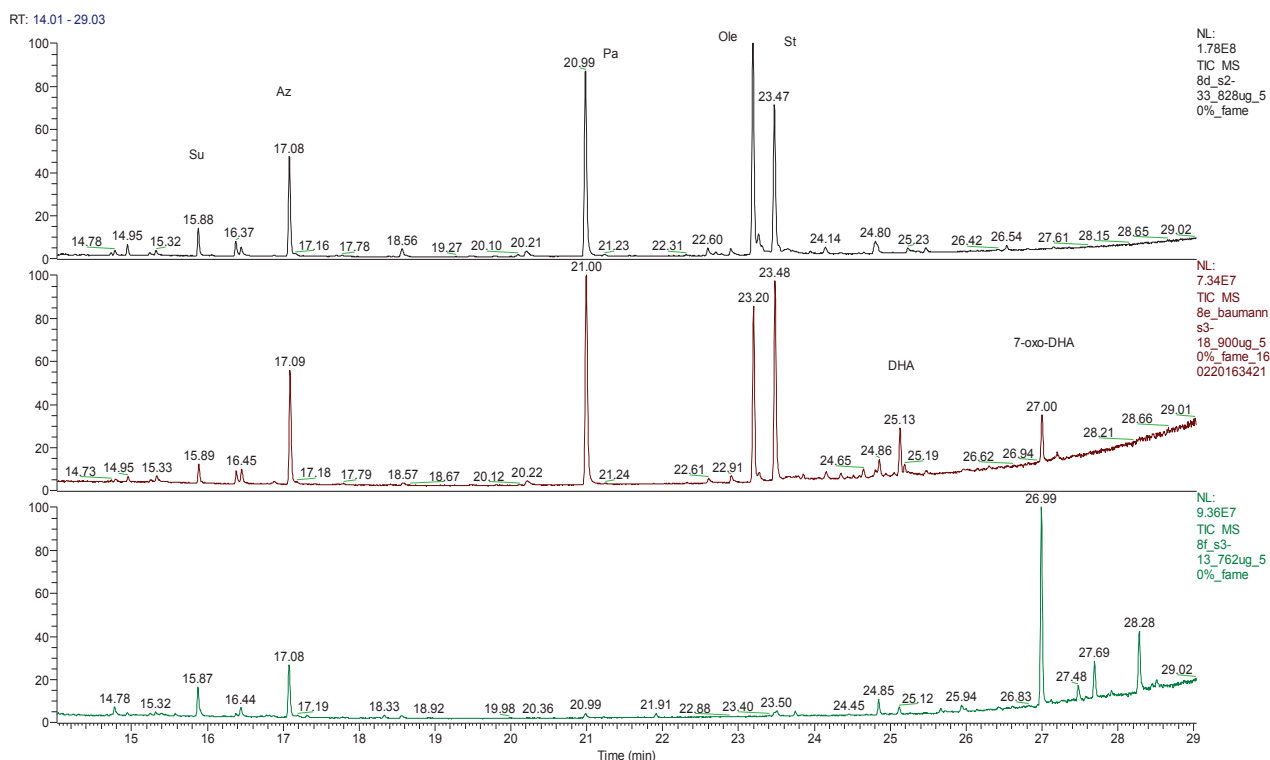


Fig. A.14 Fatty acid profile of Baumann studio “printing varnishes”: A-S2-33 (top), D-S3-18 (middle) and H-S3-13 (bottom).

A.4 CONCLUSION

The results from Phase 1 testing against pure standards and raw materials showed reproducible peaks for each analyte in the individual fractions. Phase 2, however, demonstrates some difficulties in interpretation when more than one binder class exists in a sample. In particular, the amino acid recovery in egg yolks is lower than other proteinaceous samples and gum tragacanth cannot be identified in a gum arabic/ gum tragacanth mixture, even though present. The samples tested in Phase 2 are less than 2 months old, thus the data is not representable for aged samples. The composition of analytes can vary qualitatively or quantitatively when the sample undergoes oxidation in air, degradation with pollutants and chemical changes in the presence of other binders and pigments. To achieve credible characterisation, validation of this protocol is necessary using naturally aged and artificially aged mockup pigment/ binder

mixtures. Phase 3 shows that the results from FTIR and Py-GC/MS are comparable to results obtained with the GC/MS analytical procedure implemented here, with the exception of waxy sample H-S3-13. The analysis of Baumann paint studio samples illustrates the importance of employing a combination of spectroscopy and chromatography techniques to characterise organic binders.

A.5 REFERENCES

- Andreotti, A., Bonaduce, I., Colombini, M.P., Gautier, G., Modugno, F. & Ribechini, E. 2006, 'Combined GC/MS Analytical Procedure for the Characterization of Glycerolipid, Waxy, Resinous, and Proteinaceous Materials in a Unique Paint Microsample', *Analytical Chemistry*, vol. 78, no. 13, pp. 4490-500.
- Biermann, C.J., Kinoshita, C.M., Marlett, J.A. & Steele, R.D. 1986, 'Analysis of amino acids as tert.-butyldimethylsilyl derivatives by gas chromatography', *Journal of Chromatography A*, vol. 357, pp. 330-4.
- Blackburn, S. 1989, *CRC Handbook of Chromatography: Amino Acids and Amines*, Taylor & Francis.
- Bonaduce, I., Cito, M. & Colombini, M.P. 2009, 'The development of a gas chromatographic–mass spectrometric analytical procedure for the determination of lipids, proteins and resins in the same paint micro-sample avoiding interferences from inorganic media', *Journal of Chromatography A*, vol. 1216, no. 32, pp. 5931-9.
- Bonaduce, I. & Colombini, M.P. 2004, 'Characterisation of beeswax in works of art by gas chromatography–mass spectrometry and pyrolysis–gas chromatography–mass spectrometry procedures', *Journal of Chromatography A*, vol. 1028, no. 2, pp. 297-306.
- Chen, S.T., Chiou, S.H., Chu, Y.H. & Wang, K.T. 1987, 'Rapid hydrolysis of proteins and peptides by means of microwave technology and its application to amino acid analysis', *International Journal of Peptide and Protein Research*, vol. 30, no. 4, pp. 572-6.
- Colombini, M.P. & Modugno, F. 2004, 'Characterisation of proteinaceous binders in artistic paintings by chromatographic techniques', *Journal of Separation Science*, vol. 27, no. 3, pp. 147-60.
- Colombini, M.P. & Modugno, F. 2009, *Organic Mass Spectrometry in Art and Archaeology*, Wiley, Chichester.
- Colombini, M.P., Modugno, F., Fuoco, R. & Tognazzi, A. 2002, 'A GC-MS study on the deterioration of lipidic paint binders', *Microchemical Journal*, vol. 73, no. 1–2, pp. 175-85.

- Colombini, M.P., Modugno, F., Giacomelli, M. & Francesconi, S. 1999, 'Characterisation of proteinaceous binders and drying oils in wall painting samples by gas chromatography–mass spectrometry', *Journal of Chromatography A*, vol. 846, no. 1–2, pp. 113-24.
- Derrick, M.R., Stulik, D. & Landry, J.M. 1999, *Infrared Spectroscopy in Conservation Science*, The Getty Conservation Institute, USA.
- Dhakal, B. & Armitage, R.A. 2013, 'GC-MS Characterization of Carbohydrates in an Archaeological Use Residue: A Case Study from the Coahuila Desert', *Archaeological Chemistry VIII*, vol. 1147, American Chemical Society, pp. 157-70.
- Dowsett, M. & Adriaens, A. 2004, 'The role of SIMS in cultural heritage studies', *Nuclear Instruments and Methods in Physics Research Section B: Beam Interactions with Materials and Atoms*, vol. 226, no. 1–2, pp. 38-52.
- Edwards, H.G.M. & Vandenabeele, P. 2012, *Analytical Archaeometry: Selected Topics*, Royal Society of Chemistry, Cambridge, United Kingdom.
- Gilman, L.B. & Woodward, C. 2012, 'An evaluation of microwave heating for the vapor phase hydrolysis of proteins', in Villafranc (ed.), *Current Research in Protein Chemistry: Techniques, Structure, and Function*, pp. 23-36.
- Gimeno-Adelantado, J.V., Mateo-Castro, R., Doménech-Carbó, M.T., Bosch-Reig, F., Doménech-Carbó, A., De la Cruz-Cañizares, J. & Casas-Catalán, M.J. 2002, 'Analytical study of proteinaceous binding media in works of art by gas chromatography using alkyl chloroformates as derivatising agents', *Talanta*, vol. 56, no. 1, pp. 71-7.
- Hyotylainen, T. & Wiedmer, S. 2013, *Chromatographic Methods in Metabolomics*, Royal Society of Chemistry.
- Jurado-López, A. & Luque de Castro, M.D. 2005, 'Optimisation of focused microwave digestion of proteinaceous binders prior to gas chromatography', *Talanta*, vol. 65, no. 4, pp. 1059-62.
- Lliveras-Tenorio, A., Mazurek, J., Restivo, A., Colombini, M.P. & Bonaduce, I. 2012a, 'Analysis of plant gums and saccharide materials in paint samples: comparison of GC-MS analytical procedures and databases', *Chemistry Central Journal*, vol. 6, no. 1, pp. 115-30.
- Lliveras-Tenorio, A., Mazurek, J., Restivo, A., Colombini, M.P. & Bonaduce, I. 2012b, 'The Development of a New Analytical Model for the Identification of Saccharide Binders in Paint Samples', *PLoS ONE*, vol. 7, no. 11, p. e49383.
- Lliveras, A., Bonaduce, I., Andreotti, A. & Colombini, M.P. 2010, 'GC/MS Analytical Procedure for the Characterization of Glycerolipids, Natural Waxes, Terpenoid Resins, Proteinaceous and Polysaccharide Materials in the Same Paint Microsample Avoiding Interferences from Inorganic Media', *Analytical Chemistry*, vol. 82, no. 1, pp. 376-86.
- Margolis, S.A., Jassie, L. & Kingston, H.M. 1991, 'The hydrolysis of proteins by microwave energy', *The Journal of Automatic Chemistry*, vol. 13, no. 3, pp. 93-5.
- Mayer, R. 1950, *The artist's handbook of materials and techniques*, The Viking Press, New York.

- Pitthard, V. & Finch, P., 'GC-MS analysis of monosaccharide mixtures as their diethylthioacetal derivatives: Application to plant gums used in art works', *Chromatographia*, vol. 53, no. 1, pp. S317-S21.
- Robinet, L. & Corbeil, M.-C. 2003, 'The Characterization of Metal Soaps', *Studies in Conservation*, vol. 48, no. 1, pp. 23-40.
- Schilling, M.R., Khanjian, H.P. & Luiz, A.C.S. 1996, 'Gas Chromatographic Analysis of Amino Acids as Ethyl Chloroformate Derivatives. Part 1, Composition of Proteins Associated with Art Objects and Monuments', *Journal of the American Institute for Conservation*, vol. 35, no. 1, pp. 45-59.
- Schummer, C., Delhomme, O., Appenzeller, B.M.R., Wennig, R. & Millet, M. 2009, 'Comparison of MTBSTFA and BSTFA in derivatization reactions of polar compounds prior to GC/MS analysis', *Talanta*, vol. 77, no. 4, pp. 1473-82.
- Smith, G.D., Newton, K.E. & Altherr, L. 2015, 'Hydrofluoric acid pre-treatment of matte artists' paints for binding medium analysis by Fourier transform infrared microspectroscopy', *Vibrational Spectroscopy*, vol. 81, pp. 46-52.
- Spoto, G. 2000, 'Secondary ion mass spectrometry in art and archaeology', *Thermochimica Acta*, vol. 365, no. 1-2, pp. 157-66.
- Voras, Z.E., Ghetaldi, K., Baade, B., Gordon, E., Gates, G. & Beebe, T.P. 2016, 'Comparison of oil and egg tempera paint systems using time-of-flight secondary ion mass spectrometry', *Studies in Conservation*, pp. 1-14.
- Yang, Y. & Wang, T. 1997, 'Fourier transform Raman spectroscopic characterization of humic substances', *Vibrational Spectroscopy*, vol. 14, no. 1, pp. 105-12.